

1-1-1989

# Towards an understanding of the effects of bubble nucleation, growth and rupture on devolatilization/

John Robert Bric

*University of Massachusetts Amherst*

Follow this and additional works at: [https://scholarworks.umass.edu/dissertations\\_1](https://scholarworks.umass.edu/dissertations_1)

---

## Recommended Citation

Bric, John Robert, "Towards an understanding of the effects of bubble nucleation, growth and rupture on devolatilization/" (1989).  
*Doctoral Dissertations 1896 - February 2014*. 756.  
[https://scholarworks.umass.edu/dissertations\\_1/756](https://scholarworks.umass.edu/dissertations_1/756)

This Open Access Dissertation is brought to you for free and open access by ScholarWorks@UMass Amherst. It has been accepted for inclusion in Doctoral Dissertations 1896 - February 2014 by an authorized administrator of ScholarWorks@UMass Amherst. For more information, please contact [scholarworks@library.umass.edu](mailto:scholarworks@library.umass.edu).

UMASS/AMHERST



312066007688521

**TOWARDS AN UNDERSTANDING OF THE EFFECTS OF BUBBLE  
NUCLEATION, GROWTH AND RUPTURE ON DEVOLATILIZATION**

A Dissertation Presented

By

**JOHN ROBERT BRIC**

Submitted to the Graduate School of the  
University of Massachusetts in partial fulfillment  
of the requirements for the degree of

**DOCTOR OF PHILOSOPHY**

May, 1989

Polymer Science and Engineering Department

© Copyright by John Robert Bric, 1989.

All Rights Reserved.

TOWARDS AN UNDERSTANDING OF THE EFFECTS OF BUBBLE  
NUCLEATION, GROWTH AND RUPTURE ON DEVOLATILIZATION


A Dissertation Presented

By

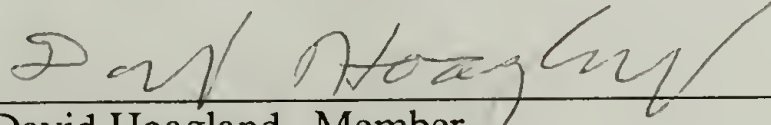
JOHN ROBERT BRIC

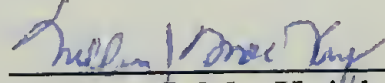
Approved as to style and content by:

  
Robert L. Laurence, Chairman of Committee

  
Julio M. Ottino, Member

  
Michael F. Malone, Member

  
David Hoagland, Member

  
William J. MacKnight, Department Head  
Polymer Science and Engineering Department

## DEDICATION

This dissertation is dedicated with love to Mom, Dad and Aunt Kae. Without their immeasurable love, support and self-sacrifice, this achievement would have been quite impossible.

## ACKNOWLEDGEMENTS

I thank my advisor, Professor Robert L. Laurence for his guidance, support and kindness during the course of this research. I also thank my committee members, Professors Julio Ottino, Michael Malone and David Hoagland, for their constructive input and their commitment to high standards. I am particularly indebted to Julio for his brief but enlightening introduction to bubble dynamics in flow fields.

Special thanks are due to Craig Pawlisch for his patience in passing on to me the art of inverse gas chromatography and to Steve Fundakowski for his enthusiasm in providing assistance on any problem in any capacity. Special thanks also to Ravi Chella and Osman Aboul-Nasr for providing valuable insights into devolatilization.

Partial support of this research by the industrial sponsors of the University of Massachusetts's CUMIRP program is gratefully acknowledged.

## ABSTRACT

### TOWARDS AN UNDERSTANDING OF THE EFFECTS OF BUBBLE NUCLEATION, GROWTH AND RUPTURE ON DEVOLATILIZATION

MAY, 1989

JOHN ROBERT BRIC, B.S.Ch.E., UNIVERSITY OF MASSACHUSETTS

Ph.D., UNIVERSITY OF MASSACHUSETTS

Directed by: Professor Robert L. Laurence

A theoretical investigation into the effects of bubble nucleation, growth and rupture on foam-enhanced devolatilization (DV) has been conducted. A methodology is proposed for constructing models of foam-enhanced DV, the first to allow incorporation of realistic descriptions of bubble birth, growth and death into models of the process. This methodology uses a population balance to track the evolution of the foam, described as a distribution over bubble sizes. A mass balance, coupled to the population balance, predicts the devolatilization rate.

Using this methodology, models of the single screw devolatilizer and the rolling drum devolatilizer were constructed which include conceptually realistic descriptions of bubble nucleation, growth and rupture. These models include two empirical parameters which quantify the rate of nucleation. The models correlate available data on the performance of these devolatilizers well. Also, they offer significant improvements over Latinen's (1962) model, which is the model most commonly used in single screw devolatilizer design.

Approximate models were derived from the single screw and rolling drum devolatilizer models. These are significantly less complex than the complete models and the computation time required for their numerical solution is reduced by more than two



orders of magnitude. Simplifications introduced into the empirical model of bubble nucleation allow the derivation of explicit, analytical model solutions, valuable for use in devolatilizer design.

Descriptors of the bubble distribution were introduced which characterize the nature of the foam. These are integral averages over the bubble distribution and are usually more practical for characterizing the foam phase than the distribution itself. Descriptors calculated using the rolling drum model reveal the predicted foam volume fractions and bubble radii to be unrealistically large. An empirical model of bubble rupture by film draining was added to this model to reduce these values. Although this decreased the average bubble age to unrealistically small values, the foam volume fraction and bubble radii were reduced to reasonable values.

## TABLE OF CONTENTS

ACKNOWLEDGEMENTS .....	v
ABSTRACT .....	vi
LIST OF TABLES .....	xi
LIST OF FIGURES .....	xii
LIST OF SYMBOLS .....	xvi
 Chapter	
I. INTRODUCTION.....	1
1.1 Modelling of Foam-Enhanced Devolatilization .....	4
1.2 Scope of Work .....	7
II. BACKGROUND .....	10
2.1 A Compilation of Experimental Studies of DV .....	10
2.2 A Review of Existing Models of Devolatilization .....	12
2.2.1 Models Neglecting Foaming .....	12
2.2.2 Models Including Foaming .....	14
2.3 Inadequacies of Existing Models .....	16
III. A METHODOLOGY FOR MODELLING FOAM-ENHANCED DV .....	18
IV. MODEL OF A SINGLE SCREW DEVOLATILIZER .....	21
4.1 Geometry and Operation .....	21
4.2 Bubble Radius and Age Distributions .....	23
4.3 Mass Balance .....	27
4.3.1 Mass Transfer to Bubbles .....	28
4.3.2 Mass Transfer by Interfacial Diffusion .....	30
4.3.2.1 Models of Latinen .....	30
4.3.2.2 Contribution of Surface Stretching to Interfacial Diffusion .....	32
4.3.3 Bubble Growth Rate .....	34
4.4 Population Balance .....	35
4.4.1 Bubble Birth Rate .....	36
4.4.2 Bubble Death Rate .....	39
4.5 Model Equations .....	42

4.6	Model Solution .....	47
4.7	Model Behavior .....	47
4.8	Model Evaluation .....	52
4.8.1	Experimental Data .....	52
4.8.2	Correlation of Experimental Data .....	58
4.8.3	Comparison with Latinen's Model .....	59
V.	MODEL OF A ROLLING DRUM DEVOLATILIZER .....	64
5.1	Geometry and Operation .....	64
5.2	Model Equations .....	64
5.3	Model Evaluation .....	70
5.3.1	Experimental Data .....	70
5.3.2	Correlation of Experimental Data .....	77
5.3.3	Comparison with Latinen's Model .....	90
VI.	APPROXIMATE MODELS AND A DESIGN MODEL OF DV .....	94
6.1	Approximate Models of DV .....	94
6.1.1	The Quasi-Steady State Model .....	94
6.1.2	The Inner Model .....	98
6.1.3	The Patched Model .....	99
6.1.4	The Instantaneous Quasi-Steady State Model .....	99
6.1.5	Comparison of Approximate Models with the Full Model .....	101
6.2	A Design Model for Foam-Enhanced DV .....	112
VII.	DESCRIPTORS OF THE BUBBLE DISTRIBUTION AND A MODEL OF DV WITH RUPTURE BY FILM DRAINING .....	118
7.1	Definition of Descriptors .....	118
7.2	Descriptors of the Rolling Drum Model .....	120
7.3	A General Model of DV .....	132
7.4	Rolling Drum Devolatilizer Model with Rupture by Film Draining .....	140
VIII.	CONCLUSIONS AND RECOMMENDATIONS .....	151
8.1	Conclusions .....	151
8.2	Recommendations for Future Work .....	152
Appendices		
A	BUBBLE GROWTH IN QUIESCENT POLYMER SOLUTIONS AND THE EFFECT OF SHEAR ON THE BUBBLE GROWTH RATE .....	156

B	BUBBLE RUPTURE RATES BY FILM DRAINING AND MECHANICAL SHEARING IN A SINGLE SCREW DEVOLATILIZER .....	161
C	ESTIMATION OF $E_a$ FROM NUCLEATION ONSET STUDIES AND THE SHEAR RATE DEPENDENCE OF THE BUBBLE BIRTH RATE .....	169
	REFERENCES .....	173

## LIST OF TABLES

<b>Table 4.1</b>	Summary of the conditions of Coughlin and Canevari's (1969) experiments on the single screw devolatilizer. ....	55
<b>Table 4.2</b>	Inlet and outlet conditions of Coughlin and Canevari's (1969) experiments on the single screw devolatilizer and the single screw devolatilizer model parameters that best correlate this data. ....	57
<b>Table 5.1</b>	Variables in Biesenberger and Lee's (1986) experiments on the rolling drum devolatilizer. ....	71
<b>Table 5.2</b>	Physical property data for solvents used in Biesenberger and Lee's (1986) experiments on the rolling drum devolatilizer. ....	77
<b>Table 5.3</b>	Physical property data on polydimethylsiloxane (PDMS) used in Biesenberger and Lee's (1986) experiments on the rolling drum devolatilizer. ....	78
<b>Table 5.4</b>	Dimensions of the rolling drum devolatilizer and of the bulk film of Biesenberger and Lee's (1986) experiments used in our model correlations. ....	78
<b>Table 5.5</b>	Conditions of Biesenberger and Lee's (1986) experiments on the rolling drum devolatilizer. ....	78
<b>Table 5.6</b>	Model parameters that best correlate the rolling drum devolatilizer model to the DV performance data measured by Biesenberger and Lee (1968) on the rolling drum devolatilizer. ....	84

## LIST OF FIGURES

<b>Figure 4.1</b>	Schematic of the cross section of a single screw devolatilizer. ....	22
<b>Figure 4.2</b>	Schematic of the idealized, unwrapped cross section of a single screw devolatilizer. ....	22
<b>Figure 4.3</b>	Schematic of the unwound single screw devolatilizer channel. ....	24
<b>Figure 4.4</b>	Schematic of the unwound single screw devolatilizer channel showing the differential volume element over which the mass balance is made. ....	29
<b>Figure 4.5</b>	Plots of reduced nucleation rate versus superpressure calculated from the empirical nucleation rate expression for $T = 220\text{ }^{\circ}\text{C}$ . ....	40
<b>Figure 4.6</b>	Plot of the characteristics of the population balance equation. ....	48
<b>Figure 4.7</b>	Plots showing the dependence of the DV rate predicted by the Full Model of the single screw devolatilizer on (a) $\alpha_1$ and (b) $\alpha_3$ . ....	50
<b>Figure 4.8</b>	Surface plot of the bubble age distribution given by the Complete Model of the rolling drum devolatilizer. $\alpha_1 = 0.02$ , $\alpha_2 = 0.00136$ , $\alpha_3 = 0.4$ and $\alpha_4 = 336$ . ....	51
<b>Figure 4.9</b>	Surface plot of the bubble age distribution given by the Complete Model of the rolling drum devolatilizer. $\alpha_1 = 0.02$ , $\alpha_2 = 0.00136$ , $\alpha_3 = 0.4$ and $\alpha_4 = 336$ . ....	53
<b>Figure 4.10</b>	Plots of the nucleation rate parameter, $F$ , estimated from the data of Coughlin and Canevari (1969) versus (a) run number and (b) characteristic shear rate for $E_a = 2.64\text{ atm}^2\text{ K}$ . ....	60
<b>Figure 4.11</b>	Plots of the dimensionless outlet concentration of xylene in polypropylene from a single screw devolatilizer measured by Coughlin and Canevari (1969) versus (a) the outlet concentration predicted by our model and (b) the outlet concentration predicted by Latinen's (1962) model. ....	61
<b>Figure 5.1</b>	Schematic of the cross section of a rolling drum devolatilizer showing (a) the actual geometry and (b) the idealized geometry used in our model. ....	65
<b>Figure 5.2</b>	Plots of data set 1 of Biesenberger and Lee's (1986) rolling drum devolatilizer performance experiments showing the effect of varying rotation speed on the DV performance of MeCl in PDMS for $X_0 \cong 8000\text{ ppm}$ and $P = 5\text{ torr}$ . (a) dimensionless concentration, (b) supersaturation and (c) superpressure. ....	72

<b>Figure 5.3</b>	Plots of data set 2 of Biesenberger and Lee's (1986) rolling drum devolatilizer performance experiments showing the effect of varying solvent concentration and pressure on the DV performance of MeCl in PDMS for $N = 75$ rpm. (a) dimensionless concentration, (b) supersaturation and (c) superpressure. ....	73
<b>Figure 5.4</b>	Plot of dimensionless concentration from data 3 of Biesenberger and Lee's (1986) rolling drum devolatilizer performance experiments taken on MeCl in PDMS and containing short time data. $X_0 = 7900$ ppm, $N = 75$ rpm, $P = 8$ torr. ....	75
<b>Figure 5.5</b>	Plots of data set 4 of Biesenberger and Lee's (1986) rolling drum devolatilizer performance experiments taken on a series of Freons <sup>®</sup> in PDMS with varying solubilities: (a) dimensionless concentration, (b) supersaturation and (c) superpressure. $X_0 = 4250$ ppm, $N = 75$ rpm, $P = 7$ torr. ....	76
<b>Figure 5.6</b>	Plot of the rolling drum devolatilizer model's correlation of Biesenberger and Lee's (1986) data 3 for MeCl in PDMS. $X_0 = 7900$ ppm, $N = 75$ rpm, $P = 8$ torr. ....	81
<b>Figure 5.7</b>	Plots of the rolling drum devolatilizer model's correlation of Biesenberger and Lee's (1986) data set 1 for MeCl in PDMS for $X_0 \cong 8000$ ppm and $P = 5$ torr: (a) data 1A, $N = 4$ rpm (b) data 1B with data 3 for comparison, $N = 75$ rpm and (c) data 1C, $N = 120$ rpm. ....	82
<b>Figure 5.8</b>	Plots of the rolling drum devolatilizer model's correlation of Biesenberger and Lee's (1986) data set 2 for MeCl in PDMS at $N = 75$ rpm and $P = 8$ torr: (a) data 2.A, $X_0 = 9000$ ppm and (b) data 2.B, $X_0 = 3800$ ppm ....	85
<b>Figure 5.9</b>	Plot of the rolling drum devolatilizer model's correlation of Biesenberger and Lee's (1986) data 4.A for Freon-114 <sup>®</sup> in PDMS. $X_0 = 4300$ ppm, $N = 75$ rpm, $P = 7$ torr. ....	87
<b>Figure 5.10</b>	Plot of the rolling drum devolatilizer model's correlation of Biesenberger and Lee's (1986) data 4.B for Freon-22 <sup>®</sup> in PDMS. $X_0 = 4260$ ppm, $N = 75$ rpm, $P = 7$ torr. ....	87
<b>Figure 5.11</b>	Plot of the rolling drum devolatilizer model's correlation of Biesenberger and Lee's (1986) data 4.C for Freon-13 <sup>®</sup> in PDMS. $X_0 = 4200$ ppm, $N = 75$ rpm, $P = 7$ torr. ....	88
<b>Figure 5.12</b>	Plots of correlations of Biesenberger and Lee's (1986) data 3 given by Latinen's (1962) model for varying values of the effective diffusivity. ....	91
<b>Figure 6.1</b>	Surface plot of the dimensionless bubble age distribution predicted by the Full Model of the rolling drum devolatilizer. $\alpha_1 = 0.02$ , $\alpha_2 = 0.00136$ and $\alpha_3 = 0.4$ . ....	96

<b>Figure 6.2</b>	Plots of the DV performance and the dimensionless moments of the bubble age distribution predicted by the Full Model of the rolling drum devolatilizer. $\alpha_1 = 0.02$ , $\alpha_2 = 0.00136$ and $\alpha_3 = 0.4$ . .....	97
<b>Figure 6.3</b>	Comparison of the solution of the Full Model of the rolling drum devolatilizer with the solutions given by the approximate models. $\alpha_1 = 0.02$ , $\alpha_2 = 0.00182$ and $\alpha_3 = 0.4$ . .....	102
<b>Figure 6.4</b>	Comparison of the solution of the Full Model of the rolling drum devolatilizer with the solutions given by the approximate models. $\alpha_1 = 0.02$ , $\alpha_2 = 0.00182$ and $\alpha_3 = 0.4$ . .....	103
<b>Figure 6.5</b>	Comparison of the solution of the Full Model of the rolling drum devolatilizer with the solutions given by the approximate models. $\alpha_1 = 0.02$ , $\alpha_2 = 0.00182$ and $\alpha_3 = 0.4$ . .....	104
<b>Figure 6.6</b>	Comparison of the solution of the Full Model of the rolling drum devolatilizer with the solutions given by the approximate models. $\alpha_1 = 0.2$ , $\alpha_2 = 0.00182$ and $\alpha_3 = 0.4$ . .....	106
<b>Figure 6.7</b>	Comparison of the solution of the Full Model of the rolling drum devolatilizer with the solutions given by the approximate models. $\alpha_1 = 0.2$ , $\alpha_2 = 0.00182$ and $\alpha_3 = 0.4$ . .....	107
<b>Figure 6.8</b>	Comparison of the solution of the Full Model of the rolling drum devolatilizer with the solutions given by the approximate models. $\alpha_1 = 0.2$ , $\alpha_2 = 0.00182$ and $\alpha_3 = 0.4$ . .....	108
<b>Figure 6.9</b>	Comparison of the solution of the Full Model of the rolling drum devolatilizer with the solutions given by the approximate models. $\alpha_1 = 0.2$ , $\alpha_2 = 0.00182$ and $\alpha_3 = 0.4$ . .....	109
<b>Figure 6.10</b>	Plot of the DV performance predicted by the Design Model. $\alpha_1 = 0.02$ , $\alpha_2 = 0.00182$ and $Y_{cr} = 0.507$ . .....	115
<b>Figure 7.1</b>	Plots of the descriptors predicted by the Full Model of the rolling drum devolatilizer for conditions of experiment 3 of Biesenberger and Lee (1986). $F = 798 \text{ cm}^{-3} \text{ s}^{-1}$ , $E_a = 15.2 \text{ atm}^2 \text{ K}$ , $\alpha_1 = 0.02$ , $\alpha_2 = 0.00136$ , $\alpha_3 = 0.4$ . .....	122
<b>Figure 7.2</b>	Plots of the descriptors predicted by the Complete Model of the rolling drum devolatilizer for conditions of experiment 3 of Biesenberger and Lee (1986). $F = 798 \text{ cm}^{-3} \text{ s}^{-1}$ , $E_a = 15.2 \text{ atm}^2 \text{ K}$ , $\alpha_1 = 0.02$ , $\alpha_2 = 0.00136$ , $\alpha_3 = 0.4$ and $\alpha_4 = 336$ . .....	124
<b>Figure 7.3</b>	Surface plot of the bubble age distribution predicted by the Complete Model of the rolling drum devolatilizer. $\alpha_1 = 0.02$ , $\alpha_2 = 0.00136$ , $\alpha_3 = 0.4$ and $\alpha_4 = 336$ . .....	125



<b>Figure 7.4</b>	Plots of the descriptors predicted by the Complete Model of the rolling drum devolatilizer for conditions of experiment 3 of Biesenberger and Lee(1986). $F = 80 \text{ cm}^{-3} \text{ s}^{-1}$ , $E_a = 15.2 \text{ atm}^2 \text{ K}$ , $\alpha_1 = 0.002$ , $\alpha_2 = 0.00136$ , $\alpha_3 = 0.4$ and $\alpha_4 = 336$ . .....	126
<b>Figure 7.5</b>	Surface plot of the bubble age distribution predicted by the Complete Model of the rolling drum devolatilizer. $\alpha_1 = 0.002$ , $\alpha_2 = 0.00136$ , $\alpha_3 = 0.4$ and $\alpha_4 = 336$ . .....	127
<b>Figure 7.6</b>	Plots of the descriptors predicted by the Complete Model of the rolling drum devolatilizer for conditions of experiment 3 of Biesenberger and Lee (1986). $F = 8 \text{ cm}^{-3} \text{ s}^{-1}$ , $E_a = 15.2 \text{ atm}^2 \text{ K}$ , $\alpha_1 = 0.0002$ , $\alpha_2 = 0.00136$ , $\alpha_3 = 0.4$ and $\alpha_4 = 336$ . .....	128
<b>Figure 7.7</b>	Surface plot of the bubble age distribution predicted by the Complete Model of the rolling drum devolatilizer. $\alpha_1 = 0.0002$ , $\alpha_2 = 0.00136$ , $\alpha_3 = 0.4$ and $\alpha_4 = 336$ . .....	129
<b>Figure 7.8</b>	Plots of the descriptors predicted by the Complete Model of the rolling drum devolatilizer of experiment 3 of Biesenberger and Lee (1986). $F = 20 \text{ cm}^{-3} \text{ s}^{-1}$ , $E_a = 15.2 \text{ atm}^2 \text{ K}$ , $\alpha_1 = 0.0005$ , $\alpha_2 = 0.00136$ , $\alpha_3 = 0.4$ and $\alpha_4 = 336$ . .....	131
<b>Figure 7.9</b>	Surface plot of the bubble age distribution predicted by the F.D. Complete Model of the rolling drum devolatilizer. $\alpha_1 = 0.02$ , $\alpha_2 = 0.00136$ , $\alpha_3 = 0.4$ and $\alpha_4 = 336$ . .....	144
<b>Figure 7.10</b>	Surface plot of the bubble age distribution predicted by the F.D. Complete Model of the rolling drum devolatilizer. $\alpha_1 = 0.002$ , $\alpha_2 = 0.00136$ , $\alpha_3 = 0.4$ and $\alpha_4 = 336$ . .....	145
<b>Figure 7.11</b>	Plots of the descriptors predicted by the F.D. Complete Model of the rolling drum devolatilizer for values of $F$ and $E_a$ which correlate data 3 of Biesenberger and Lee (1986). $F = 19500 \text{ cm}^{-3} \text{ s}^{-1}$ , $E_a = 15.2 \text{ atm}^2 \text{ K}$ , $\tau_R = 0.005 \text{ s}$ , $\alpha_1 = 0.008$ , $\alpha_2 = 0.000263$ , $\alpha_3 = 0.4$ and $\alpha_4 = 336$ . .....	147
<b>Figure 7.12</b>	Plots of the descriptors predicted by the F.D. Complete Model of the rolling drum devolatilizer fit to data 3 Biesenberger and Lee (1986). $F = 1.7 \times 10^5 \text{ cm}^{-3} \text{ s}^{-1}$ , $E_a = 15.2 \text{ atm}^2 \text{ K}$ , $\tau_R = 0.0005 \text{ s}$ , $\alpha_1 = 0.0015$ , $\alpha_2 = 5.67 \times 10^{-5}$ , $\alpha_3 = 0.4$ and $\alpha_4 = 336$ . .....	148
<b>Figure B-1</b>	Schematic of a cross sectional element of the single screw devolatilizer. ....	162
<b>Figure B-2</b>	Schematic of a cross sectional element of the single screw devolatilizer. ....	166

## LIST OF SYMBOLS

$A_c$	cross sectional area of the bulk film before foaming [ $L^2$ ]
$A_t$	cross sectional area of the bulk film during foaming [ $L^2$ ]
$b$	bubble birth rate variable in the general model [ $L^{-1} t^{-1}$ ]
$B$	birth rate of bubbles [ $L^{-1} t^{-2}$ ]
$C$	average concentration of solvent in continuous phase [ $M L^{-3}$ ]
$Ca$	bubble capillary number []
$C_e$	concentration of solvent in the continuous phase at the bubble surface which is in equilibrium with the solvent vapor in the bubble [ $M L^{-3}$ ]
$C_{max}$	$C_0 - C_e$ , the supersaturation of the fluid entering the devolatilizer [ $M L^{-3}$ ]
$C_0$	concentration of solvent in the feed to the devolatilizer [ $M L^{-3}$ ]
$d$	depth of the bulk film in the single screw devolatilizer [ $L$ ]
$dY/dt$	devolatilization rate [ $t^{-1}$ ]
$D$	solvent diffusivity [ $L^2 t^{-1}$ ]
$e$	bubble death rate variable in the general model [ $L^{-r} t^{-1}$ ]
$E$	death rate of bubbles [ $L^{-1} t^{-2}$ ]
$E_a$	empirical nucleation parameter [ $F^2 L^{-4} K$ ]
$f$	bubble age distribution [ $L^{-3} t^{-1}$ or $L^{-1} t^{-1}$ ]
$F$	empirical nucleation parameter [ $L^{-3} t^{-1}$ ]
$g$	bubble radius distribution [ $L^{-4}$ or $L^{-2}$ ]
$G$	shear rate far from bubble [ $t^{-1}$ ]
$H_b$	length of free surface of bulk film during foaming [ $L$ ]
$H_{b0}$	length of free surface of bulk film before foaming [ $L$ ]
$J$	nucleation rate of bubbles [ $L^{-3} t^{-1}$ ]
$k$	Boltzman's constant [ $F L K^{-1}$ ]
$K_C$	Henry's Law constant based on concentration [ $F L M^{-1}$ ]
$K_w$	Henry's Law constant based on mass fraction [ $F L^{-2}$ ]
$L_f$	length of the barrel film in the direction of barrel motion [ $L$ ]
$m$	mass of a solvent molecule [ $M$ ]
$M_n$	n'th dimensionless moment of the bubble age distribution []
$N$	number density of molecules [ $L^{-3}$ ]
$Pe$	Peclet number []
$P$	mechanical pressure in fluid [ $F L^{-2}$ ]
$P_v$	vapor pressure of solvent [ $F L^{-2}$ ]
$q$	exponent of $R$ in general growth rate expression []
$r$	exponent of $R$ in general death rate expression []
$Q$	$[1-(1/3)(1-P_v/P_l)]$ []
$R$	bubble radius [ $L$ ]
$R_{av}$	average bubble radius [ $L$ ]
$Re$	bubble Reynold's number []
$R_v/R_c$	foam volume expansion variable []
$R_0$	bubble radius at nucleation [ $L$ ]
$S$	fractional reduction in the free energy required to form a bubble nucleus at a surface relative to that in the interior of the solution []
$Sh$	Sherwood Number []
$T$	dimensionless bubble age []
$\mathbf{T}$	dimensionless time []

$T_{cr}$	dimensionless time at which $Y_{cr}$ is reached []
$\dot{V}$	volumetric flow rate of the bulk film in the z direction in the single screw devolatilizer [ $L^3 t^{-1}$ ]
$V_c$	volume of the bulk film (continuous phase only) before foaming [ $L^3$ ]
$V_t$	volume of the bulk film (continuous phase and bubbles) during foaming [ $L^3$ ]
$V_b$	velocity component of the bulk film surface normal to the flights [ $L t^{-1}$ ]
$V_f$	velocity component of the barrel film in the direction of barrel rotation [ $L t^{-1}$ ]
$V_w$	velocity of the barrel [ $L t^{-1}$ ]
$V_z$	average velocity of the bulk film in the z direction in the single screw devolatilizer [ $L t^{-1}$ ]
w	width of the single screw devolatilizer channel measured normal to the flights []
x	rectangular coordinate in the cross channel direction [L]
y	rectangular coordinate normal to the screw surface [L]
Y	dimensionless solvent concentration []
$Y_{cr}$	critical dimensionless solvent concentration at which nucleation ceases []
z	rectangular coordinate in the down channel direction [L]
Z	dimensionless distance in the down channel direction []

### Greek Symbols

$\alpha_i$	i'th dimensionless model parameter []
$\gamma(\Delta C)$	growth rate variable in general model [ $L t^{-q}$ ]
$\delta(\tau)$	Dirac-Delta function in $\tau$
$\Delta C$	$C - C_e$ , solvent supersaturation [ $M L^{-3}$ ]
$(\Delta C)_{cr}$	critical solvent supersaturation at which nucleation ceases [ $M L^{-3}$ ]
$\theta$	single screw helix angle [degrees]
$\lambda$	ratio of bubble viscosity to fluid viscosity []
$\mu_B$	viscosity of solvent vapor in bubble [ $F L^{-2} t$ ]
$\mu_f$	viscosity of fluid surrounding bubble [ $F L^{-2} t$ ]
$\mu_n$	n'th moment of the bubble age distribution [ $t^n L^{-1}$ ]
$\rho_b$	number density of bubbles in foam [ $L^{-3}$ ]
$\rho_g$	density of solvent vapor in bubbles [ $M L^{-3}$ ]
$\sigma$	surface tension [ $F L^{-1}$ ]
$\tau$	bubble age [t]
$\tau_{av}$	average bubble age [t]
$\tau_R$	time for a surface bubble to rupture by film draining [t]
$\phi$	foam phase volume fraction []
$\psi$	dimensionless bubble age distribution []

## CHAPTER I

### INTRODUCTION

*Devolatilization* (DV) is the name applied in polymer production to the process of separation of volatile, low molecular weight materials from nonvolatile, high molecular weight polymers. Devolatilization is analogous to the more familiar process of flashing, common to the chemical process industry. In both processes, a volatile material is separated from a less volatile host by reducing the pressure over the solution, preferentially evaporating the more volatile species. However, a distinction is made between the two processes because the physical properties of long chain molecules are sufficiently different from those of small molecules to require highly specialized equipment for devolatilization.

Devolatilization processes are commonly applied in polymer production for many reasons. Toxic, low molecular weight residuals are devolatilized from polymers for consumer safety. An example is residual styrene in polystyrene produced for food packaging. Polystyrene must be devolatilized to reduce its concentration of styrene monomer from per cent levels to concentrations on the order of parts per million to meet federal safety regulations. DV is commonly used in condensation polymerization processes also. The condensation polymerization reaction is driven to form higher molecular weight polymer by concurrently removing the volatile condensate by devolatilization. Other reasons for devolatilizing polymer solutions are to improve the performance or increase the consumer appeal of polymer products by devolatilizing solvents that are detrimental to these properties. As well, devolatilization is commonly used to recover expensive monomers and solvents to reduce materials costs.

The high viscosity of polymer solutions prevents them from being separated with standard flash equipment. Specialized equipment, called *devolatilizers*, are required to pump the solutions, usually by dragging or pushing, while simultaneously devolatilizing

the solvent. A desirable design feature of devolatilizers is *surface renewal*. Surface renewal is the process by which fluid at the solution/vapor interface is replaced with fluid from the interior of the liquid. This increases the concentration of solvent near the surface, thereby increasing the solvent mass flux. Rapid surface renewal is useful in DV to increase the rate of mass transfer, which usually limits the DV efficiency. These limitations arise from the small diffusivities of solvents in polymers, usually between  $10^{-7}$  to  $10^{-10}$  cm<sup>2</sup>/s.

The devolatilizers applied most commonly in industrial DV operations are the *single* and *twin screw devolatilizers*, the *falling strand devolatilizer* and the *wiped film evaporator*. The single and twin screw devolatilizers are standard screw extruders which are modified to operate with the screw channel in the DV section partially occupied by vapor. This vapor space is evacuated through a vacuum port on the extruder barrel. The falling strand devolatilizer consists of a strand die through which the polymer solution is pumped into an evacuated chamber where DV occurs. The wiped film evaporator is a blade and drum assembly through which the solution is dragged by scraping the polymer between the blade and drum wall forming thin films for DV.

The cost of a DV process can be a significant fraction of the total polymer production cost. According to estimates in 1979, DV costs ranged from \$.15 to \$6.30 per Kg of polymer produced (Devolatilization of Plastics, 1980). Capital costs of DV, such as costs for devolatilizers and vacuum equipment, are considerable. Also, the operating costs of DV can be significant, as the power consumption of extruders and vacuum equipment is substantial. Cost efficient design of devolatilizers can provide large economic returns. To develop cost efficient designs of devolatilizers, models are beneficial.

The earliest models constructed for devolatilizers often underestimate their efficiency (i.e. the time rate of change of the solvent concentration) by more than an order of magnitude. This has been generally attributed to neglect of *foaming*. Foaming contributes additional interfacial area for mass transfer and can significantly increase the DV efficiency.

The earliest models of DV include descriptions of mass transfer by diffusion through the liquid/vapor free surface only.

Foaming has been observed to occur in devolatilizers operating under vacuum. The reduced pressure in the devolatilizer supersaturates the solvent and bubbles containing solvent vapor are formed initiating foaming. Solvent diffuses into these bubbles causing them to grow to larger sizes. These bubbles rupture at the liquid/vapor interface and transfer the solvent contained in the bubbles to the vapor phase. The many bubbles which comprise the foam increase the surface area through which solvent can diffuse. This increases the mass transfer rate. The rate of mass transfer by foaming is usually many times greater than that by interfacial diffusion. Exclusion of foaming in models of DV has precluded them from providing an adequate *a priori* prediction of the performance of devolatilizers when foaming occurs.

Recognizing the limitations of these early models of DV, subsequent investigators developed models which include contributions to mass transfer by foaming. However, these models incorporate descriptions of the foaming process which differ conceptually with practical observations. This prevents these models from adequately predicting the performance of devolatilizers.

Models of DV developed to date are inadequate in that they function only in a correlative capacity. They contain empirical parameters that can only be determined from direct experimental measurements on the devolatilizer. These are costly and time-consuming. It would be advantageous to construct rigorous models of DV from first principles which would provide an *a priori* prediction of the performance of devolatilizers, obviating the need for experiment and empiricism.

The ultimate goal of this research program is it to develop models of foam-enhanced DV capable of predicting the performance of devolatilizers from first principles. As a preliminary step towards this goal, this thesis work has as its objective the development of a better understanding of foam-enhanced devolatilization. Specifically, we aim to better

understand how bubble birth, growth and death affect the nature of the foaming process and the devolatilizer's performance. A second objective is to apply this better understanding of foam-enhanced DV towards the rational construction of models of common industrial devolatilizers.

### **1.1 Modelling of Foam-Enhanced Devolatilization**

The significant complexity of the foaming process makes modelling of foam-enhanced DV a difficult task. The difficulty of constructing and solving a physically realistic model of foam-enhanced devolatilization becomes clear upon examining the large amounts of physical information it must include in a tractable form. To provide some perspective on the task of modelling DV, this information, its availability and its implementation into a tractable model will be addressed in this section.

The objective of any model of foam-enhanced DV is to predict the concentration of solvent in the solution leaving the devolatilizer. To do this, we must estimate the total mass transfer rate of solvent into the foam phase. This is given by the sum of the mass transfer rates to individual bubbles. Since the mass transfer rate to a bubble is a function of its radius, information on the number and sizes of bubbles in the devolatilizer is required to model foam-enhanced DV. The number and sizes of bubbles is governed by the complex interactions among the bubble birth, growth and death processes. Assuming the number and sizes of bubbles can be adequately represented by a distribution over bubble sizes, if the rates of bubble birth, growth and death are known, in theory, the bubble distribution can be solved for using standard population balance techniques.

Bubble birth in devolatilizers has been proposed to occur by nucleation according to the postulates of classical nucleation theory, both homogeneously and heterogeneously. Another proposed birth mechanism is pinch-off of bubbles from gas pockets trapped in the small crevices of container walls and entrained particles. Entrainment of bubbles at the dynamic liquid-solid-vapor contact line of moving surfaces has also been proposed as a

mechanism for birth. Unfortunately, there have been no conclusive studies revealing the mechanism of bubble birth or its frequency during devolatilization.

Bubble growth is probably the best understood of all the physical processes that comprise foaming during DV. Yet nearly all models of bubble growth have been for a single bubble growing in an infinite fluid, either stagnant or undergoing a time-independent flow. The flows which bubbles experience in typical devolatilizers are time-dependent rendering existing models inapplicable. A complication not included in most models of bubble growth is the presence of neighboring bubbles. As well, the large viscous and elastic stresses which can occur in flowing polymer solutions could considerably complicate the bubble growth rate description and must be considered in any bubble growth model. We are not aware of any models of bubble growth that include all these physical phenomena, a prerequisite if the model is to describe with rigor the growth rate of bubbles during DV.

Bubble death in devolatilizers can occur by rupture of bubbles at the vapor/liquid free surface. This has been observed to occur by two distinct mechanisms: *film draining* and *mechanical shearing*. Bubble rupture by film draining occurs when the thin liquid film surrounding surface bubbles drains into the surrounding liquid. Rupture occurs when this film thins enough so that London-van der Waal's forces become significant and drive instabilities in the film thickness, causing rupture. Bubble death by mechanical rupture can occur at the dynamic liquid-solid-gas contact line associated with a moving solid boundary. Shearing of the bubbles at the contact line causes their rupture. Nearly all studies available in the literature on bubble rupture have addressed rupture by the film draining mechanism, for which the bubbles are driven to the surface of low molecular weight, quiescent liquids by buoyancy forces. However, in DV, the liquid is a viscous polymer solution and bubbles are expected to be driven to the surface by convection rather than by buoyancy. The applicability of existing studies of bubble rupture to bubble rupture occurring during DV is unclear.



Bubble birth and death can also occur by bubble coalescence and breakage. Bubble coalescence has been observed to occur during DV, but its frequency has never been measured. The frequency of bubble breakage during DV has never been investigated and its frequency is unknown. Theories of bubble coalescence and breakage are not developed well enough yet to accurately predict their frequencies in the complex flows of most devolatilizers. Also, it should be noted that, if adequate theories of coalescence and breakage were available, their inclusion into models of DV would significantly increase the complexity of the model. It would introduce expressions into the model equations which include integral convolutions over the bubble size distribution. This is because coalescence can occur between bubbles of all sizes and breakage can form bubbles smaller than the original but of varying sizes.

Implicit in this discussion so far is the assumption that the bubbles are spherical. Yet, bubbles have been observed to deform from their spherical shape in the flow fields of devolatilizers. This could significantly increase the mass transfer rate to bubbles by increasing the surface area of the bubble and its mass transfer coefficient. If the bubble's deformation were to be included into models of DV, a measure of the deformation, such as the bubble's extension ratio, would be required, in addition to the effective bubble radius (i.e. the radius of the bubble relaxed to its undeformed, spherical state), to uniquely specify the mass transfer rate to a bubble. A multivariate distribution would be necessary to describe the bubble phase. This would increase the dimension of the solution vector, considerably complicating the problem description and its solution.

Bubble deformation has been investigated both theoretically and experimentally, mostly for time-independent flows. These studies may not be directly applicable to the time-dependent flows experienced by bubbles in typical devolatilizers. Also, we are not aware of any studies on the mass transfer rates to bubbles undergoing deformation. Only when bubble deformation and mass transfer to deforming bubbles in devolatilizers are

better understood will it be clear what their contributions to the devolatilizer's performance are and how these processes should be included into models of foam-enhanced DV.

Since the physical processes that comprise bubble birth, growth and death and their interactions are not well understood, it is clear that much of the information required in a complete model of DV is not yet available. Without this information it is unlikely that a tractable model of DV could soon be developed that would incorporate accurate descriptions of all aspects of the DV process. Without further fundamental investigations of these processes, attempts at rigorous modelling of foam-enhanced DV will not be very fruitful.

Advances in modelling of DV need not await these investigations, however. Although rigorously accurate descriptions of bubble birth, growth and death during DV are not yet available, models of DV that include approximate descriptions of these processes may be constructed and would be very valuable. If these approximate descriptions are at least conceptually realistic, unlike descriptions incorporated into preceding models, they could reveal valuable insights into this poorly understood operation. For instance, an approximate model of DV might reveal qualitatively the effects of varying physical properties or process variables on the devolatilizer's performance. This would make these models valuable in guiding rational devolatilizer experimentation and design. As well, since errors of approximately 15% in the predicted size of a devolatilizer are often tolerable, approximate models might be sufficiently accurate to be used for sizing devolatilizers *a priori*, without the need for costly and time-consuming experiments.

## 1.2 Scope of Work

We will investigate the effects of bubble birth, growth and death on foaming and mass transfer during DV. To do this, we will construct models of common industrial devolatilizers that include approximate descriptions of the bubble birth, growth and death rates which, unlike those incorporated into existing models of DV, are conceptually

realistic. A methodology for modelling DV will be formulated to guide the construction of these models. Model predictions of the nature of the foaming process and its effect on the DV rate will be investigated to provide insights into foam-enhanced DV.

The abilities of these models to describe the performance of industrial devolatilizers will also be investigated. These models will be used to analyze available devolatilizer performance data so that the model's correlative abilities can be evaluated. Also, the model's ability to describe the state of the foam phase will be evaluated by comparing the model's predictions of the state of the foam with experimental observations made by previous investigators. Comparison of the performance of our models with those of existing models will also be made to determine the advantages and improvements in our models.

This dissertation includes firstly, in **Chapter 2**, a compilation of published experimental studies of devolatilization for which the devolatilizer's performance was measured or its operation observed. A detailed review of existing models of devolatilization is also presented. The inadequacies of these models are revealed and the need for a new methodology for constructing models of DV which can incorporate realistic descriptions of bubble birth, growth and death is discussed.

In **Chapter 3**, a methodology for constructing models of DV is presented which can incorporate realistic descriptions of bubble birth, growth and death. This methodology is based on population balance techniques. Reasons why this methodology is more appropriate for modelling foam-enhanced devolatilization than the methods chosen by preceding investigators are presented.

In **Chapter 4**, the methodology proposed in Chapter 3 is used to construct a model of a single screw devolatilizer. This model is evaluated through its ability to correlate experimental measurements of DV rates in a single screw devolatilizer taken by Coughlin and Canevari (1969). This model is compared with Latinen's (1962) model, which is the

model most commonly used for sizing single screw devolatilizers, to identify the advantages and improvements in our model.

In **Chapter 5**, a model of a rolling drum devolatilizer is constructed, also according to the methodology proposed in Chapter 3. This apparatus was designed by Biesenberger and Lee (1986) to simulate the operation of the single screw devolatilizer. The model is evaluated by correlating rolling drum devolatilizer performance data measured by Biesenberger and Lee (1986). Comparisons with Latinen's (1962) model, modified to apply to the rolling drum devolatilizer, are also made.

In **Chapter 6**, approximate models of the single screw and rolling drum devolatilizer models are developed which are much less complex than the complete model and which require significantly reduced computation times for their numerical solution. Additional simplifications are introduced into the empirical birth rate expression of these approximate models which allow the derivation of explicit, analytical expressions describing the devolatilizer's performance. These solutions are valuable as design equations for the single screw and rolling drum devolatilizers.

Descriptors of the bubble distribution, which are useful in characterizing the state of the foam, are introduced in **Chapter 7**. To provide insight into the effects of the rates of bubble birth, growth and death on the state of the foam phase, a general model of DV is constructed. Using insight derived from this general model, a model of DV which incorporates bubble rupture by the mechanism of film draining is constructed with the objective of predicting more realistic foaming behavior.

## CHAPTER II

### BACKGROUND

In this chapter, a compilation of prior experimental studies of DV will be presented. Also, a review of important models of DV developed to date will be given and the inadequacies of these models will be discussed.

#### 2.1 A Compilation of Experimental Studies of DV

Most experimental studies of devolatilization have been conducted on the single screw, twin screw or falling strand devolatilizers. In nearly all experiments, measurements were made under vacuum and only measurements of the concentration of solvent at the inlet and outlet of the equipment were taken.

For the single screw devolatilizer, Latinen (1962) was the first to publish DV performance measurements. He measured the DV rates of styrene from polystyrene. Measurements of the single screw devolatilizer's performance were also made for xylene and methanol in polypropylene by Coughlin and Canevari (1969) and for styrene in polystyrene by Biesenberger and Kessidis (1982). The performance of the single screw devolatilizer for the devolatilization of styrene from polystyrene during depolymerization was measured by Blanks, Meyer and Grulke (1981). Kearney and Hold (1985) measured the devolatilization performance of a novel rotating drum devolatilizer, similar to a single screw devolatilizer with three screw flights. The DV rates of hexane/heptane solutions from polyethylene and polyethylene/polyethyl methacrylate copolymer were measured.

Biesenberger and Lee (1985, 1986 and 1987) investigated the performance of the rolling drum devolatilizer, which is a batch device that they designed to simulate the operation of a single screw devolatilizer. They measured the concentrations of methyl chloride and a series of Freons<sup>®</sup> in polydimethylsiloxane as a function of time. Since time in the rolling drum devolatilizer is analogous to distance in the single screw extruder, these

measurements correspond to the concentrations that would be measured as a function of distance through a single screw devolatilizer.

Most experiments on the performance of multi-screw devolatilizers were conducted for intermeshing, corotating screws. In the twin screw devolatilizer, Todd (1974) measured the devolatilization rates of thiophene, toluene and ethylbenzene from styrene and of cyclohexane from polyethylene. Gras and Eise (1975) measured the performance of a four screw devolatilizer with one and two vacuum stages. The materials devolatilized were not revealed. Collins, Denson and Astarita (1985) measured the DV rates of Freon<sup>®</sup>/polybutene mixtures in a twin screw devolatilizer. Measurements were made at atmospheric pressure by passing nitrogen over the solution to suppress foaming.

Han and Han (1985) made visual observations of the foaming behavior occurring during devolatilization in a model single screw devolatilizer and in a model counter-rotating and co-rotating twin screw devolatilizer. Nichols and Lubiejewski (1985) measured the performance of a twin screw devolatilizer for the devolatilization of cyclohexane/benzene mixtures from styrene-butadiene copolymers. Secor (1986) measured the performance of a twin screw devolatilizer operating at atmospheric pressure (i.e. without foaming) by passing dry air over the solution. The devolatilization rates of Freon-113<sup>®</sup> from polybutene were measured. Mack (1986) compared the performance of single and twin screw devolatilizers for the devolatilization of ethylene from polyethylene. The devolatilization rates of octene/n-hexane mixtures from polyethylene and carbon tetrachloride from a chloroprene rubber slurry were measured by Sakai and Hashimoto (1986) in a twin screw devolatilizer. Meder (1987) measured the devolatilization rates of water in polymethyl methacrylate in the twin screw devolatilizer. Shah, Wang, Schott and Grossman (1987) measured the DV performance for a tetra-methylene sulfone/polyamide solution in a twin screw devolatilizer operating as a finishing reactor.

In the falling strand devolatilizer, Newman and Simon (1980) measured the devolatilization rates of styrene/polystyrene solutions. Albalak, Tadmor and Talmon

(1987) made observations of the foaming behavior occurring during falling strand devolatilization of styrene from polystyrene. They investigated the foam structure of strands by freeze fracturing them and observing their cross sections using a scanning electron microscope.

Experimental studies of DV in other equipment include measurements of the DV rates of vinyl chloride from polyvinyl chloride in a batch slurry devolatilizer by Chan, Patel, Gupta, Worman and Grandin (1982). Mehta, Valsamis and Tadmor (1984) made DV rate measurements of styrene/polystyrene solutions in a novel rotating disk processor.

## 2.2 A Review of Existing Models of Devolatilization

A brief review will be presented of important DV models developed to date. Models which neglect foaming will be discussed first. For the single screw devolatilizer, these include models by Latinen (1962), Coughlin and Canevari (1969), Roberts (1970), and Biesenberger (1980). For the twin screw devolatilizer, models by Todd (1974), Collins, Denson and Astarita (1983 and 1985) and Secor (1986) will be discussed.

The few published models of DV that include foaming will also be discussed. The first was developed by Newman and Simon (1980) for the falling strand devolatilizer. A model of foam-enhanced DV in a twin screw devolatilizer was developed by Yoo and Han (1984). Powell and Denson (1983) and Chella and Lindt (1986) have developed models of foam-enhanced DV in batch devolatilizers.

### 2.2.1 Models Neglecting Foaming

Latinen's (1962) model of the single screw devolatilizer is the first successful model to be published for this equipment. It consists of a mass balance on the solvent applied over a differential cross sectional element of the screw channel. Included in the model are contributions to the loss of solvent by diffusion through the surface of the *bulk film*, comprised of solution contained in the screw channel, and by diffusion from the surface of

the *barrel film*, comprised of solution that adheres to the barrel wall after being dragged through the narrow clearance between the screw flight and the barrel wall. Latinen described the mass transfer using *penetration theory*. Penetration theory treats the film as being infinitely deep, simplifying the model's solution. This is usually an acceptable assumption for polymer/solvent solutions, considering the very small diffusivities of solvents in polymers. In his description of the interfacial mass transfer, Latinen also included surface renewal induced by the cross channel circulatory flow. The axial flow of fluid through the channel was described by a standard convective-diffusion expression which incorporates both the plug-like and axial dispersive characters of the flow. The mass balance, expressed as a second order, ordinary differential equation, was solved analytically to give an expression for the solvent concentration as a function of distance through the devolatilizer.

Coughlin and Canevari (1969) also developed a model for the single screw devolatilizer. Their's is a simplification of Latinen's model. They constructed a similar mass balance, although they neglected axial dispersion and surface renewal. They modelled mass transfer from the bulk film as diffusion from a slab of finite thickness, yet they neglected mass transfer from the barrel film. Roberts (1970) developed a model of a single screw devolatilizer similar to Latinen's. The major difference between the two is that Roberts assumed axial dispersion to occur solely by leakage over the screw flights, for which he was able to derive an approximate, explicit expression.

Biesenberger (1980) developed general models of staged and continuous DV processes. A staged model consists of a plug flow section connected to a well mixed section, each of which can transfer volatiles by diffusion through the interface of the fluid contained in the section. Each stage could contain either a feed forward or feed back loop to simulate axial dispersion. A devolatilizer could be simulated by connecting a number of stages in series. To illustrate the concept of a continuous devolatilizer, Biesenberger developed a model for a single screw devolatilizer which is similar to the model developed



by Roberts. However, Biesenberger includes a more general description of the contribution to axial dispersion by gap leakage.

For the twin screw devolatilizer, Todd (1974) developed a correlative model based on Latinen's approach for modelling the single screw devolatilizer. Two empirical parameters were included in the model, the effective diffusivity, quantifying the DV efficiency, and the Peclet number, quantifying the extent of axial dispersion. Collins, Denson and Astarita (1983) constructed an empirical model of the twin screw devolatilizer based on the length of a transfer unit concept borrowed from theories for stripping and extraction. Collins, Denson and Astarita (1985) refined their first model to include a description of the solvent mass transfer derived from first principles. Their theory closely parallels that of Latinen (1962) for the single screw devolatilizer. Secor (1985) also developed a model of the twin screw devolatilizer. Secor treated the DV in the twin screw devolatilizer as a staged process. He defined one stage as occurring from the time a fluid element enters screw A from adjacent screw B to the time later when it returns to screw B. He incorporated penetration theory to describe the mass transfer, although surface renewal was neglected. From a mass balance, Secor solved for the concentration change over each stage. After each stage he assumed that the transfer of the solution between flights induced sufficient mixing to homogenize the solvent.

### **2.2.2 Models Including Foaming**

Newman and Simon (1980) developed a model for the falling strand devolatilizer which is the earliest published model of DV to include foaming. Newman et al. assumed that the devolatilizer is fed a melt stream that is swollen with vapor bubbles from the previous processing step. Additional bubbles were not allowed to enter the solution beyond the entrance of the devolatilizer. The number of bubbles was estimated empirically by choosing values which best fit available experimental data on the devolatilizer's performance. The bubbles were modelled as growing in a stagnant, Newtonian fluid of

infinite extent so that the effects of bubble-bubble interactions and flow induced convection on the bubble growth could be neglected. Henry's law was chosen to relate the bubble pressure to the solvent concentration in the liquid at the bubble interface. The bubble's radius was calculated versus time by numerically integrating the coupled species balance (specifying the solvent flux to the bubble) and momentum balance (specifying the bubble growth rate). From a mass balance over all bubbles, the average solvent concentration in the continuous phase was calculated as a function of time. All bubbles were assumed to rupture simultaneously at some later time causing DV to cease. The time to rupture was determined empirically as that value for which the predicted value of the outlet concentration agreed with the experimental value.

Powell and Denson (1983) developed a model of batch DV (foaming of a quiescent solution) that is conceptually similar to the model by Newman and Simon. Powell et al. assumed that a set of bubbles are born simultaneously at the start of devolatilization and that no bubbles enter the solution at later times. No means were given for estimating the number of bubbles in the solution. For the purposes of model demonstration, the number of bubbles was chosen arbitrarily. To include interactions with neighboring bubbles, the bubble growth was modelled using a cell model. A cell model confines each bubble to a spherical cell of fluid and diffusion across the outer boundary of the cell is forbidden. The cell was assumed to contain a Newtonian fluid and Henry's Law was applied to couple the species and momentum balances which were solved numerically. A mass balance over all bubbles was constructed giving the average solvent concentration as a function of time. No model of bubble rupture was proposed.

Yoo and Han (1984) modelled foam-enhanced DV in a twin screw devolatilizer. They considered a devolatilizer with five DV sections. Bubbles were assumed to be born at, and only at, the entrance of each DV section. How they chose values for the number of bubbles was not clearly stated. The bubbles were assumed to travel in plug flow through the devolatilizer. Models were constructed for growth of bubbles in a Newtonian fluid, in

a linear viscoelastic fluid and in a three-constant Oldroyd fluid. Interactions among neighboring bubbles were neglected and the model was simplified to the growth of a set of isolated bubbles. The coupled momentum and mass balances were solved numerically. A mass balance over all bubbles gave the average solvent concentration as a function of time. All bubbles were assumed to rupture only upon exiting each DV section.

Chella and Lindt (1986) constructed a model of a batch devolatilizer which is very similar to the model by Powell and Denson. They assumed that a set of bubbles are born at the start of DV and that no bubbles enter the solution at later times. The number of bubbles was estimated from experimental data by first determining the change in the solution volume at the start of DV attributed to instantaneous bubble birth. From the bubble radius at birth, estimated to be that value which balances the opposing forces of surface tension and solvent vapor pressure, the number of bubbles was calculated from a volume balance on the solution. The bubble growth was described using a cell model. The major distinction between it and the cell model used by Powell and Denson is that Chella et al. include a heat balance in addition to the mass and momentum balances. This is to track the reduction in temperature due to the latent heat of vaporization of the solvent. Also, the Flory-Huggins thermodynamic model was used in place of Henry's Law. These modifications were necessary to apply the model to systems with moderately high solvent concentrations (less than 60% by mass). The average solvent concentration was calculated versus time from a mass balance over all bubbles. No description of bubble rupture was included in the model.

### 2.3 Inadequacies of Existing Models

Existing models of foam-enhanced DV cannot provide an adequate description of the performance of devolatilizers. This is because unrealistic descriptions of foaming were incorporated into these models. Previous investigators treated bubble birth as occurring only at the entrance of the devolatilizer (or at startup for batch devolatilizers). Foaming was

assumed to cease abruptly, usually at the exit of the equipment, where all bubbles were assumed to rupture. These assumptions constrain all bubbles at the same position through the equipment (or at the same time for a batch process) to be of identical size and age.

Actually, observations of foaming occurring during DV reveal it to be quite different from that proposed to occur by earlier investigators. Bubbles in devolatilizers have been observed to be born and rupture continuously from the entrance of the devolatilizer to the exit. The assumptions that birth occurs only at the entrance of the devolatilizer (i.e. at the start of DV) and that rupture occurs only at the exit of the devolatilizer (i.e. at the completion of DV) are clearly unrealistic. As well, a distribution of bubble sizes is observable at any position in the equipment which is a direct result of the continuous birth, growth and death of bubbles. The constraint that the bubbles be identical in size and age is artificial.

The significant conceptual differences between existing models of DV and the actual DV process indicate that the methodologies used by preceding investigators in constructing their models is inappropriate. A new methodology is needed that can incorporate realistic descriptions of bubble birth, growth and death into models of DV.

## CHAPTER III

### A METHODOLOGY FOR MODELLING FOAM-ENHANCED DV

A methodology based on population balances has been developed which can incorporate conceptually realistic descriptions of foaming occurring during DV into models of the process. Recognizing first that a distribution of bubble sizes occurs in devolatilizers and assuming that a bubble's radius is the only internal variable necessary for specifying the mass transfer rate to any bubble, the bubble phase will be described by a distribution over bubble radii. These bubbles will be treated as being spherical. If bubble deformation is significant, a second internal variable necessary for specifying the mass transfer rate to a bubble, perhaps the bubble extension ratio, could be added.

A balance on the rate of mass transfer between the continuous phase and the bubble phase is proposed to give the time rate of change of the average solvent concentration (i.e. the DV rate) in the continuous phase. Since the DV rate depends on the distribution of bubble sizes, a population balance on the distribution is proposed to track the distribution over time. This population balance will include expressions for the rates of bubble birth, growth and death. The coupled mass and population balances, expressed as differential equations, can be simultaneously integrated to solve for the bubble distribution and solvent concentration as functions of time (if it is a batch process) or position (if it is a continuous process).

Population balance techniques have been common in the fields of biology and ecology for more than 50 years. It has been only over the past 25 years that they have become a common tool of the chemical engineer. Hulburt and Katz (1964) were the first to introduce to the chemical engineer the formal methodology for constructing population balances for chemical systems. Population balances have since been applied extensively in many areas of chemical process modelling. A small selection of investigators who have

applied this methodology to chemical systems includes Bayens and Laurence (1967) and Randolph and Larson (1971) who constructed population balances to predict the evolution of distributions of liquid and solid particles undergoing growth, coalescence and breakage. In the area of polymer reactor design, population balances are fundamental to the modelling of the reaction kinetics of polymers distributed over varying molecular weights (Tirrell, Galvan and Laurence ; 1987). Pasiuk-Bronikowska and Rudzinski (1980 and 1981) have constructed successful population balance models of gas desorption from gas/liquid solutions occurring by bubbling of gases evolved during chemical reaction. From the physical similarities evident between gas desorption and DV, the success of Pasiuk-Bronikowska et al.'s model indicates that population balances might also be successful in modelling DV. However, population balances have not yet been applied to the modelling of foam-enhanced DV.

To demonstrate the proposed methodology, we will use it to construct models of devolatilizers. It is preferable, for preliminary modelling studies, that devolatilizers be chosen for which bubble coalescence and breakage have a minimal effect on the DV performance, since coalescence and breakage can significantly complicate the model's formulation and solution. Bubbles in the falling strand devolatilizer were shown by Alabak, Tadmor and Talmon (1987) to undergo frequent coalescence. This is understandable considering the high volume fractions of foam present in falling strand devolatilizers (according to Newman and Simon (1980), foam volume fractions occurring in the falling strand devolatilization of styrene from polystyrene can be as high as 0.67). Coalescence in the batch flash devolatilizer is expected to occur even more frequently than in the falling strand devolatilizer because larger volume fractions of foam are expected. A larger foam content is expected because the surface area to volume ratio is much smaller in the batch flash devolatilizer which reduces the probability of bubble rupture at surfaces.

Single and twin screw devolatilizers are expected to exhibit smaller volume fractions of foam than both the batch flash and falling strand devolatilizers because surface renewal

in the screw devolatilizers will increase the bubble rupture rate (i.e. by transporting bubbles to the surface). Evidence of this is given in photographs of foaming occurring in the rolling drum devolatilizer constructed by Biesenberger and Lee (1986) to mimic the operation of a single screw devolatilizer. Significant increases in the solution volume during foaming (i.e volume increases greater than about 10%) are not observable from the photographs. Similarly small foam fractions are expected in single and twin screw devolatilizers and these are preferred to batch and falling strand devolatilizers as candidates for preliminary modelling studies.

Experimental data on the performance of the single screw and rolling drum devolatilizers are available in the literature which are documented well enough for use in model evaluation. Acceptable data was not found for the twin screw devolatilizer. Models for the single screw and rolling drum devolatilizers will be constructed according to the proposed methodology.

## CHAPTER IV

### MODEL OF A SINGLE SCREW DEVOLATILIZER

#### 4.1 Geometry and Operation

The single screw devolatilizer is similar to a standard single screw extruder, however, a vacuum port is added to the barrel wall of the DV section through which devolatilized solvent is removed. A common method of operation is starved feed mode, where the feed is metered to the devolatilizer at a flow rate smaller than the flow rate that the extruder would produce if operated with an unrestricted input. Since the mass flow rate into the extruder must be balanced by the flow rate through the extruder, it must operate at reduced capacity, or, partially filled. An alternative to starving the feed to the devolatilizer is to deepen a section of the screw channel (i.e. the DV section), so that the flow rate into the DV section will be insufficient to fill the channel.

A schematic of a cross section of a single screw devolatilizer taken perpendicular to the axis of the screw is shown in Figure 4.1. The screw rotates to convey the fluid through the devolatilizer and fluid is dragged against the screw flight by the barrel wall. This fluid is termed the *bulk film*. Fluid from the bulk film passes through the small clearance between the screw flight and the barrel wall and is laid down as a thin film on the barrel termed the *barrel film*.

A schematic of the channel cross section, taken perpendicular to the down channel direction (i.e. perpendicular to the screw helix) and in the idealized, unwrapped configuration, is shown in Figure 4.2. This simplifies the system's geometry by removing the small curvature in the bulk film. Although the screw is the rotating component, the problem conceptualization will be clarified by considering the barrel to rotate with the screw fixed. The barrel moves over the channel, as would be perceived by an observer rotating with the screw. The moving barrel induces a free surface cavity flow that circulates the



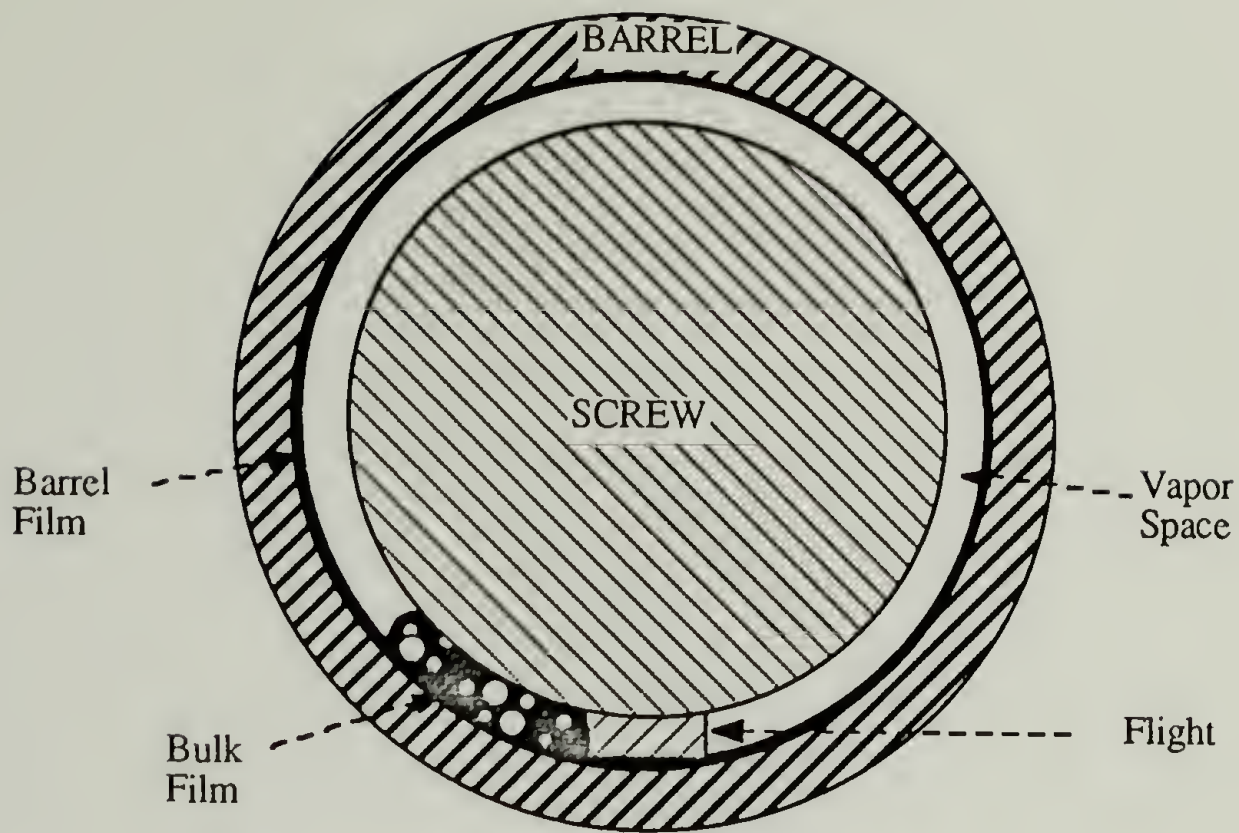


**Figure 4.1** Schematic of the cross section of a single screw devolatilizer.

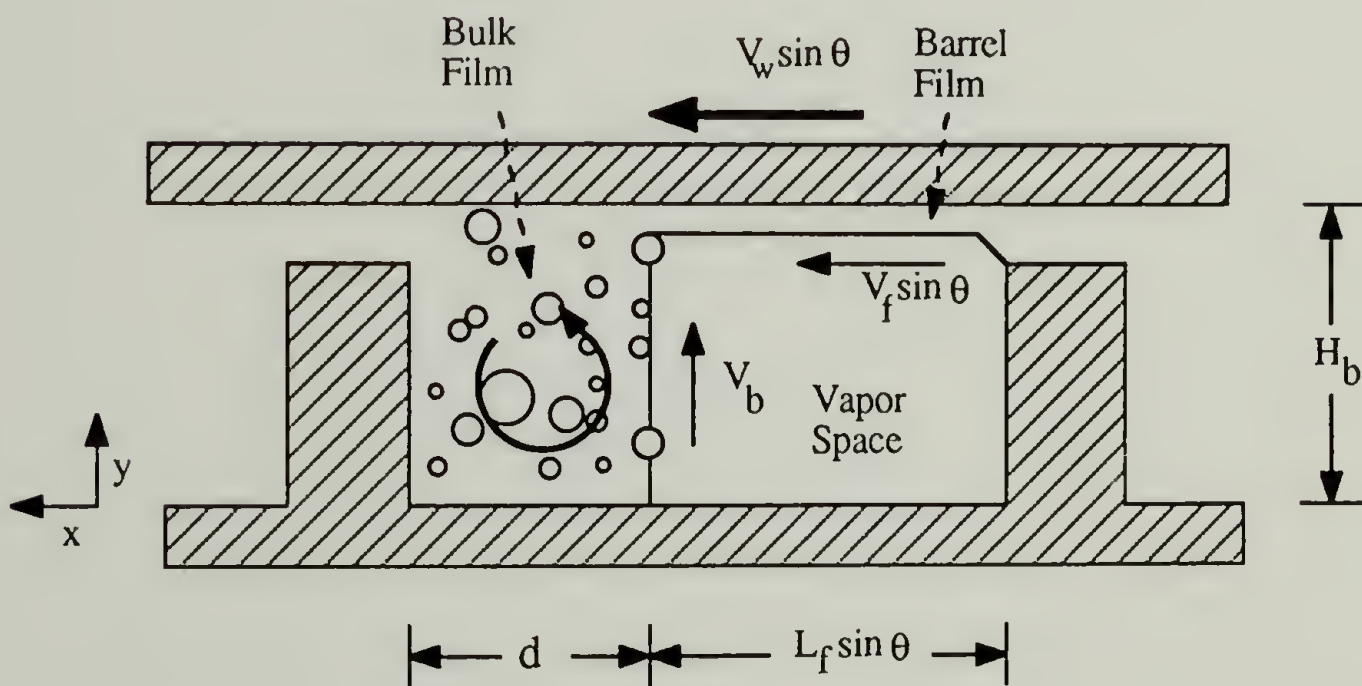


**Figure 4.2** Schematic of the idealized, unwrapped cross section of a single screw devolatilizer.

fluid in the cross section of the bulk film. The helical geometry of the screw channel will be approximated by a straight rectangular channel as shown in Figure 4.3. This rectangular conformation can be viewed as being the result of unwinding the helical channel. In this idealized, unwound configuration, the rotating barrel is perceived as a flat plate dragging diagonally across the top of the channel with a velocity  $V_w$ . The moving barrel's down-channel velocity component,  $[v_w]_z$ , drags the fluid through the screw channel.

Solvent is removed from the bulk and barrel films by diffusion into the vapor phase and by diffusion into bubbles. These bubbles are born, grow, are convected to the melt/vapor interface where they rupture, releasing the solvent into the vapor space.

## 4.2 Bubble Radius and Age Distributions

Since bubbles are born, grow, and die continuously throughout the length of the devolatilizer, a distribution of bubble sizes results. The bubble phase will be described naturally as a distribution,  $g(R)$ , over the bubble radius,  $R$ , where  $g(R)dVdR$  is the number of bubbles in volume  $dV$  between radii  $R$  and  $R + dR$ . An implicit assumption is that the bubbles are spherical. In a stagnant fluid, the bubbles will maintain a spherical shape due to the stabilizing forces of surface tension. However, in a flow field, the hydrodynamic stresses in the fluid can change the bubble shape to ellipsoidal, S-shaped or even needle-like.

For bubbles in a steady shear flow at low bubble Reynolds number (in the single screw devolatilizer at typical operating conditions, the Reynolds number was estimated to be less than 0.01), the bubble deformation is governed by two dimensionless quantities, the viscosity ratio of the fluids,  $\lambda$ , and the capillary number,  $Ca$ , defined as

$$\lambda = \frac{\mu_B}{\mu_F} \quad C_a = \frac{\mu_F G R}{\sigma}$$

$\mu_B$  and  $\mu_F$  are the viscosities of the bubble vapor and surrounding fluid,  $G$  is the shear rate in the fluid far from the bubble and  $\sigma$  is the surface tension. For gas/polymer systems,

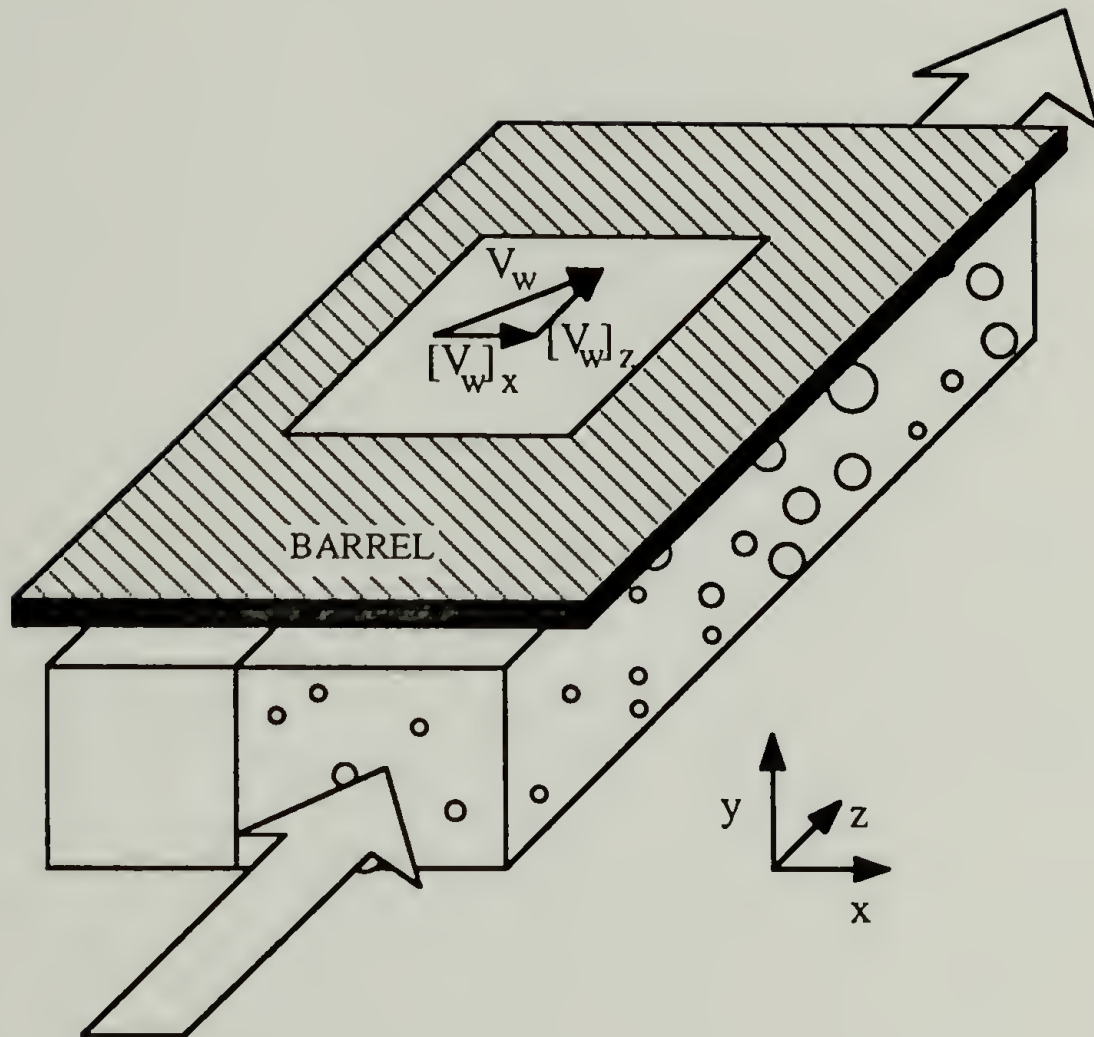


**Figure 4.3** Schematic of the unwound single screw devolatilizer channel.

$\lambda \ll 1$  and the deformation is governed solely by  $Ca$ . If  $Ca \ll 1$ , bubble deformation is negligible. If  $Ca \geq O(1)$ , bubble deformation is significant (Rallison, 1984). For polymer solutions in single screw devolatilizers,  $Ca$  can be of order 1 and greater at typical operating conditions. So bubble deformation could occur. Indeed, bubble deformation was observed by Biesenberger and Lee (1986) in their visualization studies of free surface cavity flows which are similar to the flows occurring in the single screw devolatilizer. At present, there are no means for quantifying the extent of elongation of bubbles in the complex, nonhomogeneous flows occurring in the single screw devolatilizer. For this preliminary model, bubble deformation will be neglected and all bubbles will be assumed to be spherical.

In addition to the bubble's radius, a second variable of interest is the bubble's age,  $\tau$ .  $\tau$  is defined as the time a bubble has spent in the solution measured from the time of *birth*. Birth is any process by which bubbles enter the solution. The age of a bubble can be related to its radius by the bubble growth rate,  $dR/d\tau$ . Integration of the bubble growth rate over the bubble's age gives a one-to-one mapping between radius and age. We will define the bubble age distribution,  $f(\tau)$ , such that  $f(\tau)dVd\tau$  is the number of bubbles in volume  $dV$  between ages  $\tau$  and  $\tau + d\tau$ . If the bubble's growth rate history is specified, either the radius distribution or the age distribution is sufficient to characterize the bubble phase.

A prerequisite that there exist a one-to-one mapping between the bubble's age and radius is that all bubbles be born with the same radius. However, new bubbles can be born by coalescence and breakage which results in differing bubble sizes at birth. If coalescence and breakage occur, the bubble age and radius are no longer related by a one-to-one mapping. That is, two bubbles of equal age could have different radii. One obvious instance is when, at some time  $t$ , one bubble is born by coalescence with a nonzero radius and another is born by nucleation at a zero radius. At time  $t$ , both bubbles would be the same age ( $\tau = 0$ ), but they would be different sizes. If coalescence and breakage occurs, a

bivariate distribution over both bubble age and radius would be required to describe the bubble phase uniquely.

Studies of the frequency of coalescence of bubbles in single screw devolatilizers are not available in the literature. However, Alabak, Tadmor and Talmon (1987) have studied coalescence in falling strand devolatilizers. They characterized the structure of the foamed strands by freezing them *in situ*, fracturing them and examining the bubble morphology using scanning electron microscopy. Alabak et al. observed that small bubbles on the order of 10 to 15  $\mu\text{m}$  in diameter surround larger bubbles on the order of 100  $\mu\text{m}$  in diameter. Blisters were also noticed on the surface of the macrobubbles which Alabak et al. postulate are the remnants of microbubbles that have coalesced with the larger macrobubbles. This study indicates that the surfaces of the macrobubbles may act as sites for microbubble birth. It is proposed that these microbubbles grow until the films separating the bubbles break and coalescence occurs.

The coalescence behavior of bubbles in single screw devolatilizers is probably quite different from that observed in falling strand devolatilizers. Bubbles in single screw devolatilizers move in free surface cavity flows which exhibit shear and extensional character. This could affect the formation of the small satellite bubbles at the surface of macrobubbles as well as their coalescence. Also, the volume fraction of bubbles in single screw devolatilizers is much smaller than the volume fractions in strand devolatilizers. We believe this is due to the free surface cavity flow in screw devolatilizers which increases the bubble rupture rate. The frequency of coalescence will probably be reduced for these smaller volume fractions. Biesenberger and Lee (1986) observed bubble coalescence during visualization experiments of DV from free surface cavity flows. However, the frequency of coalescence wasn't measured and its effect on DV performance is not known. As inclusion in the model would introduce significant complexities, coalescence will be neglected in this preliminary study.

Bubble breakage can occur when the flow strength, or similarly, the capillary number, is increased to a critical level beyond which the restoring force of interfacial tension is insufficient to balance the deforming forces of the flow. For bubbles deforming in a steady shear flow, Hinch and Acrivos (1980) predict that for  $Ca$  greater than  $(Ca)_{critical} = 0.054 \lambda^{-2/3}$ , breakage occurs. This expression is not strictly applicable to flow in single screw extruders, as these flows are nonhomogeneous and exhibit extensional as well as shear character. However, it is suitable as a rough indicator of the likelihood of bubble breakage if the characteristic shear rate of the devolatilizer is used in the expression for  $Ca$ . The characteristic shear rate is defined as the ratio of the barrel velocity to the channel depth.  $Ca$  was estimated for 1 mm-sized styrene bubbles in polystyrene over the range of characteristic shear rates encountered in typical single screw devolatilizers. In all cases,  $(Ca)_{critical}$  was greater than  $Ca$ . Since the diameters of most bubbles in the single screw devolatilizer are expected to be less than 1 mm, bubble breakage is not expected and will be neglected in this study.

### 4.3 Mass Balance

To develop a tractable model of devolatilization, it is necessary to introduce some simplifying assumptions. The bulk film will be assumed to travel in plug flow with the volumetric flow rate,  $\dot{V}$ . The validity of the plug flow assumption may be determined from residence time distribution (RTD) studies on single screw extruders. RTD's quantify the extent of axial dispersion in extruders. Experimental measurements of the RTD of the flow in a single screw extruder were made by Bigg and Middleman (1974) and Wolf and White (1976). They determined that 60-70% of the fluid travels in plug flow and exits the extruder at 75% of the mean residence time. 80% of the material elutes by the mean residence time. For preliminary models, the plug flow assumption is a reasonable first approximation.

The circulatory flow in the bulk film will be assumed to provide sufficient mixing so that the concentration of solvent and the bubble distribution does not vary with position in the cross section. The concentration and the bubble distribution therefore vary only in the down channel direction,  $z$ . The bubble age distribution,  $f$ , is only a function of  $z$  and is redefined such that  $f(\tau, z)d\tau dz$  is the number of bubbles between ages  $\tau$  to  $\tau + d\tau$  and between axial positions  $z$  to  $z + dz$ .

Using these simplifying assumptions, a mass balance on the solvent may be written about a differential volume element  $dz$ , shown in Figure 4.4. As the solution traverses the element  $dz$ , the average solvent concentration in the continuous phase is reduced by diffusion of the solvent from the continuous phase to the bubble phase and to the vapor space. A mass balance on the solvent equates the rate of solvent removal from the continuous phase to the rate of solvent uptake by the bubble phase and by the vapor space. This mass balance may be expressed as

$$\dot{V} \frac{dC}{dz} = - \int_0^{\infty} \underbrace{\frac{d}{dt} \left( \frac{4}{3} \pi R^3 \rho_g \right)}_{\text{Bubble Growth}} f d\tau - \int_0^{\infty} \underbrace{\rho_g \left( \frac{4}{3} \pi R_0^3 \right)}_{\text{Bubble Birth}} B d\tau$$

$$- 2 \underbrace{\left( \frac{DV_b H_b}{\pi} \right)^{1/2}}_{\text{Bulk Film Diffusion}} \Delta C - 2 \sin\theta \underbrace{\left( \frac{DV_f L_f}{\pi} \right)^{1/2}}_{\text{Barrel Film Diffusion}} \Delta C \quad 4.1$$

where  $C$  is the average concentration of solvent in the continuous phase. The terms on the right hand side quantify the rates of solvent loss by bubble growth, bubble birth, bulk film diffusion and barrel film diffusion. These are discussed next.

#### 4.3.1 Mass Transfer to Bubbles

In the Bubble Growth term,  $\rho_g$  is the density of the solvent vapor in the bubble. The mass transfer rate to a single bubble of age  $\tau$  (given by the time derivative of the total

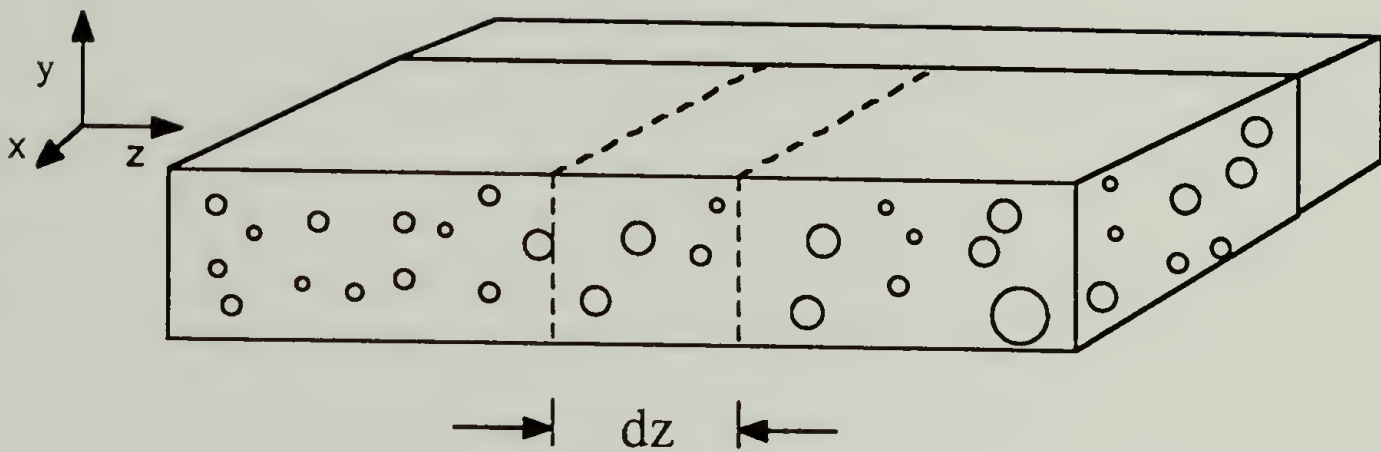


**Figure 4.4** Schematic of the unwound single screw devolatilizer channel showing the differential volume element over which the mass balance is made.



bubble mass), or similarly, radius  $R(\tau)$ , is multiplied by the number of bubbles of radius  $R$  (i.e.  $f$ ) and integrated over all bubble ages to account for the contribution to DV of bubbles of all ages. Note that the bubble radius distribution could have been used in place of the age distribution. However, the age distribution was chosen for convenience because the bubble growth rate is most naturally expressed in terms of the bubble's age rather than its radius.

Bubble birth must be accounted for in the mass balance, since upon birth solvent is transferred from the continuous phase to the bubble nuclei.  $B$  is the rate of birth, defined as the number of bubbles born per distance per time. All bubbles are assumed to be born at a radius  $R_0$ . Studies by C.D. Han (1987) on the birth of bubbles in polymer/solvent solutions indicate that values for  $R_0$  in polymer solutions are on the order of 0.1 microns. Since most bubbles grow to hundreds of times  $R_0$ , the magnitude of the bubble birth term is negligible compared to that of the bubble growth term. The bubble birth term will be neglected in further analysis.

#### 4.3.2 Mass Transfer by Interfacial Diffusion

**4.3.2.1 Models of Latinen.** The Bulk Film Diffusion term was derived from the model by Latinen (1962). Latinen modelled mass transfer from the surface of the bulk film using *penetration theory* combined with a *surface renewal* description for the flow field. Penetration theory treats the diffusion as occurring in an infinite medium. The small penetration depth of the diffusion field as compared with the film thickness, a result of the low diffusivity of polymer/solvent systems, validates the infinite film assumption. Surface renewal is the process by which material elements travel in the flow field to the interface, where the element's solvent concentration is reduced by diffusion into the vapor phase. The fluid elements are circulated back into the bulk of the fluid where they are refreshed by absorbing more solvent and this cycle is repeated.

Latinen assumed that fluid elements enter the interface along the root of the screw (see Figure 4.2) with a concentration,  $C$ , the average concentration in the cross section. The surface concentration was assumed to drop instantaneously to that in equilibrium with the vapor phase,  $C_e$ . The fluid elements were assumed to travel with a constant velocity  $V_b$  along the surface. Latinen assumed  $V_b$  to be equal to the component of the barrel wall velocity normal to the interface,  $V_w \sin \theta$ . In our analysis,  $V_b$  was taken to be  $(2/\pi)V_w \sin \theta$ , the value predicted by Moffatt (1964) to be the velocity of a free surface perpendicular to the moving wall of an infinitely deep cavity. As the material elements move along the surface, the concentration of solvent is reduced by diffusion of solvent into the vapor phase. After travelling a distance  $H_b$ , the fluid elements reach the moving barrel surface and are reintroduced into the interior of the bulk film. Integration of the local mass flux, described using penetration theory, over the interface gives the total mass transfer rate used in deriving the Bulk Film Diffusion term.

The Barrel Film Diffusion term was also derived from the model developed by Latinen (1962). Fluid travels through the gap between the screw flight and the barrel wall and is laid down as a thin film on the barrel (see Figure 4.2). Latinen assumed the concentration of solvent in the fluid exiting the gap to be equal to the average concentration of the bulk film,  $C$ , and the surface concentration was assumed to drop instantaneously to that in equilibrium with the vapor phase,  $C_e$ . As the fluid travels in a rigid body motion with the velocity of the barrel,  $V_w$ , the concentration is reduced by diffusion into the vapor phase. After travelling a distance  $L_f$ , the fluid reaches the convergence point of the bulk and barrel film and is reintroduced into the interior of the bulk film. The term  $\sin(\theta)$ , where  $\theta$  is the screw helix angle, is included in the expression due to the requirement that the components of the barrel velocity and barrel film length perpendicular to the interface be used in the derivation. The expression for the barrel film diffusion term was derived by integrating the local mass flux, described using penetration theory, over the interface.

#### 4.3.2.2 Contribution of Surface Stretching to Interfacial Diffusion.

Latinen modelled the kinematics of the flow of fluid at the surface of the bulk film as a rigid body motion with a constant velocity. By analogy with Moffat's (1964) analysis of free surface cavity flows of Newtonian fluids in infinitely deep channels, the fluid at the free surface of the single screw devolatilizer is expected to accelerate from a zero velocity at the surface of the screw to a maximum value at the moving wall. The fluid elements at the surface will stretch as they translate and Latinen's assumption of a constant velocity, rigid body flow is unrealistic.

Canedo (1985) investigated free surface flows of Newtonian fluids in driven cavities of finite depth. He estimated the kinematics of the flow from numerical simulations assuming a flat liquid/vapor interface. Canedo's prediction of the interfacial kinematics for deep channels (i.e. channels with large aspect ratios, single screw extruder channels are deep) agrees closely with the prediction by Moffat over most of the interface. However, near the moving wall, the solutions diverge. Moffat's solution exhibits a discontinuity at the wall where the tangential velocity drops to zero. For Canedo's solution, the tangential velocity approaches zero continuously.

Canedo (1985) also modelled the mass transfer from the free surface of a solution undergoing devolatilization in the driven cavity. Like Latinen (1962), he used penetration theory to model the mass flux assuming the fluid elements move in a rigid body motion along the surface. However, rather than assuming that these rigid fluid elements move with a constant velocity, Canedo allowed the surface elements to accelerate with velocities estimated from his simulations. Comparison of mass transfer rates of carbon dioxide in glycerol diffusing through the free surface of a driven cavity flow predicted by his model with experimental measurements taken by Canedo (1985) reveal that his model underestimates the mass transfer rates by an order of magnitude. A likely explanation for this discrepancy is that Canedo neglects surface stretching which enhances mass transfer.

To estimate the contribution of surface stretching to mass transfer from free surface cavity flows, we have modelled the mass transfer from the surface assuming the fluid elements moving along the surface undergo a simple one dimensional elongational flow with a constant stretch rate,  $dV_y/dy = (2/\pi)V_w/H_b$ . This results in the linear velocity profile  $V_y = (2/\pi)V_w(y/H_b)$ . For infinitely deep cavities with flat interfaces, Moffat's (1964) analytical expression for the velocity of the surface can be satisfactorily approximated by this linear velocity profile. Although single screw extruder channels are not infinitely deep, Canedo's simulation for deep channels agrees closely with the solution of Moffat over approximately 90% of the surface. We expect that the presumed linear velocity profile should give better than an order of magnitude estimate of the contribution of stretching to the mass transfer rate in the single screw devolatilizer.

Following the methodology of Latinen, the mass flux from the surface of the fluid was estimated as a function of distance along the surface. However, the mass transfer rate was not estimated assuming the free surface moves in a rigid body motion, but rather the surface elements were assumed to stretch at a constant rate. This local mass flux was integrated over the length of the free surface to give the mass transfer rate in the cross section. The resulting expression is identical to the expression derived by Latinen to within a factor of  $2/\pi^{1/2}$ . This agreement is remarkable considering Latinen neglects surface stretching in his derivation.

This fortuitous agreement can be explained as being the result of a cancellation of two errors which are introduced by Latinen's assumption of a constant surface velocity: (1) the surface residence time of a fluid element is underestimated resulting in a higher average interfacial concentration gradient of solvent; this overestimates the mass transfer rate and (2) stretching is neglected which underestimates the mass transfer rate. So Latinen's model should give an adequate estimate of the interfacial mass transfer rate despite its unrealistic description of the kinematics of the fluid surface.

### 4.3.3 Bubble Growth Rate

Inspection of the mass balance reveals that, for it to be solved, the bubble radius,  $R$ , must be specified as a function of its age,  $\tau$ . Or, equivalently, the growth rate of the bubbles must be specified. Unfortunately, there are no explicit expressions describing the growth rate of bubbles translating in a free surface cavity flow. Since an explicit expression for the growth rate is desired in this preliminary model, approximations must be made.

To derive a tractable, closed form growth rate expression, the following simplifying approximations will be made:

- (i) the bubbles remain spherical.
- (ii) the bubbles grow in a quiescent fluid.
- (iii) the bubbles do not interact with neighboring bubbles.
- (iv) the growth is diffusion-controlled.
- (v) the fluid is an isothermal, binary solution

The bubbles may deform from their spherical geometry in the shear and elongational flows of the bulk film. However, as a first approximation, a spherical shape will be assumed. Although an applied flow could enhance the mass transfer to bubbles, and hence the growth rate, bubbles will be assumed to grow in a stagnant fluid. An analysis by Acrivos (1971) of the related problem of mass transfer to rigid spheres in simple shear flows indicates that a boundary layer may form around the bubble which will approach a limiting thickness with increasing shear rate. This would limit the influence of the flow field on the bubble growth rate. The effect of flow on the bubble growth rate is discussed further in Appendix B.

The presence of neighboring bubbles could reduce the growth rate if the bubbles are close enough so that the diffusion fields overlap. We can not say *a priori* whether this will occur, as it depends on the number of bubbles per volume and on the width of the diffusion boundary layers. The effect of bubble interaction on the bubble growth will be neglected.

The diffusion-controlled growth assumption is argued in Appendix B to be reasonable for bubble growth in a stagnant polymer/solvent solution. Whether it is applicable to bubbles translating in a free surface cavity flow is not clear. The temperature of the fluid, which can decrease due to the latent heat of vaporization of the solvent, is assumed to remain constant. For the devolatilization of low solvent concentration solutions, which is the focus of this study (the polymer/solvent solutions in all experiments studied contained less than 1% by mass of solvent), this is a good assumption.

In his classic paper on phase growth, Scriven (1959) derived an implicit growth rate expression for diffusion-controlled growth of a single bubble in an infinite, quiescent fluid. From Scriven's expression, Szekely and Martin (1971) developed the following simplified, explicit approximation, valid for high supersaturations (i.e.  $10 < \Delta C/\rho_g < 1000$ ; in the experiments of Coughlin and Canevari (1969),  $\Delta C/\rho_g \approx 300$ )

$$R = R_0 + \sqrt{\frac{12D}{\pi}} \left( \frac{\Delta C}{\rho_g} \right) \tau^{1/2} \quad 4.2$$

where  $\Delta C$  is the supersaturation,  $C - C_e$ , and  $C_e$  is the concentration of solvent in the liquid at the bubble surface in equilibrium with the bubble vapor,  $R_0$  is the bubble radius at birth and  $D$  is the polymer/solvent diffusivity. This expression will be used to describe the bubble growth rate.

#### 4.4 Population Balance

To solve the mass balance, the bubble age distribution must be known as a function of distance through the devolatilizer,  $z$ . A population balance on the bubble distribution is proposed to track the distribution through the devolatilizer. Following Hulburt and Katz' (1964) formulation, the general balance equation on a bivariate distribution  $f(\tau, z)$  is

$$\frac{\partial f}{\partial t} + \frac{\partial}{\partial \tau} \left[ \left( \frac{\partial \tau}{\partial t} \right) f \right] + \frac{\partial}{\partial z} \left[ \left( \frac{\partial z}{\partial t} \right) f \right] = B - E \quad 4.3$$

where,  $Bd\tau dz$  is the rate of birth of bubbles between ages  $\tau$  to  $\tau + d\tau$  and between positions  $z$  to  $z + dz$  and  $E d\tau dz$  is the rate of extinction, or death, of bubbles between ages  $\tau$  and  $\tau + d\tau$  and between positions  $z$  to  $z + dz$ . The convection terms are simply

$$\left(\frac{\partial \tau}{\partial t}\right) = 1 \quad \left(\frac{\partial z}{\partial t}\right) = V_z$$

where  $V_z$  is the average velocity of the solution in the down channel direction. Introducing the expressions for the convection terms into the population balance yields

$$\frac{\partial f}{\partial \tau} + V_z \left(\frac{\partial f}{\partial z}\right) = B - E \quad 4.4$$

where steady state conditions have been introduced removing the time derivative of  $f$ . It remains to derive expressions for the bubble birth and death rates.

#### 4.4.1 Bubble Birth Rate

The mechanism of bubble birth in single screw devolatilizers is not known. Bubble birth may occur by homogeneous or heterogeneous nucleation according to the postulates of classical nucleation theory. Biesenberger and Lee (1986) have proposed that birth may occur by growth and pinch-off of bubbles from stable gas pockets adhering to the surfaces of equipment walls or to the surfaces of entrained particles. Entrainment of bubbles at the dynamic liquid-gas-solid contact line due to agitation from the rotating screw has also been suggested as a possible birth mechanism (Canedo, 1985). Finally, bubble coalescence and breakup can result in the birth of new bubbles. A brief discussion of past investigations into bubble birth in polymer solutions by these mechanisms follows and the likelihood of bubble birth by these mechanisms during DV is discussed.

The homogeneous nucleation rate in styrene/polystyrene solutions was estimated by Lee and Biesenberger (1987) using an expression derived by Blander and Katz (1975) from classical nucleation theory. The homogeneous nucleation rate is negligible for solvent mass fractions less than 0.5% and at temperatures less than 325 °C. As a result, bubble

birth in devolatilizers by homogeneous nucleation is not expected to contribute significantly to the total bubble birth rate. Biesenberger and Lee also estimated the frequency of classical heterogeneous nucleation for the same solution and conditions in conical cavities. This was also negligible and heterogeneous nucleation is not likely to occur in these cavities. Hoque (1986) used classical nucleation theory to correlate the onset of nucleation measured experimentally in pentane/polyisobutylene solutions flowing between two, partially-submerged rotating rollers. The surface tension was used to correlate the nucleation onset data. The value estimated for the surface tension was more than an order of magnitude smaller than the measured value given by Gaines (1972). This indicates that the bubble birth was more rapid than would be predicted by homogeneous nucleation theory and may have occurred either heterogeneously or by some other mechanism. Prud'homme, Gregory, and Andres (1985) measured the temperature of onset of homogeneous nucleation in benzene/polystyrene solutions at polymer concentrations between 0 and 60%. Nucleation was observed to occur at or near the nucleation onset temperature predicted by the theory of classical homogeneous nucleation.

The mechanism of bubble birth from stable gas pockets was proposed by Lee and Biesenberger (1987) to explain the strong dependence of the birth rate on the shear rate. This is discussed further in Appendix C. This birth mechanism has been observed to occur by Darby (1964) and is feasible. Entrainment of bubbles at the dynamic contact line was not observed at reduced pressure by Biesenberger and Lee (1986) in their apparatus designed to simulate single screw extruder operation and its occurrence is unlikely. For the same reasons discussed earlier, coalescence and breakage will also be neglected as mechanisms of bubble birth.

The experiments of Biesenberger and Lee (1986) and Hoque (1986) on the onset of bubble birth in devolatilizers reveal that a finite superpressure must be exceeded before rapid birth occurs. Since this behavior is predicted by classical nucleation theory, the



expression of bubble birth to be incorporated in our model will be based on classical nucleation theory.

Blander and Katz (1975) derived the following expression for the classical nucleation rate,  $J$ , in pure fluids.

$$J = \left[ \frac{\text{\# of bubbles born}}{\text{time volume}} \right] = N \left[ \frac{2 \sigma}{\pi m Q} \right]^{1/2} \exp \left[ \frac{-16 \pi \sigma^3 S}{3 k T (P_v - P_l)^2} \right] \quad 4.5$$

where  $N$  is the number density of molecules,  $\sigma$  is the surface tension,  $m$  is the mass of a solvent molecule,  $Q$  is approximately equal to  $(1 - 1/3(1 - P_l/P_v))$ ,  $S$  is the fractional reduction in the free energy required to form a nucleus due to the presence of a heterogeneous surface,  $k$  is Boltzmann's constant,  $T$  is temperature in Kelvin,  $P_v$  is the vapor pressure of the solution and  $P_l$  is the local fluid pressure.  $P_v - P_l$  is the thermodynamic driving force for nucleation and is termed the *superpressure*.

An empirical expression analogous to equation 4.5 will be adopted for the bubble nucleation rate which retains the same functional dependence of the nucleation rate on temperature and superpressure.

$$J = F \exp \left[ \frac{-E_a}{T (P_v - P_l)^2} \right] \quad 4.6$$

Two empirical model parameters,  $F$  and  $E_a$ , have been introduced which describe the nucleation rate. If the analogy with classical nucleation theory is valid,  $F$  is a measure of the number of nucleation sites in the fluid and  $E_a$  is a measure of the free energy barrier to nucleation (although it does not have units of energy!).  $F$  is expected to increase with increasing concentration of heterogeneous impurities in the system which can act as nucleation sites.  $F$  might also increase with increasing shear rate, as indicated by the studies of Biesenberger and Lee (1986) and Hoque (1986). This is discussed further in Appendix C.  $E_a$  is a thermodynamic parameter and is expected to depend on the temperature, pressure and composition of the solvent/polymer solution. However, it is not

expected to vary with the operating variables, unless these affect the energetics of the formation of bubble nuclei.

The effect of  $E_a$  on the dimensionless nucleation rate,  $J/F$ , calculated from equation 4.6, is shown in Figure 4.5.  $J/F$  is plotted versus superpressure for values of  $E_a$  between  $10^3$  and  $10^6$  psi<sup>2</sup> K and for  $T = 220$  °C. As observed experimentally, all curves show a critical superpressure that must be exceeded before appreciable nucleation occurs. As  $E_a$  increases, the critical superpressure required for nucleation increases and the nucleation onset is less abrupt.

The birth rate,  $B$ , is derived from  $J$  by

$$B = A_c J \delta(\tau) = A_c F \exp\left(\frac{-E_a}{T K_c^2 \Delta C^2}\right) \delta(\tau) \quad 4.7$$

where  $A_c$  is the cross sectional area of the continuous phase, or equivalently, the cross sectional area before foaming. Assuming Henry's law applies, the superpressure has been replaced by the product of the supersaturation and the Henry's Law constant,  $K_c$ .  $\delta(\tau)$  is the Dirac-Delta function and requires that all bubbles be born at age  $\tau = 0$ .

#### 4.4.2 Bubble Death Rate

Bubble death can occur by rupture at the surface of the bulk film. In their experiments on the rolling drum devolatilizer, Biesenberger and Lee (1986) observed surface rupture by two distinct mechanisms: *film draining* and *mechanical shearing*. Rupture by film draining occurs when the fluid film surrounding surface bubbles drains into the bulk of the fluid due to capillary forces. A critical film thickness is reached on the order of 500 angstroms when London-van der Waal forces amplify surface perturbations causing the film to rupture. Rupture by film draining is discussed in more detail in Appendix B. Rupture by mechanical shearing occurs at the convergence point of the bulk and barrel films (see Figure 4.2). Bubbles are driven to the convergence point by the moving fluid surface. The shearing of the bubble by the converging films causes their

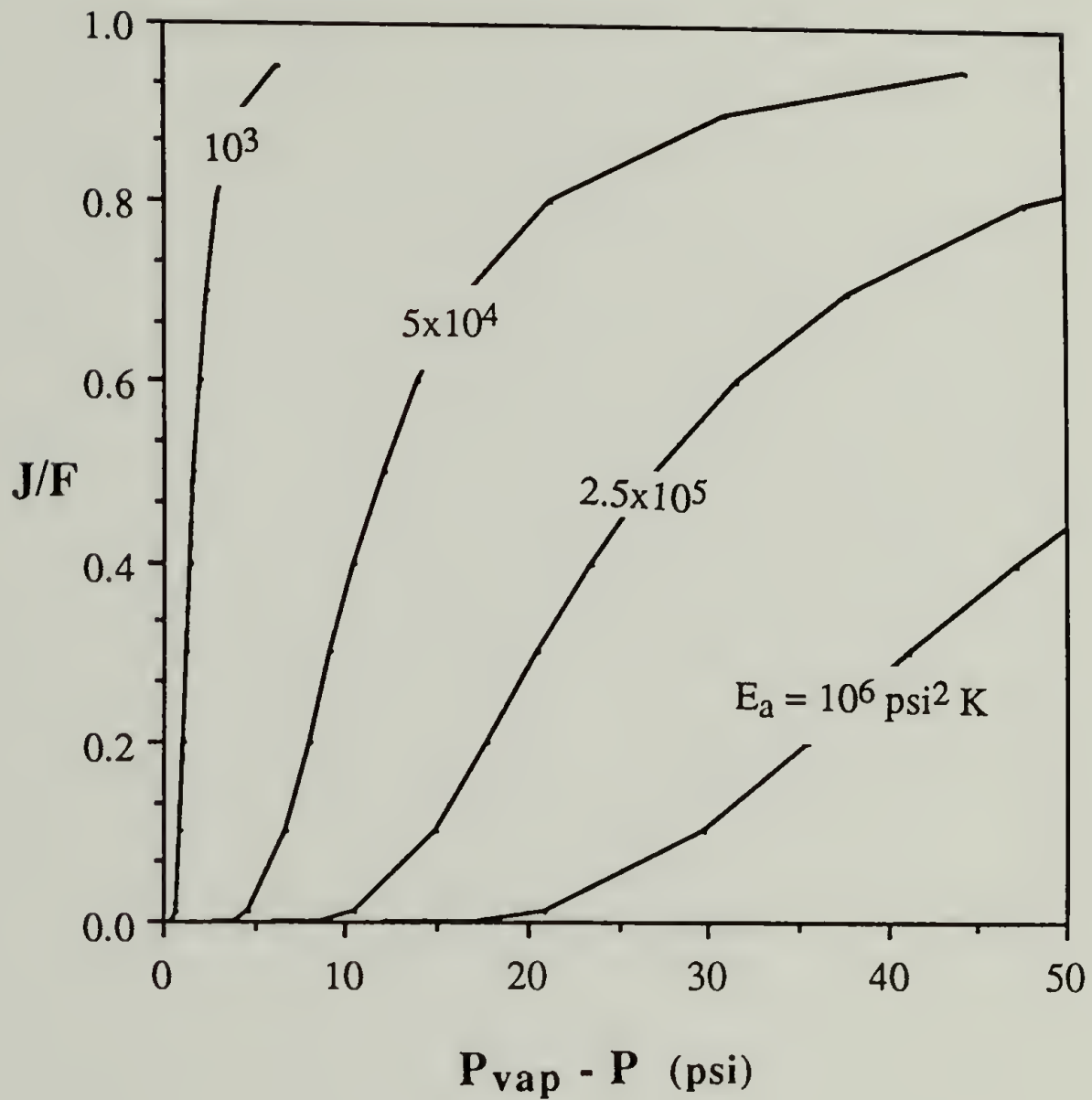


**Figure 4.5** Plots of reduced nucleation rate versus superpressure calculated from the empirical nucleation rate expression for  $T = 220 \text{ }^\circ\text{C}$ .

rupture. Since the rolling drum devolatilizer simulates the operation of a single screw devolatilizer, bubble rupture by both mechanisms is expected to occur in the single screw devolatilizer. Bubble death might also occur by coalescence and breakage. However, as discussed previously, coalescence and breakage will be neglected in the bubble death model.

There have been many studies of the film draining rupture of bubbles driven to the surface of a Newtonian fluid by buoyancy. A few of these are discussed in Appendix B. These are not directly applicable to DV, however, as the buoyancy forces a bubble experiences in a flowing, viscous polymer solutions are negligible compared to the viscous and elastic forces which arise. From the studies by Moffat (1964) and Canedo (1985) on the kinematics of free surface cavity flows, bubbles at the surface of the bulk film in the single screw extruder are expected to undergo mostly extensional flow. There have been no studies on the rate of bubble rupture by film draining at the surface of a polymer/solvent solution undergoing extensional flow. However, in a related problem, Hoffman (1985) modelled the protrusion of a rigid sphere through the surface of a fluid undergoing extensional flow. His analysis predicts that the sphere reaches an equilibrium height when the drag forces on the bubble, which drive the sphere towards the interface, are just balanced by the repelling surface tension forces. For this preliminary model, only rupture by mechanical shearing will be included. We will neglect rupture by the poorly understood mechanism of film draining. However, an empirical film draining rupture model is developed in Appendix B and will be included in a later model in Chapter 7.

The death rate expression for bubble rupture by mechanical shearing is derived in Appendix B. In this derivation, the surface bubbles are assumed to translate along the free surface of the bulk film with a constant interfacial velocity,  $V_b$ . The value of  $V_b$  was taken to be  $(2/\pi)V_w$ , the surface velocity predicted by Moffat (1964) to occur in infinitely deep channels as discussed in section 4.3. All bubbles occupying the surface of the bulk film were assumed to rupture upon reaching the convergence point of the bulk film and barrel

film (see Figure 4.2). Rupture of bubbles in the barrel film was not accounted for as Biesenberger and Lee (1986) observed that no bubbles were present in the barrel film of their rolling drum devolatilizer. The surface density of bubbles was calculated assuming the bubbles are distributed homogeneously in the cross section. The death rate expression derived in Appendix B using these assumptions is

$$E = \frac{2 V_b}{A_c} \left[ R_0 + 2 \left( \frac{3D}{\pi} \right)^{1/2} \left( \frac{\Delta C}{\rho_g} \right) \tau^{1/2} \right] f \quad 4.8$$

The death rate of bubbles is predicted to increase with the velocity of the bulk film surface,  $V_b$  (which is proportional to the screw rotation rate), since more bubbles will enter the convergence point per time. Older (or, equivalently, larger) bubbles are predicted to rupture more frequently than smaller bubbles as larger bubbles are more likely to occupy the surface simply because they occupy more space. Also, an increase in the number density of bubbles,  $f$ , which is a measure of the number of bubbles in the cross section, is predicted to increase the rupture rate.

#### 4.5 Model Equations

Introducing the expressions for the bubble birth, growth and death rates into the mass balance and population balance gives the model equations

$$\begin{aligned} \frac{d\Delta C}{dz} = & - \left( 48 \sqrt{\frac{3}{\pi}} \right) \left( \frac{D^{3/2}}{V_z A_c \rho_g^2} \right) \Delta C^3 \mu_{1/2} \\ & - \left( \frac{2}{\sqrt{\pi}} \right) \left( \frac{D^{1/2}}{V_z A_c} \right) [(V_b H_b)^{1/2} + \sin\theta (V_f L_f)^{1/2}] \Delta C \end{aligned} \quad (4.9 \text{ a})$$

$$\frac{\partial f}{\partial \tau} + V_z \frac{\partial f}{\partial z} = - \left( 4 \sqrt{\frac{3}{\pi}} \right) \left( \frac{D^{1/2} V_b}{A_c \rho_g} \right) \Delta C \tau^{1/2} f \quad (4.9 \text{ b})$$

$$\begin{aligned} \text{B.C.'s} & \\ \text{at } z=0; & \begin{cases} \Delta C = C_o - C_e \\ f(\tau, 0) = 0 \end{cases} \\ \text{at } \tau=0; & f(0, z) = F A_c \exp\left[\frac{-E_a}{T K_c^2 \Delta C^2}\right] \end{aligned}$$

where  $\mu_n$ , the n'th moment of the bubble age distribution, is defined as

$$\mu_n = \int_0^{\infty} \tau^n f d\tau$$

The supersaturation of the solution fed to the devolatilizer (i.e. at  $z = 0$ ) is  $C_o - C_e$ , where  $C_o$  is the concentration of solvent in the feed. We have assumed that the feed does not contain bubbles (i.e.  $f = 0$  at  $z = 0$ ).

To nondimensionalize the equations, the dimensionless variables

$$Y = \frac{\Delta C}{\Delta C^*}; \quad \Psi = \frac{f}{f^*}; \quad T = \frac{\tau}{\tau^*}; \quad Z = \frac{z}{z^*}$$

are introduced where the reference scales are defined as

$$\Delta C^* = C_o - C_e = C_{\max}$$

$$f^* = A_c F \exp\left(\frac{-E_a}{T K_c^2 C_{\max}^2}\right)$$

$$\tau^* = \left(\frac{A_c}{V_b}\right)^{2/3} \left(\frac{\rho_g}{C_{\max}}\right)^{2/3} \left(\frac{1}{D}\right)^{1/3}$$

$$z^* = V_z \tau^*$$

The dimensionless model equations are

$$\begin{aligned} \frac{dY}{dZ} = & - \left(48 \sqrt{\frac{3}{\pi}}\right) \alpha_1 M_{1/2} Y^3 \\ & - \left(\frac{2}{\sqrt{\pi}}\right) \left[ \alpha_5 + \alpha_6 \left(1 - \alpha_7 \left(1 + 32 \sqrt{\frac{3}{\pi}} \alpha_1 \alpha_4 Y^3 M_{3/2}\right)\right)^{1/2} \right] Y \end{aligned} \quad 4.10a$$

$$\frac{\partial \Psi}{\partial T} + \frac{\partial \Psi}{\partial Z} = - \left( 4 \sqrt{\frac{3}{\pi}} \right) \frac{1}{\left( 1 + 32 \sqrt{\frac{3}{\pi}} \alpha_1 \alpha_4 Y^3 M_{3/2} \right)} T^{1/2} Y \Psi \quad 4.10b$$

B.C.'s

$$\text{at } Z = 0; \quad \begin{cases} Y = 1 \\ \Psi(T, 0) = 0 \end{cases}$$

$$\text{at } T = 0; \quad \Psi(0, Z) = \exp \left[ \alpha_3 \left( 1 - \frac{1}{Y^2} \right) \right]$$

where the dimensionless n'th moment,  $M_n$ , is defined as

$$M_n = \int_0^\infty T^n \Psi \, dT = \left( \frac{1}{\tau^{*n+1} f^*} \right) \mu_n$$

These equations will be termed the *Complete Model*.

The independent dimensionless model parameters are defined as

$$\alpha_1 = \left( \frac{A_c}{V_b} \right)^{5/3} \left( \frac{C_{\max}}{\rho_g} \right)^{1/3} D^{2/3} F \exp(-\alpha_3)$$

$$\alpha_3 = \left( \frac{1}{T K_c^2 C_{\max}^2} \right) E_a$$

$$\alpha_4 = \left( \frac{C_{\max}}{\rho_g} \right)$$

$$\alpha_5 = \left( \frac{D^{1/6} H_b^{1/2}}{V_b^{1/6} A_c^{1/3}} \right) \left( \frac{\rho_g}{C_{\max}} \right)^{2/3}$$

$$\alpha_6 = \left( \frac{D^{1/6}}{A_c^{1/3} V_b^{2/3}} \right) (\sin \theta V_f w)^{1/2} \left( \frac{\rho_g}{C_{\max}} \right)^{2/3}$$

$$\alpha_7 = \left( \frac{A_c}{H_b w} \right)$$

During foaming, the volume of the bulk film increases due to the addition of bubbles.

Inspection of Figure 4.2 shows that this will increase the depth of the bulk film,  $d$ , and

decrease the length of the barrel film,  $L_f$ . The term in the denominator of the bubble death term in equation 4.10b is the volume expansion ratio,  $V_t/V_c$ ,

$$\frac{V_t}{V_c} = 1 + 32\sqrt{\frac{3}{\pi}} \alpha_1 \alpha_4 Y^3 M_{3/2}$$

and accounts for this effect.  $V_c$  and  $V_t$  are the volumes of the bulk film before and during foaming, respectively ("c" and "t" are mnemonics for "continuous phase volume" and "total volume").  $V_t/V_c$  is equivalent to  $A_t/A_c$ , where  $A_c$  and  $A_t$  are the cross sectional area of the bulk film before and during foaming. As the volume expansion ratio  $V_t/V_c$  increases, the surface area to volume ratio of the film decreases. This decreases the fraction of bubbles that can be located at the surface and, hence, the rupture rate.

Foam expansion introduces significant nonlinearities into the equations which can complicate the models behavior and its solution. However, as discussed in Chapter III, significant volume expansion due to foaming is not observed in typical single screw devolatilizers. As an approximation, the volume expansion will be neglected in the model equations. This is a valuable approximation as it significantly reduces the complexity of the model. It will allow further approximations to be made so that simplified models may be constructed. These simplified models will be shown in Chapter 6 to be valuable for use in devolatilizer design and for providing insight in the DV process which can be obscured by the complexity of the Complete Model.

Setting  $V_t/V_c = 1$ , the model equations reduce to

$$\frac{dY}{dZ} = -\left(48\sqrt{\frac{3}{\pi}}\right) \alpha_1 M_{1/2} Y^3 - \left(\frac{2}{\sqrt{\pi}}\right) \alpha_2 Y \quad 4.11a$$

$$\frac{\partial \Psi}{\partial T} + \frac{\partial \Psi}{\partial Z} = -\left(4\sqrt{\frac{3}{\pi}}\right) T^{1/2} Y \Psi \quad 4.11b$$



$$\text{B.C.'s} \quad \text{at } Z = 0; \quad \begin{cases} Y = 1 \\ \Psi(T, 0) = 0 \end{cases}$$

$$\text{at } T = 0; \quad \Psi(0, Z) = \exp\left[\alpha_3 \left(1 - \frac{1}{Y^2}\right)\right]$$

where a new parameter  $\alpha_2$  is introduced in which are lumped the variables in the parameters  $\alpha_4$  to  $\alpha_7$ .

$$\alpha_2 = \left(\frac{1}{A_c V_b^2}\right)^{1/3} \left(\frac{\rho_g}{\Delta C_{\max}}\right)^{2/3} D^{1/6} [(V_b H_b)^{1/2} + \sin(\theta) (V_f L_f)^{1/2}]$$

The negligible volume expansion assumption removes the nonlinearities in the population balance and reduces the number of model parameters to three. These equations will be referred to as the *Full Model*. In this chapter, the Full Model, rather than the Complete Model, will be used to simulate the performance of the single screw devolatilizer.

It will be useful in later chapters to use the population balance expressed as an infinite set of ODE's in terms of the moments of the distribution. These are derived by multiplying the population balance by  $T^n$  and integrating over  $T$  from 0 to  $\infty$ . The resulting moment equations and initial conditions are

$$\begin{aligned} \frac{dM_0}{dZ} &= \exp\left[\alpha_3 \left(1 - \frac{1}{Y^2}\right)\right] - \left(4\sqrt{\frac{3}{\pi}}\right) Y M_{1/2} \\ \frac{dM_{1/2}}{dZ} &= \left(\frac{1}{2}\right) M_{-1/2} - \left(4\sqrt{\frac{3}{\pi}}\right) Y M_1 \\ \frac{dM_1}{dZ} &= M_0 - \left(4\sqrt{\frac{3}{\pi}}\right) Y M_{3/2} \\ &\bullet \qquad \bullet \qquad \bullet \\ &\bullet \qquad \bullet \qquad \bullet \\ &\bullet \qquad \bullet \qquad \bullet \\ \frac{dM_n}{dZ} &= n M_{n-1} - \left(4\sqrt{\frac{3}{\pi}}\right) Y M_{n+1/2} \end{aligned} \tag{4.12}$$

I.C.'s at  $Z = 0$ ;  $M_j = 0$ , ( $j = -1/2, 0, 1/2, \dots, n+1/2$ )

Note that the moment equations are not closed. To solve for the moments between 0 and  $n$ , information on the  $-1/2$  and  $n+1/2$  moments is required.

#### 4.6 Model Solution

The model equations consist of the mass balance, an ordinary differential equation, coupled to the population balance, a first order partial differential equation. The population balance was simplified to the ordinary differential equation

$$\frac{d\Psi}{dZ} = -\left(4\sqrt{\frac{3}{\pi}}\right) T^{1/2} Y \Psi \quad \text{along } Z = T + c \quad 4.13$$

where the derivative is taken in the direction along the characteristics of the PDE. The characteristics, shown in Figure 4.6, are defined by  $Z = T + c$ , where  $c$  is an arbitrary constant.

Equations 4.11a and 4.13 were solved numerically by the method of lines using the DGEAR IMSL integration algorithm (Gear, 1971). The solution procedure was to integrate  $Y$  along  $Z$  and  $\Psi$  along the characteristics. At each step in the integration, the  $1/2$  moment of the distribution was determined by numerical integration of the discrete values of  $\Psi$  which have been estimated along the characteristics. Characteristics were added at intervals along  $Z$ ,  $\Delta Z$ . The value of  $\Psi$  for each newly added characteristic (i.e. at  $T = 0$ ) is specified by the boundary condition for  $\Psi$  at  $T = 0$ . The solution accuracy increases as more characteristics are added, or equivalently, as  $\Delta Z$  is decreased.  $\Delta Z$  was chosen by reducing it to a value at which an acceptable limiting solution was approached.

#### 4.7 Model Behavior

The model's behavior is governed by the three dimensionless parameters  $\alpha_1$ ,  $\alpha_2$  and  $\alpha_3$ .  $\alpha_1$  is a measure of the rate of mass transfer by foaming,  $\alpha_2$  is a measure of the rate of

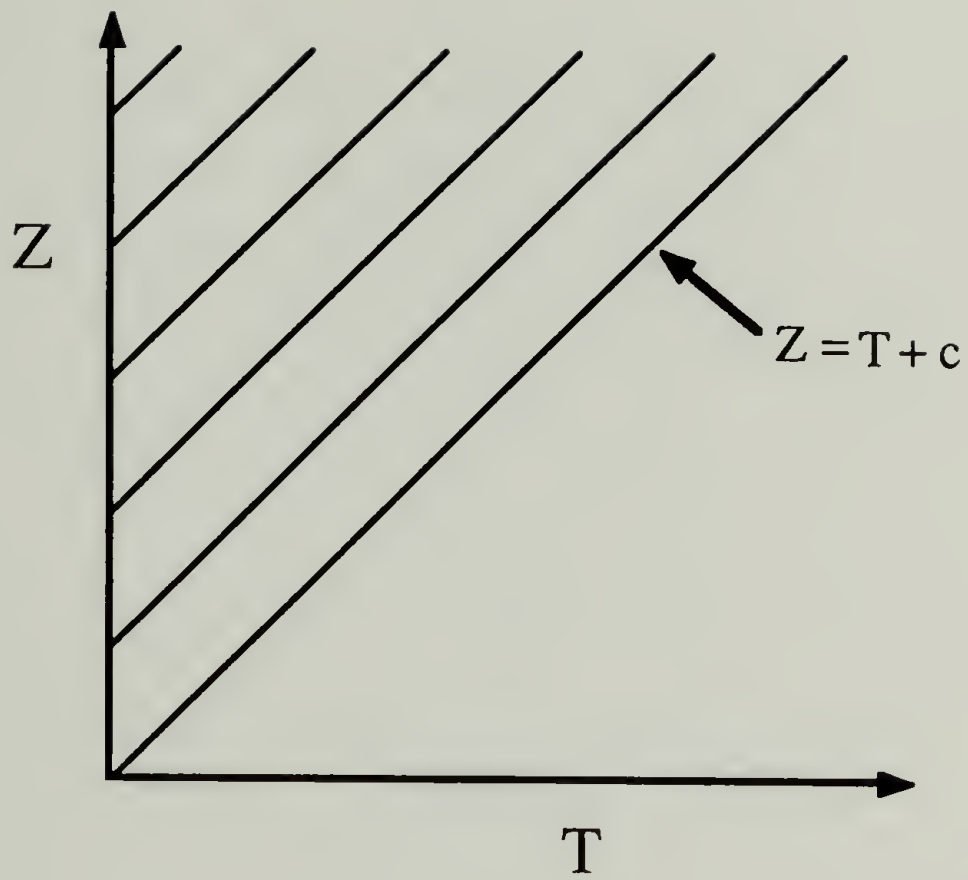


**Figure 4.6** Plot of the characteristics of the population balance equation.

mass transfer by interfacial diffusion, and  $\alpha_3$  is a measure of the concentration dependence of the nucleation rate. The effect of  $\alpha_1$ , or equivalently,  $F$ , as  $\alpha_1$  is proportional to  $F$ , on the DV performance is shown in Figure 4.7a. For a value of  $\alpha_2 = 0.0013$  (calculated by choosing values for the variables in the expression for  $\alpha_2$  that are typical of industrial processes) and  $\alpha_3 = 0.1$ , the dimensionless concentration,  $Y$ , is plotted versus the dimensionless distance,  $Z$ , for values of  $\alpha_1$  equal to 0.01, 0.1 and 0.5. As  $\alpha_1$  increases, the total mass transfer rate to bubbles increases proportionally and the DV performance improves. The effect of varying  $\alpha_3$  is shown in Figure 4.7b for values of  $\alpha_1 = 0.1$  and  $\alpha_2 = 0.0013$ . As  $\alpha_3$  is increased from 0.01 to 0.1 to 0.5, the initial DV rates remain unchanged. However, at greater distances through the equipment, the DV performance deteriorates with increasing  $\alpha_3$ . The effect of increasing  $\alpha_2$  is not shown, but its effect is to increase the slope of the  $Y$  versus  $Z$  plot for  $Z \gg 1$ .

Two regimes of DV are evident in these plots. Over short distances, both foaming and interfacial diffusion contribute to the DV performance. Although for these values of the model parameters, mass transfer by foaming dominates mass transfer by interfacial diffusion. At large  $Z$ , however, DV becomes controlled solely by interfacial diffusion. This transition occurs when the supersaturation (i.e.  $Y$ ) is decreased below the critical value necessary to sustain nucleation. As  $\alpha_3$ , or equivalently,  $E_a$ , increases, this critical value of the supersaturation increases and the transition occurs at larger values of  $Y$ .

In Figure 4.8, a surface plot of a typical bubble age distribution is presented revealing how it evolves through the devolatilizer. This sample distribution was calculated from the Complete Model of the rolling drum devolatilizer (to be presented in the next chapter) for values of  $\alpha_1 = 0.02$ ,  $\alpha_2 = 0.00136$ ,  $\alpha_3 = 0.4$  and  $\alpha_4 = 336$ . The effects of all aspects of the bubble nucleation, growth and rupture processes on the bubble age distribution are evident in this plot. At the entrance to the devolatilizer ( $Z = 0$ ), only bubbles of age  $T = 0$  exist. Travelling through the devolatilizer (increasing  $Z$ ), the bubbles grow to larger ages

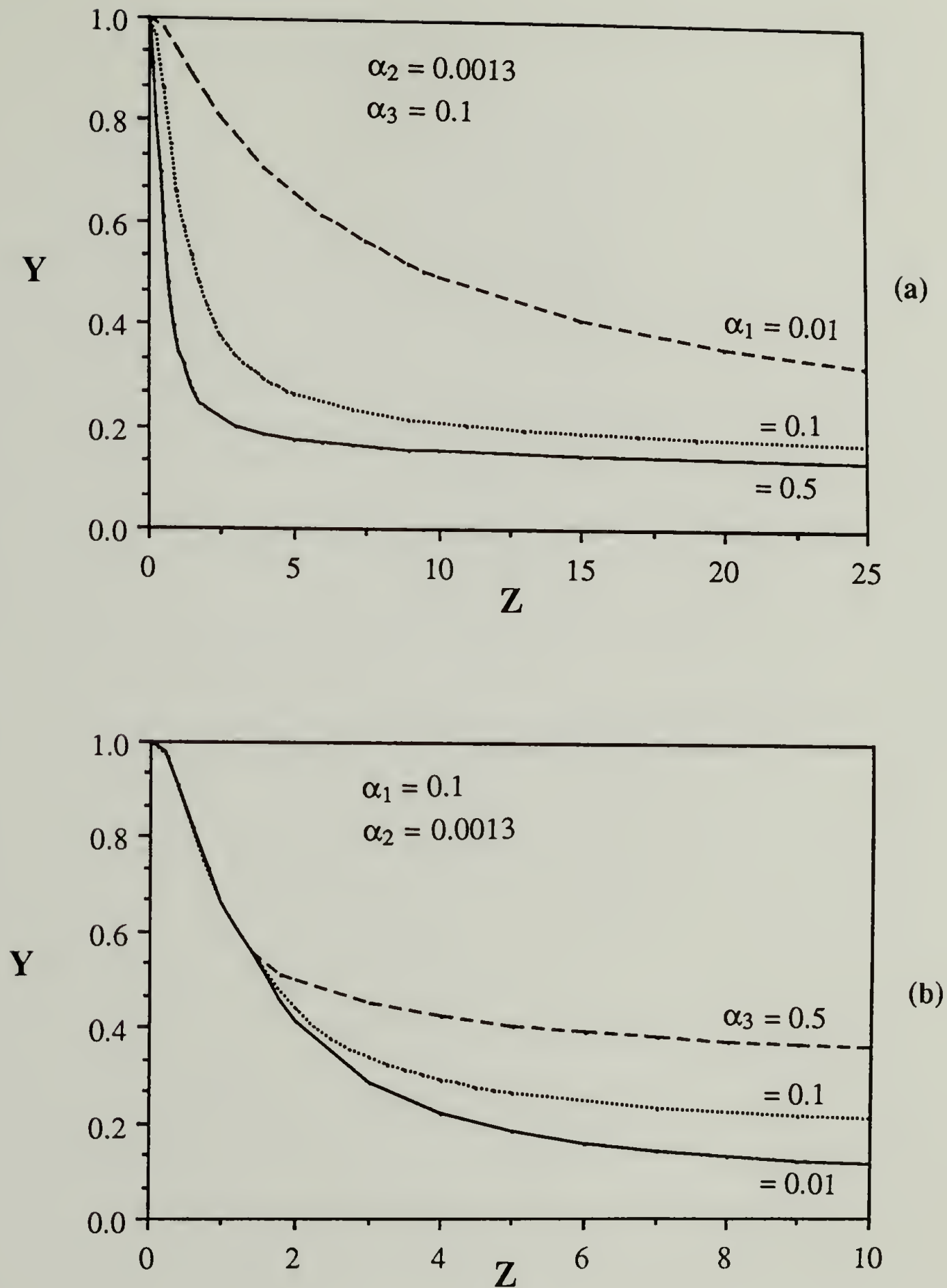


**Figure 4.7** Plots showing the dependence of the DV rate predicted by the Full Model of the single screw devolatilizer on (a)  $\alpha_1$  and (b)  $\alpha_3$ .

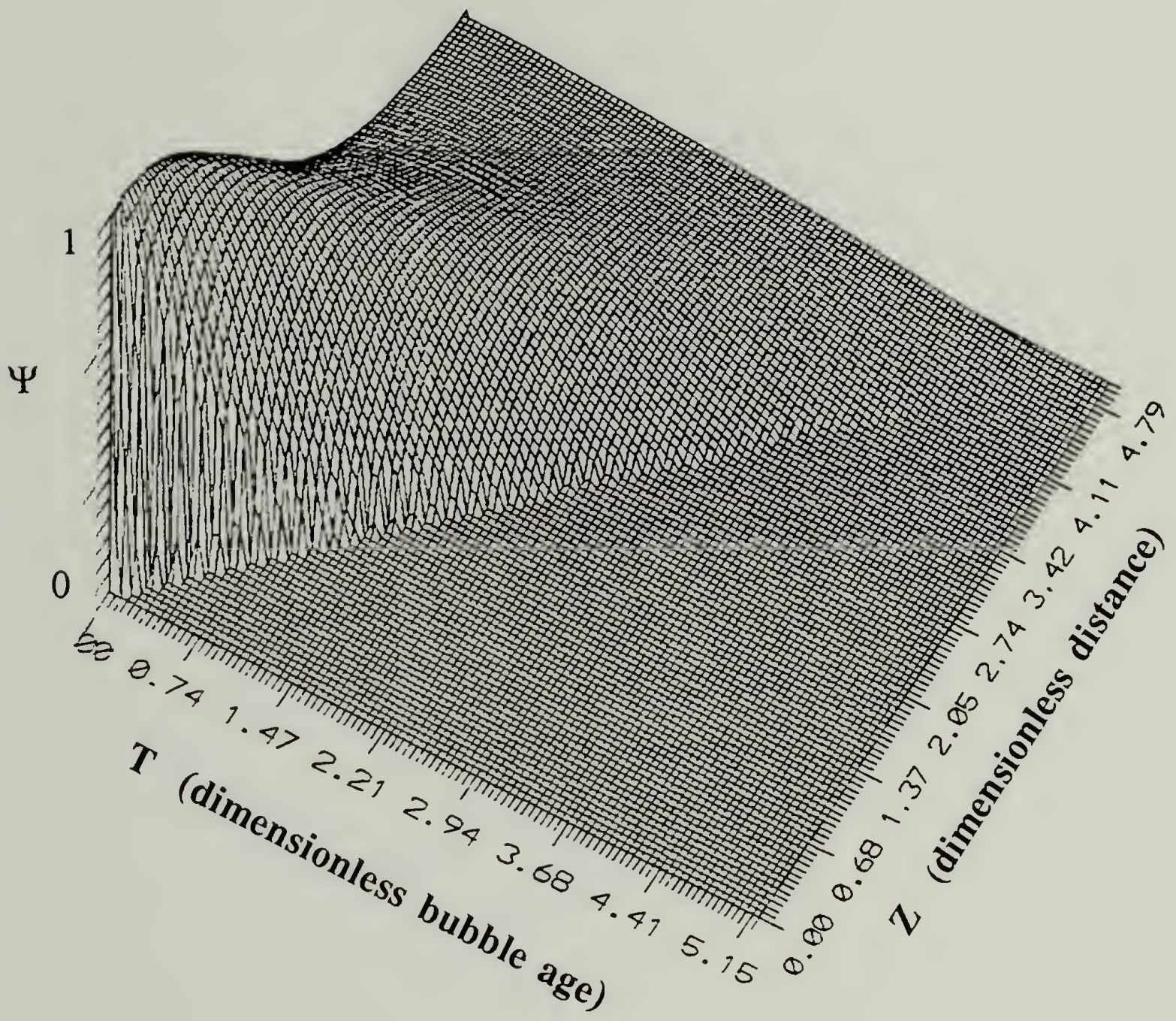


**Figure 4.8** Surface plot of the bubble age distribution given by the Complete Model of the rolling drum devolatilizer.  $\alpha_1 = 0.02$ ,  $\alpha_2 = 0.00136$ ,  $\alpha_3 = 0.4$  and  $\alpha_4 = 336$ .

which is reflected by an increase in the width of the bubble age distribution. The discontinuous drop in the distribution along the line  $T = Z$  is due to the plug flow assumption. Bubbles in any fluid element can not be older than the residence time of that fluid element which moves in plug flow through the devolatilizer. The effects of nucleation and rupture on the distribution can be seen more clearly in the different perspective of the same distribution given in Figure 4.9. Rupture reduces the number of bubbles, as is exhibited by the drop in  $\Psi$  with increasing  $Z$ . The decrease in the nucleation rate due to the reduction in the supersaturation is also evident, as  $\Psi(T = 0)$ , which is proportional to the nucleation rate, decreases with increasing  $Z$ .

## 4.8 Model Evaluation

The most effective means of evaluating the model would be to compare the model's prediction of a single screw devolatilizer's performance with that measured experimentally. However, our model has two empirical parameters,  $F$  and  $E_a$ , which characterize the rate of nucleation. Since values of  $F$  and  $E_a$  can't be determined from first principles, our model is not a predictive model. However, if  $F$  and  $E_a$  could be determined from independent measurements of the nucleation rate, the model could function in a predictive capacity. Indeed, in Appendix C, a method is presented for estimating  $E_a$  from nucleation onset data.

Since  $F$  and  $E_a$  were not measured experimentally, the model was evaluated by correlating existing experimental data. Values of  $F$  and  $E_a$  were estimated to be those values for which the model gives the best correlation of experimental devolatilizer performance data. The utility of the model was evaluated from its ability to correlate data taken over varying operating conditions.

### 4.8.1 Experimental Data

The experimental data used in the model evaluation were taken from the literature. For the single screw devolatilizer, only the experiments by Coughlin and Canevari (1969)

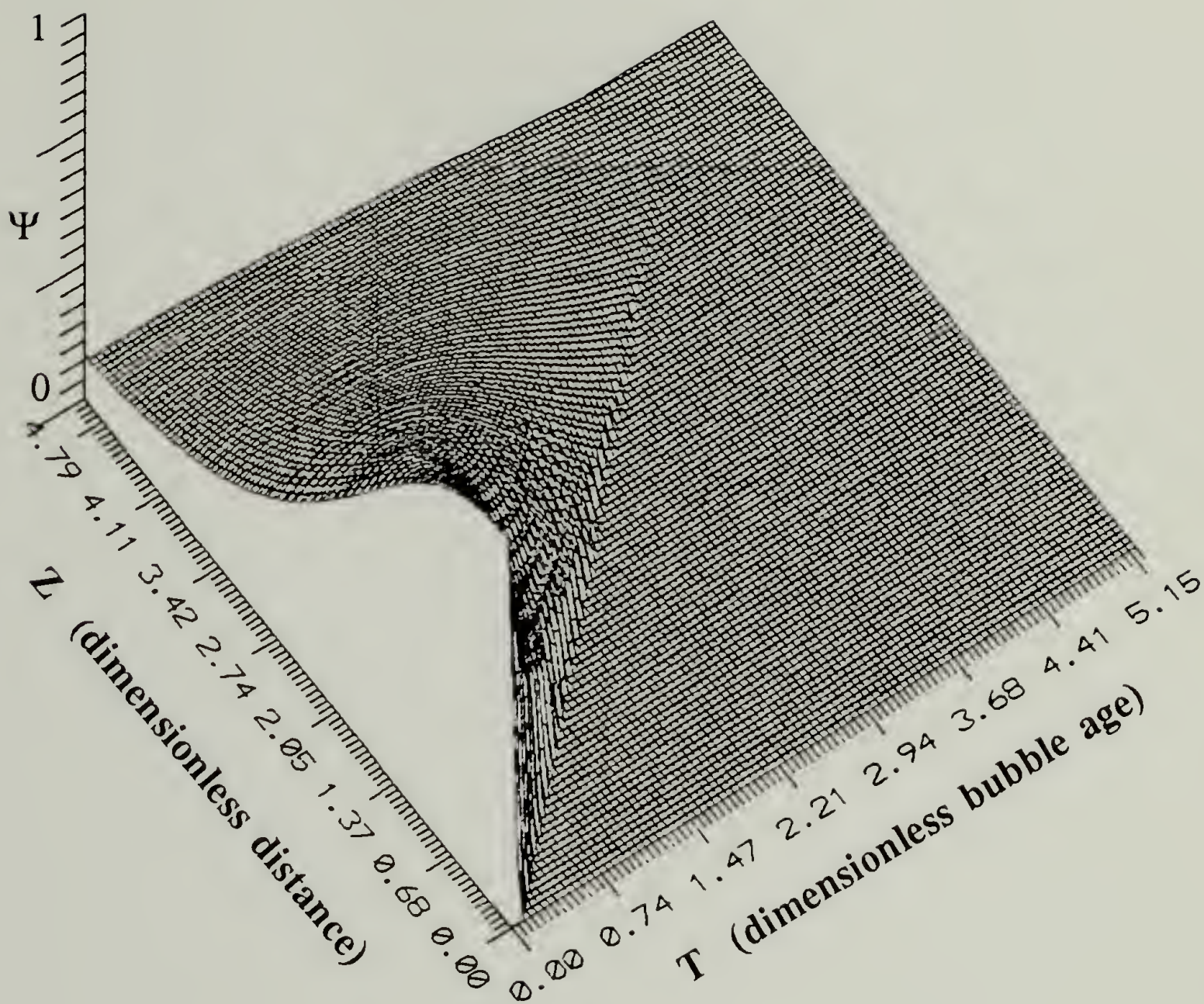


**Figure 4.9** Surface plot of the bubble age distribution given by the Complete Model of the rolling drum devolatilizer.  $\alpha_1 = 0.02$ ,  $\alpha_2 = 0.00136$ ,  $\alpha_3 = 0.4$  and  $\alpha_4 = 336$ .



were documented well enough to be used for model evaluation. Coughlin et al. measured the concentration of xylene in polypropylene (PP) exiting from a commercial-sized, single screw devolatilizer. This data was used for model evaluation. Coughlin et al. also measured the DV rates of methanol in polypropylene. This data was not used, however, since greater than 99.7% of the solvent was removed in each run. At these low solvent concentrations, the DV rate is dominated by interfacial diffusion and the contribution to mass transfer by foaming can not be unambiguously extracted from this data. Reliable estimation of values of  $F$  and  $E_a$  would be impossible.

A summary of the physical property data, extruder dimensions and operating conditions for each run by Coughlin et al. are presented in Table 4.1. Data on the diffusivity and solubility of xylene in PP could not be found in the literature. However, diffusivity and solubility data for xylene in polyethylene (PE) was available and was used as an estimate. PE is chemically similar to PP and should have similar values for the diffusivity and solubility of xylene. The diffusivity of xylene in PP at 260 °C was estimated to be  $4.8 \times 10^{-5} \text{ cm}^2/\text{s}$ . This value was determined by extrapolating the diffusivity measured by Duda and Vrentas (1982) for xylene in PE at 175 °C and 0.05 weight fraction of solvent to 260 °C using the measured activation energy of 5.1 Kcal/mole. For the same system and conditions, Duda et al. measured a value of the Flory-Huggins interaction parameter,  $\chi$ , equal to 0.2. From this value of  $\chi$ , a Henry's Law constant of 45.3 atm  $\text{cm}^3/\text{g}$  was estimated for xylene in PP using Flory-Huggins theory. The solution density was calculated to be  $0.72 \text{ g}/\text{cm}^3$  by dividing the mass flow rate by the volumetric flow rate.

The extruder dimensions were varied among runs. Two different barrels were used with diameters,  $D_b$ , of 8.9 cm and 11.4 cm. The axial lengths over the DV section,  $L_b$ , for these barrels are approximately 44.5 and 57.2 cm. These values for  $L_b$  were not given by Coughlin et al. Rather, we estimated them from values given for the volume and cross sectional area of the bulk film. The screw in the smaller barrel had a channel height,  $H_b$ , of 1.11 cm, a channel width,  $w$ , of 7.59 cm and a channel length,  $L_c$ , (measured helically

**Table 4.1** Summary of the conditions of Coughlin and Canevari's (1969) experiments on the single screw devolatilizer.

PHYSICAL PROPERTY DATA

Polymer	Solvent	D	K <sub>c</sub>	Mol. Wt.	Solution Density
		(cm <sup>2</sup> /s)	(atm cm <sup>3</sup> /g)	(g/mole)	(g/cm <sup>3</sup> )
polypropylene	xylene	4.76x10 <sup>-5</sup>	45.3	106.17	0.717

EXTRUDER DIMENSIONS

Run	D <sub>b</sub>	H <sub>b</sub>	w	θ	L <sub>b</sub>	L <sub>c</sub>
	(cm)	(cm)	(cm)	(radians)	(cm)	(cm)
1	8.89	1.11	7.59	0.3084	44.5	146.6
2	8.89	1.11	7.59	"	44.4	146.3
3	8.89	1.11	7.59	"	44.5	146.6
4	11.43	1.27	9.70	"	57.3	188.9
5	11.43	1.27	9.70	"	57.2	188.6
6	11.43	1.90	9.70	"	57.3	188.8
7	11.43	1.90	9.70	"	57.2	188.4
8	11.43	1.90	9.70	"	57.1	188.3

OPERATING CONDITIONS

Run	N	T	P	Fraction Full	Mass Flow Rate	Vol. Flow Rate	Residence Time
	(s <sup>-1</sup> )	(°C)	(atm)		(lbs/hr)	(cm <sup>3</sup> /s)	(s)
1	0.67	260	0.01	0.41	150	26.2	19.3
2	1.33	260	"	0.40	290	50.8	9.7
3	2.00	260	"	0.39	405	70.7	6.8
4	2.00	260	"	0.20	425	74.8	6.2
5	1.25	260	"	0.27	345	60.6	10.4
6	0.67	260	"	0.27	198	34.1	27.6
7	1.00	260	"	0.24	330	57.9	14.4
8	1.50	260	"	0.21	458	79.8	9.2

FILM DIMENSIONS, FILM VELOCITIES and SHEAR RATE

Run	d	A <sub>c</sub>	L <sub>f</sub>	V <sub>ext</sub>	V <sub>z</sub>	V <sub>f</sub>	V <sub>b</sub>	G
	(cm)	(cm <sup>2</sup> )	(cm)	(cm <sup>3</sup> )	(cm/s)	(cm/s)	(cm/s)	(s <sup>-1</sup> )
1	3.11	3.45	14.75	506.4	7.58	18.6	3.6	16.7
2	3.04	3.37	15.00	493.3	15.07	37.2	7.1	33.5
3	2.96	3.29	15.25	481.8	21.52	55.8	10.7	50.3
4	1.94	2.46	25.57	465.4	30.36	71.8	13.8	56.5
5	2.62	3.33	23.33	627.6	18.22	44.8	8.6	35.3
6	2.62	4.99	23.33	942.3	6.83	23.9	4.6	12.5
7	2.33	4.43	24.29	835.7	13.06	35.9	6.9	18.8
8	2.04	3.88	25.25	730.9	20.56	53.8	10.4	28.2

along the channel) of approximately 146.6 cm. This value was also calculated from given values of the bulk film volume and cross sectional area. For the larger barrel, two screws were used with identical channel widths and lengths over the DV section equal to 9.7 cm and 188.5 cm, respectively. However, one screw channel was deepened from 1.27 cm to 1.9 cm. All screws had a screw helix angle,  $\theta$ , of 0.3084 rad (17.67 °).

The screw rotation rate,  $N$ , was also varied among runs. Measurements were made over  $N$  varying between 30 and 120 rpm (.67 to 2 s<sup>-1</sup>) at a temperature of 260 °C. The pressure was not given and we assumed it to be constant at 0.01 atm (7.6 torr), which is representative of operating pressures in industrial single screw devolatilizers. The fraction of the channel volume filled, the mass flow rate, the volumetric flow rate and the mean residence time in the DV section were also given by Coughlin et al. and are presented in Table 4.1.

The dimensions of the bulk and barrel films varied from run to run due to variations in the channel width, channel height and fraction of channel fill. For the bulk film, the depth,  $d$ , cross sectional area,  $A_c$ , and total volume of the film in the DV section (extraction section),  $V_{ext}$ , are given in Table 4.1 along with the length of the barrel film,  $L_f$ . The velocities of the films are also presented. The average velocity of the bulk film in the down channel direction,  $V_z$ , was calculated as the ratio of the volumetric flow rate to the cross sectional area,  $A_c$ . The velocity of the barrel film,  $V_f$ , was set equal to the velocity of the barrel. The velocity of the bulk film surface was taken to be  $2/\pi$  times that of the component of the barrel velocity normal to the bulk film surface,  $\sin\theta V_f$ . The characteristic shear rate in the bulk film, defined as the velocity of the barrel,  $V_f$ , divided by the height of the bulk film,  $H_b$ , is also given in Table 4.1.

In Table 4.2, the inlet and outlet concentrations are presented for each run. The mass fraction of solvent at the start of DV,  $X_{w0}$ , was given by Coughlin et al. as ranging from 0.003 to 0.01.  $C_0$  and  $C_{max}$  (where  $C_{max} = C_0 - C_e$ ), were estimated assuming the initial solvent mass fraction,  $X_w$ , was 0.01. The equilibrium concentration of solvent,  $C_e$ , was

**Table 4.2** Inlet and outlet conditions of Coughlin and Canevari's (1969) experiments on the single screw devolatilizer and the single screw devolatilizer model parameters that best correlate this data.

#### INLET AND OUTLET CONDITIONS

Run	$X_{w0}$	$C_0$ (g/cm <sup>3</sup> )	$C_e$ (g/cm <sup>3</sup> )	$C_{max}$ (g/cm <sup>3</sup> )	$\rho_g$ (g/cm <sup>3</sup> )	$(C_0 - C)/C_0$	$X_w$	$C$ (g/cm <sup>3</sup> )
1	0.01	$7.17 \times 10^{-3}$	$2.21 \times 10^{-4}$	$6.95 \times 10^{-3}$	$2.43 \times 10^{-5}$	0.68	0.00320	0.00229
2	"	"	"	"	"	0.47	0.00530	0.00380
3	"	"	"	"	"	0.49	0.00510	0.00366
4	"	"	"	"	"	0.42	0.00580	0.00416
5	"	"	"	"	"	0.61	0.00390	0.00280
6	"	"	"	"	"	0.87	0.00130	0.00093
7	"	"	"	"	"	0.76	0.00244	0.00175
8	"	"	"	"	"	0.59	0.00410	0.00294

#### CORRELATION RESULTS

Run	$Z_{exp}$	$Y_{exp}$	$E_a$ (atm <sup>2</sup> K)	$F$ (cm <sup>-3</sup> s <sup>-1</sup> )	$Y_{pred}$
1	31.2	0.320	2.64	0.84	0.19
2	25.3	0.530	"	1.23	0.35
3	23.7	0.510	"	2.97	0.52
4	31.0	0.580	"	3.58	0.60
5	30.8	0.390	"	2.59	0.37
6	41.3	0.130	"	4.63	0.15
7	30.6	0.244	"	3.26	0.25
8	27.8	0.410	"	2.71	0.40

#### REFERENCE SCALES AND MODEL PARAMETERS

Run	$f^*$ (cm <sup>-1</sup> s <sup>-1</sup> )	$\tau^*$ (s)	$z^*$ (cm)	$\Delta C^*$ (g/cm <sup>3</sup> )	$\alpha_1$	$\alpha_2$	$\alpha_3$
1	10.36	0.62	4.69	0.00695	0.02424	0.00868	0.050
2	10.11	0.38	5.78	"	0.00733	0.00784	"
3	9.86	0.29	6.18	"	0.00357	0.00744	"
4	7.39	0.20	6.09	"	0.00145	0.00967	"
5	9.98	0.34	6.11	"	0.00525	0.00914	"
6	14.97	0.67	4.56	"	0.02943	0.00937	"
7	13.30	0.47	6.15	"	0.01231	0.00924	"
8	11.64	0.33	6.77	"	0.00501	0.00915	"

calculated from Henry's Law and the gas density in the bubble was calculated from the ideal gas law. Coughlin et al. measured the fraction of solvent removed,  $(C_0 - C)/C_0$ , in each run. From this, the solvent concentration,  $C$ , and mass fraction,  $X_w$ , at the outlet of the devolatilizer were estimated.

#### 4.8.2 Correlation of Experimental Data

The procedure used in correlating Coughlin and Canevari's (1969) data was to choose a single value of  $F$  and a single value of  $E_a$  which gave the best agreement between the outlet concentrations predicted by the model and those measured experimentally. The fitting procedure was to choose an arbitrary value of  $E_a$  and determine the values of  $F$ , for each run, that gave predictions of the outlet concentrations equivalent to those measured experimentally. The goodness of the correlation was determined from the degree of scatter in the values of  $F$ . This procedure was repeated over a range of values of  $E_a$ . That value of  $E_a$  that minimized the scatter in  $F$  was chosen as the best estimate for  $E_a$ . The best estimate of  $F$  was then chosen as the average value about which the scatter was minimized.

The data was fit in terms of the dimensionless concentration,  $Y$ , rather than  $C$ , because the uncertainties in the estimates of  $C$  are greater than those of  $Y$ . To calculate values of  $Y$ , where  $Y = [C - C_e]/[C_0 - C_e]$ , at the extruder outlet, the value of  $C$  and  $C_0$  is required. However, values of  $C$  were not given by Coughlin et al. and only bounds on the initial concentration,  $C_0$ , were given.  $Y$  could be approximated by assuming a value of  $C_0$  within the given range and solving for  $C$  from given values of the fraction of solvent removed,  $(C_0 - C)/C_0$ . However, the uncertainty in  $C_0$  alone could be as high as 300%. A more precise estimate is to approximate  $Y$  by  $[1 - (C_0 - C)/C_0]$ , by setting  $C_e$  equal to zero. This is a good approximation to  $Y$  when  $C_e \ll C$ .  $Y$  was approximated using this expression. The maximum uncertainty in  $Y$  was estimated to be  $\pm 0.03$ . These values of  $Y$ , designated  $Y_{exp}$ , and the corresponding dimensionless length of the DV section,  $Z_{exp}$ , are presented in Table 4.2.

The value of  $E_a$  which gives the least scatter in the fitted values of  $F$  is  $E_a = 2.64 \text{ atm}^2 \text{ K}$ . The values of  $F$  which fit the data for this value of  $E_a$  are presented in Table 4.2.  $F$  varies five fold from  $0.84$  to  $4.6 \text{ cm}^{-3} \text{ s}^{-1}$ . These values of  $F$  are plotted versus run number in Figure 4.10a. Most of the values of  $F$  are located near  $F = 3 \text{ cm}^{-3} \text{ s}^{-1}$ , with the exception of the first two values which are significantly lower. In Figure 4.10b,  $F$  is plotted versus the characteristic shear rate, as studies by Biesenberger and Lee (1987) indicate that the nucleation rate,  $F$ , may increase with increasing shear rate. However, this trend is not evident in Coughlin et al.'s data.

To evaluate the model's ability to correlate the DV performance over varying operating conditions, a single value of  $F$  was chosen to correlate the data. A value of  $F = 3 \text{ cm}^{-3} \text{ s}^{-1}$  was chosen to be the best estimate of  $F$ , as the scatter in  $F$  about this value is minimized. The dimensionless concentration predicted for each run,  $Y_{\text{pred}}$ , for  $F = 3 \text{ cm}^{-3} \text{ s}^{-1}$  and  $E_a = 2.64 \text{ atm}^2 \text{ K}$  are presented in Table 4.2. The reference scales,  $f^*$ ,  $\tau^*$ ,  $z^*$ , and  $\Delta C^*$ , and the model parameters,  $\alpha_1$ ,  $\alpha_2$ , and  $\alpha_3$  used in calculating  $Y_{\text{pred}}$  are also presented. The reference scales and model parameters were calculated from their definitions in section 4.5.

In Figure 4.11a,  $Y_{\text{pred}}$  is plotted versus the experimental value,  $Y_{\text{exp}}$ . If the correlation were exact, all the points would lie along the solid line  $Y_{\text{pred}} = Y_{\text{exp}}$ . The correlation is excellent for most of the data with data points for runs 1 and 2 exhibiting the greatest deviation.

### 4.8.3 Comparison With Latinen's Model

Our model gives a good correlation of the Coughlin and Canevari data. It would be of interest to compare our model's correlative ability with that of Latinen's (1962) model, since Latinen's model is the model most commonly used for sizing single screw devolatilizers. We used Latinen's model to correlate Coughlin and Canevari's data. To simplify the comparison, we neglected the contribution of axial dispersion to the DV

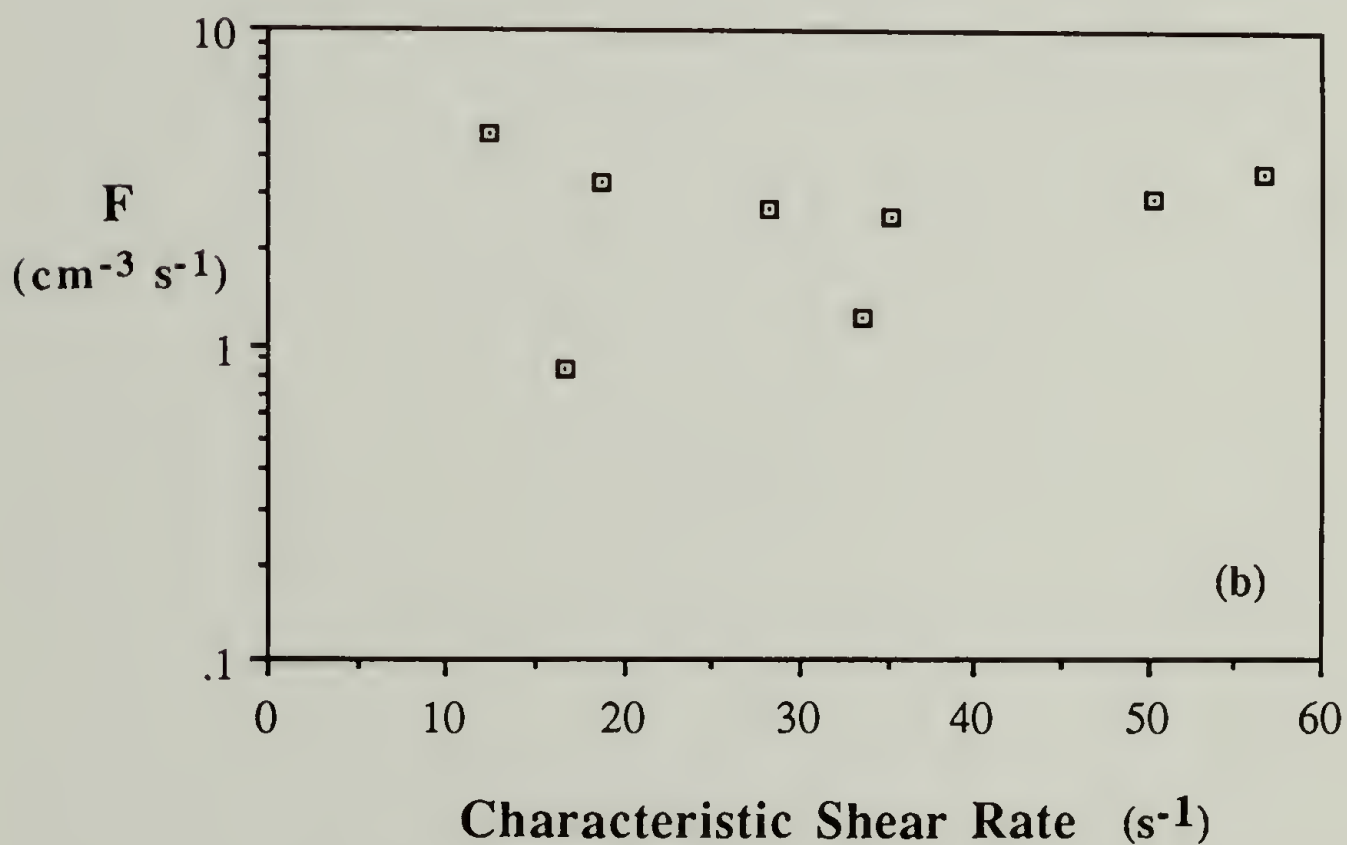
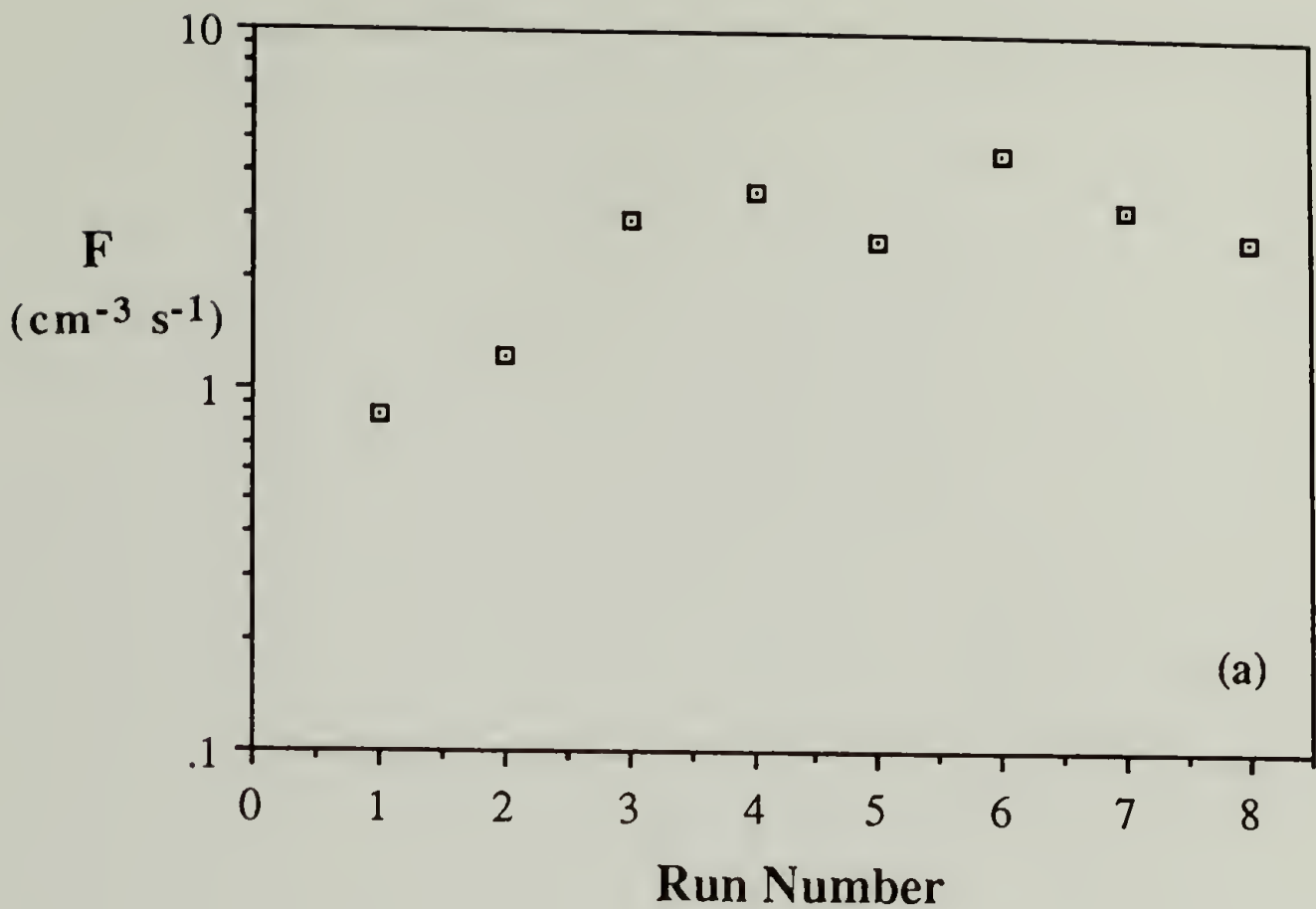


**Figure 4.10** Plots of the nucleation rate parameter,  $F$ , estimated from the data of Coughlin and Canevari (1969) versus (a) run number and (b) characteristic shear rate for  $E_a = 2.64 \text{ atm}^2 \text{ K}$ .

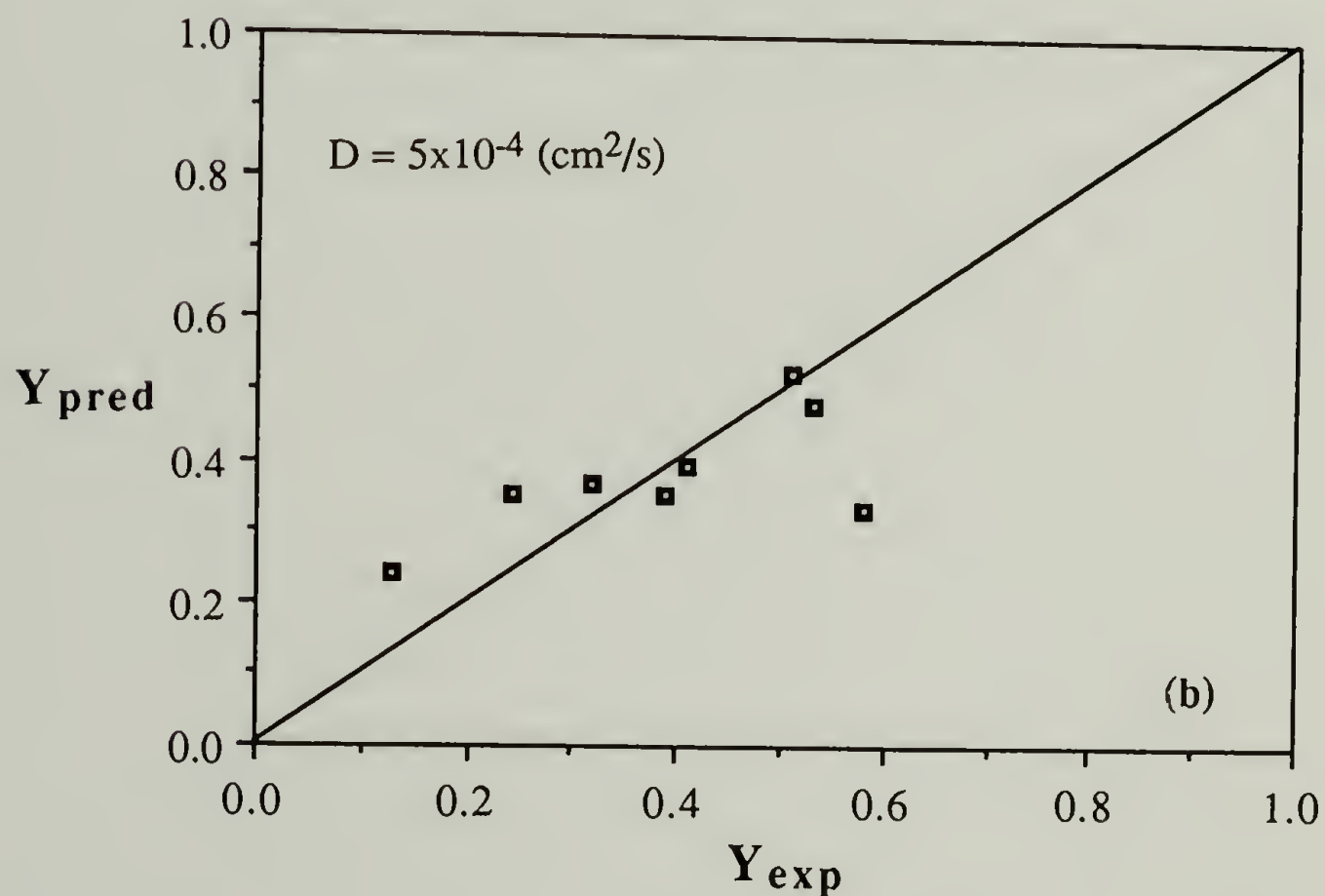
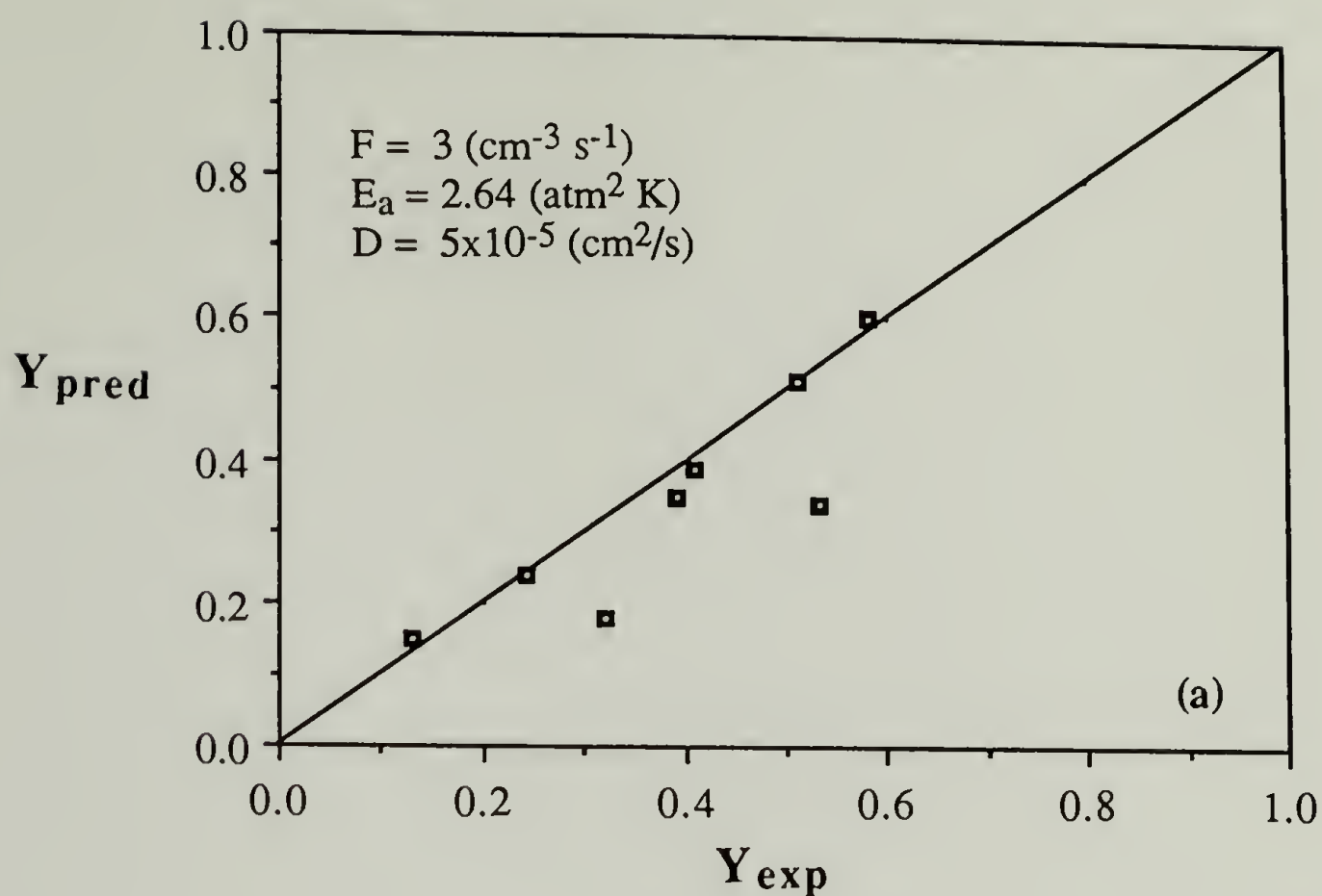


**Figure 4.11** Plots of the dimensionless outlet concentration of xylene in polypropylene from a single screw devolatilizer measured by Coughlin and Canevari (1969) versus (a) the outlet concentration predicted by our model and (b) the outlet concentration predicted by Latinen's (1962) model.



performance. The importance of the axial dispersion is quantified by the reciprocal of the Peclet number. Latinen (1962) measured a Peclet number in the single screw devolatilizer of order 5. For this value of the Peclet number, axial dispersion has a small effect on the DV rate and can be neglected.

To correlate the data using Latinen's model, a value of the effective diffusivity was chosen which best correlates the outlet concentrations predicted by Latinen's model to the experimental measurements. A value of  $D = 5 \times 10^{-4} \text{ cm}^2/\text{s}$  was found to give the best correlation. In Figure 4.11b, the dimensionless concentration predicted by Latinen's model,  $Y_{\text{pred}}$ , for  $D = 5 \times 10^{-4} \text{ cm}^2/\text{s}$  is plotted versus  $Y_{\text{exp}}$ . Comparison of Figures 4.11a and 4.11b reveals more scatter is present in Latinen's correlation.

This comparison indicates that our model is superior to Latinen's model in its ability to correlate experimental data. However, one might argue that this should be expected, as our model has two adjustable parameters and Latinen's model has only one. Yet, the two empirical parameters of our model,  $F$  and  $E_a$ , are both physically meaningful. They describe the nucleation rate of bubbles in polymer solutions and both should be essential in any model of foam enhanced DV. In contrast, the physical interpretation of Latinen's fitting parameter, the effective diffusivity, is lost when foaming is significant, as Latinen does not include foaming in his model. In this case, it can only be interpreted as a measure of the overall DV efficiency. Evidence of this loss of physical meaning is the fact that the value of the effective diffusivity required to fit the data is an order of magnitude larger than the measured value.

Despite the better relative abilities of our model, the design engineer might not be persuaded to use our model in favor of Latinen's model for devolatilizer design. This is because Latinen's model has an analytical solution and can frequently give an adequate correlation of the devolatilizer's performance. Our model is significantly more complex and requires a numerical solution procedure.

In the next chapter, reasons for using our model of the single screw devolatilizer in favor of Latinen's model will become clear. A model constructed for the rolling drum devolatilizer, designed to simulate the operation of the single screw devolatilizer, is presented next. Significant improvements in the correlative abilities of our model over Latinen's model will become evident upon comparison of these models using data available on the performance of the rolling drum devolatilizer

## CHAPTER V

### MODEL OF A ROLLING DRUM DEVOLATILIZER

#### 5.1 Geometry and Operation

The rolling drum devolatilizer was designed by Biesenberger and Lee (1985) to simulate the operation of a single screw devolatilizer. It consists of a blade housed within a rotating drum, as shown in Figure 5.1a. Polymer solution is poured between the blade and drum and the drum is set in motion inducing a free surface flow in the fluid, similar to that occurring in the single screw devolatilizer. DV is initiated by reducing the pressure in the vapor space.

#### 5.2 Model Equations

We have developed a model of the rolling drum devolatilizer. Although there are significant differences between the rolling drum and single screw devolatilizers, from a modelling standpoint, they are very similar in nature as both induce free surface flows in the polymer solution. The model of the rolling drum devolatilizer was constructed using assumptions and approximations similar to those used in the single screw devolatilizer model. These include:

- (1) The bubble phase is described by a distribution over bubble ages.
- (2) The solvent concentration and bubble age distribution is homogeneous in the cross section and through the length of the devolatilizer.
- (3) Bubble deformation, breakage and coalescence are neglected.
- (4) Models for the bubble birth, growth and death rates are identical to those incorporated into the single screw devolatilizer model.
- (5) The description of the rate of mass transfer through the interface of the bulk film is derived from the model of Latinen (1962).
- (6) Mass transfer from the barrel film is negligible as the barrel film thickness was made very small by Biesenberger et al. by using Teflon-tipped blades.

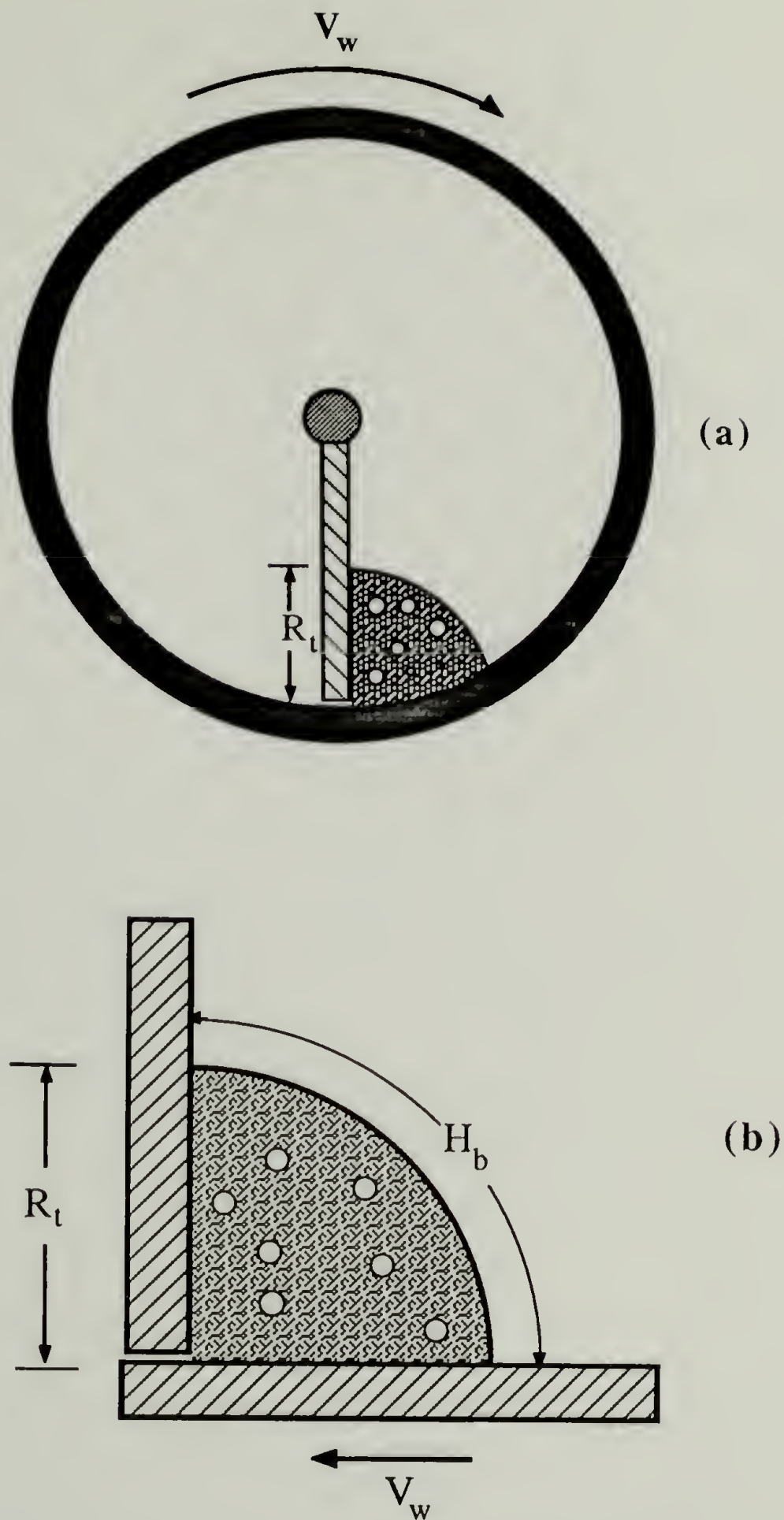


**Figure 5.1** Schematic of the cross section of a rolling drum devolatilizer showing (a) the actual geometry and (b) the idealized geometry used in our model.

The two most obvious differences between the single screw and rolling drum devolatilizers is the differences in the geometries of the cross sections of the bulk films and the differences in the modes of operation. Biesenberger et al. observed that the shape of the bulk film cross section in the rolling drum devolatilizer was similar to the shape of an arc of a circle. This differs from the rectangular shape of the bulk film cross section in the single screw devolatilizer. However, due to the assumption of good cross sectional mixing, the differing shape of the cross section will not affect the form of the resulting model equations. Only the cross sectional area,  $A_c$ , is required in the equations. The variables characterizing the shape of the cross section are lumped into this variable and these will affect only the value of  $A_c$ .

The operation of the single screw devolatilizer is continuous with inflow and outflow, whereas the rolling drum devolatilizer is operated in batch mode. In the rolling drum devolatilizer, the solvent concentration varies with time and the model is properly posed in terms of time rather than distance. However, the models of the two devolatilizers are closely related. The plug flow assumption in the single screw model allows that the distance  $z$  that a fluid element has travelled at a velocity  $V_z$  can be related to its time of travel  $t$  by  $t = z/V_z$ . Following a translating cross sectional fluid element over distance in the single screw devolatilizer is equivalent to following a stationary cross sectional fluid element as a function of time in the rolling drum devolatilizer. The equations of the single screw devolatilizer model expressed in terms of the residence time of a fluid element (rather than distance travelled) reduce identically to the equations of the rolling drum model.

To derive the equations for the rolling drum model, we note that equations 4.9a and b for the single screw extruder model are identical with the rolling drum model equations when  $z$  is replaced by  $V_z t$ . Replacing  $z$  with  $V_z t$  in these equations yields the mass balance, population balance and boundary conditions for the rolling drum model

$$\frac{d\Delta C}{dt} = - \left( 48 \sqrt{\frac{3}{\pi}} \right) \left( \frac{D^{3/2}}{A_c \rho_g^2} \right) \Delta C^3 \mu_{1/2} - \left( \frac{2}{\sqrt{\pi}} \right) \left( \frac{D V_b H_b}{A_c^2} \right)^{1/2} \Delta C \quad 5.1a$$

$$\frac{\partial f}{\partial \tau} + \frac{\partial f}{\partial t} = - \left( 4 \sqrt{\frac{3}{\pi}} \right) \left( \frac{D^{1/2} V_b}{A_t \rho_g} \right) \Delta C \tau^{1/2} f \quad 5.1b$$

B.C.'s

$$\text{at } t = 0; \quad \begin{cases} \Delta C = C_o - C_e \\ f(\tau, 0) = 0 \end{cases}$$

$$\text{at } \tau = 0; \quad f(0, t) = F A \exp \left[ \frac{-E_a}{T K_c^2 \Delta C^2} \right]$$

Note that the barrel film diffusion term in the mass balance is not included, as the barrel film is negligibly thick.

Introducing the dimensionless variables

$$Y = \frac{\Delta C}{\Delta C^*}; \quad \Psi = \frac{f}{f^*}; \quad T = \frac{\tau}{\tau^*}; \quad \Gamma = \frac{t}{\tau^*}$$

where the characteristic reference scales are defined as

$$\Delta C^* = C_o - C_e = C_{\max}$$

$$f^* = A_c F \exp \left[ \frac{-E_a}{T K_c^2 C_{\max}^2} \right]$$

$$\tau^* = \left( \frac{A_c}{V_b} \right)^{2/3} \left( \frac{\rho_g}{C_{\max}} \right)^{2/3} \left( \frac{1}{D} \right)^{1/3}$$

the dimensionless model equations become

$$\begin{aligned} \frac{dY}{dT} = & - \left( 48 \sqrt{\frac{3}{\pi}} \right) \alpha_1 M_{1/2} Y^3 \\ & - \left( \frac{2}{\pi^{1/4}} \right) \alpha_2 \left[ 1 + 32 \sqrt{\frac{3}{\pi}} \alpha_1 \alpha_4 Y^3 M_{3/2} \right]^{1/4} Y \end{aligned} \quad 5.2a$$

$$\frac{\partial \Psi}{\partial T} + \frac{\partial \Psi}{\partial T} = - \left( 4 \sqrt{\frac{3}{\pi}} \right) \frac{1}{\left( 1 + 32 \sqrt{\frac{3}{\pi}} \alpha_1 \alpha_4 Y^3 M_{3/2} \right)} T^{1/2} Y \Psi \quad 5.2b$$

B.C.'s

$$\text{at } T = 0; \quad \begin{cases} Y = 1 \\ \Psi(T, 0) = 0 \end{cases}$$

$$\text{at } T = 0; \quad \Psi(0, Z) = \exp \left[ \alpha_3 \left( 1 - \frac{1}{Y^2} \right) \right]$$

where the dimensionless model parameters are defined as

$$\alpha_1 = \left( \frac{A_c}{V_b} \right)^{5/3} \left( \frac{C_{\max}}{\rho_g} \right)^{1/3} D^{2/3} F \exp(-\alpha_3)$$

$$\alpha_2 = \left( \frac{D}{A_c^{1/2} V_b} \right)^{1/6} \left( \frac{\rho_g}{C_{\max}} \right)^{2/3}$$

$$\alpha_3 = \left( \frac{1}{T K_c^2 C_{\max}^2} \right) E_a$$

$$\alpha_4 = \left( \frac{C_{\max}}{\rho_g} \right)$$

These equations will be referred to as the *Complete Model* of the rolling drum devolatilizer.

The numerical prefactor of the bulk film diffusion term in the dimensionless mass balance differs slightly from that of the single screw model by a factor of  $\pi^{1/4}$ . This results during transformation to the dimensionless equations, where  $H_b$ , the length of the bulk film surface, was expressed in terms of  $A_t$ , the cross sectional area of the film, using the relation  $H_b = (\pi A_t)^{1/2}$ . This expression was derived assuming that the cross section of the bulk film was in the shape of a quarter circle with radius  $R_t$ , as shown in Figure 5.1b.

Biesenberger et al. observed that this is an adequate approximation to the actual shape of the film. In fact, they modelled the flow of fluid in the cross section assuming that the cross section was in the shape of a quarter circle

An additional factor is also evident in the bulk film diffusion term of the mass balance which is not present in the corresponding term in the single screw model, (i.e. the  $\alpha_5$  term in equation 4.10a). This term in the rolling drum model contains  $A_t/A_c$ , defined as

$$\frac{A_t}{A_c} = 1 + 32\sqrt{\frac{3}{\pi}} \alpha_1 \alpha_4 Y^3 M_{3/2} \quad 5.3$$

which is the fractional increase in the cross sectional area of the bulk film and is identical to that derived for the single screw model. This factor accounts for the increase in the length of the free surface of the bulk film,  $H_b$ , due to volume expansion during foaming. In the single screw model, the length of the free surface of the bulk film does not change during foaming (see Figure 4.2) and this factor is absent.

As discussed in Chapter 3, the volume expansion due to foaming in the rolling drum devolatilizer experiments was small. The value of  $A_t/A_c$  will be approximated as unity and the model equations simplify to

$$\frac{dY}{dT} = -\left(48\sqrt{\frac{3}{\pi}}\right) \alpha_1 M_{1/2} Y^3 - \left(\frac{2}{\pi^{1/4}}\right) \alpha_2 Y \quad 5.4a$$

$$\frac{\partial \Psi}{\partial T} + \frac{\partial \Psi}{\partial \mathbf{T}} = -\left(4\sqrt{\frac{3}{\pi}}\right) T^{1/2} Y \Psi \quad 5.4b$$

These equations will be referred to as the *Full Model* of the rolling drum devolatilizer. Due to its reduced complexity, the Full Model will be used in this chapter to correlate experimental data.

The population balance of the Full Model, equation 5.4b, may be expressed as an infinite set of ODE's in the moments of the distribution. Since the resulting moment equations are identical to equations 4.12 with  $Z$  replaced by  $\mathbf{T}$ , they need not be presented here.



### 5.3 Model Evaluation

As for the single screw devolatilizer model, the utility of the rolling drum devolatilizer model was evaluated from its ability to correlate experimental data. Data measured by Biesenberger and Lee (1987) on the performance of the rolling drum devolatilizer was analyzed. This data consists of the rates of devolatilization of methyl chloride (MeCl) and a series of Freons<sup>®</sup> (Freon<sup>®</sup> is a registered trademark of the DuPont Company) in polydimethylsiloxane (PDMS) at room temperature. Measurements were made over varying drum rotation rates, initial solvent concentrations and pressures.

#### 5.3.1 Experimental Data

Biesenberger and Lee (1987) measured the fraction of solvent removed from the rolling drum devolatilizer,  $(C_0 - C)/C_0$ , versus time. We converted these variables into  $Y$ ,  $X - X_e$  and  $P_{vap} - P$ , where  $Y$  is the dimensionless concentration,  $X$  is the mass fraction of solvent,  $X_e$  is the mass fraction of solvent in equilibrium with the applied pressure,  $P$ , and  $P_{vap}$  is the vapor pressure of the solution.  $X - X_e$  is the supersaturation and  $P_{vap} - P$  is the superpressure. Both are important, as they are measures of two distinct driving forces. The supersaturation drives diffusion and the superpressure drives nucleation.

Plots of  $Y$ ,  $X - X_e$  and  $P_{vap} - P$  are presented in Figures 5.2 to 5.5 for four different data sets measured by Biesenberger and Lee (1987). Within a data set, the pressure, rotation rate, initial supersaturation or initial superpressure were varied to determine its effect on the DV performance. At each experimental condition, two experiments were usually run to test the reproducibility of the measurements. The initial conditions of each data set are listed in Table 5.1.

**Table 5.1** Variables in Biesenberger and Lee's (1986) experiments on the rolling drum devolatilizer. Devolatilization of PDMS at 20 °C.

RUN	SOLVENT	X <sub>0</sub>	P	N <sub>r</sub>	SUPER-SATURATION	SUPER-PRESSURE
		(ppm)	(torr)	(rpm)	(ppm)	(torr)
1.A	MeCl	8000	5	4	7860	280.7
1.B	"	8100	"	75	7960	284.3
1.C	"	8000	"	120	7860	280.7
2.A	MeCl	9000	8	75	8776	313.5
2.B	"	3800	"	"	3576	127.7
2.C	"	9100	200	"	9100	125.0
3.A	MeCl	7900	8	75	7676	274.2
4.A	Freon-114®	4300	7	75	3532	32.2
4.B	Freon-22®	4260	"	"	4024	119.2
4.C	Freon-13®	4200	"	"	4134	439.9

In data set 1, the rotation rate,  $N$ , was varied from 4 to 120 rpm. In data set 2, from a base case of  $P = 8$  torr and  $X_0 = 9000$  ppm, the pressure was increased to 200 torr in one experiment and the initial concentration was reduced to 3800 ppm in the other. In data set 3, no variations in operating conditions were made, as it consists of only one experiment. Rather, measurements were started after 5 seconds, as compared with 30 seconds for the other data sets. For data set 4, the superpressure was varied by using a series of Freons® with differing solubilities as the solvent.

Data set 1 is presented in Figure 5.2 where  $Y$ ,  $X - X_e$  and  $P_{vap} - P$  of MeCl in PDMS are plotted versus time. All plots are for initial mass fractions between 80-8100 ppm and a pressure of 5 torr. The drum rotation rates vary, however, from 4 to 75 to 120 rpm. From Figure 5.2, it is evident that the DV rate increases with increasing rotation rate.

Data set 2 is presented in Figure 5.3. Plots of  $Y$ ,  $X - X_e$  and  $P_{vap} - P$  versus time for MeCl in PDMS are given for a rotation rate of 75 rpm. Data was measured for a base case of  $X_0 = 9000$  ppm and  $P = 8$  torr (data 2.A). For comparison with the base case, data was

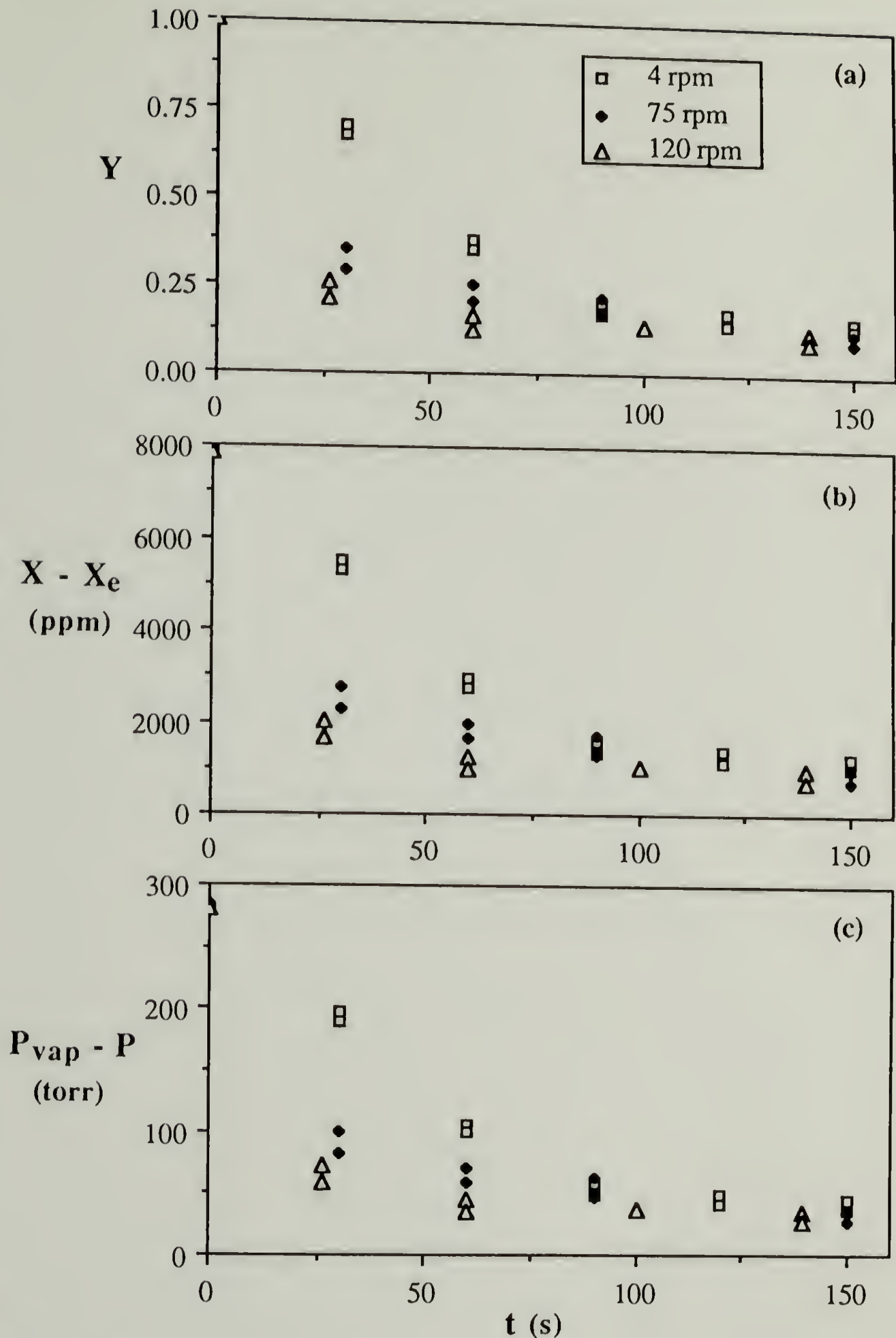


**Figure 5.2** Plots of data set 1 of Biesenberger and Lee's (1986) rolling drum devolatilizer performance experiments showing the effect of varying rotation speed on the DV performance of MeCl in PDMS for  $X_0 \cong 8000$  ppm and  $P = 5$  torr. (a) dimensionless concentration, (b) supersaturation and (c) superpressure.

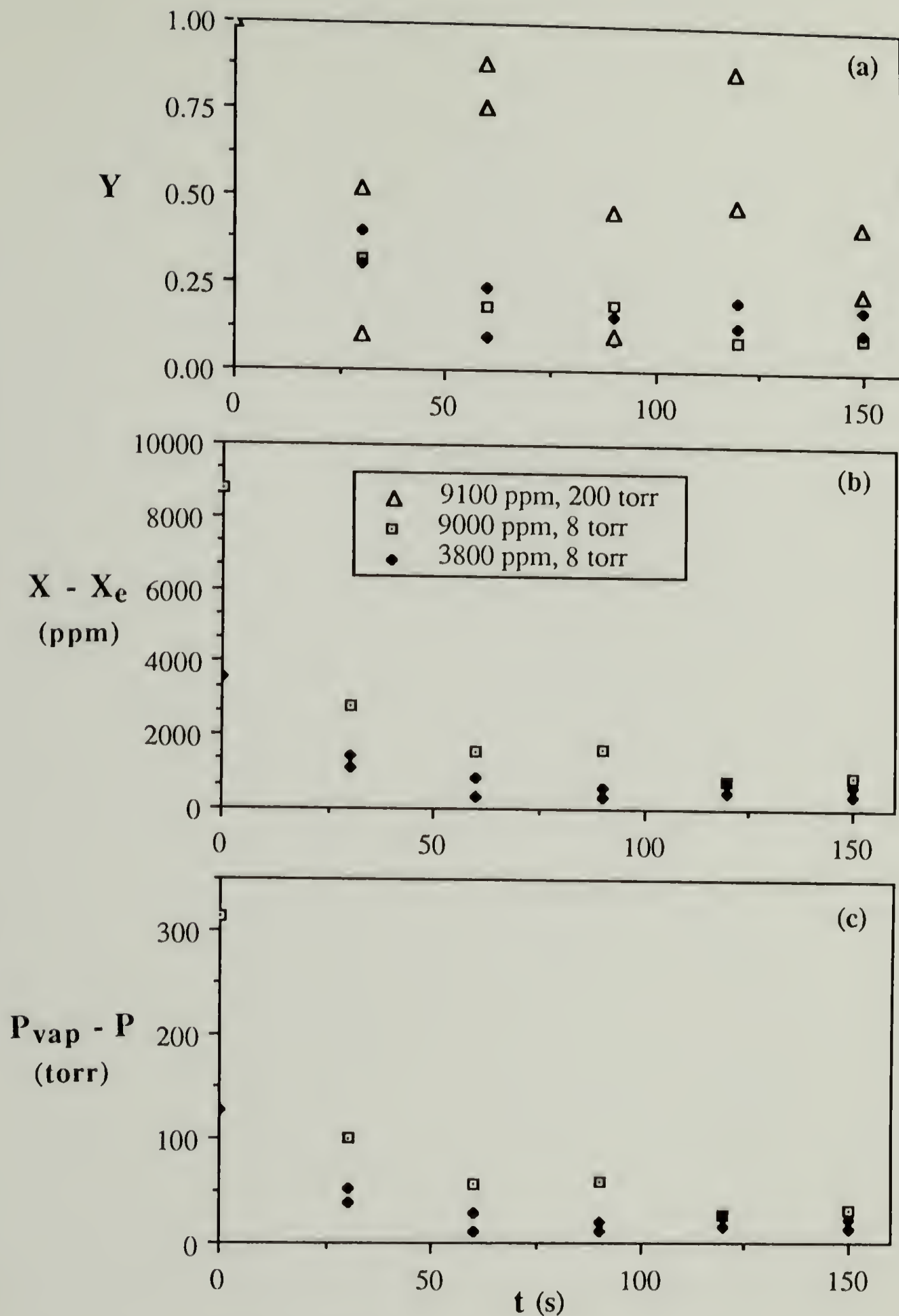


**Figure 5.3** Plots of data set 2 of Biesenberger and Lee's (1986) rolling drum devolatilizer performance experiments showing the effect of varying solvent concentration and pressure on the DV performance of MeCl in PDMS for  $N = 75$  rpm. (a) dimensionless concentration, (b) supersaturation and (c) superpressure.

also measured for the concentration reduced to 3800 ppm (data 2.B) and for the pressure increased to 200 torr (data 2.C). Data 2.C exhibits enough scatter to remove any confidence in the precision of the data fitting. It will not be used in the model evaluation and is presented in Figure 5.3a only. For data 2.B, the supersaturation curves are consistently lower than those of the base case. This is expected since the initial supersaturation is also lower. However, the dimensionless concentration plots are very similar.

Data set 3, which includes measurements taken at short time, is presented in Figure 5.4. Only a single plot,  $Y$  of MeCl in PDMS versus  $t$ , is necessary, as the conditions of this experiment ( $W_0 = 7900$  ppm, at  $P = 8$  torr and  $N_r = 75$  rpm) are similar to the conditions of data 1.B. Two regimes of DV can be clearly distinguished in this plot: fast DV at short times, where 60% of the solvent is removed within five seconds, followed by considerably slower DV at longer times.

In Figure 5.5, the results of data set 4 are presented.  $Y$ ,  $X - X_e$  and  $P_{vap} - P$  of a series of Freons<sup>®</sup> in PDMS are plotted versus time for  $W_0 = 42-4300$  ppm,  $P = 7$  torr and  $N_r = 75$  rpm. The trade names of these Freons<sup>®</sup> are Freon-114<sup>®</sup>, Freon-22<sup>®</sup> and Freon-13<sup>®</sup>. The solubilities of Freon-114<sup>®</sup>, Freon-22<sup>®</sup> and Freon-13<sup>®</sup> are quantified by their Henry's Law constants,  $K_w$  (on a mass fraction basis), which are 11.7, 39, and 140 atms respectively. Their differing solubilities cause the initial superpressures to vary from 32.2 torr, for the most soluble Freon<sup>®</sup> (Freon-114<sup>®</sup>) in data 4.A, to 439.9 torr for the least soluble Freon<sup>®</sup> (Freon-13<sup>®</sup>) in data 4.C. Inspection of the supersaturation plots show that the least soluble Freon<sup>®</sup> (i.e. with the largest superpressure) is devolatilized most rapidly and the most soluble Freon<sup>®</sup> (i.e. with the smallest superpressure) is devolatilized least rapidly. As the diffusion driving forces (i.e. the supersaturations) are equivalent, this behavior is probably related to differences in the nucleation driving forces (i.e. the superpressures). This indicates that increasing the superpressure can increase the DV rate, probably by increasing the nucleation rate of bubbles.

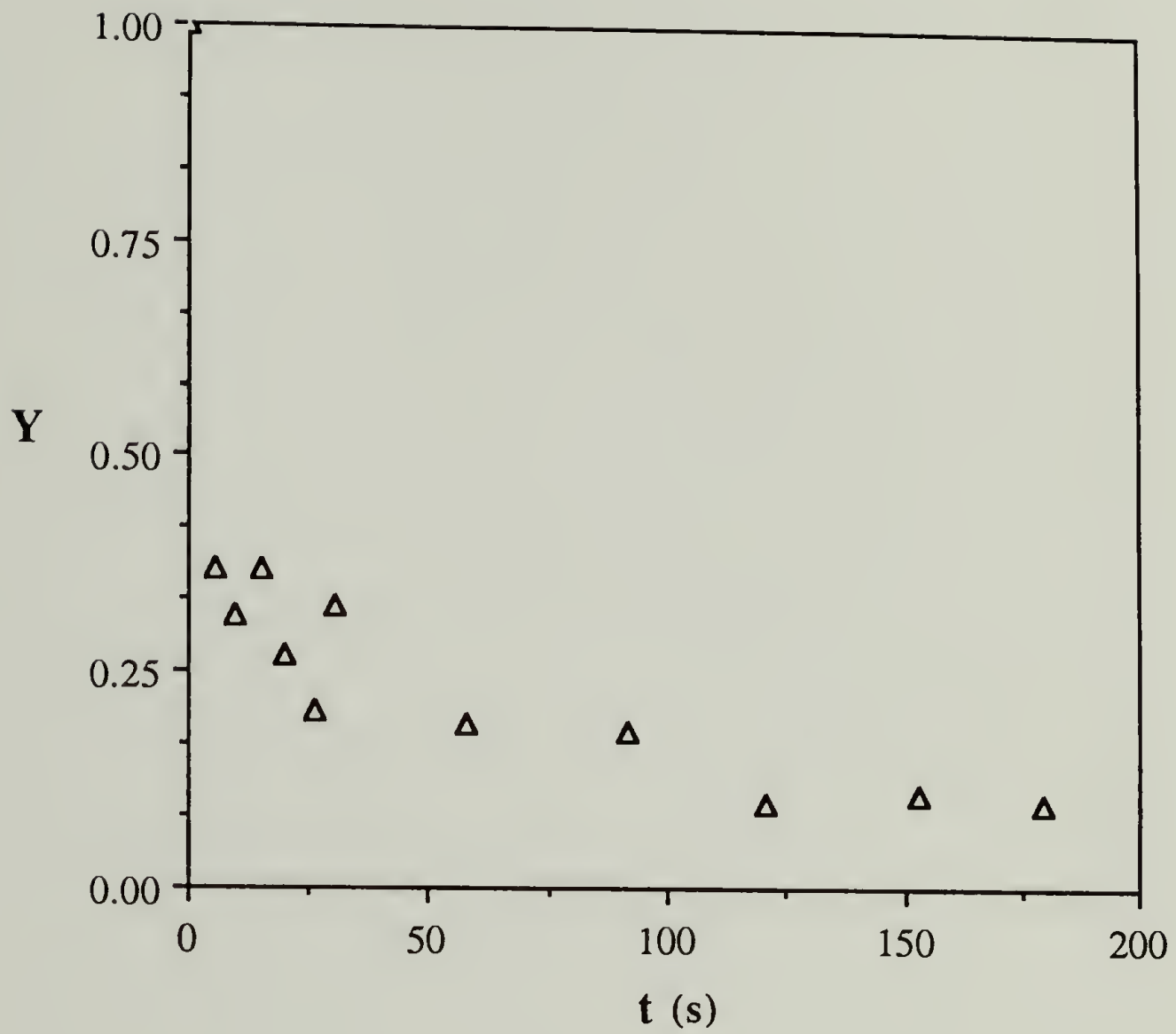


**Figure 5.4** Plot of dimensionless concentration from data 3 of Biesenberger and Lee's (1986) rolling drum devolatilizer performance experiments taken on MeCl in PDMS and containing short time data.  $X_0 = 7900$  ppm,  $N = 75$  rpm,  $P = 8$  torr.

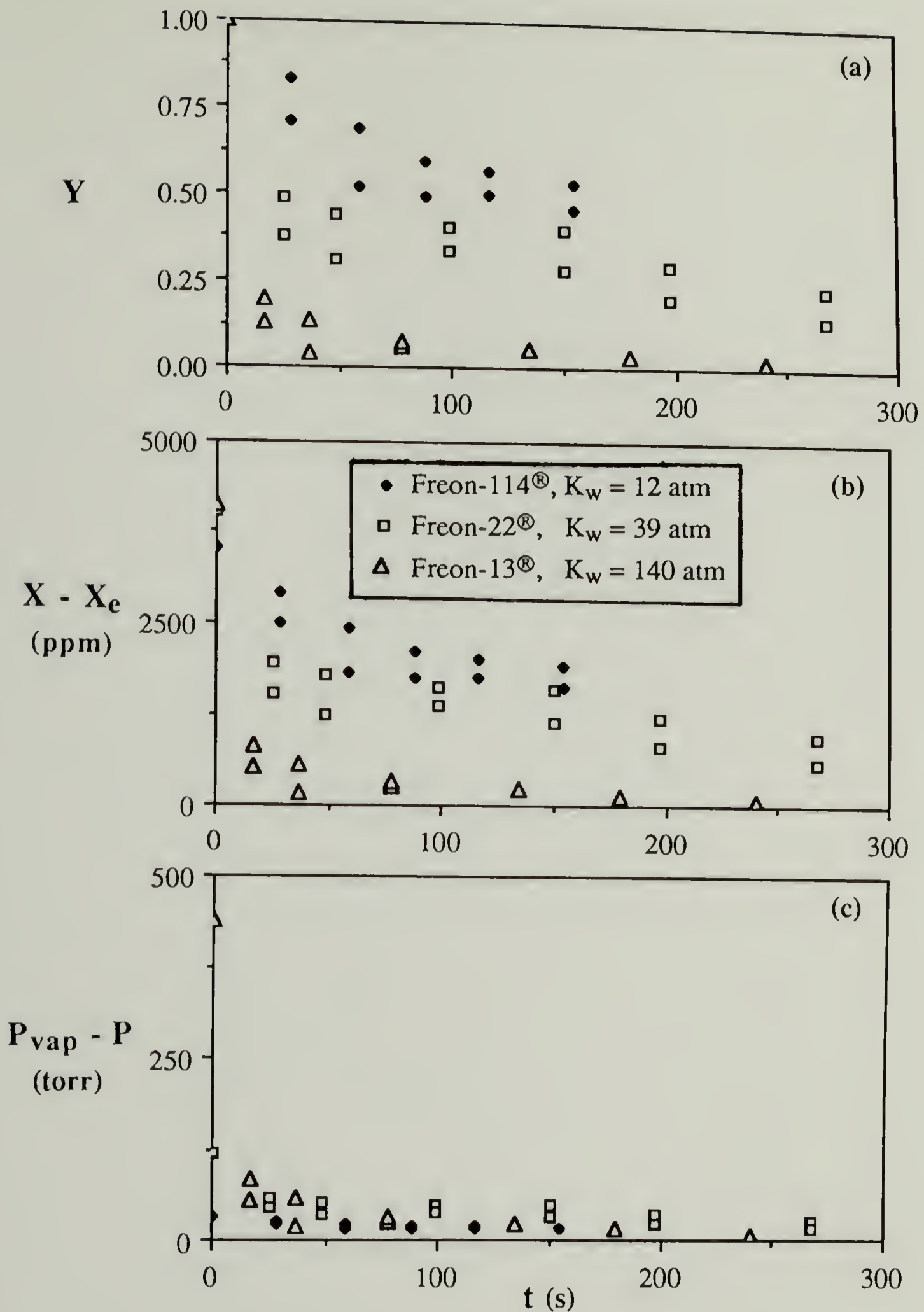


**Figure 5.5** Plots of data set 4 of Biesenberger and Lee's (1986) rolling drum devolatilizer performance experiments taken on a series of Freons<sup>®</sup> in PDMS with varying solubilities: (a) dimensionless concentration, (b) supersaturation and (c) superpressure.  $X_0 \cong 4250$  ppm,  $N = 75$  rpm,  $P = 7$  torr.

### 5.3.2 Correlation of Experimental Data

Physical property data for MeCl, Freon-114<sup>®</sup>, Freon-22<sup>®</sup> and Freon-13<sup>®</sup> given by Biesenberger and Lee (1987) are presented in Table 5.2. Included in this table are the chemical formulae, the Henry's law constants in PDMS,  $K_w$ , the normal boiling points,  $T_b$ , the molecular weights,  $M_w$ , and the pure component densities. The value of the diffusivity of MeCl in PDMS was not available in the literature. It was estimated to be  $4.7 \times 10^{-6}$  cm<sup>2</sup>/s by extrapolating values of the diffusivities of a series of n-alkanes for  $n > 5$  measured by Millen and Hawkes (1977) to a value for ethane ( $n = 2$ ). Ethane is similar in size to MeCl and should have a diffusivity of the same order of magnitude. Values for the diffusivities of the Freons<sup>®</sup> were also not available. These diffusivities were estimated to be those values which best correlate the DV model to the long time Y vs t data measured by Biesenberger and Lee (1987). At long times, foaming does not occur and the DV performance can be adequately described by the interfacial diffusion model.

**Table 5.2** Physical property data for solvents used in Biesenberger and Lee's (1986) experiments on the rolling drum devolatilizer.

SOLVENT	FORMULA	$K_w$ (atm)	$T_b$ (°F)	$M_w$ (g/mole)	Density (g/cc)
MeCl	CH <sub>3</sub> Cl	47	-11.2	50.5	0.915 @ -11.6 °F.
Freon-114 <sup>®</sup>	C <sub>2</sub> Cl <sub>2</sub> F <sub>4</sub>	11.7	-137	170.9	1.46 @ 86 °F
Freon-22 <sup>®</sup>	CHClF <sub>2</sub>	39	-256	86.5	1.17 @ 86 °F
Freon-13 <sup>®</sup>	CClF <sub>3</sub>	140	-294	104.5	1.32 @ 30 °F

Physical property data for PDMS given by Lee (1987) are presented in Table 5.3. Values for the dimensions of the rotating drum and bulk film are presented in Table 5.4. Biesenberger and Lee (1986) did not give the depth of the solution in the devolatilizer, which is equivalent to  $R_1$  for a quarter circular film. We assumed it to be 1.9 cm, which is



75% of the height of the wiping blade (1 inch). In Table 5.5, the initial solvent concentrations, bubble vapor density, solvent vapor pressure and the velocities of the drum wall and of the surface of the bulk film are presented for each run.

**Table 5.3** Physical property data on polydimethylsiloxane (PDMS) used in Biesenberger and Lee's (1986) experiments on the rolling drum devolatilizer.

Product Name:	Dow Corning 200 Fluid®
Viscosity:	1,000 poise
$M_w$ :	75,000 g/mole
Density:	0.97 g/cc
Surface Tension:	20.9 dyne/cm

**Table 5.4** Dimensions of the rolling drum devolatilizer and of the bulk film of Biesenberger and Lee's (1986) experiments used in our model correlations.

Barrel Diameter, $D_b$ :	11.42 cm
Film Depth, $R_t$ :	1.9 cm
Area of Cross-Section, $A_c$ :	2.84 cm <sup>2</sup>
Length of Free Surface, $H_{b0}$ :	2.98 cm

**Table 5.5** Conditions of Biesenberger and Lee's (1986) experiments on the rolling drum devolatilizer.

RUN	$X_0$ (ppm)	$X_e$ (ppm)	$C_0$ (g/cc)	$C_e$ (g/cc)	$\rho_g$ (g/cc x 10 <sup>5</sup> )	$P_{vap}$ (torr)	$V_w$ (cm/s)	$V_b$ (cm/s)
1.A	8000	140	.00776	.000136	1.38	285.7	2.39	1.52
1.B	8100	140	.00785	.000136	1.38	289.3	44.8	28.5
1.C	8000	140	.00776	.000136	1.38	285.7	71.7	45.7
2.A	9000	224	.00873	.000217	2.21	321.4	44.8	28.5
2.B	3800	224	.00369	.000217	2.21	135.7	"	"
2.C	9100	5599	.00882	.005428	55.2	325.1	"	"
3.A	7900	224	.00766	.000217	2.21	282.2	44.84	28.55
4.A	4300	767	.004180	.000746	6.54	39.2	44.8	28.55
4.B	4260	236	.004136	.000229	3.31	126.2	"	"
4.C	4200	65	.004080	.000063	4.01	446.8	"	"

The data were correlated by choosing values of  $F$  and  $E_a$  which give the best agreement of the dimensionless concentrations predicted by the Full Model to those values measured experimentally. In Figures 5.6 to 5.11, the results of the correlations are presented as plots of the dimensionless concentration versus time measured in seconds along with the experimental data from each data set. Unfortunately, unique values of  $F$  and  $E_a$  which best correlate the data could not be chosen for each run, since a range of values can give equally satisfactory correlations. This is evident in Figure 5.8b showing the correlation of data 2.B. Values of  $F=114 \text{ cm}^{-3} \text{ s}^{-1}$ ,  $E_a = .83 \text{ atm}^2 \text{ K}$  and  $F = 43500 \text{ cm}^{-3} \text{ s}^{-1}$ ,  $E_a = 15.2$  both give an adequate correlation of the data, which were taken at long times only. Yet the short time solutions for the two correlations are very different. This makes clear the necessity of short time data for discriminating between values for the model parameters.

Although it is not clear what values to choose for  $F$  and  $E_a$  when short time data is absent, lower bounds on  $F$  and  $E_a$  can be determined. This is also evident in Figure 5.8b. The values of  $F=114 \text{ cm}^{-3} \text{ s}^{-1}$  and  $E_a = .83 \text{ atm}^2 \text{ K}$  are the smallest values of  $F$  and  $E_a$  which can give an acceptable fit of the data. A smaller value of  $F$  will reduce the short time DV rate (i.e. the slope of  $Y$  vs  $t$  at  $t = 0$ ) and overshoot the first two data points regardless of the value chosen for  $E_a$ . A smaller value of  $E_a$  will decrease the supersaturation at which nucleation ceases. If  $E_a$  were decreased, the first two data points in Figure 5.8b could be correlated but the curve would underestimate the long time data.

To minimize the uncertainty in the lower bound estimates of  $F$  and  $E_a$  for the MeCl experiments, we will take advantage of the expectation that the values of  $E_a$  should be equivalent for experiments run at equivalent temperature, pressure and composition. This is expected since, by analogy with classical nucleation theory,  $E_a$  is a thermodynamic parameter and should depend only on the composition, temperature and pressure of the polymer/solvent system. If so, we may estimate  $E_a$  for all experiments at the same temperature, composition and pressure using a value determined from only one experiment.

Data 1A-C, 2A and B and 3 for MeCl in PDMS were all taken at similar temperatures and pressures and a single lower bound value of  $E_a$  will be assumed to apply for these data sets. This value will be taken to be the lower bound value of  $E_a$  which fits data 3, as data 3 contains data taken at the shortest time and should be the least conservative of the lower bound estimates for  $E_a$  of all the data sets.

The value of  $E_a$  fit to data 3 will be used in fitting data sets 1.A-C and 2.A and B. However, different values of  $F$  will be chosen to fit each run, as these may depend on the rotation rate or on the heterogeneous impurities concentration (i.e. concentration of nucleation sites) which may vary among runs. For data set 4, which contains the DV data for a series of Freons<sup>®</sup>,  $E_a$  is expected to vary among runs as the composition of the polymer solutions varies. Lower bound values of  $F$  and  $E_a$  will be determined individually for each experiment in data set 4.

In Figure 5.6, the correlation of data 3, the data set which includes the short time measurements, using the Full Model is presented as a plot of dimensionless concentration versus time. The lower bound values of  $F$  and  $E_a$  which best fit the data are  $F = 798 \text{ cm}^{-3} \text{ s}^{-1}$  and  $E_a = 15.2 \text{ atm}^2 \text{ K}$ . The goodness of this correlation was estimated visually as were the correlations of all the data sets. Considering the appreciable scatter, the fit of the data is excellent. The precision of this estimate is better than 20% as changes of 20% in both  $F$  and  $E_a$  caused a noticeable deterioration in the goodness of the fit.

In Figure 5.7, the correlation results are presented for data set 1, within which the drum rotation rates were varied. In Figure 5.7a, data taken at the lowest rotation rate, 4 rpm, are correlated. For  $E_a = 15.2 \text{ atm}^2 \text{ K}$ , the least conservative lower bound on  $E_a$ , a value of  $F = 1 \text{ cm}^{-3} \text{ s}^{-1}$  was determined to give the best correlation. The model overestimates the short time DV rate and underestimates the long time DV rate. This is a result of the sigmoidal shape of the data which the model can not reproduce even qualitatively. A second set of values of  $E_a = 0.8 \text{ atm}^2 \text{ K}$  and  $F = .7 \text{ cm}^{-3} \text{ s}^{-1}$  was chosen to give a better correlation of the long time data, at the expense, however, of a poorer

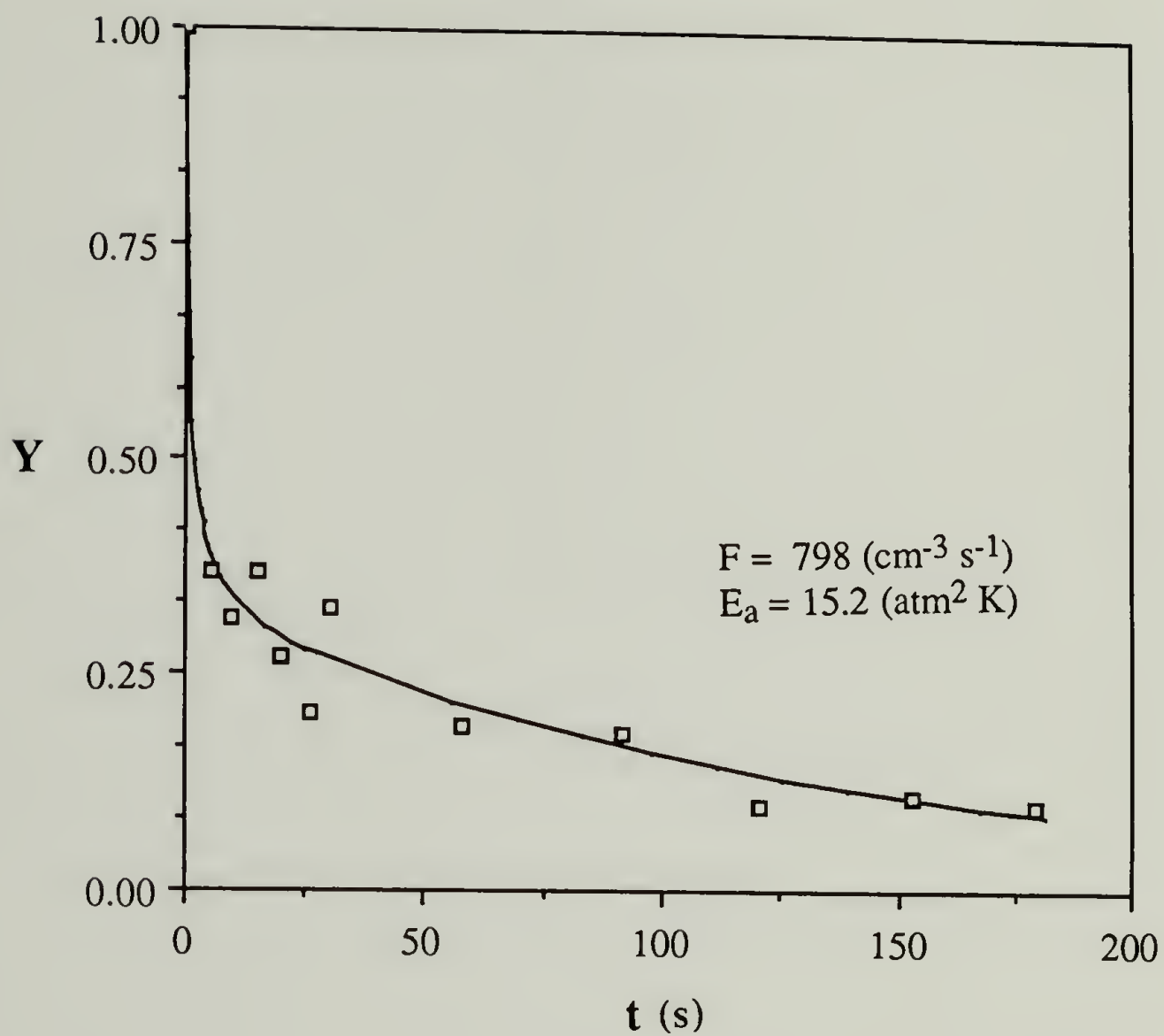


**Figure 5.6** Plot of the rolling drum devolatilizer model's correlation of Biesenberger and Lee's (1986) data 3 for MeCl in PDMS.  $X_0 = 7900$  ppm,  $N = 75$  rpm,  $P = 8$  torr.

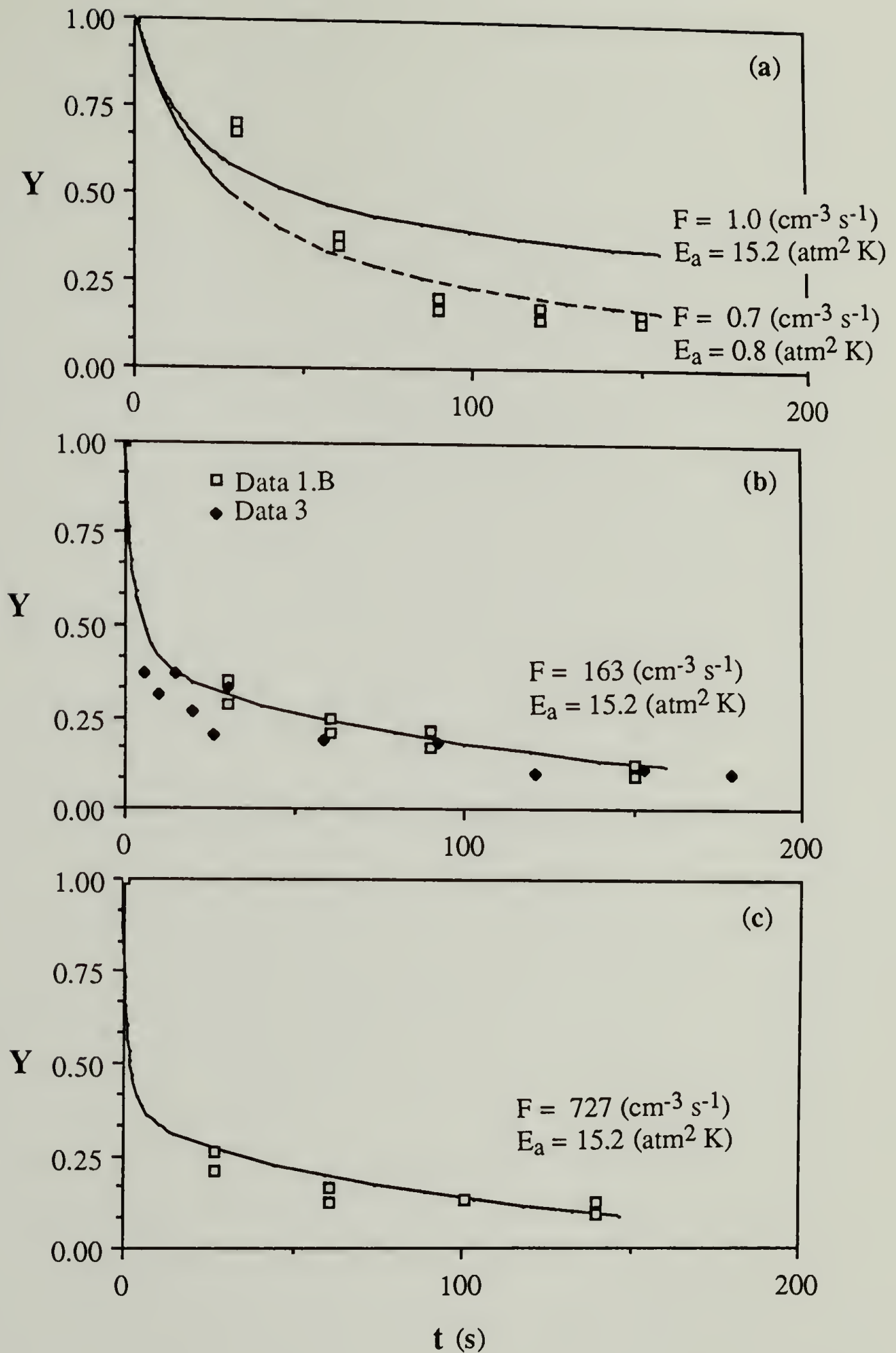


**Figure 5.7** Plots of the rolling drum devolatilizer model's correlation of Biesenberger and Lee's (1986) data set 1 for MeCl in PDMS for  $X_0 \cong 8000$  ppm and  $P = 5$  torr: (a) data 1.A,  $N = 4$  rpm, (b) data 1.B with data 3 for comparison,  $N = 75$  rpm and (c) data 1.C,  $N = 120$  rpm.

correlation of the short time data. The origin of the sigmoidal shape of the data is unclear and cannot be reproduced using our model.

In Figures 5.7b and 5.7c, data sets 1.B and 1.C are plotted along with the model correlations. Data 3 is also plotted in Figure 5.7b for comparison with data 1.B, since the experimental conditions of both data sets are similar. The least conservative lower-bound value of  $E_a = 15.2 \text{ atm}^2 \text{ K}$  was also used to correlate data sets 1.B and 1.C. An excellent correlation is given for  $F$  equal  $163 \text{ cm}^{-3} \text{ s}^{-1}$  for data set 1.B and  $F$  equal  $727 \text{ cm}^{-3} \text{ s}^{-1}$  for data set 1.C.

From the summary of the correlation results given in Table 5.6, it is clear that the model predicts an increase in the nucleation rate,  $F$ , with increasing drum rotation rate, or, equivalently, shear rate. The model's prediction of increasing nucleation rates with increasing shear rates is consistent with Biesenberger and Lee's (1986) observation of more vigorous foaming at higher rotation rates, which they proposed was due to increases in the nucleation rate.

Comparison of data 3, which includes measurements at short times, with data 1.B in Figure 5.7b shows that the data sets agree to within the scatter of the data. However, the correlation of data 1.B gives a poor correlation for data 3. The values of  $F$  fit to the individual data sets differ by a factor of five. This further emphasizes the sensitivity of the correlation to the presence of data at short time.

**Table 5.6** Model parameters that best correlate the rolling drum devolatilizer model to the DV performance data measured by Biesenberger and Lee (1968) on the rolling drum devolatilizer.

RUN	D	$\tau^*$	$f^*$	$\Delta C^*$	$\alpha_1$	$\alpha_2$	$\alpha_3$	$E_a$	F
	( $\text{cm}^2/\text{s}$ )	(s)	( $\text{cm}^{-1} \text{s}^{-1}$ )	(g/cc)				( $\text{atm}^2 \text{K}$ )	( $\text{cm}^{-3} \text{s}^{-1}$ )
1.A	$4 \times 10^{-6}$	1.41	1.947	.00762	.004	.00160	.38	15.2	1.0
"	"	"	"	"	.004	"	.02	0.80	0.70
1.B	"	.199	320.7	.00772	.005	.000976	.37	15.2	163.8
1.C	"	.147	1410	.00762	.01	.000908	.38	"	727.8
2.A	$4 \times 10^{-6}$	.255	726.2	.00851	.01	.00124	.30	15.2	347.7
2.B	"	.464	19590	.00347	.2	.00227	1.8	"	43540
"	"	"	293.8	"	.003	"	.1	.828	114.5
2.C	"	4.02	-	.00339				NO FIT POSSIBLE	
3.A	$4 \times 10^{-6}$	.279	1519	.00744	.02	.00136	.39	15.2	798.6
4.A	$4 \times 10^{-7}$	2.07	1310	.00343	.002	.00321	1.0	.527	1256
"	$4 \times 10^{-8}$	4.47	22800	"	.0075	.00218	1.0	"	21860
4.B	$4 \times 10^{-6}$	.561	808.0	.00391	.0075	.00274	.5	3.61	469.8
"	$4 \times 10^{-7}$	1.21	25000	"	.05	.00187	.5	"	14540
4.C	$4 \times 10^{-6}$	.625	11370	.00402	.1	.00305	.05	4.91	4215

In Figure 5.8, the correlation results are presented for data 2.A and 2.B for which the initial concentration was varied. In Figure 5.8a, data 2.A for  $X_0 = 9000$  ppm is plotted along with the model correlation. For  $E_a = 15.2 \text{ atm}^2 \text{K}$  (the value expected to be a least conservative lower bound), a value of  $F = 347 \text{ cm}^{-3} \text{s}^{-1}$  gives an excellent fit of the data. In Figure 5.8b, data 2.B, for which  $X_0$  was reduced to 3800 ppm, is plotted along with our model correlations. For  $E_a = 15 \text{ atm}^2 \text{K}$ , a value of  $F = 43540 \text{ cm}^{-3} \text{s}^{-1}$  gives the best correlation. The correlation is good, considering that the data exhibits a minimum which is physically unrealistic. However, the value of  $F$  equal to  $43500 \text{ cm}^{-3} \text{s}^{-1}$  required to fit this data is unrealistically high. This value results in a 60% reduction in the solvent content over microseconds. Lower bound values for  $F = 114 \text{ cm}^{-3} \text{s}^{-1}$  and  $E_a = .83 \text{ atm}^2 \text{K}$  give an adequate correlation and a more realistic DV rate. This value of  $E_a$  is 20 times smaller than the least conservative lower bound value. Since without short time data we cannot

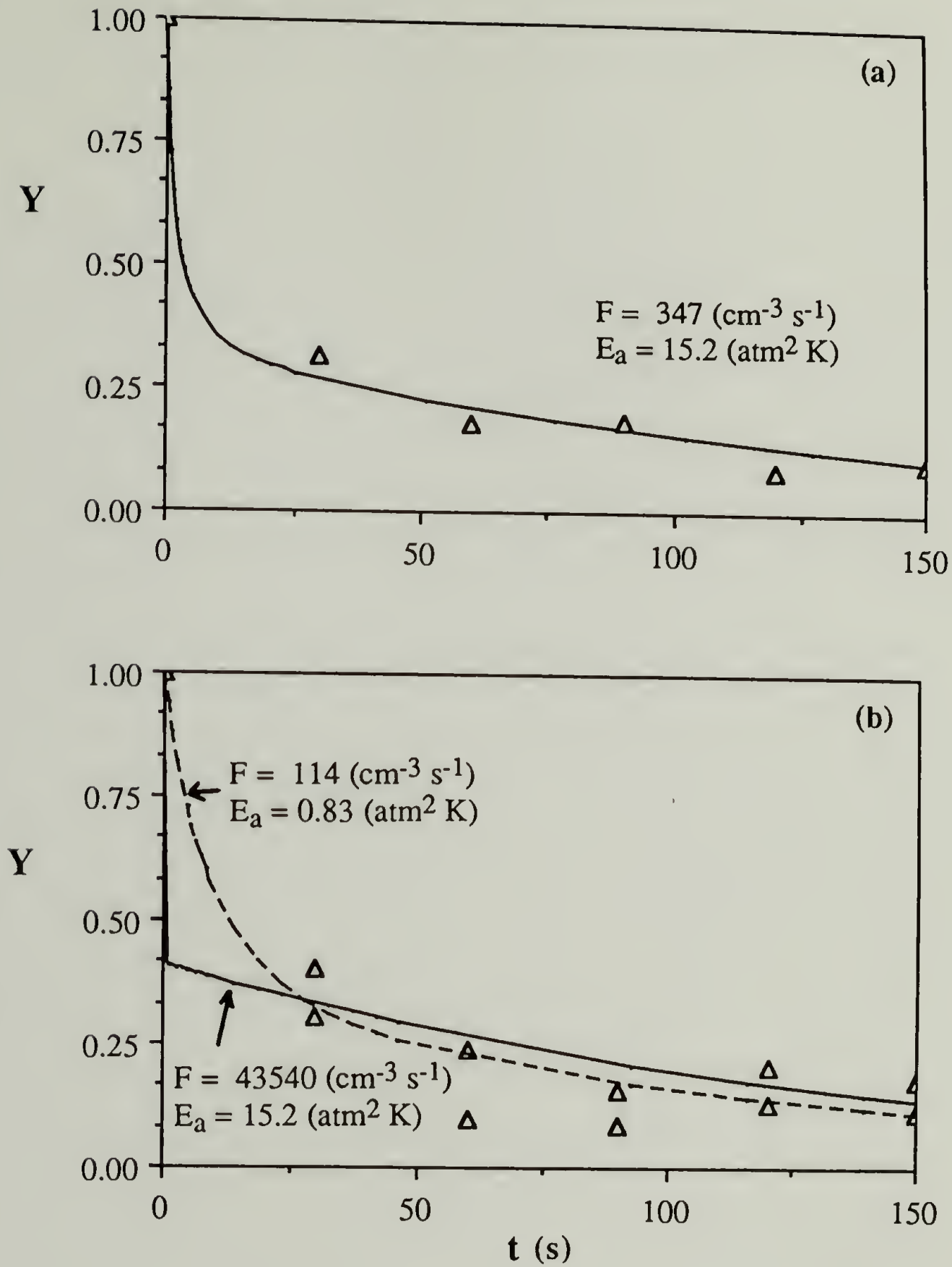


**Figure 5.8** Plots of the rolling drum devolatilizer model's correlation of Biesenberger and Lee's (1986) data 2.A and 2.B for MeCl in PDMS at  $N = 75$  rpm and  $P = 8$  torr: (a) data 2.A,  $X_0 = 9000$  ppm and (b) data 2.B,  $X_0 = 3800$  ppm.



unambiguously estimate the actual value for  $E_a$ , but only some lower bound, we cannot confidently conclude that the value of  $E_a$  varies with the concentration of solvent.

The results of the correlation of data set 4, for which a series of Freons<sup>®</sup> were devolatilized from PDMS, are presented in Figures 5.9 to 5.11. Values of the diffusivities of these Freons<sup>®</sup> in PDMS were not available in the literature. They were estimated by choosing values of  $D$  which could give an acceptable correlation of the data in the interfacial diffusion-controlled regime, approached at long times after foaming ceases. In Figure 5.9, results of the correlation of data 4.A for the most soluble Freon<sup>®</sup>, Freon-114<sup>®</sup>, are plotted. Due to the appreciable scatter in the data, a range of values of  $D$  between  $4 \times 10^{-8}$  to  $4 \times 10^{-7}$   $\text{cm}^2/\text{s}$  was found to give an acceptable correlation for the long time data. Values of  $D$  larger than  $4 \times 10^{-7}$   $\text{cm}^2/\text{s}$  overestimated the long time DV rate and values of  $D$  smaller than  $4 \times 10^{-8}$   $\text{cm}^2/\text{s}$  underestimated the long time DV rate. A value of  $E_a = .53 \text{ atm}^2 \text{ K}$  gives a good correlation of the data for both values of  $D$ . However, the values of  $F$  which best correlate the data depend on the value chosen for the diffusivity. For  $D = 4 \times 10^{-8}$   $\text{cm}^2/\text{s}$ ,  $F = 21800 \text{ cm}^{-3} \text{ s}^{-1}$  gave an acceptable correlation of the data. For  $D = 4 \times 10^{-7}$   $\text{cm}^2/\text{s}$ ,  $F = 1250 \text{ cm}^{-3} \text{ s}^{-1}$  also gave an acceptable correlation.

In Figure 5.10, data 4.B for Freon-22<sup>®</sup> is correlated. Values of  $D$  between  $4 \times 10^{-7}$  and  $4 \times 10^{-6}$   $\text{cm}^2/\text{s}$  give a good correlation of the long time data. Comparison with the diffusivities which best correlate the Freon-114<sup>®</sup> data indicates that Freon-22<sup>®</sup> should have a larger diffusivity. This is reasonable, as Freon-114<sup>®</sup> is a larger molecule. A value of  $E_a = 3.6 \text{ atm}^2 \text{ K}$  gave a good correlation of the data over the range of  $D$ . However, the values of  $F$  which could correlate the data over the range of acceptable diffusivities varied between 470 to 14500  $\text{cm}^{-3} \text{ s}^{-1}$ .

In Figure 5.11, data 4.C for the least soluble Freon<sup>®</sup>, Freon-13<sup>®</sup>, is correlated. A large range of values of  $D$  between  $10^{-5}$  to  $10^{-8}$   $\text{cm}^2/\text{s}$  could give an acceptable fit of this data. This is due to the insensitivity in the slope of  $Y$  versus  $t$  plots at long times to changes in  $D$  when  $Y$  is small ( $Y < .1$ ). Since it is not clear what are acceptable values of

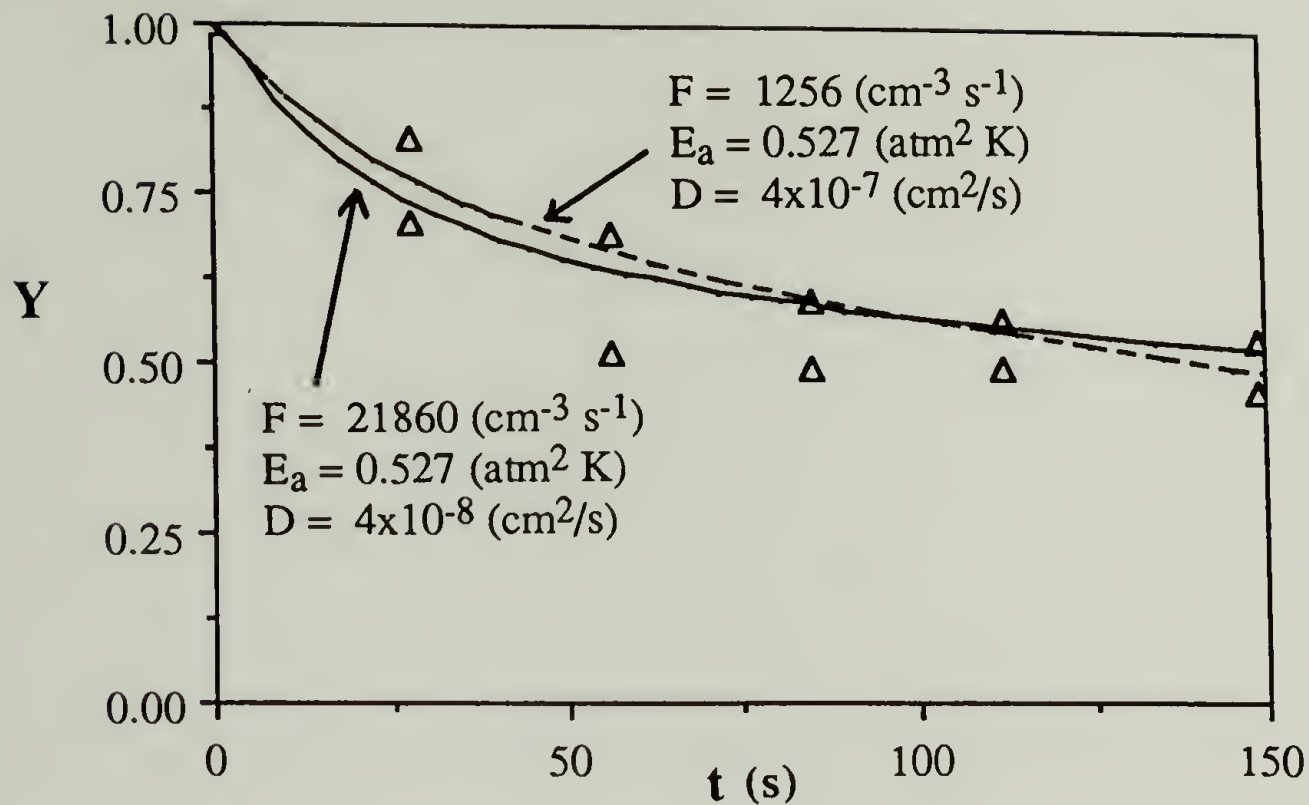


**Figure 5.9** Plot of the rolling drum devolatilizer model's correlation of Biesenberger and Lee's (1986) data 4.A for Freon-114<sup>®</sup> in PDMS.  $X_0 = 4300$  ppm,  $N = 75$  rpm,  $P = 7$  torr.

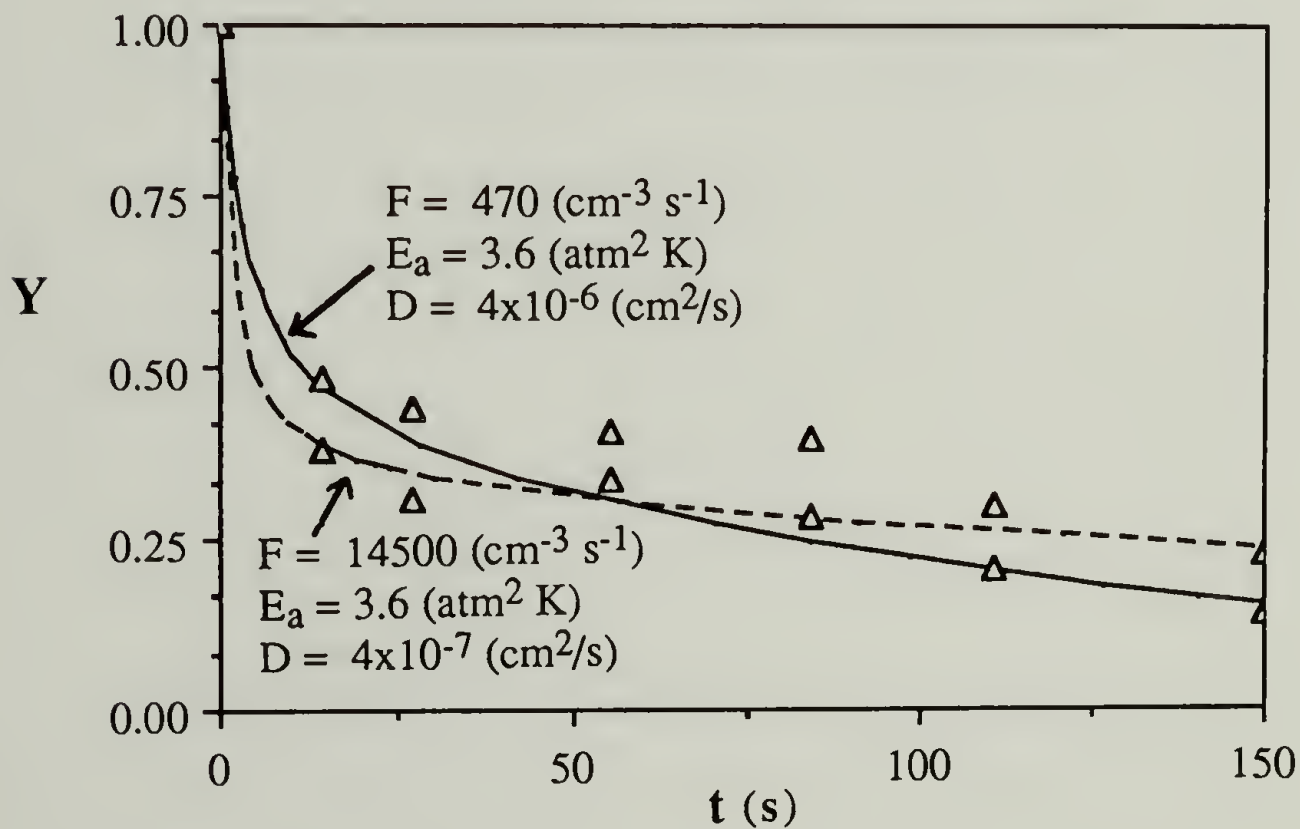


**Figure 5.10** Plot of the rolling drum devolatilizer model's correlation of Biesenberger and Lee's (1986) data 4.B for Freon-22<sup>®</sup> in PDMS.  $X_0 = 4260$  ppm,  $N = 75$  rpm,  $P = 7$  torr.

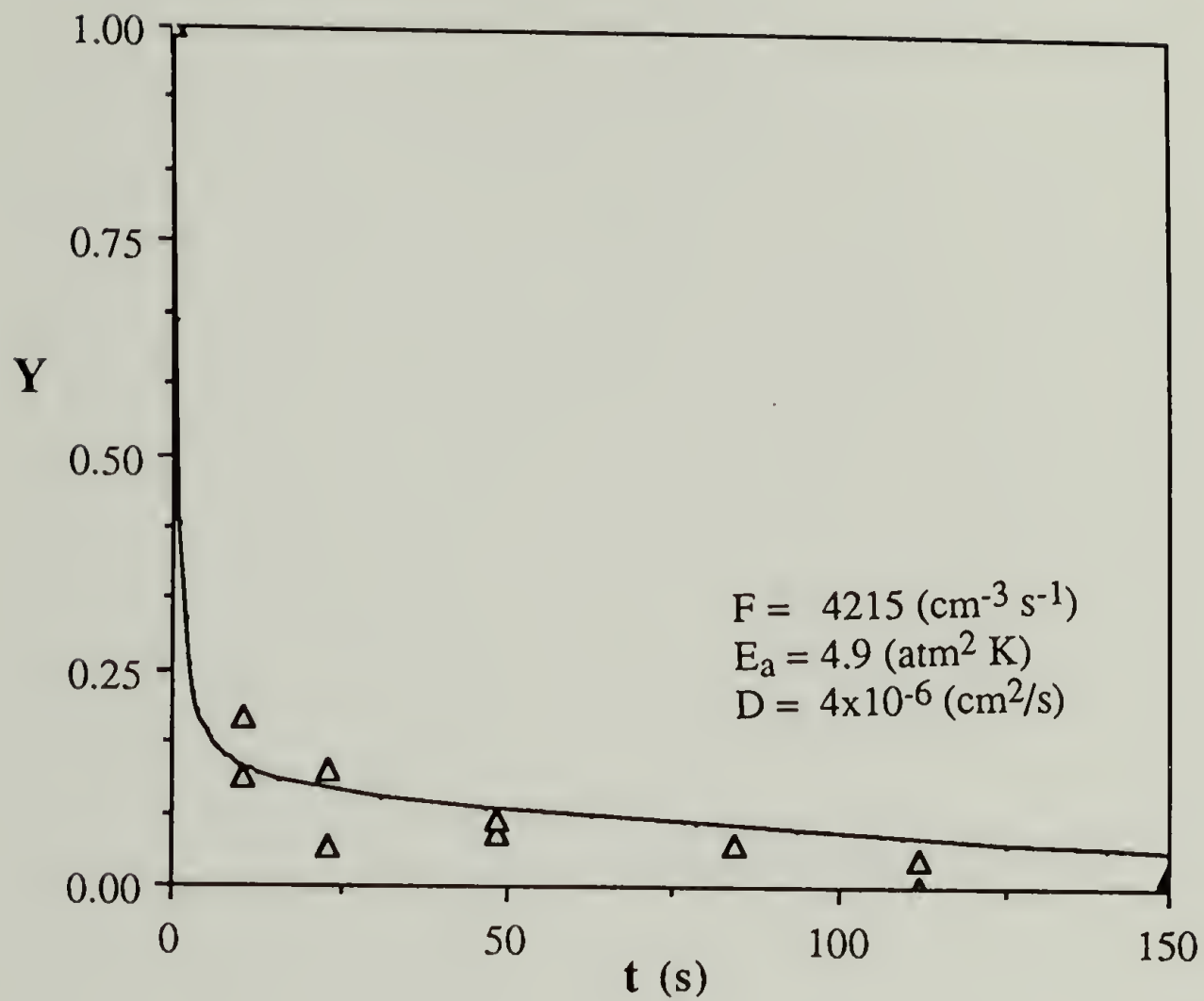


**Figure 5.11** Plot of the rolling drum devolatilizer model's correlation of Biesenberger and Lee's (1986) data 4.C for Freon-13<sup>®</sup> in PDMS.  $X_0 = 4200$  ppm,  $N = 75$  rpm,  $P = 7$  torr.

D, a value of  $D = 4 \times 10^{-6} \text{ cm}^2/\text{s}$  was chosen. This value was chosen because the diffusivity of Freon-13<sup>®</sup> is expected to be of order of the diffusivity of Freon-22<sup>®</sup>, since the sizes and atomic constituents of the two molecules are similar. For  $D = 4 \times 10^{-6} \text{ cm}^2/\text{s}$ , values of  $F = 4215 \text{ cm}^{-3} \text{ s}^{-1}$  and  $E_a = 4.9 \text{ atm}^2 \text{ K}$  gave a good correlation of the data. The small overprediction of the data at long times is tolerable as the long time data is expected to be slightly greater than that shown in Figure 5.11. Errors introduced while extracting data from graphs published by Biesenberger and Lee (1986) resulted in negative values of Y at 120 and 150 s (set to a value of zero in Figure 5.11). Since negative values of Y are impossible, the data probably err systematically low.

The model's predictions of the effects of decreasing solubility of the solvent on the DV performance are qualitatively consistent with the effects evident in data set 4. The model predicts that the effect of decreasing the solubility (i.e. increasing  $K_c$ , which decreases  $\alpha_3$ ) is to decrease the supersaturation at which nucleation ceases. This behavior was demonstrated previously in Figure 4.7b and is consistent with trends observed in the DV performance data shown in Figure 5.5 for data set 4. So the model predicts, at least qualitatively, how changes in the solubility of the solvent will affect the DV performance. This indicates that the observed improvements in the DV performance accompanying decreases in the solvent's solubility are likely due to an increase in the time over which bubble nucleation can be sustained, rather than due to an increase in the rate of mass transfer to bubbles. Decreasing the solubility allows that rapid DV by foaming can continue down to smaller supersaturations, extending the time over which foam-enhanced DV occurs and delaying the onset of mass transfer control by the much slower mechanism of interfacial diffusion.

The values of F and  $E_a$  estimated by correlating Biesenberger and Lee's data contain large uncertainties for several reasons. The data exhibit significant scatter within runs and a lack of reproducibility among experiments at identical conditions. As well, counter-intuitive behavior is displayed, such as a sigmoidal shape in the Y vs t plot for Data 1.A.

Also, physically unrealistic minima were observed in some of these plots. The lack of short time data precludes unique estimates for  $F$  and  $E_a$ . In addition, accurate values of the diffusivity were not available, which introduces great uncertainty into the estimates of  $F$ .

In spite of the significant uncertainties in the data and in the parameter estimates, valuable insights may be gained from these experiments. The observed increases in the DV performance with increasing shear rate are real, as the differences between the data measured at varying rotation rates are greater than the scatter in the data. Our model indicates that this is caused by an increase in the nucleation rate with increasing shear rate. As well, improvements in the DV performance with decreasing solubility of the solvent are clearly real and could not be attributed to experimental uncertainty. Our model indicates that these improvements accompanying decreases in the solvent solubility result from a lowering of the critical supersaturation required to sustain nucleation.

### 5.3.3 Comparison With Latinen's Model

As was done for the single screw devolatilizer model, the correlative abilities of the rolling drum devolatilizer model were compared with those of Latinen's (1962) model. Although Latinen did not develop a model for the rolling drum devolatilizer, his model for the single screw devolatilizer was modified to describe the rolling drum devolatilizer in the same manner that our single screw devolatilizer model was modified. Since there is no axial flow in the rolling drum devolatilizer, axial dispersion was neglected in Latinen's model.

Data 3 of Biesenberger and Lee's experiments was chosen as the best data to be used for comparison, as it contains data taken at the shortest times and should give the most reliable comparison. Data 3 is plotted in Figure 5.12 along with the predictions of Latinen's model for effective diffusivities ranging between  $4 \times 10^{-6}$  to  $4 \times 10^{-3}$  cm<sup>2</sup>/s. The prediction of Latinen's model using the predicted diffusivity for MeCl in PDMS,  $4 \times 10^{-6}$

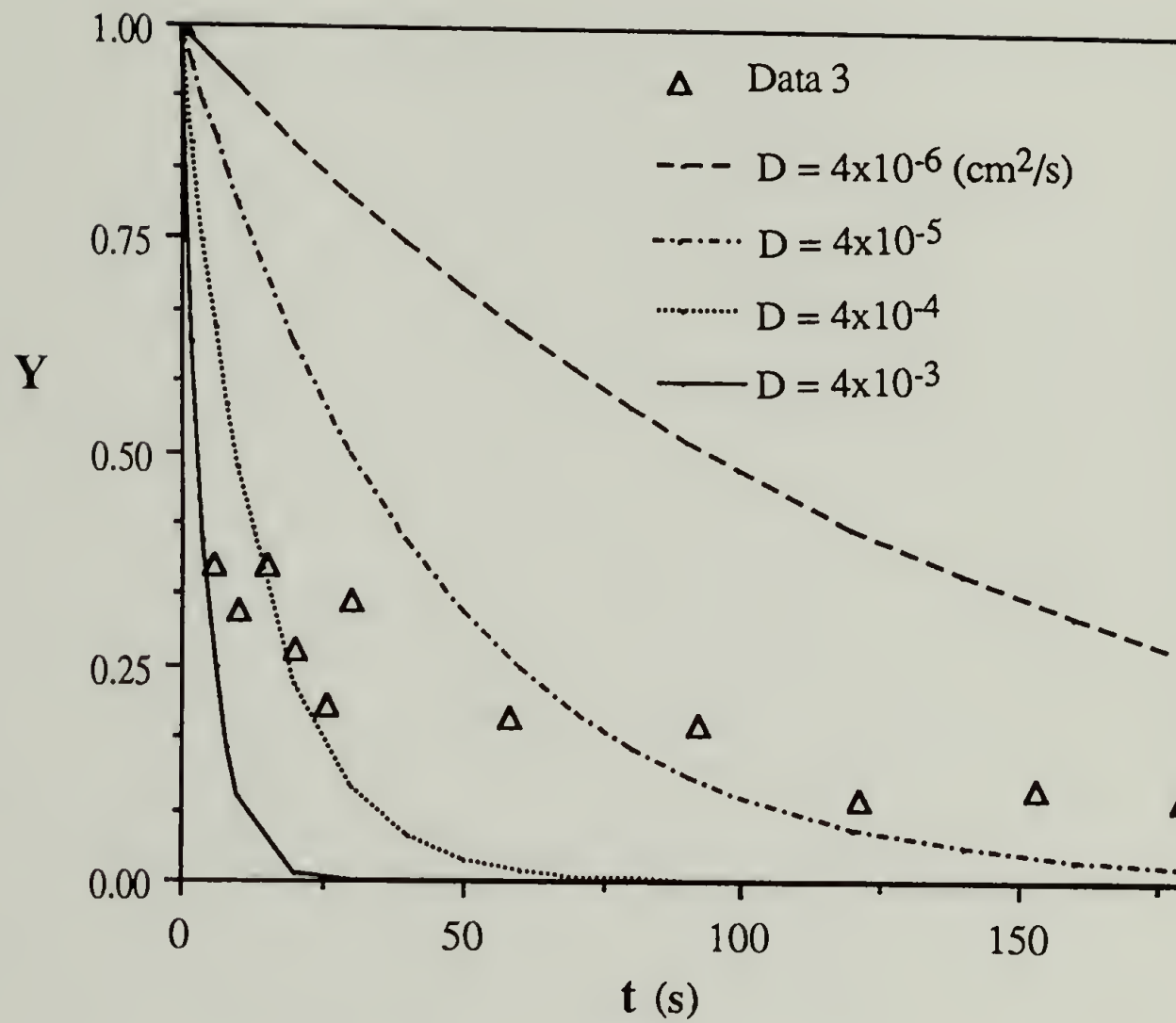


**Figure 5.12** Plots of correlations of Biesenberger and Lee's (1986) data 3 given by Latinen's (1962) model for varying values of the effective diffusivity.

cm<sup>2</sup>/s, grossly underestimates the DV rate. To fit the short time data, Latinen's model requires an effective diffusivity three orders of magnitude larger than the actual value. Although the short time data is adequately fit for  $D = 4 \times 10^{-3}$  cm<sup>2</sup>/s, the long time data is grossly underestimated.

This comparison reveals firstly that our model is superior to Latinen's model, since it can correlate both the short and long time DV regimes well, while using the actual value of the diffusivity. Secondly, it reveals that any realistic model of foam-enhanced DV must account for the *two* time scales of DV associated with the distinct processes of foaming and interfacial diffusion. Latinen's model includes only one time scale, that for interfacial diffusion, and cannot correlate both regimes of DV.

The experiments of Biesenberger and Lee (1988) show that DV can occur very rapidly over short times during which foaming dominates the DV rate. At later times when the supersaturation has been reduced below the critical level required to sustain nucleation, foaming ceases and DV occurs by the much slower mechanism of interfacial diffusion. This suggests that the performance of a devolatilizer may be limited by the critical superpressure required to sustain nucleation. Attempts at optimizing the DV performance might be best directed at reducing the critical superpressure of the solution, or, equivalently,  $E_a$ . This might be done by adding nucleating agents, perhaps heterogeneous particles or surfactants (i.e. which lower the surface tension), to reduce the energetics of nucleation.

A common industrial practice for improving the performance of a devolatilizer is the addition of a *stripping agent*, usually a volatile, low molecular weight liquid (water is the most commonly used stripping agent). The beneficial effect of a stripping agent on the DV performance has been attributed to the fact that it adds free volume to the solution and enhances DV by increasing the diffusivity (Vrentas, Duda and Ling; 1985) and, hence, the mass transfer rate to bubbles. However, these performance improvements are more likely caused by an increase in the solution vapor pressure attending the addition of the volatile

stripping agent. According to our model, this would sustain nucleation and foaming for longer times, down to lower concentrations of the solvent. Although both effects would enhance the DV performance, the extension of the foaming regime to smaller supersaturations has the potential for making the greater contribution.

The existence of a critical supersaturation required to sustain foaming has important implications in the design of DV equipment. In a typical devolatilizer, rapid foam enhanced DV might occur only over a fraction of the length of the equipment, during which the superpressure exceeds the critical value. After this section, foaming would cease and DV would occur by the much slower mechanism of interfacial diffusion. For the single screw devolatilizer, it may be most economical to design the length of the DV section to be only as long as the length over which foaming occurs. Since extruders are expensive, the cost of the section of the devolatilizer over which the inefficient interfacial diffusion regime would occur may not be worth the return from the attendant small increase in the devolatilizer's performance. If DV beyond the foaming regime is required, a cheaper alternative to a long, single screw devolatilizer may be a staged process consisting of a shorter single screw devolatilizer operating in the foam-controlled regime only, followed by a less expensive devolatilizer, perhaps a wiped film evaporator, designed to operate efficiently and cheaply in the diffusion-controlled regime.



## CHAPTER VI

### APPROXIMATE MODELS AND A DESIGN MODEL OF DV

#### 6.1 Approximate Models of DV

The models we have developed of foam-enhanced DV are complicated. As well, they must be solved by numerical methods using a computer which can be costly and time consuming. It would be useful to reduce the complexity of the models and the computation time required for their solution. Simplified models would be valuable to engineers for use in devolatilizer design.

##### 6.1.1 The Quasi-Steady State Model

Our models of DV may be simplified if the bubble age distribution approaches a *quasi-steady state (QSS)*. A quasi-steady state distribution is one that changes slowly relative to the characteristic time scale of the process. If a quasi-steady state is approached, we may simplify the rolling drum model equations by approximating the time derivative of the moments of the distribution to be zero

$$\frac{dM_n}{dT} \cong 0 \quad 6.1$$

This is the *quasi-steady state assumption*. For the single screw devolatilizer model, the spatial derivative of the moments are set equal to zero.

Applying the quasi-steady state assumption to the rolling drum model, the left hand side of the moment expressions, equations 4.12 with Z replaced by T, are replaced by zeros. Solving explicitly for the 1/2 moment gives

$$(M_{1/2})_{QSS} = \frac{1}{4} \sqrt{\frac{\pi}{3}} \exp\left[\alpha_3 \left(1 - \frac{1}{Y^2}\right)\right] \frac{1}{Y} \quad 6.2$$

Substituting this expression into the mass balance for  $M_{1/2}$  gives a single ODE describing the rolling drum devolatilizer's performance.

$$\left(\frac{dY}{dT}\right)_{\text{QSS}} = -12\alpha_1 \exp\left[-\alpha_3\left(\frac{1}{Y^2} - 1\right)\right]Y^2 - \frac{2}{\pi^{1/4}}\alpha_2 Y \quad 6.3$$

This will be called the *Quasi-Steady State Model*.

The expression for the QSS 1/2 moment for the single screw devolatilizer model is identical to that of the rolling drum model with  $T$  replaced by  $Z$ . The QSS DV rate expression for the single screw devolatilizer is identical to that for the rolling drum devolatilizer, equation 6.3, with the exception that the  $\alpha_2$  term is smaller by a factor of  $1/\pi^{1/4}$ . In addition to the approximate QSS Model, other approximate models will be developed in the following sections for the single screw and rolling drum devolatilizers. Since for all these approximate models, the single screw and rolling drum devolatilizer models will differ by only a factor of  $1/\pi^{1/4}$  in the  $\alpha_2$  term, only the approximate models of the rolling drum devolatilizer will be presented.

To determine if the bubble age distribution indeed approaches a quasi-steady state, we may inspect the distribution predicted by the Full Model of the rolling drum devolatilizer. In Figure 6.1, a surface plot of the dimensionless bubble age distribution predicted by this model is presented. This is the distribution predicted for the model parameters that best correlated data 3 of Biesenberger and Lee:  $\alpha_1 = 0.02$ ,  $\alpha_2 = 0.00136$  and  $\alpha_3 = 0.4$ . From this surface plot it is evident that, after a short induction time of about one dimensionless time unit, the bubble age distribution changes slowly relative to the characteristic time scale. Additional evidence that a quasi-steady state distribution exists is presented in Figure 6.2, which plots both the dimensionless moments of this distribution and the dimensionless concentration versus dimensionless time. After the short induction time, the moments level off as the distribution approaches a quasi-steady state. This indicates that, for these values of the model parameters, the QSS model is valid at long times but is invalid at short times. It is therefore desirable to construct a short time solution.

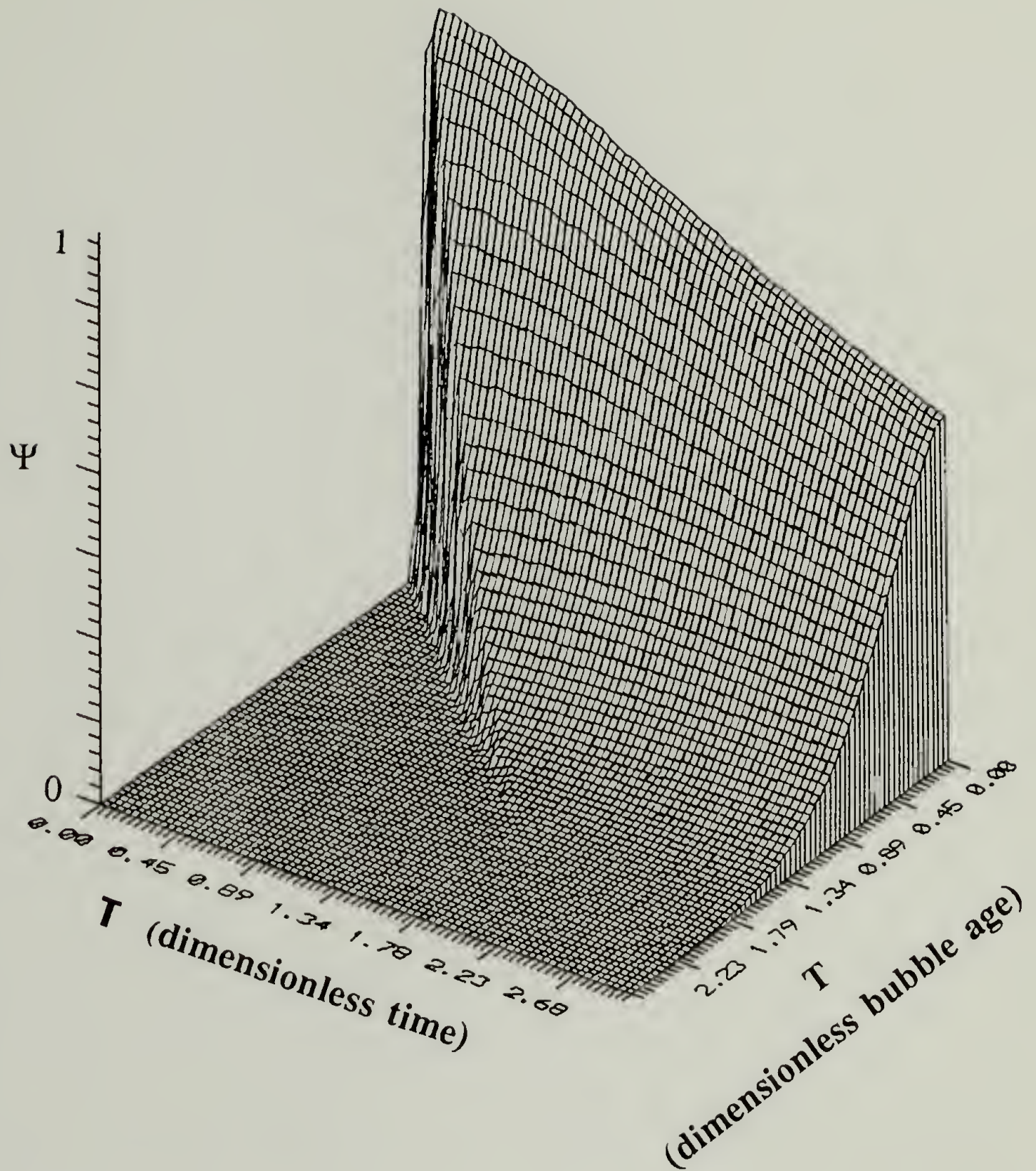


**Figure 6.1** Surface plot of the dimensionless bubble age distribution predicted by the Full Model of the rolling drum devolatilizer.  $\alpha_1 = 0.02$ ,  $\alpha_2 = 0.00136$  and  $\alpha_3 = 0.4$ .

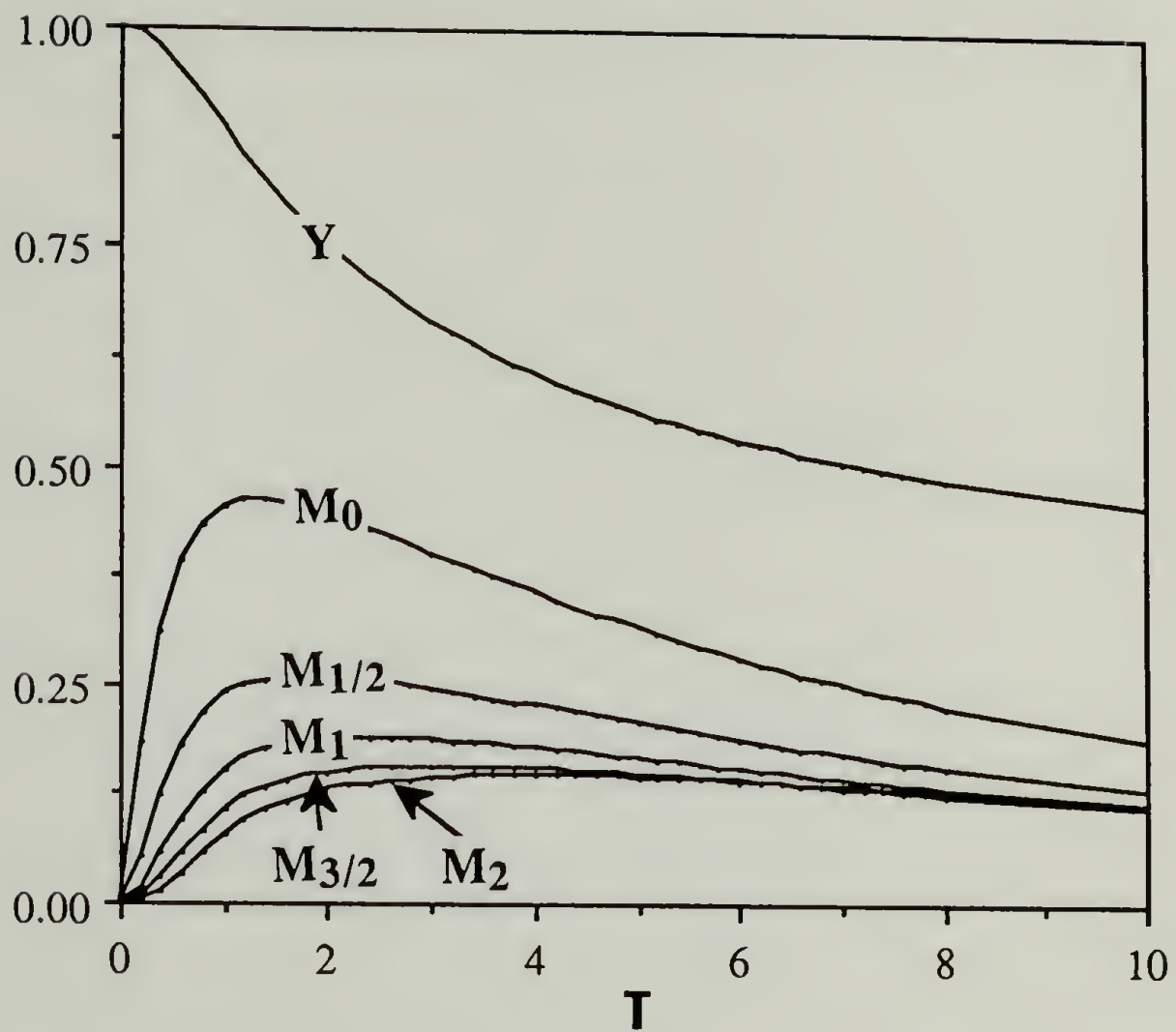


**Figure 6.2** Plots of the DV performance and the dimensionless moments of the bubble age distribution predicted by the Full Model of the rolling drum devolatilizer.  $\alpha_1 = 0.02$ ,  $\alpha_2 = 0.00136$  and  $\alpha_3 = 0.4$ .

### 6.1.2 The Inner Model

Aiken and Lapidus (1974) gave a clear discussion of the equivalence between the QSS representation of a set of ODE's (i.e. the mass balance and population balance expressed in terms of the moments) and the zero'th order approximation to the singularly perturbed representation of these same equations. This equivalence indicates that our model equations may exhibit behavior similar to that occurring for singular perturbation type problems. There could be two time scales for the solution vector (i.e. composed of  $Y$  and the moments) and the solution could exhibit a *boundary layer*. Indeed, a boundary layer is predicted by the model at short times, as is evident in Figure 6.2. The QSS model will be valid at long times, beyond the boundary layer, after which a quasi-steady state distribution is reached. The region beyond the boundary layer is commonly referred to as the *outer region* and the boundary layer region is referred to as the *inner region*. The solution which is valid over the boundary layer is termed the *inner solution*.

If the dimensionless concentration changes negligibly over the boundary layer, we may decouple the population balance from the mass balance by approximating the dimensionless concentration to be constant and equal to 1. Setting  $Y$  equal to 1, an explicit expression for the bubble age distribution is derived by integrating the population balance analytically along the characteristics. This gives

$$\Psi_{\text{inner}} = \begin{cases} \exp\left[-8\sqrt{\frac{3}{\pi}} T^{3/2}\right] & T \leq \mathbf{T} \\ 0 & T > \mathbf{T} \end{cases} \quad 6.4$$

Integrating this expression gives an expression for the 1/2 moment of the distribution

$$(M_{1/2})_{\text{inner}} = \frac{1}{4}\sqrt{\frac{\pi}{3}} \left( 1 - \exp\left[-\frac{8}{\sqrt{3\pi}} T^{3/2}\right] \right) \quad 6.5$$

which when substituted into the mass balance gives the *Inner Model*.

$$\left(\frac{dY}{dT}\right)_{\text{inner}} = -12 \alpha_1 \left[ 1 - \exp\left(\frac{-8}{\sqrt{3\pi}} T^{3/2}\right) \right] Y^3 - \frac{2}{\pi^{1/4}} \alpha_2 Y \quad 6.6$$

Inspection of Figure 6.2 shows that over the boundary layer between  $T$  greater than zero and less than about one, the dimensionless concentration changes by approximately 10%. Comparison of the solution of the Inner Model with that of the Full Model would be necessary to determine the acceptability of the Inner Model's approximation that  $Y$  is nearly constant and equal to 1 over the boundary layer.

### 6.1.3 The Patched Model

A more accurate approximation to the Full Model solution over both the boundary layer and the outer region can be derived by patching the Inner Model together with the QSS Model. This model is called the *Patched Model*. The Patched Model consists of the Inner Model, equation 6.6, applied over the boundary layer and the QSS Model, equation 6.3, applied over the outer region. The boundary layer is defined to be between  $0 < T < T_{\text{patch}}$  and the outer region is defined to be between  $T_{\text{patch}} < T$ , where  $T_{\text{patch}}$  is the edge of the boundary layer. The Patched Model is expected to be more accurate than the Inner and QSS Models if the concentration changes negligibly over the boundary layer, since the approximations of the Patched Model will be valid over the entire time domain rather than over just the boundary layer or the outer region.

### 6.1.4 The Instantaneous Quasi-Steady State Model

An alternate approach to developing an approximate solution to the Full Model equations can be applied if the dimensionless concentration,  $Y$ , changes negligibly over the lifetime of the bubbles. If so, when solving for the population balance, we may approximate  $Y$  is being constant, although not necessarily equal to 1 as for the Inner Model. Treating  $Y$  as a constant, the population balance is solved independently of the mass balance by integrating along the characteristics.

$$(\Psi)_{IQSS} = \begin{cases} \exp\left[-\alpha_3\left(\frac{1}{Y^2} - 1\right)\right] \exp\left[-\frac{8}{\sqrt{3\pi}} Y T^{3/2}\right] & T \leq \mathbf{T} \\ 0 & T > \mathbf{T} \end{cases} \quad 6.7$$

This simple expression approximates the distribution over all time, provided the concentration changes slowly over the lifetimes of most of the bubbles. This distribution will be called the *instantaneous quasi-steady state (IQSS) distribution*. It is analogous to the instantaneous QSS distribution of polymer chain lengths that can occur in a batch free radical polymerization reactor. Consider a well mixed polymer batch reactor for which the average lifetime of a growing free radical chain is on the order of 1 second (a value typical of industrial reactors). The distribution of polymer chain lengths that are formed over this period depends on the monomer concentration. If the monomer concentration changes negligibly over 1 second, as is commonly the case in industrial batch free radical polymerization operations, the majority of the free radical chains formed at any instant will have grown in an environment of constant monomer concentration. Under these circumstances, the analysis of the polymer reaction kinetics can be well approximated assuming the monomer concentration to be constant over the lifetime of the growing chains (Tirrell, Galvin and Laurence; 1986). This is the quasi-steady state assumption in polymer reaction kinetics. The result is a quasi-steady state distribution of free radical chain lengths which changes slowly with time due to the slowly decreasing monomer concentration.

The expression for the 1/2 moment of the IQSS distribution is derived by integrating equation 6.7.

$$(M_{1/2})_{IQSS} = \frac{1}{4} \sqrt{\frac{\pi}{3}} \exp\left(-\alpha_3 \left[\frac{1}{Y^2} - 1\right]\right) \left(1 - \exp\left[-\frac{8}{\sqrt{3\pi}} Y T^{3/2}\right]\right) \frac{1}{Y} \quad 6.8$$

In the limit as  $\mathbf{T}$  approaches zero (i.e. at short times when  $Y$  equals 1), the second exponential in equation 6.8 can be expressed as an infinite series in integer powers of  $\mathbf{T}$  and truncated to first order in  $\mathbf{T}$ .  $(M_{1/2})_{IQSS}$  then reduces identically to that for the Inner

Model, equation 6.5. As well, at long times, the expression for  $(M_{1/2})_{IQSS}$  approaches that of the QSS Model, equation 6.2.

Substituting this expression for  $(M_{1/2})_{QSS}$  into the mass balance gives a single ODE describing the performance of the devolatilizer.

$$\left(\frac{dY}{dT}\right)_{IQSS} = -12 \alpha_1 \exp\left[-\alpha_3 \left(\frac{1}{Y^2} - 1\right)\right] \left[1 - \exp\left(\frac{-8}{\sqrt{3\pi}} Y T^{3/2}\right)\right] Y^2 - \frac{2}{\pi^{1/4}} \alpha_2 Y \quad 6.9$$

This will be called the *IQSS Model*.

### 6.1.5 Comparison of the Approximate Models with the Full Model

The accuracy of the solutions to the approximate models was estimated by comparison with the Full Model solution. Figures 6.3 to 6.5 present comparisons of the solution for the Full Model with solutions for the approximate models. The values of the dimensionless model parameters used in the simulations are  $\alpha_1 = 0.02$ ,  $\alpha_2 = 0.00182$  and  $\alpha_3 = 0.4$ . These values are similar to the values of the model parameters which gave a good correlation of the DV performance data of Coughlin and Canevari (1969) and Biesenberger and Lee (1986).

In Figure 6.3a and b, the dimensionless concentration and the dimensionless 1/2 moment are plotted for times less than  $T = 10$  for the Full Model and for the approximate models. In Figure 6.4, the same data is plotted as the fractional differences between the Full model solution and the approximate model solution. The fluctuations shown at short times in Figure 6.4b are contributed by numerical errors in the integration of  $M_{1/2}$ . Increasing the number of characteristics can remove these fluctuations. For  $T < 10$ , the dimensionless concentrations predicted by the Inner, Patched ( $T_{patch}$  was chosen to be 1.5, approximately the width of the boundary layer) and IQSS Models agree to better than about 2% with the Full Model solution. The QSS solution agrees to better than about 8%. Notice that, at  $T = 0$ , the QSS Model predicts a finite value for  $M_{1/2}$ , whereas the initial



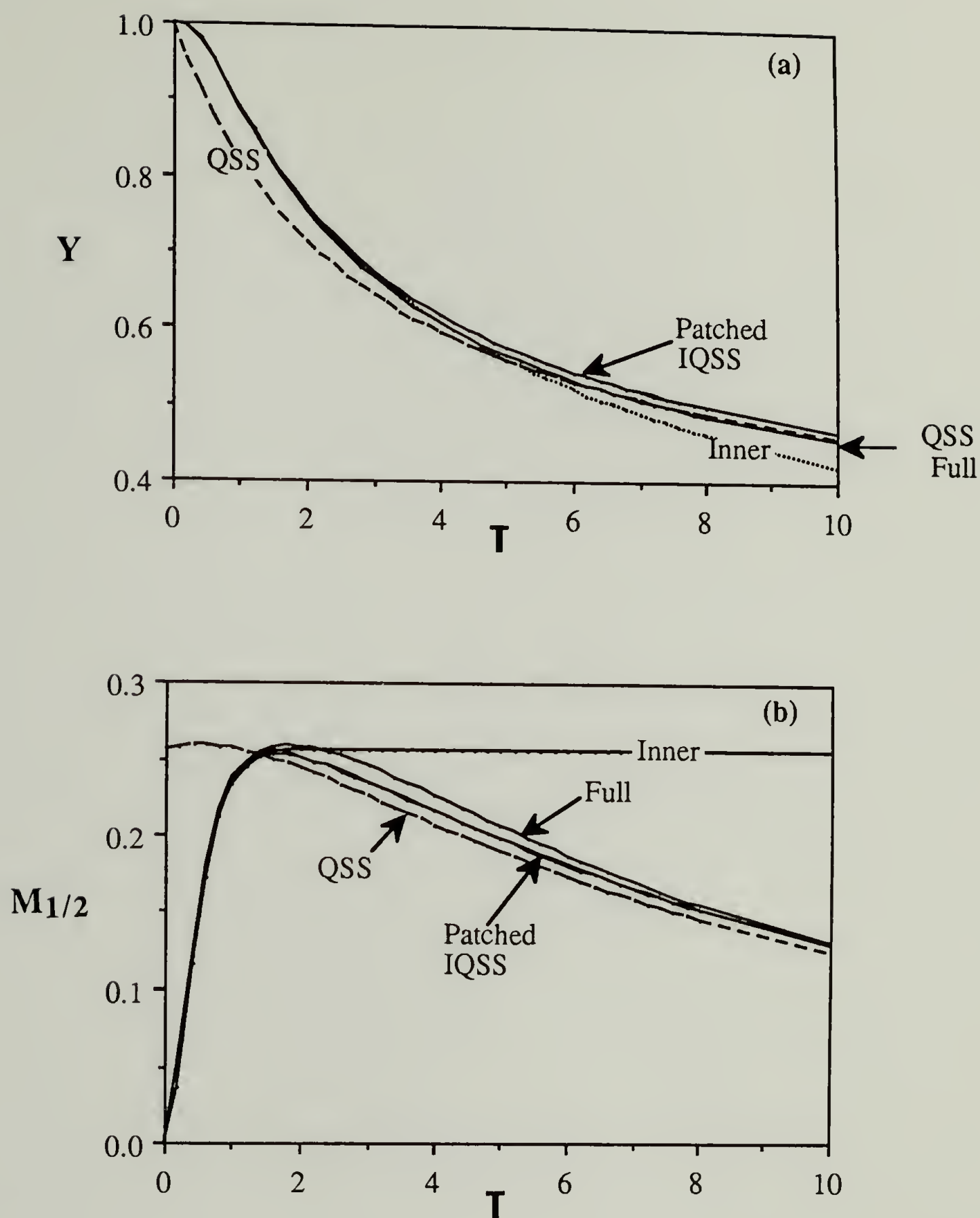


**Figure 6.3** Comparison of the solution of the Full Model of the rolling drum devolatilizer with the solutions given by the approximate models.  $\alpha_1 = 0.02$ ,  $\alpha_2 = 0.00182$  and  $\alpha_3 = 0.4$ .

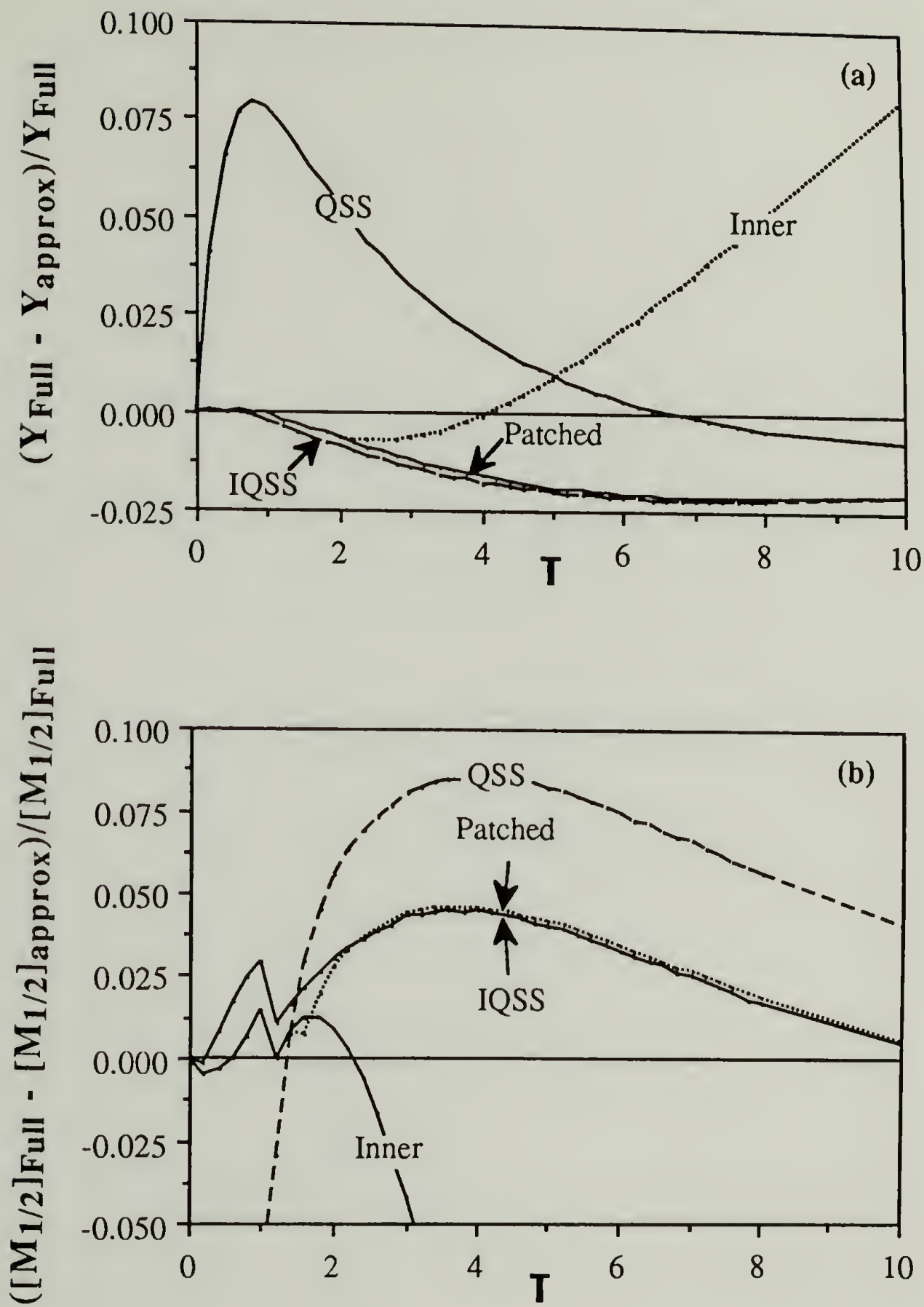


**Figure 6.4** Comparison of the solution of the Full Model of the rolling drum devolatilizer with the solutions given by the approximate models.  $\alpha_1 = 0.02$ ,  $\alpha_2 = 0.00182$  and  $\alpha_3 = 0.4$ .

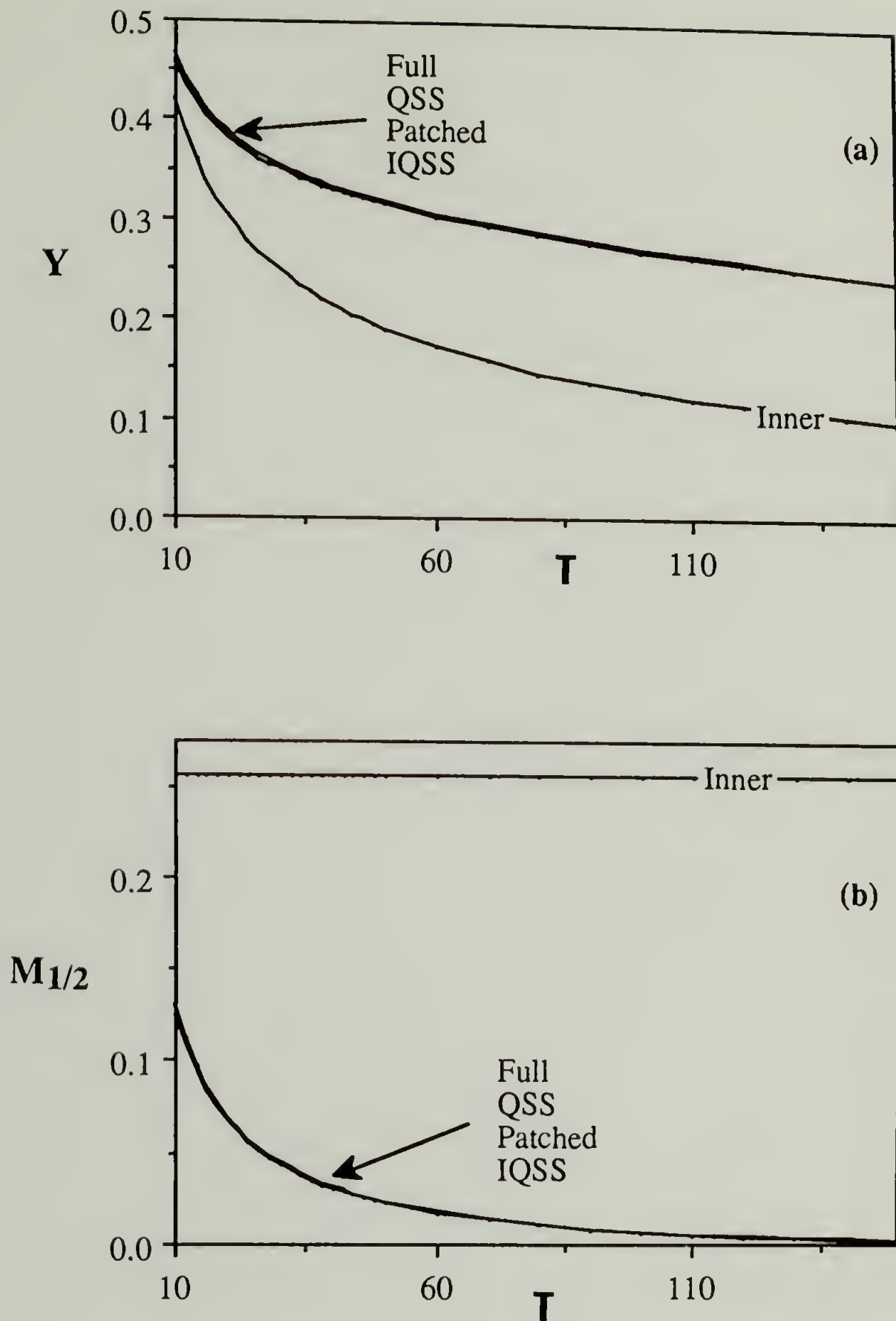


**Figure 6.5** Comparison of the solution of the Full Model of the rolling drum devolatilizer with the solutions given by the approximate models.  $\alpha_1 = 0.02$ ,  $\alpha_2 = 0.00182$  and  $\alpha_3 = 0.4$ .

condition is  $M_{1/2} = 0$ . This is consistent with the expectation that the QSS Model will not be valid over the boundary layer. Figure 6.5 presents comparisons of the Full Model and the approximate models for  $10 < T < 150$ . The QSS, Patched and IQSS Model solutions all agree closely with the Full Model solution over this range. However, the inner model solution diverges from the Full Model solution at long times as anticipated.

In Figures 6.6 to 6.9, plots of comparisons of the Full Model and the approximate model solutions are presented for values of  $\alpha_1 = 0.2$ ,  $\alpha_2 = 0.00182$  and  $\alpha_3 = 0.4$ .  $\alpha_1$  was increased by an order of magnitude to investigate the effect of increasing the DV rate on the accuracy of the approximate solutions. At short times,  $0 < T < 2$ , the Inner and Patched Models agree closely with the Full Model, whereas the IQSS and QSS Models show a maximum error in  $Y$  of approximately 20 and 30% respectively. For  $T > 2$ , the QSS and Patched Models solutions are similar and give a slightly better agreement with the Full Model than does the IQSS Model. They exhibit a maximum relative error in  $Y$  less than about 15%. At long times, the Inner Model diverges from the Full Model.

Comparison of Figures 6.3 to 6.5 with Figures 6.6 to 6.9 shows that increasing the DV rate (i.e. increasing  $\alpha_1$  from 0.02 to 0.2) results in a loss of QSS behavior and in a decrease in the accuracy of the approximate models. To explain the reason for this it will be helpful if we first develop a physical understanding of the quasi-steady state distribution. The quasi-steady state distribution is the distribution that would result if the solvent concentration were held constant and the distribution were allowed to evolve to the steady state corresponding to this concentration. This same distribution can be approached if the concentration changes slowly relative to the time it takes to evolve to the steady state. However, if the concentration changes significantly over the time it takes to reach a steady state, the changing concentration changes the nature of the distribution faster than the quasi-steady state can be achieved. So, the criterion that must be satisfied to reach a quasi-steady state bubble distribution in a devolatilizer is that the characteristic time required to reach a steady state distribution be small relative to the characteristic time for solvent removal.

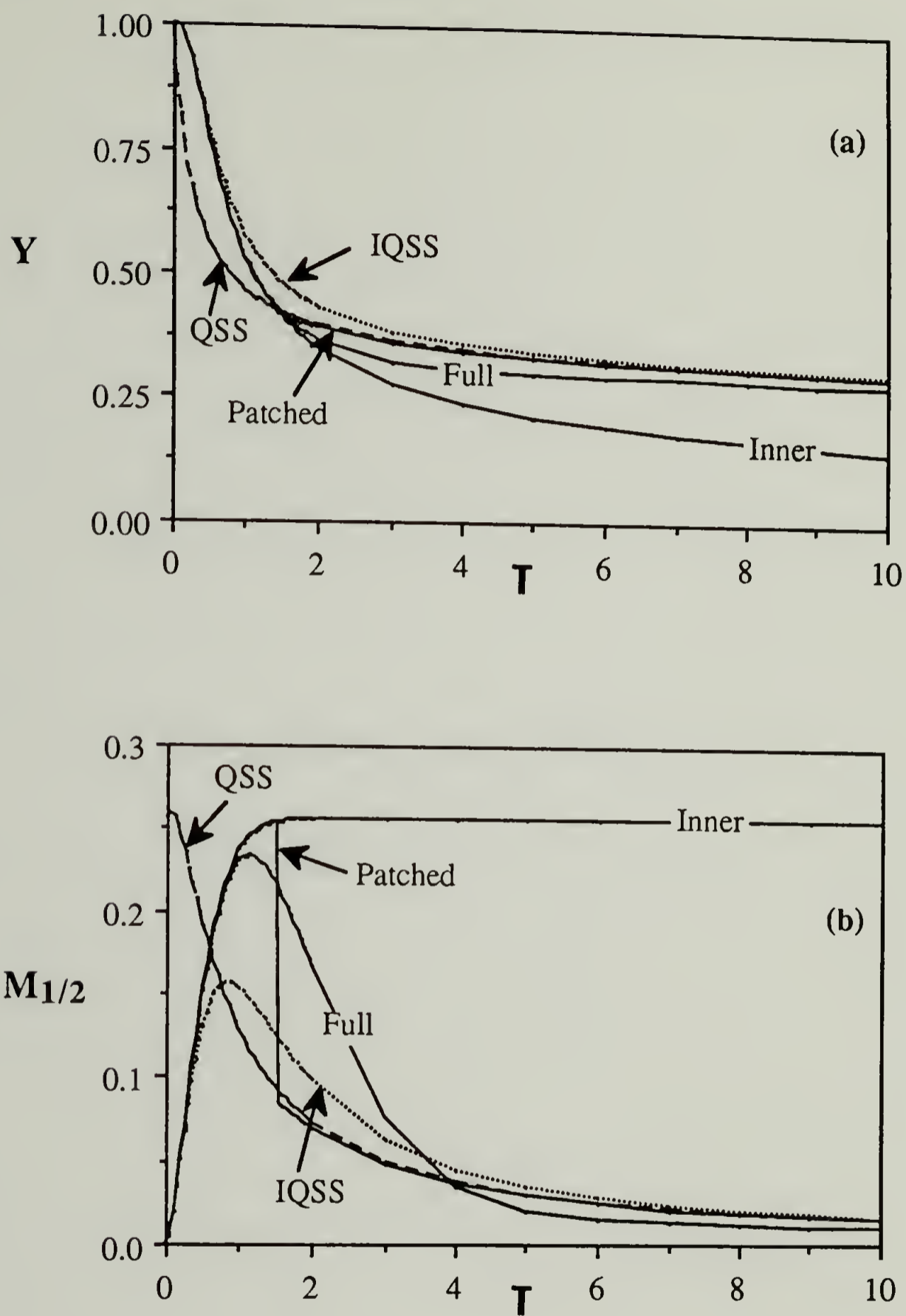


**Figure 6.6** Comparison of the solution of the Full Model of the rolling drum devolatilizer with the solutions given by the approximate models.  $\alpha_1 = 0.2$ ,  $\alpha_2 = 0.00182$  and  $\alpha_3 = 0.4$ .

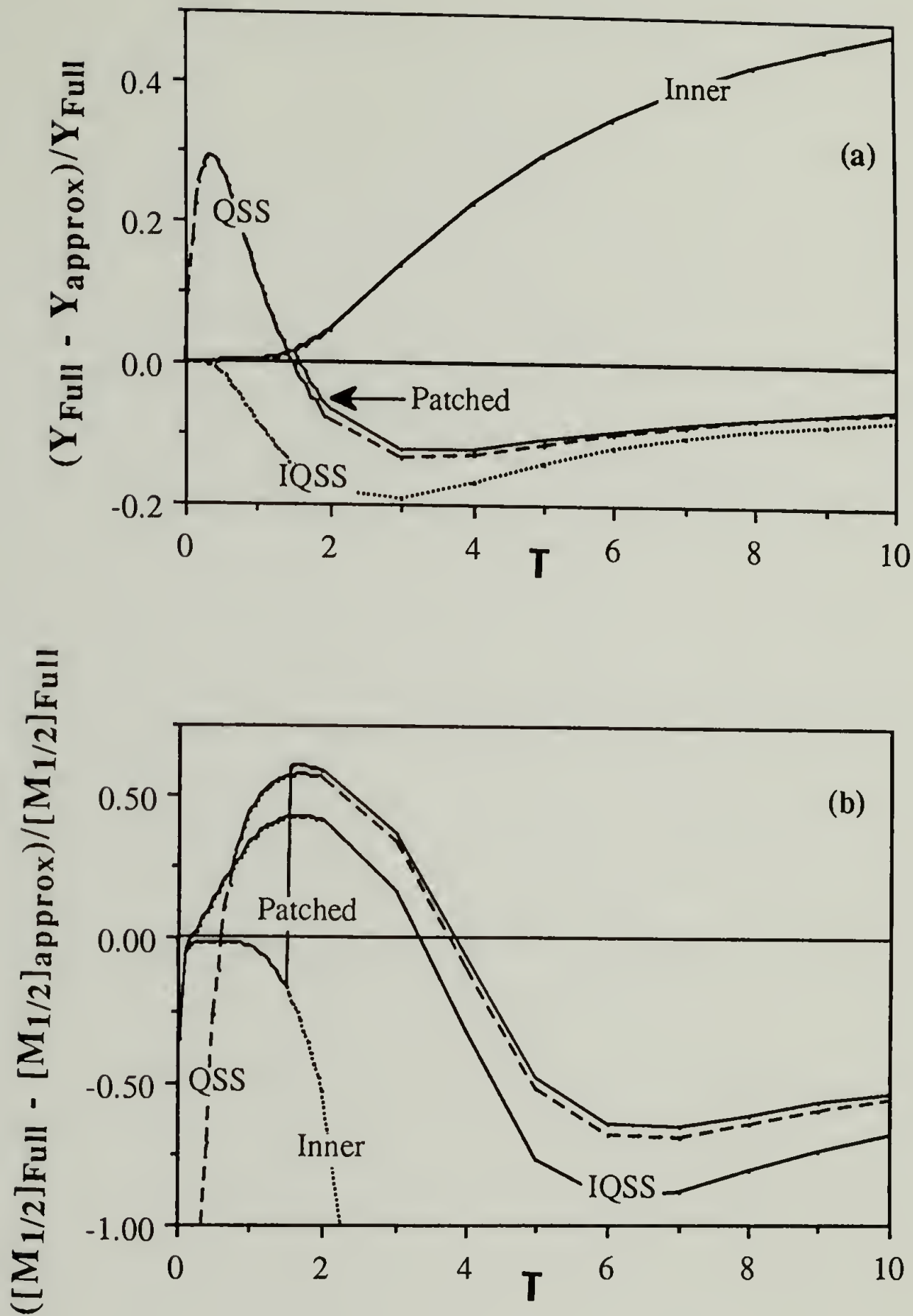


**Figure 6.7** Comparison of the solution of the Full Model of the rolling drum devolatilizer with the solutions given by the approximate models.  $\alpha_1 = 0.2$ ,  $\alpha_2 = 0.00182$  and  $\alpha_3 = 0.4$ .

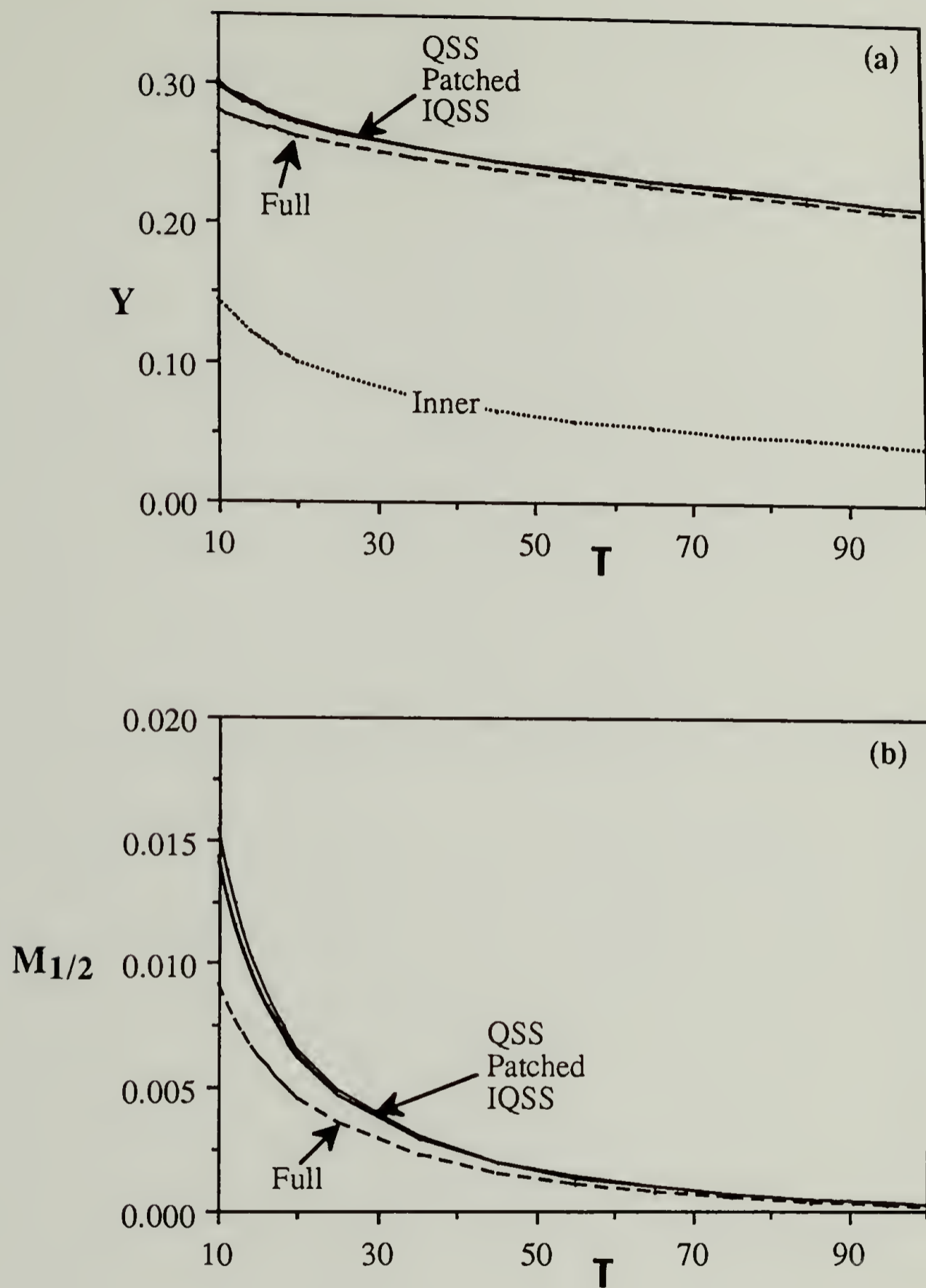


**Figure 6.8** Comparison of the solution of the Full Model of the rolling drum devolatilizer with the solutions given by the approximate models.  $\alpha_1 = 0.2$ ,  $\alpha_2 = 0.00182$  and  $\alpha_3 = 0.4$ .

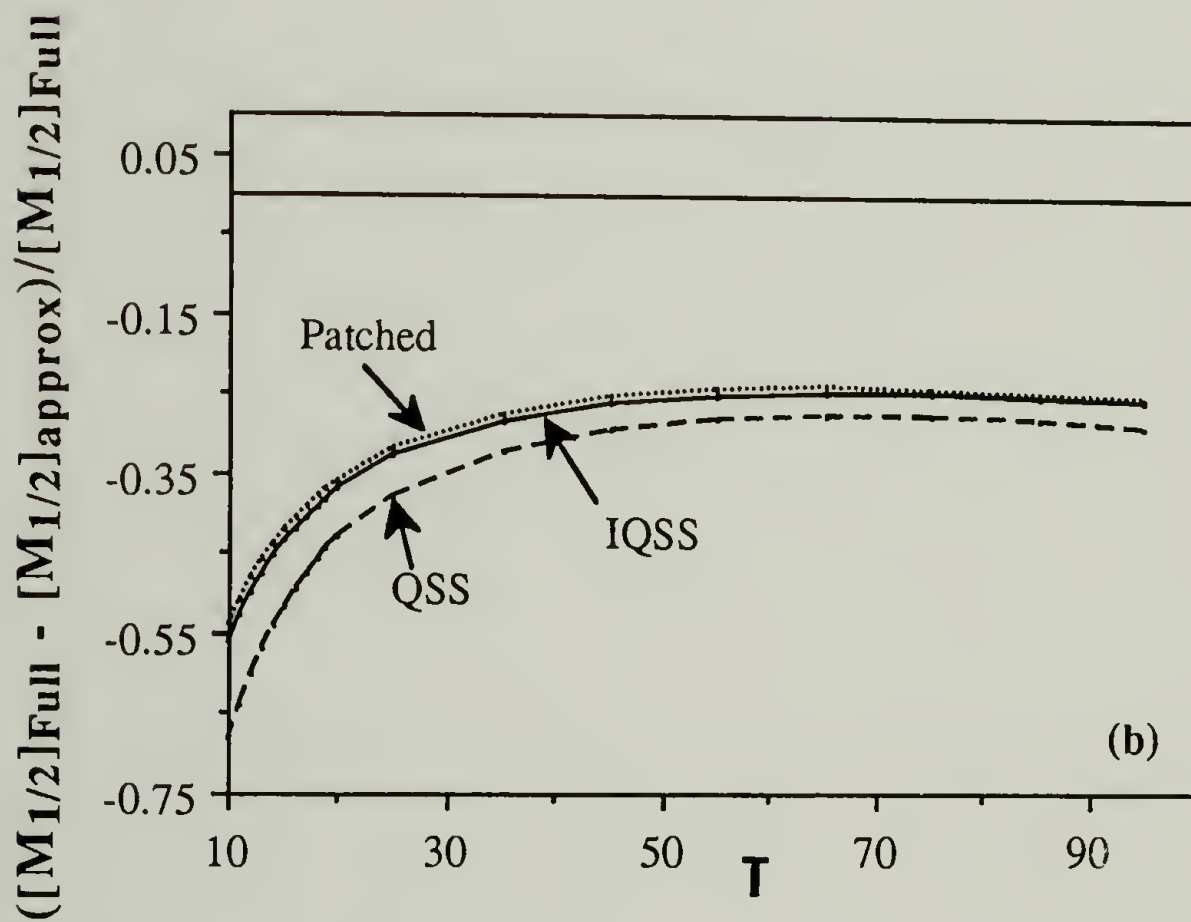
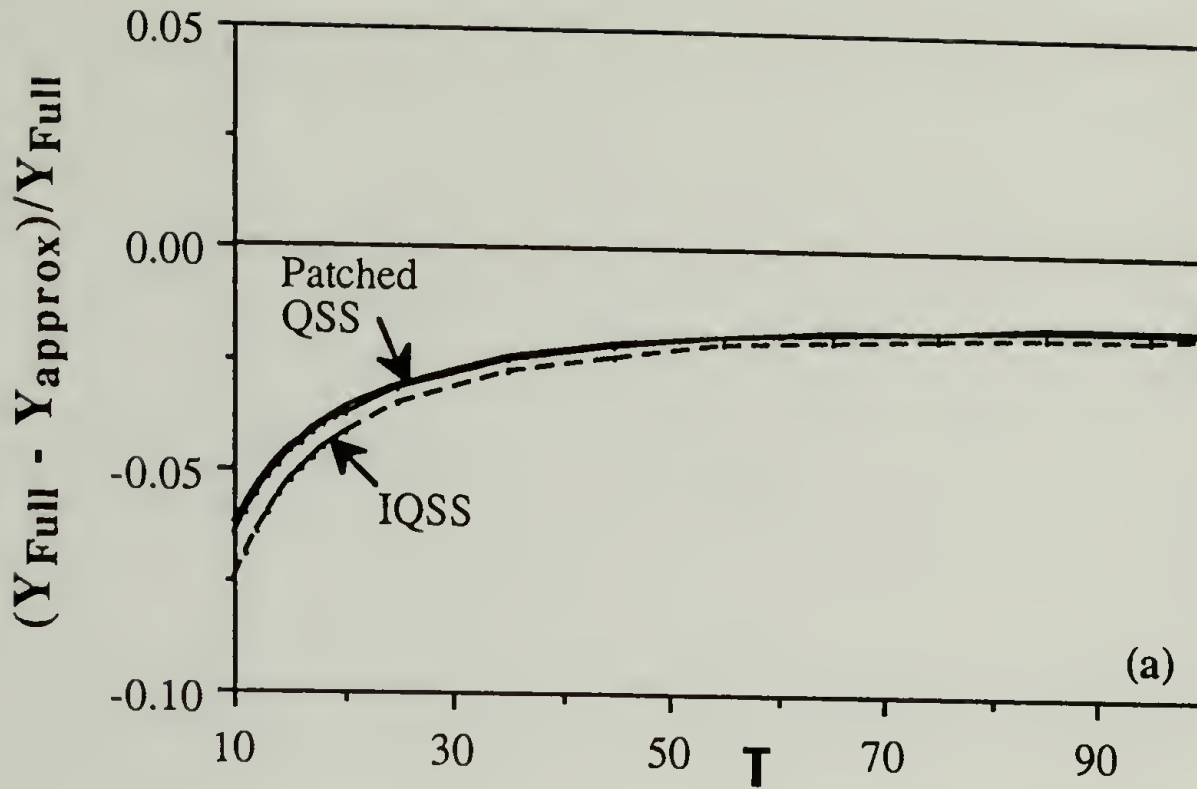


**Figure 6.9** Comparison of the solution of the Full Model of the rolling drum devolatilizer with the solutions given by the approximate models.  $\alpha_1 = 0.2$ ,  $\alpha_2 = 0.00182$  and  $\alpha_3 = 0.4$ .



It would be useful to express this criterion mathematically so that it could be used as an indicator of the likelihood that a quasi-steady state bubble distribution will be reached. A rough rule of thumb would be to assume that a quasi-steady state will be approached if the concentration changes less than 10% over the boundary layer. Or, equivalently,  $\Delta Y < 0.1$ , where  $\Delta Y$  is the absolute value of the change in the concentration over the boundary layer.  $\Delta Y$  can be estimated from the mass balance if we approximate the time derivative of  $Y$  to be constant over the boundary layer with some average value

$$\left(\frac{dY}{dT}\right)_{av} \cong -48\sqrt{\frac{3}{\pi}} \alpha_1 (M_{1/2})_{av} (Y^3)_{av}$$

where  $(M_{1/2})_{av}$  is an average value of  $M_{1/2}$  over the boundary layer and  $(Y^3)_{av}$  is an average value of  $Y^3$  over the boundary layer. The small contribution of interfacial diffusion to the mass transfer rate has been neglected in the above expression.

We are interested in estimating an average value for  $M_{1/2}$  over the boundary layer. Equation 6.5 indicates that  $M_{1/2}$  will be independent of values of the model parameters, as long as a QSS distribution is approached. Inspection of Figure 6.3b, which exhibits QSS behavior, reveals that a reasonable estimate for  $(M_{1/2})_{av}$  is 0.13. A reasonable average value of  $Y$  is 0.95 if  $Y$  is not to change by more than 10% over the boundary layer. Substituting these values into the above expression gives

$$\left(\frac{dY}{dT}\right)_{av} \cong -5.3 \alpha_1$$

The change in  $Y$  over the boundary layer,  $\Delta Y$ , is given by multiplying the absolute value of  $(dY/dT)_{av}$  by the width of the boundary layer. Estimating the width of the boundary layer from Figure 6.1 to be 1 dimensionless time unit, the resulting expression for  $\Delta Y$  is  $\Delta Y \cong 5.3 \alpha_1$ . The condition that a quasi-steady state be reached, or, equivalently that  $\Delta Y$  be less than 0.1, is  $\alpha_1 < 0.02$ .

Considering the approximations in the derivation of this expression, it can only be considered an order of magnitude estimate. For values of  $\alpha_1$  considerably larger than

0.02, this criterion predicts that a quasi-steady state will not occur. For values of  $\alpha_1$  considerably smaller than 0.02, a quasi-steady state is predicted. This criterion is consistent with the model's prediction of a QSS distribution at  $\alpha_1 = 0.02$  and the prediction of a deviation from QSS behavior at  $\alpha_1 = 0.2$ .

The fact that the time to reach a quasi-steady state, that is, the width of the boundary layer, is approximately 1 dimensionless time unit, is an important observation. This reveals the physical interpretation of the characteristic time scale for the problem,  $\tau^*$ . It may be interpreted as being the time required to reach a quasi-steady state distribution.

In summary, the approximate models based on the quasi-steady state assumption are much less complex than the Full Model. Also, the computation time required for their solution is significantly reduced (by approximately two orders of magnitude) relative to the time required to solve the Full Model. At experimental conditions typically encountered in practice, the existence of a quasi-steady state is predicted and the agreement of the approximate solutions with the Full Model solutions is excellent. At conditions for which the DV rates are significantly greater and the QSS assumption becomes invalid, the approximate solutions give a less accurate approximation. However, these solutions can still be valuable as they retain the qualitative character of the exact solution and can give better than an order of magnitude estimate of the DV rate.

These results indicate that the bubble distribution might reach a quasi-steady state in industrial DV processes. This is a significant finding, as the nature of a foaming process which exhibits QSS behavior is quite different than that of foaming processes depicted in the models developed by all previous investigators. Prior investigators have assumed that all bubbles are born at the entrance of the devolatilizer (or at startup for a batch devolatilizer) and that they persist until they exit the equipment with the fluid. If a QSS bubble distribution is approached, the bubbles are born and persist for very short times before they are removed from the system by rupture and this process repeats continuously.

## 6.2 A Design Model for Foam-Enhanced DV

It is desirable to develop explicit, analytical solutions to our complete and approximate DV models, as these would be beneficial for applications of the model to devolatilizer design. However, the complexity of the equations of the complete models prevented us from deriving analytical solutions. Likewise, the approximate models, although less complex, could not be solved analytically.

It is possible, however, to choose different models of the bubble nucleation, growth and rupture rates which simplify the model equations sufficiently so that analytical expressions can be derived. In doing this, however, one should be careful to retain the essential physics of the process in the simplified model.

A simplified model of the rolling drum devolatilizer has been constructed which admits an analytical solution. This model consists of the Quasi-Steady State Model with a simplified nucleation rate expression. The original nucleation expression includes the empirical parameter  $E_a$ , which determines the critical supersaturation at which nucleation ceases. The new nucleation model sets  $E_a$  to zero and the nucleation rate is assumed to be constant and equal to  $F$  for values of the supersaturation greater than the critical value,  $(\Delta C)_{cr}$ . At  $(\Delta C)_{cr}$ , the nucleation is assumed to cease and foaming stops. This nucleation model may be expressed mathematically as

$$J = \begin{cases} F & \text{for } \Delta C > (\Delta C)_{cr} \\ 0 & \text{for } \Delta C \leq (\Delta C)_{cr} \end{cases} \quad 6.10$$

Replacing the original nucleation model expression in the population balance with this new expression, nondimensionalizing the model equations, and applying the QSS assumption gives the Design Model

$$\left(\frac{dY}{d\Gamma}\right)_{\text{Design}} = \begin{cases} -12 \alpha_1 Y^2 - \frac{2}{\pi^{1/4}} \alpha_2 Y & Y > Y_{\text{cr}} \\ -\frac{2}{\pi^{1/4}} \alpha_2 Y & Y < Y_{\text{cr}} \end{cases} \quad 6.11$$

where  $Y_{\text{cr}}$  is defined as  $(\Delta C)_{\text{cr}}/C_{\text{max}}$  and  $\alpha_1$  and  $\alpha_2$  retain their original definitions, with the exception that  $E_a$  is set to zero.

Since the Design Model is based on the QSS Model, it is an outer model and is strictly valid at long times only. However, as the QSS Model was shown to give reasonable agreement with the complete model over short times, it will be assumed to apply at short times (i.e. over the boundary layer) also. This approximation should be adequate for design purposes. Note that the exponential term in the original QSS Model is not present in the Design Model. This exponential term contributes significantly to the nonlinearity in the QSS Model and its removal allows the derivation of an analytical solution.

The question which must be answered is whether this simplification has seriously compromised the correlative abilities of the model. What is required of a useful design model is that it give a reasonable estimate of the two time scales of DV associated with foaming and interfacial diffusion. The Design Model will give slightly different performance predictions from the QSS Model. At equal values of the parameter  $F$  in both models, these differences will grow with increases in the value of  $E_a$ , as the Design Model for  $Y > Y_{\text{cr}}$  is equivalent to the QSS Model in the limit as  $E_a$  approaches 0. Yet, the models are similar and both exhibit two time scales for DV. The Design Model should be adequate for correlating the DV performance data. As well, one should note that the the QSS Model is not necessarily more correct than the Design Model, as the nucleation models incorporated into both are empirical. We can not say as yet which is the more appropriate description.

Equation 6.11, for  $Y > Y_{cr}$  is a Bernoulli type equation with constant coefficients (Ince, 1956). The standard method of solution is to make the substitution  $U = 1/Y$  which reduces the equation to a first-order, linear differential equation in terms of  $U$ . Solving this equation using an integrating factor gives an explicit expression for  $U$ , which upon substitution for  $Y$  gives

$$Y_{Design} = \frac{1}{\left(6\pi^{1/4} \frac{\alpha_1}{\alpha_2} + 1\right) \exp\left(\frac{2}{\pi^{1/4}} \alpha_2 \mathbf{T}\right) - 6\pi^{1/4} \frac{\alpha_1}{\alpha_2}} \quad Y > Y_{cr} \quad 6.12a$$

Equation 6.11 for  $Y < Y_{cr}$  can be solved by direct integration to give

$$Y_{Design} = Y_{cr} \exp\left[-\frac{2}{\pi^{1/4}} \alpha_2 (\mathbf{T} - \mathbf{T}_{cr})\right] \quad Y \leq Y_{cr} \quad 6.12b$$

where  $\mathbf{T}_{cr}$  is the dimensionless time at which  $Y = Y_{cr}$ .

When mass transfer by foaming is so small that it can be neglected in comparison to interfacial diffusion, as is usually the case when foaming occurs, equation 6.12a in the limit as  $\alpha_2$  approaches zero reduces to

$$(Y_{Design})_{\alpha_2 \rightarrow 0} = \frac{1}{1 + 12 \alpha_1 \mathbf{T}} \quad Y > Y_{cr} \quad 6.13$$

Over short times, 6.12a can be further simplified in the limit as  $\mathbf{T}$  approaches zero.

$$(Y_{Design})_{\mathbf{T} \rightarrow 0} = \frac{1}{1 + \left[12 \alpha_1 + \frac{2}{\pi^{1/4}} \alpha_2\right] \mathbf{T}} \quad Y > Y_{cr} \quad 6.14$$

In Figure 6.10,  $Y_{Design}$  is plotted for values of  $\alpha_1 = 0.02$  and  $\alpha_2 = 0.00182$ . These values are similar to the values of the model parameters of the single screw and rolling drum devolatilizer models that gave a good correlation of the data of Coughlin and Canevari (1969) and Biesenberger and Lee (1986). For purposes of model demonstration, the critical time,  $\mathbf{T}_{cr}$ , was chosen arbitrarily to be 4.0, which corresponds to a value of  $Y_{cr}$  of 0.507. At  $Y = Y_{cr}$ , the nucleation is presumed to cease after which the DV becomes

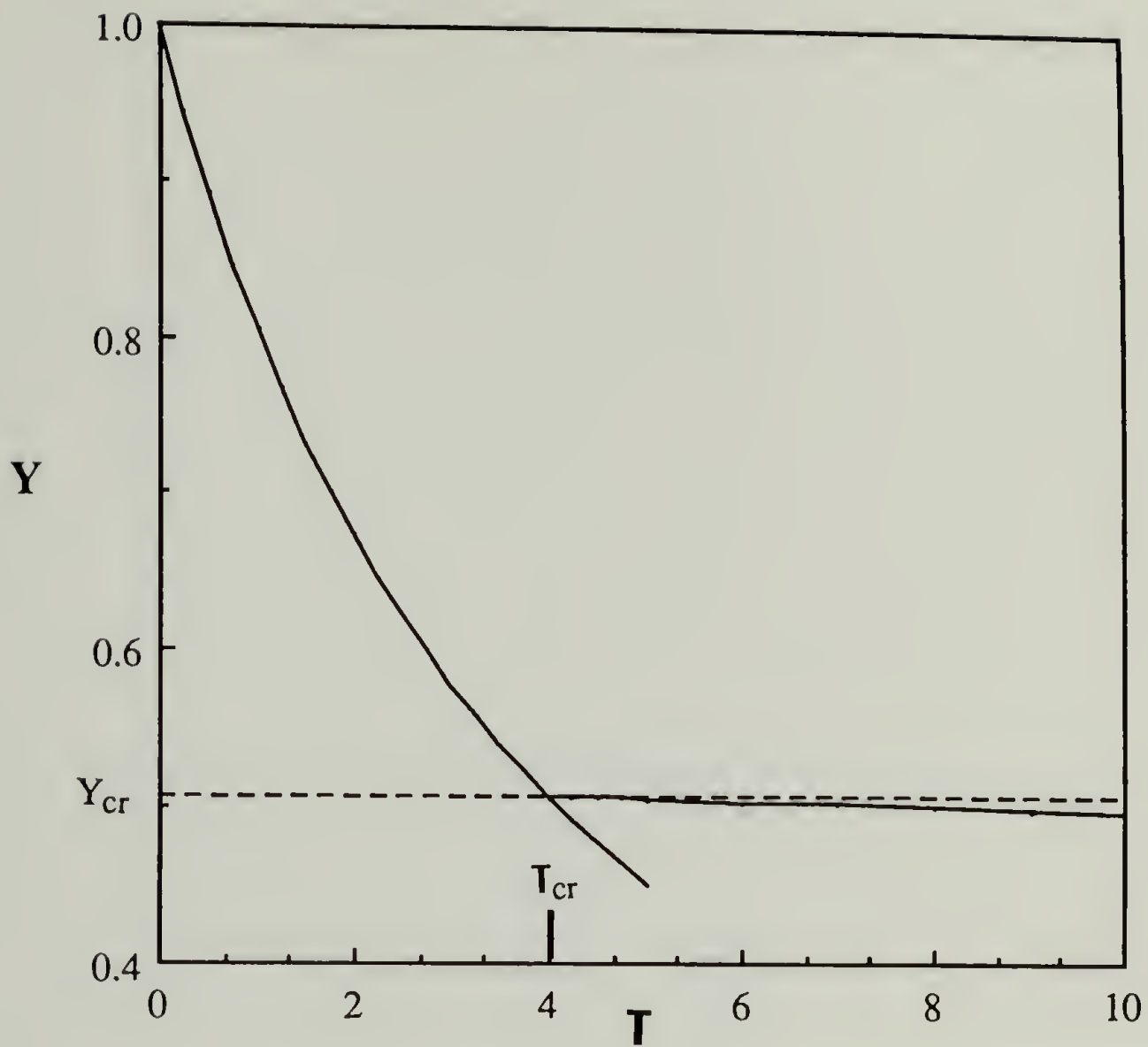


**Figure 6.10** Plot of the DV performance predicted by the Design Model.  
 $\alpha_1 = 0.02$ ,  $\alpha_2 = 0.00182$  and  $Y_{cr} = 0.507$ .

controlled by interfacial diffusion only. Inspection of Figure 6.10 reveals that this model clearly exhibits two distinct time scales for DV, as desired, and should have correlative abilities similar to those of the approximate models.

The Design Model of the rolling drum devolatilizer has two unknown, empirical parameters,  $F$  and  $(\Delta C)_{cr}$ . If the Design Model is to be applied to devolatilizer design, it is necessary that methods for estimating  $F$  and  $(\Delta C)_{cr}$  be available that do not require measurements on the devolatilizer to be designed. As well, it would be advantageous if these methods did not consume significant amounts of the polymer solution to be devolatilized, as the solution may not be available in appreciable quantities before the production process is started up. Bench scale experiments for measuring  $F$  and  $(\Delta C)_{cr}$  would be very valuable.

As discussed in Appendix C, nucleation onset experiments would give a direct measure of  $(\Delta C)_{cr}$ . An experiment would consist of measuring the superpressure at which nucleation onset occurs. It would be desirable to conduct these experiments on solutions undergoing a simple shear flow, as the shear rate has been suggested by Biesenberger and Lee (1986) to enhance nucleation rates. This could be done with a transparent cone-and-plate device between which the polymer solution could be sheared with a homogeneous shear rate. Exposure of the cone and plate to a reduced ambient pressure would induce nucleation in the fluid which would be observable through the transparent plates.

Experimental methods for measuring  $F$ , the nucleation rate of bubbles, would be much more complex. The nucleation rate could be measured directly by counting the number of bubbles nucleated as a function of time. This measurement could also be performed on the transparent cone-and-plate device discussed previously. High speed photographic methods could be used to track the number of bubbles over time. An alternative method for estimating  $F$  would be to use a bench scale devolatilizer, preferably modelled after the simple rolling drum devolatilizer. Measurement of the concentration of solvent versus time would allow  $F$  to be estimated from a correlation of the data given by

the Design Model. Measurements could be made over varying drum rotation rates to determine the dependence of  $F$  on the shear rate. This device would also be suitable for estimating  $(\Delta C)_{cr}$  from nucleation onset experiments.

In summary, the Design Model, which is based on the QSS Model, should serve as a valuable tool for the design engineer. It has an analytical solution which greatly simplifies its application to devolatilizer design problems. As well, the model includes the two time scales for devolatilization associated with foaming and interfacial diffusion. These two time scales are required in any model of foam-enhanced DV if it is to provide a reasonable correlation of devolatilizer performance data.



## CHAPTER VII

### DESCRIPTORS OF THE BUBBLE DISTRIBUTION AND A MODEL OF DV WITH RUPTURE BY FILM DRAINING

In correlating the experimental DV data in Chapters 4 and 5, the volume expansion due to foaming was assumed to be small and was neglected in the model evaluation. The extent of volume expansion can be quantified by the fraction of volume occupied by the bubbles or by the ratio of the volumes of the fluid film before and during foaming. These quantities describe the character of the bubble phase and will be termed *descriptors*. Other descriptors of the bubble phase which are of interest include the average bubble age, the average bubble radius, the number of bubbles per volume, the surface area of bubbles per volume, the surface area of bubbles per surface area of vapor/liquid interface, etc. Descriptors are single-valued quantities and are often more practical for describing the nature of the bubble phase than the bubble distribution itself. Indeed, experimental measurement of the bubble distribution is usually quite difficult, whereas, measurement of descriptors of the distribution can be much simpler.

#### 7.1 Definition of Descriptors

Descriptors are averages over the distribution. A few of the more important descriptors are defined below

$$\tau_{av} = \frac{\int_0^{\infty} \tau f d\tau}{\int_0^{\infty} f d\tau} = \frac{\mu_1}{\mu_0} = \tau^* \frac{M_1}{M_0} \quad 7.1a$$

$$R_{av} = \frac{\int_0^{\infty} R f d\tau}{\int_0^{\infty} f d\tau} = \gamma(Y) \frac{\mu_{1/2}}{\mu_0} = \gamma(Y) \tau^{*1/2} \frac{M_{1/2}}{M_0} \quad 7.1b$$

$$\begin{aligned} \phi &= \frac{\int_0^\infty \left( \frac{4}{3} \pi R^3 \right) f \, d\tau \, dz}{\int_0^\infty \left( \frac{4}{3} \pi R^3 \right) f \, d\tau \, dz + A_c \, dz} = \frac{1}{1 + \frac{A_c}{\frac{4}{3} \pi \gamma(Y)^3 \mu_{3/2}}} \\ &= \frac{1}{1 + \frac{A_c}{\frac{4}{3} \pi \gamma(Y)^3 \tau^{*5/2} f^* M_{3/2}}} \end{aligned} \quad 7.1c$$

$$\begin{aligned} \rho_b &= \frac{\int_0^\infty f \, d\tau \, dz}{\int_0^\infty \left( \frac{4}{3} \pi R^3 \right) f \, d\tau \, dz + A_c \, dz} = \frac{\mu_0}{\frac{4}{3} \pi \gamma(Y)^3 \mu_{3/2} + A_c} \\ &= \frac{M_0}{\frac{4}{3} \pi \gamma(Y)^3 \tau^{*3/2} M_{3/2} + \frac{A_c}{\tau^* f^*}} \end{aligned} \quad 7.1d$$

$$\begin{aligned} \frac{R_t}{R_c} &= \frac{\left( \frac{4 \left[ \int_0^\infty \left( \frac{4}{3} \pi R^3 \right) f \, d\tau \, dz + A_c \, dz \right]}{\pi \, dz} \right)^{1/2}}{R_c} = \frac{2 \left[ \frac{4}{3} \gamma(Y)^3 \mu_{3/2} + \frac{A_c}{\pi} \right]^{1/2}}{R_c} \\ &= \left[ 1 + \frac{16}{3} \frac{\gamma(Y)^3 \tau^{*5/2} f^* M_{3/2}}{R_c^2} \right]^{1/2} \end{aligned} \quad 7.1e$$

where  $\tau_{av}$  is the mean age of the bubbles,  $R_{av}$  is the mean radius of the bubbles,  $\phi$  is the volume fraction of bubbles,  $\rho_b$  is the number of bubbles per volume and  $R_t/R_c$  is the ratio of the radius of the bulk film in the rolling drum devolatilizer during foaming,  $R_t$ , to that before foaming,  $R_c$ . In these descriptor equations, a general growth rate expression was chosen to relate the bubble's radius to its age

$$R = \gamma(Y) \tau^{1/2}$$

where  $\gamma(Y)$  gives the dependence of the growth rate on the supersaturation. The integrals over the distribution have been expressed in terms of the moments which have in turn been

expressed in terms of the dimensionless moments and the characteristic reference scales of the model.

Note that the descriptor expression for the average bubble age, equation 7.1a, reveals some additional information on the physical meaning of the characteristic time,  $\tau^*$ . When a quasi-steady state distribution is approached,  $M_1/M_0$  approaches a nearly constant value of order 1 (see Figure 6.2). From equation 7.1a,  $\tau^*$  can be understood as being a measure of the average residence time of bubbles in the fluid.

## 7.2 Descriptors of the Rolling Drum Model

We will investigate the nature of the foam phase predicted by our DV model to occur in the rolling drum devolatilizer by calculating the descriptors of the bubble distribution. Expressions for the descriptors in terms of the physical property and process variables and the dimensionless moments of the distribution were derived by substituting the expressions for  $\gamma(Y)$  and for the characteristic reference scales of the rolling drum model into the general descriptor equations 7.1. The resulting expressions are

$$\tau_{av} = \left( \frac{A_c}{V_b D^{1/2}} \frac{\rho_g}{C_{max}} \right)^{2/3} \frac{M_1}{M_0} \quad 7.2 a$$

$$R_{av} = \sqrt{\frac{12}{\pi}} \left( \frac{A_c D}{V_b} \right)^{1/3} \left( \frac{C_{max}}{\rho_g} \right)^{2/3} Y \frac{M_{1/2}}{M_0} \quad 7.2 b$$

$$\phi = \frac{1}{1 + \frac{1}{32 \sqrt{\frac{3}{\pi}} \left( \frac{C_{max}}{\rho_g} \right)^{4/3} \left( \frac{D^{2/3} A_c^{5/3} F}{V_b^{5/3}} \right) \exp[-\alpha_3] Y^3 M_{3/2}}} \quad 7.2 c$$

$$\rho_b = \frac{M_0}{32 \sqrt{\frac{3}{\pi}} \left( \frac{C_{max}}{\rho_g} \right)^2 \left( \frac{D A_c^2 F}{V_b^2} \right) \exp[-\alpha_3] Y^3 M_{3/2} + \frac{1}{\left( \frac{A_c^{2/3} F}{V_b^{2/3} D^{1/3}} \right) \exp[-\alpha_3]}} \quad 7.2 d$$

$$\frac{R_t}{R_c} = \left[ 1 + \frac{128 \sqrt{3}}{\pi^{3/2}} \left( \frac{A_c^{8/3} D^{2/3}}{V_b^{5/3}} \right) \left( \frac{C_{\max}}{\rho_g} \right)^{4/3} F \exp(-\alpha_3) Y^3 M_{3/2} \right]^{1/2} \quad 7.2 e$$

$$\frac{dY}{dt} \cong -48 \sqrt{\frac{3}{\pi}} \left( \frac{D A_c F \exp(-\alpha_3)}{V_b} \right) \left( \frac{C_{\max}}{\rho_g} \right) Y^3 M_{1/2} \quad 7.2 f$$

where the DV rate,  $dY/dt$ , has been included. For purposes of clarity, this expression for  $dY/dt$  excludes the interfacial diffusion term which will be negligible in comparison with the bubble growth term when foaming occurs.

Descriptors were calculated for the experimental conditions of data 3 of Biesenberger and Lee's (1986) rolling drum experiments using these expressions. The values of  $F$  and  $E_a$  used in these calculations are the same values that were used in correlating data 3 in Chapter V. Figures 7.1a and b plot these descriptors versus dimensionless time. The model predicts a very large volume expansion upon foaming. The maximum volume fraction of bubbles,  $\phi$ , is about 0.94 which corresponds to a radial expansion ratio,  $R_t/R_c$  of about 4. The number density of bubbles,  $\rho_b$ , shows an unexpected maximum at short times. This can be explained by investigating the expression for  $\rho_b$ . At short time,  $\rho_b$  grows proportionally with  $M_0$ , the total number of bubbles. However, the denominator of the expression is the total volume of the solution which increases due to foaming and reduces  $\rho_b$ .

The large foam expansion predicted by the Full Model to occur during operation of the single screw devolatilizer is much larger than could be accommodated by the equipment. As well, this large foam expansion is inconsistent with the assumption of negligible foam expansion used in constructing the Full Model. The simulation was rerun for identical values of the process variables and model parameters using the Complete Model. The Complete Model includes the effect of reduction in the bubble rupture rate in response to bulk film volume expansion due to foaming. For data 3 of Biesenberger and Lee (1986),

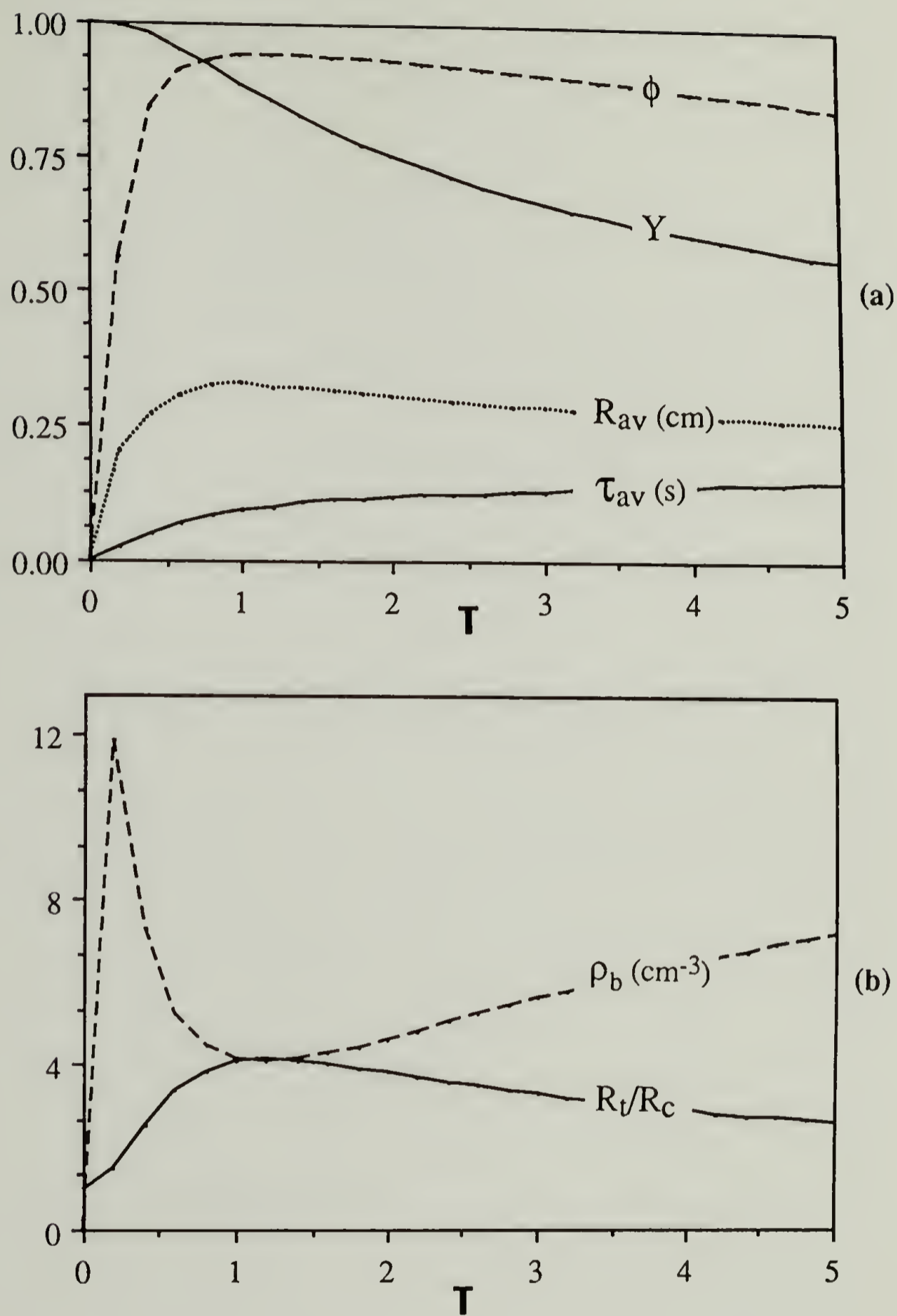


**Figure 7.1** Plots of the descriptors predicted by the Full Model of the rolling drum devolatilizer for conditions of experiment 3 of Biesenberger and Lee (1986).  $F = 798 \text{ cm}^{-3} \text{ s}^{-1}$ ,  $E_a = 15.2 \text{ atm}^2 \text{ K}$ ,  $\alpha_1 = 0.02$ ,  $\alpha_2 = 0.00136$ ,  $\alpha_3 = 0.4$ .

the model parameter  $\alpha_4$ , neglected in the Full Model, has a value of 336. The descriptors of the distribution predicted by the Complete Model are presented in Figure 7.2. These descriptors differ significantly with those predicted by the Full Model. The volume expansion is much larger with a maximum radial expansion ratio of 8. A decrease in the rupture rate has an autocatalytic effect on the volume expansion. Volume expansion reduces the bubble rupture rate which fuels further expansion. The DV rate is much greater for the Complete Model due to the greater number of bubbles contained within the larger volume of foam. As a result, the DV rate of data 3 for the rolling drum devolatilizer is overestimated for these values of the model parameters.

The differences between the Complete and Full Model's solutions are also evident in the shapes of their bubble age distributions. The distribution predicted by the Full Model, presented in Figure 6.1, exhibits typical QSS behavior, which requires that, at constant time  $\mathbf{T}$ , the bubble distribution decreases monotonically with increasing age  $\mathbf{T}$ . The distribution predicted by the Complete Model is presented in Figure 7.3. QSS behavior is not observed. A ridge is present in the surface plot running along the characteristic  $\mathbf{T} = \mathbf{T}$ . Nucleation ceases near  $\mathbf{T} = 3$  when the supersaturation has decreased below the critical supersaturation necessary to sustain nucleation. Bubbles born before this live for very long times due to a significant reduction in the rupture rate caused by the large foam expansion.

For comparison, the simulation was rerun for values of the nucleation rate  $F$ , proportional to  $\alpha_1$ , decreased by one and two orders of magnitude. The descriptors and surface plot of the distribution for  $\alpha_1 = 0.002$  are presented in Figures 7.4 and 7.5 and for  $\alpha_1 = 0.0002$  in Figures 7.6 and 7.7. For the nucleation rate decreased by one order of magnitude,  $\alpha_1 = 0.002$ , the maximum radial expansion ratio decreased slightly to about 7.5 and was reached at later times. A larger average bubble radius and smaller number density of bubbles is predicted. From the surface plot in Figure 7.5 it is evident that a QSS distribution is not predicted. The shape of the distribution is similar to that for  $\alpha_1 = 0.02$ ,

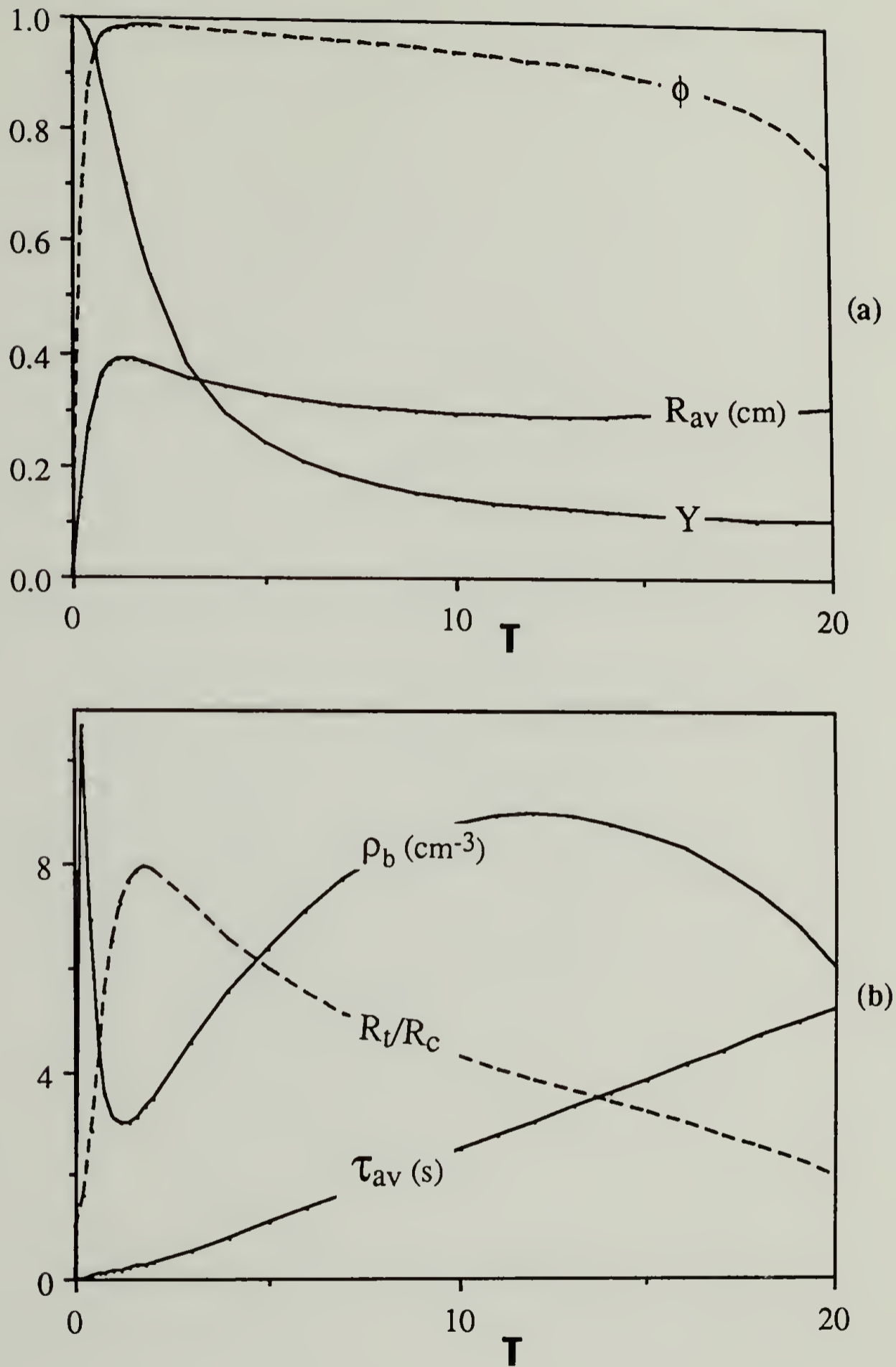


**Figure 7.2** Plots of the descriptors predicted by the Complete Model of the rolling drum devolatilizer for conditions of experiment 3 of Biesenberger and Lee (1986).  $F = 798 \text{ cm}^{-3} \text{ s}^{-1}$ ,  $E_a = 15.2 \text{ atm}^2 \text{ K}$ ,  $\alpha_1 = 0.02$ ,  $\alpha_2 = 0.00136$ ,  $\alpha_3 = 0.4$  and  $\alpha_4 = 336$ .

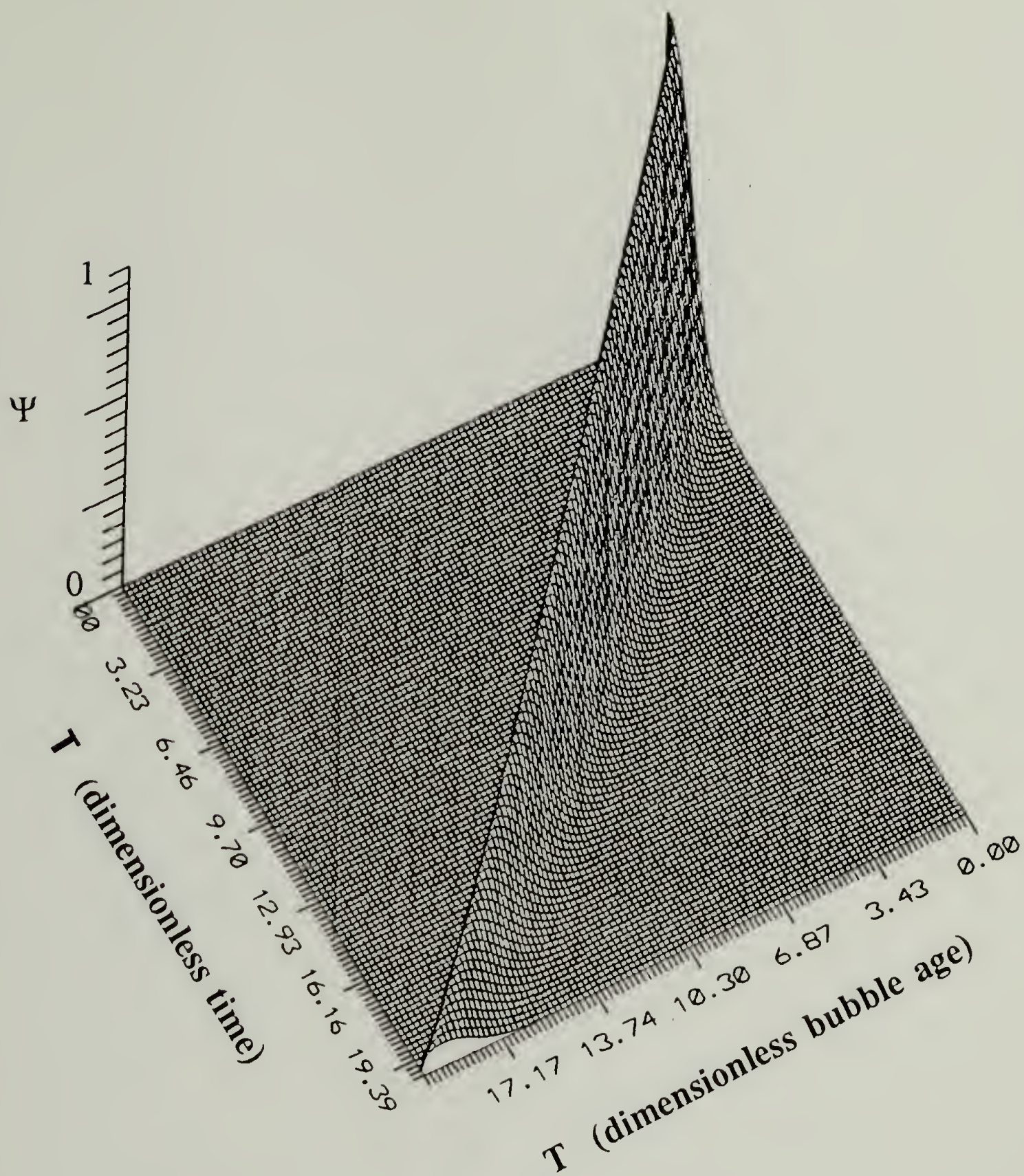


**Figure 7.3** Surface plot of the bubble age distribution predicted by the Complete Model of the rolling drum devolatilizer.  $\alpha_1 = 0.02$ ,  $\alpha_2 = 0.00136$ ,  $\alpha_3 = 0.4$  and  $\alpha_4 = 336$ .



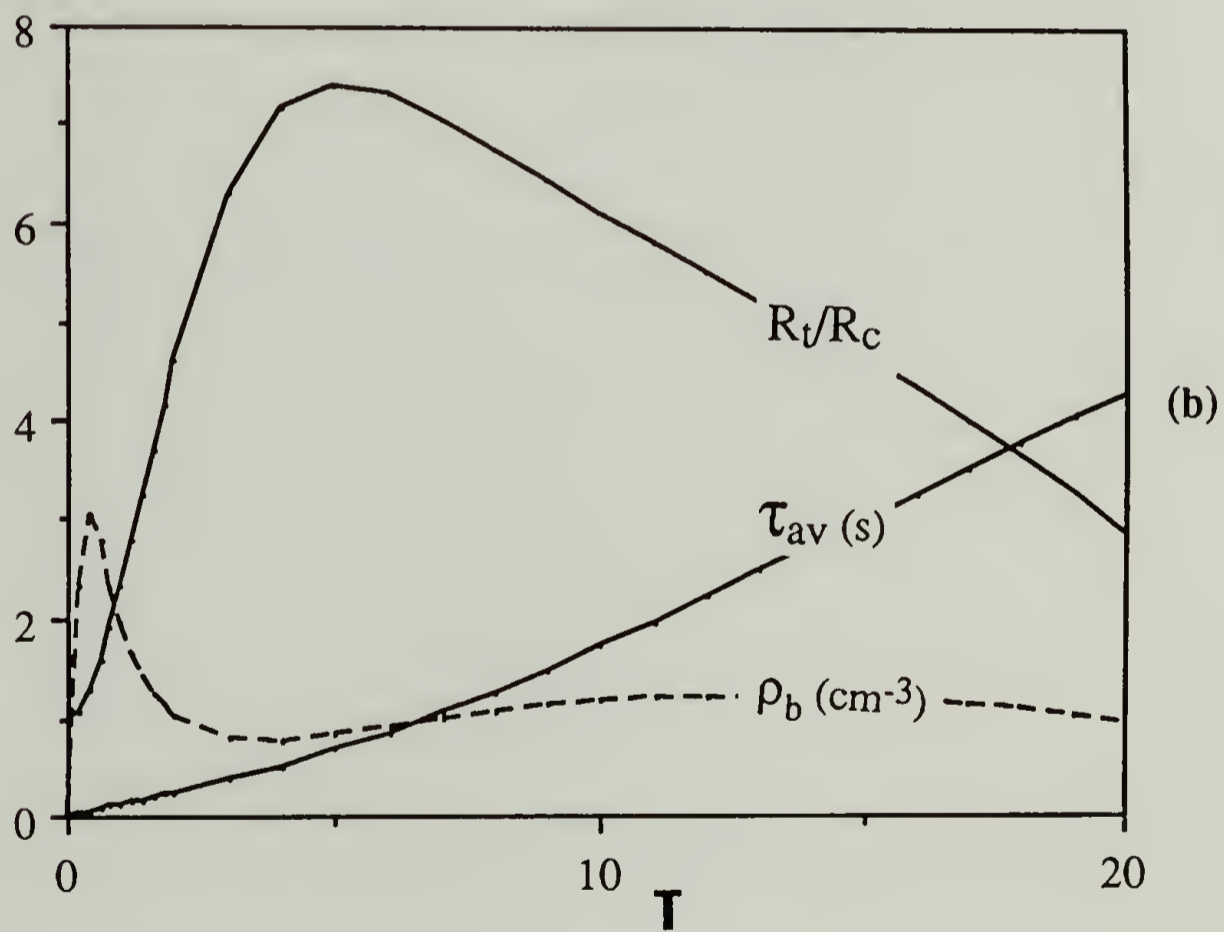
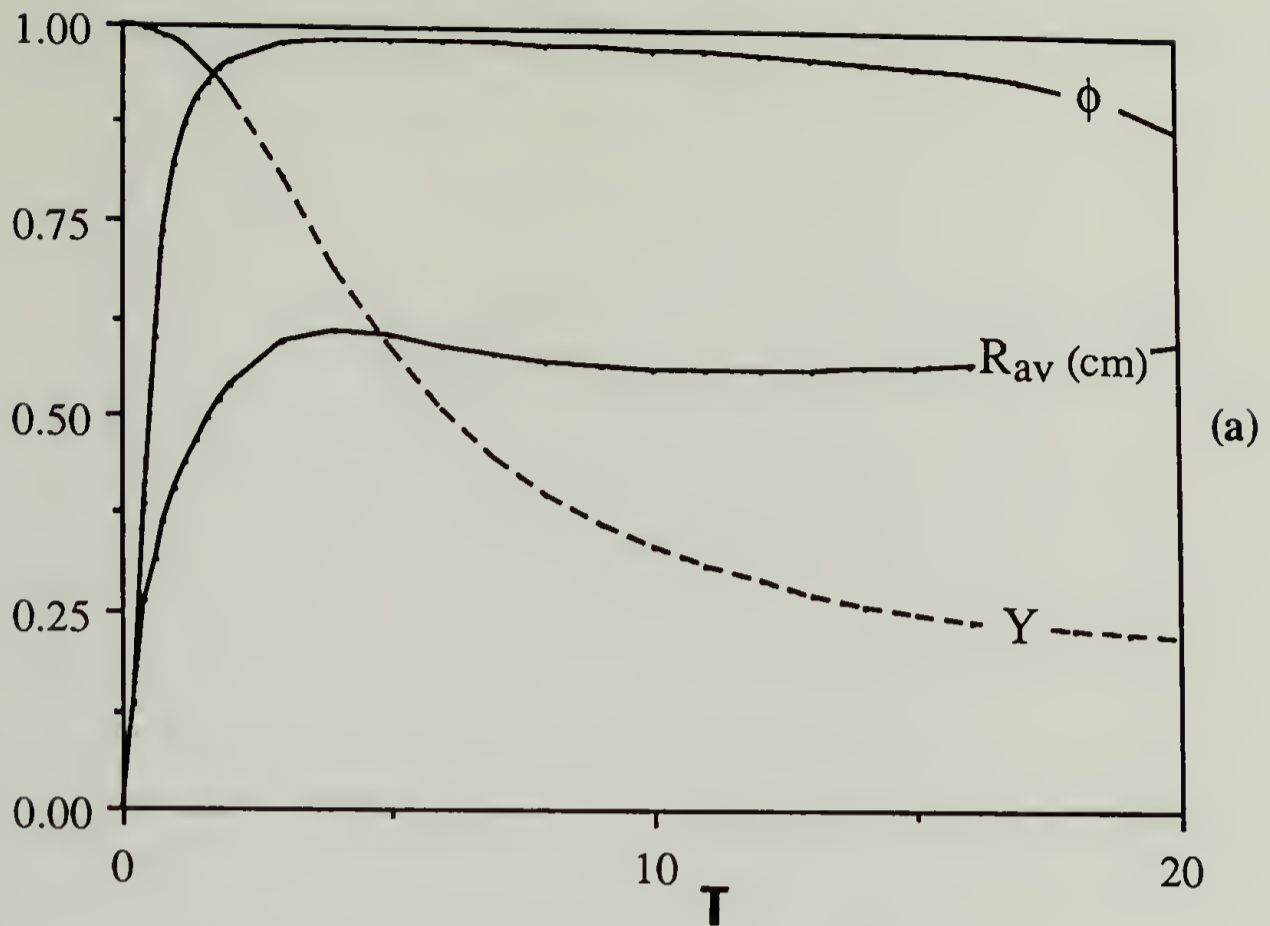


**Figure 7.4** Plots of the descriptors predicted by the Complete Model of the rolling drum devolatilizer for conditions of experiment 3 of Biesenberger and Lee (1986).  $F = 80 \text{ cm}^{-3} \text{ s}^{-1}$ ,  $E_a = 15.2 \text{ atm}^2 \text{ K}$ ,  $\alpha_1 = 0.002$ ,  $\alpha_2 = 0.00136$ ,  $\alpha_3 = 0.4$  and  $\alpha_4 = 336$ .

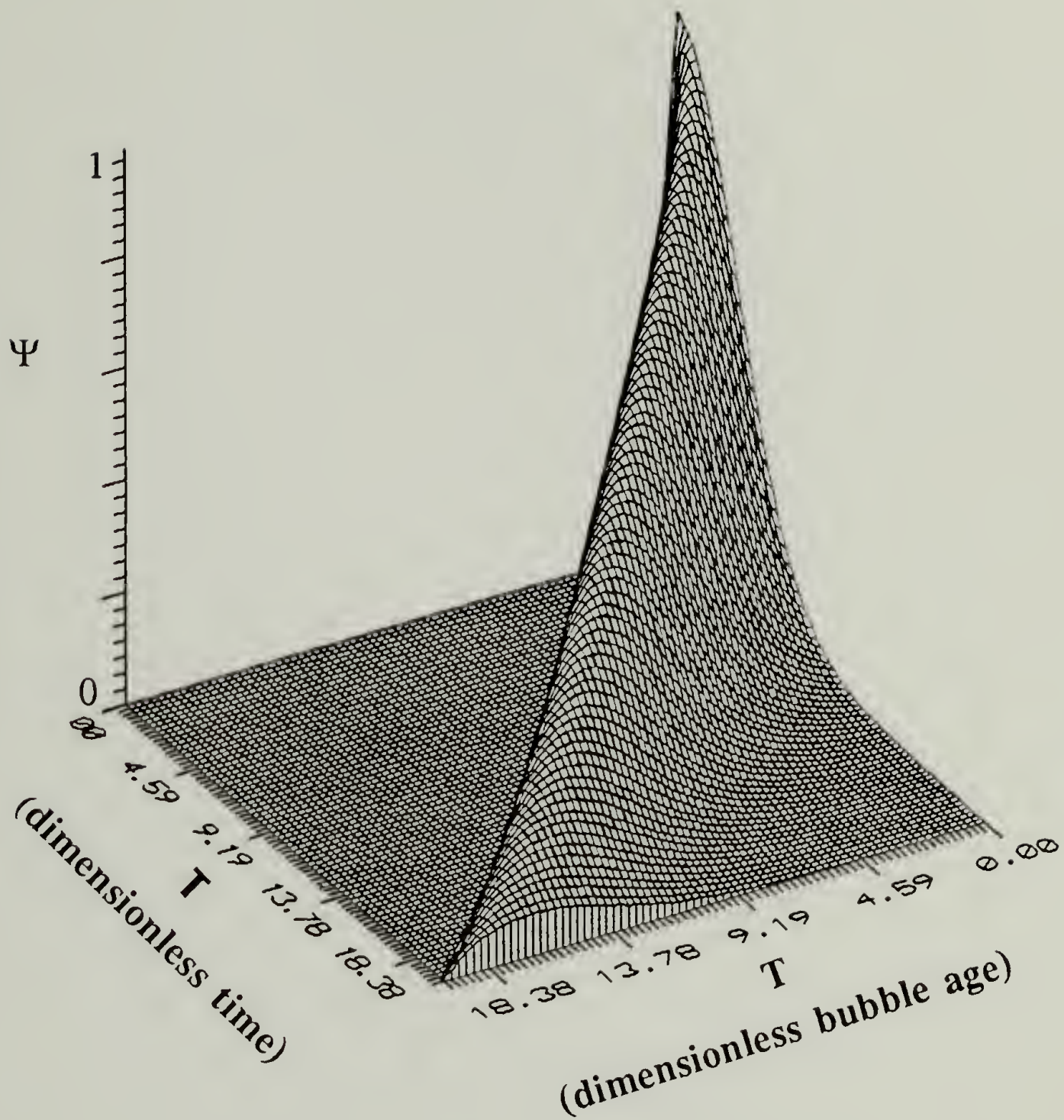


**Figure 7.5** Surface plot of the bubble age distribution predicted by the Complete Model of the rolling drum devolatilizer.  $\alpha_1 = 0.002$ ,  $\alpha_2 = 0.00136$ ,  $\alpha_3 = 0.4$  and  $\alpha_4 = 336$ .

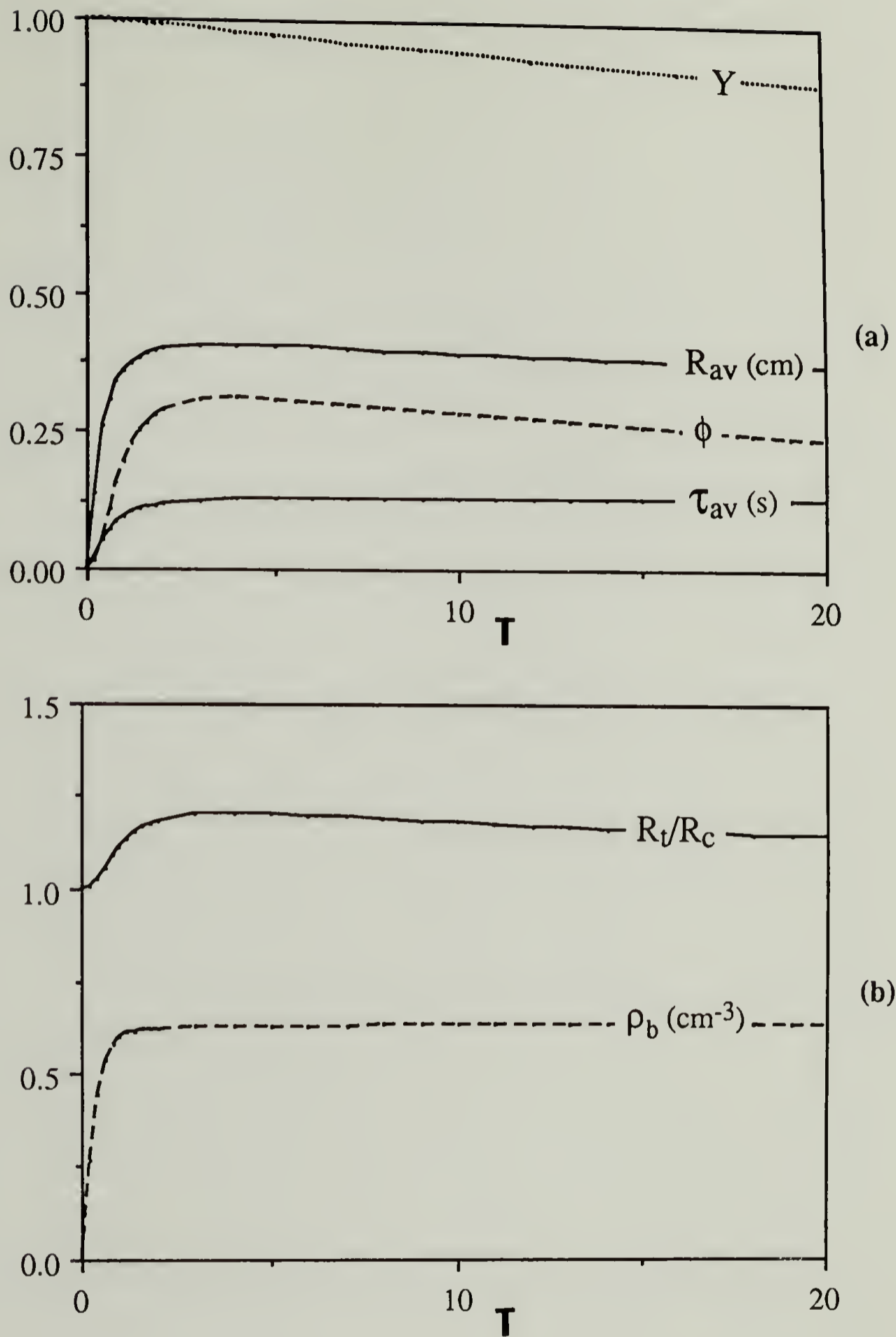


**Figure 7.6** Plots of the descriptors predicted by the Complete Model of the rolling drum devolatilizer for conditions of experiment 3 of Biesenberger and Lee (1986).  $F = 8 \text{ cm}^{-3} \text{ s}^{-1}$ ,  $E_a = 15.2 \text{ atm}^2 \text{ K}$ ,  $\alpha_1 = 0.0002$ ,  $\alpha_2 = 0.00136$ ,  $\alpha_3 = 0.4$  and  $\alpha_4 = 336$ .

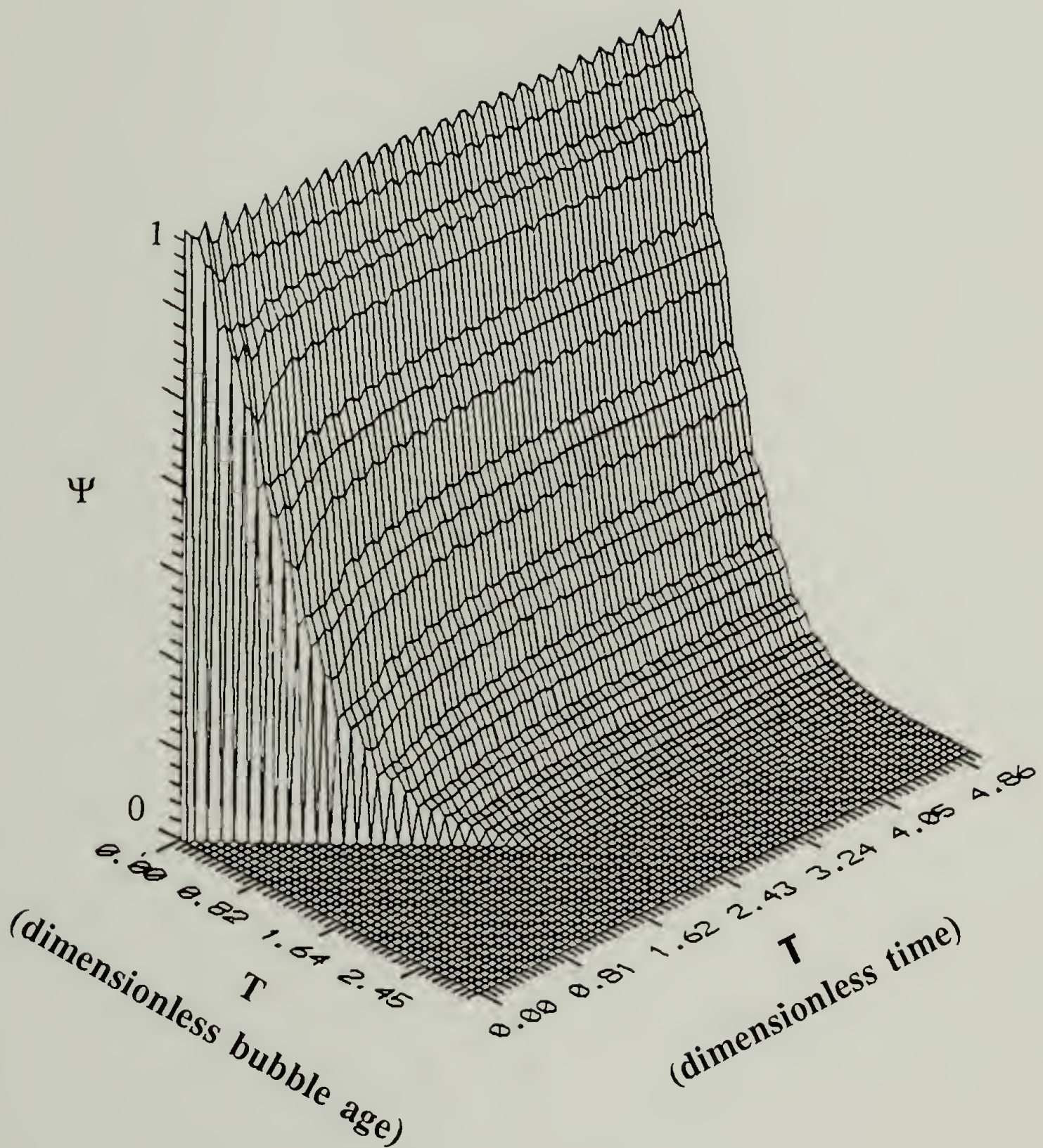


**Figure 7.7** Surface plot of the bubble age distribution predicted by the Complete Model of the rolling drum devolatilizer.  $\alpha_1 = 0.0002$ ,  $\alpha_2 = 0.00136$ ,  $\alpha_3 = 0.4$  and  $\alpha_4 = 336$ .

however, the nucleation is sustained over longer times resulting in a broader ridge along  $T = T$ . Reducing the nucleation rate another order of magnitude to  $\alpha_1 = 0.0002$ , the radial expansion ratio, shown in Figure 7.6, has been significantly reduced to a value less than 1.5. The distribution shown in Figure 7.7 approaches a QSS. This is expected, since in the limit as  $R_1/R_c$  approaches 1, the solution for the Complete Model should approach that of the Full Model, which, for these values of the model parameters, approaches a quasi-steady state.

For comparison with the Full Model, the Complete Model was also used to correlate data 3 of Biesenberger and Lee. The same value of  $E_a = 15.2 \text{ atm}^2 \text{ K}$  used in correlating the Full Model gave an acceptable fit of the data. However, the value of  $F$  which best fit the data was reduced from  $798 \text{ cm}^{-3} \text{ s}^{-1}$  for the Full Model to  $20 \text{ cm}^{-3} \text{ s}^{-1}$  for the Complete Model. The goodness of the fit was indistinguishable from that given by the Full Model. A smaller nucleation rate was required to compensate for the decreased rupture rates caused by the volume expansion. The descriptors predicted by the Complete Model are plotted in Figure 7.8. The maximum radial expansion ratio is predicted to be approximately 6, corresponding to a volume fraction of about 0.97.

The large foam expansion predicted by the Complete Model is unrealistic. Also, the maximum average bubble radius, predicted to be approximately 7 mm, is at least an order of magnitude too large. So, although the model was able to give a good correlation of the DV rate, its description of the bubble distribution is not realistic. Apparently, one or more of the model assumptions are invalid. The descriptions of the bubble nucleation, growth and rupture may be inaccurate, or, perhaps, bubble coalescence, breakage or deformation may make a significant contribution to the DV rate and should have been included in the model.

The most effective means of determining the validity of our model assumptions would be to conduct experimental studies of the nature of foaming occurring during DV.

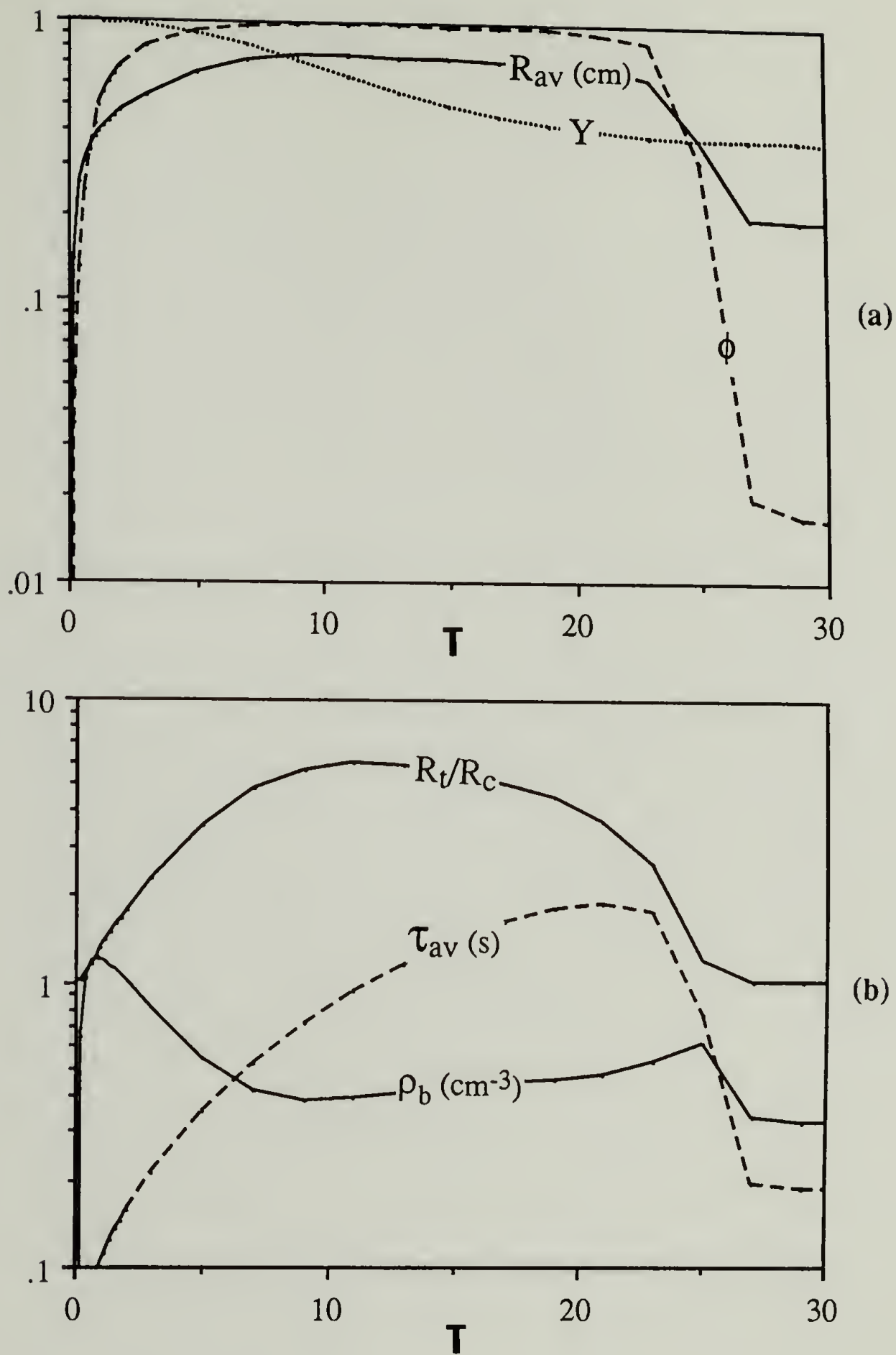


**Figure 7.8** Plots of the descriptors predicted by the Complete Model of the rolling drum devolatilizer for conditions of experiment 3 of Biesenberger and Lee (1986).  $F = 20 \text{ cm}^{-3} \text{ s}^{-1}$ ,  $E_a = 15.2 \text{ atm}^2 \text{ K}$ ,  $\alpha_1 = 0.0005$ ,  $\alpha_2 = 0.00136$ ,  $\alpha_3 = 0.4$  and  $\alpha_4 = 336$ .

Unfortunately, the equipment and facilities necessary for these studies were not available. Rather, the models were investigated to determine if changes in the magnitudes of the nucleation, growth and rupture rates can provide more realistic descriptions of the state of the foam.

To guide us in this task, a general model of DV will first be constructed which will include our DV models as special cases. This general model will be analyzed to obtain insight into the effects of bubble birth, growth and death on the nature of the foaming. It will provide information valuable in determining how the rates of these processes should be varied so that more realistic foaming is predicted while maintaining the DV rate which correlates the DV performance data.

### 7.3 A General Model of DV

The general model of DV will include general descriptions of the bubble nucleation, growth and rupture. Bubble coalescence, breakage and deformation will be neglected. By analogy with classical nucleation theory, the nucleation rate will be assumed to depend on the supersaturation according to the general expression.

$$B = b(\Delta C) \delta(\tau) \quad 7.3$$

where  $b(\Delta C)$  is an arbitrary function of the supersaturation,  $\Delta C$ , and quantifies the frequency of nucleation. The Dirac-Delta function,  $\delta(\tau)$ , forces all bubbles to be born at age  $\tau = 0$ . We have assumed that other variables which might affect the nucleation rate, such as temperature or surface tension, will not vary with time and therefore can be treated as constants embedded in the expression for  $b(\Delta C)$ .

To derive a general expression for the bubble growth rate, we will assume that the growth is diffusion-controlled and that the bubbles remain spherical. We will also assume that the mass flux to the bubble can be described by the expression

$$\text{Mass Flux} = k_c \Delta C \quad 7.4$$

where  $k_c$  is the instantaneous mass transfer coefficient. A mass balance over the bubble relates the bubble growth rate,  $dR/dt$ , to  $k_c$ .

$$\frac{dR}{dt} = k_c \left( \frac{\Delta C}{\rho_g} \right) \quad 7.5$$

Integrating over the bubble's age  $\tau$  gives the bubble's radius as a function of its age

$$R = R_0 + \int_0^\tau k_c \left( \frac{\Delta C}{\rho_g} \right) d\tau \quad 7.6$$

where  $R_0$  is the radius of the bubble at birth ( $\tau = 0$ ).  $k_c$  remains within the integral, as it can be a function of time, as will be shown below.

To gain insight into the time dependence of  $k_c$ , we will examine the expression for  $k_c$  corresponding to the bubble growth rate expression developed by Szekely and Martin (1971) for the diffusion-controlled growth of a gas bubble in a stagnant, binary fluid of infinite extent. This expression was used in our DV models presented in Chapters 4 and 5 and is restated here

$$R = R_0 + \sqrt{\frac{12D}{\pi}} \left( \frac{\Delta C}{\rho_g} \right) \tau^{1/2} \quad 7.7$$

The bubble growth rate is determined by differentiating with respect to  $t$

$$\frac{dR}{dt} = \frac{1}{2} \sqrt{\frac{12D}{\pi}} \left( \frac{\Delta C}{\rho_g} \right) \tau^{-1/2} \quad 7.8$$

Comparison with equation 7.5 gives this expression for the mass transfer coefficient

$$k_c = \sqrt{\frac{3D}{\pi}} \tau^{-1/2} \quad 7.9$$

The form of this expression indicates that a suitable, general, instantaneous mass transfer coefficient might take the form of a power law in  $\tau$

$$k_c \propto \tau^{q-1}$$

where  $q - 1$  is an arbitrary power law exponent. A general expression for  $dR/dt$  results



$$\frac{dR}{dt} = q \gamma(\Delta C) \tau^{q-1} \quad 7.10$$

where  $\gamma(\Delta C)$  is a proportionality factor which quantifies the growth rate and is assumed to be an arbitrary function of the supersaturation,  $\Delta C$ .

The general expression for the time dependence of the bubble radius is

$$R(\tau) = \int_0^\tau q \gamma(\Delta C) t^{q-1} dt \quad 7.11$$

where the radius at birth,  $R_0$ , was set equal to zero. This will be a valid approximation if the bubble grows many times larger in radius than  $R_0$ , as is expected. If  $\gamma(\Delta C)$  changes negligibly over the life time of the bubbles,  $\gamma(\Delta C)$  may be removed from within the integral and the expression for  $R$  may be approximated as

$$R = \gamma(\Delta C) \tau^q \quad 7.12$$

The constraint that the concentration change slowly over the lifetime of the bubbles is met if a quasi-steady state bubble distribution is approached.

This rigorous derivation of the time dependence of a bubble's radius reveals a subtle assumption embedded in the derivation of the bubble growth rate expressions used in our DV models. The growth rate expression used is that of Szekely et al., derived assuming the concentration far from the bubble to be constant. However, in a devolatilizer, the solvent concentration far from the bubble is the average solvent concentration. It will decrease with time and this expression is not strictly valid. At any instant, equation 7.12 presumes that all bubbles have grown over their entire lifetimes with the instantaneous value of the supersaturation. Actually, the average supersaturation over the bubbles lifetime is greater than this instantaneous value and this expression underestimates the radius of the bubbles. If a quasi-steady state is approached, then the concentration changes negligibly over the bubbles lifetimes and the approximation is valid. Otherwise, the bubble radius will be underestimated.

Bubble death will be assumed to occur by rupture of bubbles at the vapor-liquid free surface. Death by coalescence and breakage will not be included. Surface rupture can occur by the mechanisms of mechanical shearing or film draining. The expression for the bubble rupture rates by mechanical shearing presented in Chapters 4 and 5 and the expression for rupture by film draining which will be presented later in this chapter are both proportional to the surface density of bubbles. Since the surface density of homogeneously distributed bubbles is proportional to the product of  $f$  (the age distribution) and  $R$ , by analogy we will propose the following general expression for the bubble rupture rate

$$E = e f R^r \quad 7.13$$

The arbitrary exponent on  $R$ ,  $r$ , is included to make the expression more general.  $e$  is a proportionality constant and is a measure of the frequency of rupture of surface bubbles.

Substituting these general expressions for the bubble birth, growth and death rates into the mass balance and population balance expressions derived in Chapter 5 for the rolling drum model gives equations for the general model

$$\frac{d\Delta C}{dt} = -4\pi \frac{\rho_g}{A_c} \int_0^\infty R^2 \frac{dR}{dt} f d\tau \quad 7.14a$$

$$\frac{\partial f}{\partial t} + \frac{\partial f}{\partial \tau} = -e R^r f \quad 7.14b$$

$$R = \int_0^\tau q \gamma(\Delta C) t^{q-1} dt$$

$$\text{at } t = 0 \quad \begin{cases} \Delta C = C_0 - C_e \\ f = 0 \end{cases}$$

$$\text{at } \tau = 0 \quad f = b(\Delta C)$$

Assuming the solvent concentration changes slowly over the lifetime of the bubbles such that  $\gamma(\Delta C)$  remains nearly constant, the model equations simplify to

$$\frac{d\Delta C}{dt} = -4\pi q \frac{\rho_g}{A_c} \gamma(\Delta C)^3 \mu_{3q-1} \quad 7.15a$$

$$\frac{\partial f}{\partial t} + \frac{\partial f}{\partial \tau} = -e \gamma(\Delta C)^r \tau^{rq} f \quad 7.15b$$

$$\text{at } t=0 \quad \begin{cases} \Delta C = C_0 - C_e \\ f = 0 \end{cases}$$

$$\text{at } \tau=0 \quad f = b(\Delta C)$$

Introducing the dimensionless variables,  $Y$ ,  $\Psi$ ,  $\mathbf{T}$  and  $\mathbf{T}$  defined in Chapter 5 with the reference scales

$$\Delta C^* = C_0 - C_e = C_{\max}$$

$$f^* = b(1)$$

$$t^* = [e \gamma(1)^r]^{-1/(rq+1)}$$

$$\tau^* = t^*$$

the dimensionless general model equations reduce to

$$\frac{dY}{d\mathbf{T}} = -4\pi q \left( \frac{\rho_g}{C_{\max}} \right) \left( \frac{b(1)}{[e^{3q+1} \gamma(1)^{r-3}]^{1/(rq+1)} A_c} \right) \left[ \frac{\gamma(Y)}{\gamma(1)} \right]^3 M_{3q-1} \quad 7.16a$$

$$\frac{\partial \Psi}{\partial \mathbf{T}} + \frac{\partial \Psi}{\partial \mathbf{T}} = - \left[ \frac{\gamma(Y)}{\gamma(1)} \right]^r \mathbf{T}^{rq} \Psi \quad 7.16b$$

$$\text{at } \mathbf{T} = 0 \quad \begin{cases} Y = 1 \\ \Psi = 0 \end{cases}$$

$$\text{at } \mathbf{T} = 0 \quad \Psi = \frac{b(Y)}{b(1)}$$

As was done for the single screw and rolling drum model, the population balance will be expressed as an infinite set of ODE's in terms of the moments of the distribution

$$\begin{aligned}
\frac{dM_0}{dT} &= \frac{b(Y)}{b(1)} - \left[ \frac{\gamma(Y)}{\gamma(1)} \right]^r M_{Tq} \\
\frac{dM_1}{dT} &= M_0 - \left[ \frac{\gamma(Y)}{\gamma(1)} \right]^r M_{Tq+1} \\
&\vdots \quad \quad \quad \vdots \\
\frac{dM_n}{dT} &= n M_{n-1} - \left[ \frac{\gamma(Y)}{\gamma(1)} \right]^r M_{Tq+n}
\end{aligned}
\tag{7.17}$$

We will investigate the general model for the special case  $r = 1$  and  $q = 1/2$ . These are the values used in the models of the single screw and rolling drum devolatilizers. For these values of  $r$  and  $q$ , the general model equations reduce to

$$\frac{dY}{dT} = -2\pi \left( \frac{\rho_g}{C_{\max}} \right) \left( \frac{b(1) \gamma(1)^{4/3}}{e^{5/3} A_c} \right) \left[ \frac{\gamma(Y)}{\gamma(1)} \right]^3 M_{1/2}
\tag{7.18a}$$

$$\frac{\partial \Psi}{\partial T} + \frac{\partial \Psi}{\partial T} = - \left[ \frac{\gamma(Y)}{\gamma(1)} \right] T^{1/2} \Psi
\tag{7.18b}$$

$$\text{at } T = 0 \quad \begin{cases} Y = 1 \\ \Psi = 0 \end{cases}$$

$$\text{at } T = 0 \quad \Psi = \frac{b(Y)}{b(1)}$$

and the reference scales become

$$\Delta C^* = C_0 - C_e = C_{\max}$$

$$f^* = b(1)$$

$$t^* = [e \gamma(1)]^{-2/3}$$

$$\tau^* = t^*$$

Expressions for the descriptors of the distribution predicted by the general model were derived by substituting the above expressions for the characteristic reference scales into the definitions of the descriptors, equations 7.1

$$\tau_{av} = \frac{1}{[e \gamma(1)]^{2/3}} \frac{M_1}{M_0} \quad 7.19a$$

$$R_{av} = \left( \frac{\gamma(Y)}{[e \gamma(1)]^{1/3}} \right) \frac{M_{1/2}}{M_0} = \left( \frac{\gamma(1)^{2/3}}{e^{1/3}} \right) \frac{M_{1/2}}{M_0} \quad 7.19b$$

$$\phi = \left( \frac{1}{1 + \frac{[e \gamma(1)]^{5/3} A_c}{\frac{4}{3} \pi b(1) \gamma(Y)^3 M_{3/2}}} \right) = \left( \frac{1}{1 + \frac{A_c e^{5/3}}{\frac{4}{3} \pi b(1) \gamma(1)^{4/3} M_{3/2}}} \right) \quad 7.19c$$

$$\rho_b = \frac{M_0}{\frac{4}{3} \pi \frac{\gamma(Y)^3}{e \gamma(1)} M_{3/2} + \frac{e^{2/3} \gamma(1)^{2/3} A_c}{b(1)}} = \frac{M_0}{\frac{4}{3} \pi \frac{\gamma(1)^2}{e} M_{3/2} + \frac{e^{2/3} \gamma(1)^{2/3} A_c}{b(1)}} \quad 7.19d$$

$$\frac{R_t}{R_c} = \left[ 1 + \frac{16}{3} \left( \frac{b(1)}{e^{5/3} \gamma(1)^{5/3}} \right) \gamma(Y)^3 M_{3/2} \right]^{1/2} = \left[ 1 + \frac{16}{3} \left( \frac{b(1) \gamma(1)^{4/3}}{e^{5/3}} \right) M_{3/2} \right]^{1/2} \quad 7.19e$$

$$\frac{dY}{dt} = -2\pi \left( \frac{\rho_g}{C_{max}} \right) \left( \frac{b(1) \gamma(1)^2}{e A_c} \right) \left( \frac{\gamma(Y)}{\gamma(1)} \right)^3 M_{1/2} = -2\pi \left( \frac{\rho_g}{C_{max}} \right) \left( \frac{b(1) \gamma(1)^2}{e A_c} \right) M_{1/2} \quad 7.19f$$

The expressions in the limit as  $\mathbf{T}$  approaches zero (i.e.  $Y = 1$ ) are also presented. This clarifies the dependence of the descriptors on the birth, growth and death rates by removing the dependence on  $Y$ . The expression for the DV rate,  $dY/dt$ , is included in equation 7.19. Given these expressions for the descriptors of the general model, we will investigate whether changes in the magnitudes of the bubble birth, growth or death rates (i.e.  $b$ ,  $\gamma$  and  $e$ ) can reduce the bubble volume fraction to acceptable values while maintaining the DV rate,  $dY/dt$ , constant and equal to the experimentally measured DV rate.

Note that if a quasi-steady state bubble distribution occurs, the dimensionless moments of the distribution will approach a nearly constant value after the short-lived boundary layer is passed (see, for example, Figure 6.2). The dependence of the

descriptors on the model variables can be quantified solely by the prefactors  $b(1)$ ,  $\gamma(1)$ ,  $e$ ,  $\rho_g/C_{\max}$  and  $A_c$  multiplying the moments in the descriptor expressions.

Examining the dependence of the descriptor expressions on the birth, growth and death rates reveals how the character of the bubble distribution is affected by changes in the rates of these processes. The average age of the bubbles,  $\tau_{av}$ , is predicted to decrease with increasing growth rate,  $\gamma(1)$ , and rupture rate,  $e$ . The predicted decrease in the bubble age with increasing growth rate can be explained by the fact that larger bubbles rupture more frequently than smaller bubbles as they are more likely to be located at the vapor/liquid interface. Increasing the growth rate causes the bubbles to reach larger radii earlier and, therefore, rupture earlier.

The average radius of the bubbles,  $R_{av}$ , is predicted to increase with increasing growth rate and decrease with increasing rupture rate, as anticipated. Note that the nucleation rate,  $b$ , is predicted to have no effect on the average bubble age and radius. Note also that the average radius of the bubbles does not increase linearly with the bubble growth rate,  $\gamma(1)$ , as might be anticipated from inspection of the growth rate expression, equation 7.10. This is because increases in the growth rate result in a decrease in the average age of a bubble, as indicated by the expression for  $\tau_{av}$ . So, although bubbles grow faster with increasing growth rate, the time over which they grow is reduced.

The volume fraction of bubbles,  $\phi$ , is predicted to increase with increasing birth and growth rates but decrease with increasing rupture rate. The radial expansion ratio,  $R_l/R_c$ , behaves exactly as the volume fraction, since it is also a measure of the volume of the bubble phase. For the number of bubbles per volume,  $\rho_b$ , at small volume fractions such that the second term in the denominator dominates, the general model predicts that the number density of bubbles increases with increasing birth rate and decreasing rupture and growth rates.

The DV rate,  $dY/dt$ , is predicted to increase proportionally with the bubble nucleation rate but vary inversely with the bubble rupture rate. This is physically reasonable.

However, the DV rate is predicted to increase with the square of the bubble growth rate. This is interesting, as one might anticipate that the DV rate would increase linearly with the cube of the growth rate, since the rate of mass uptake to any bubble is predicted by the growth model to increase proportionally with the cube of  $\gamma(1)$  (see equation 7.15a). Indeed, models of DV proposed by previous investigators, which include very naive descriptions of bubble birth and death, would predict this behavior. It can be explained if one investigates the effect on the bubble distribution of an increase in the bubble growth rate. Increasing the bubble growth rate will decrease the total number of bubbles, as shown by equation 7.19d. This will reduce the total rate of mass uptake by the foam phase. So increases in the bubble growth rate could have an effect on the DV performance diminished from that which might be expected intuitively.

The descriptor expressions derived from the general model of DV demonstrate the complex effects that the bubble birth, growth and death can have on the DV performance and on the nature of the resulting foam. This reveals the usefulness of conceptually realistic DV models, even if approximate, in providing insight into the nature of the foaming process that might not otherwise be correctly intuited.

#### **7.4 Rolling Drum Devolatilizer Model with Rupture by Film Draining**

Inspection of the descriptor expressions reveals that a means for reducing the volume fraction of bubbles while maintaining a constant DV rate is to increase the birth and death rates proportionally. A larger rupture rate can be justified if rupture by film draining makes a significant contribution to the total rupture rate. Bubble rupture by film draining was not included in the preliminary model and would provide a means for increasing the rupture rate. As well, the nucleation expression used in our DV models is empirical and has no constraints on its magnitude. It may be increased as necessary.

In Appendix B an expression for the rate of rupture of bubbles by film draining in a single screw devolatilizer,  $E_{F,D}$ , is derived in detail. An analogous derivation was used to

determine the following expression for the bubble rupture rate by film draining in the rolling drum devolatilizer

$$E_{F.D.} = \begin{cases} \frac{2 R H_b f}{A_t} \left( \frac{1}{\tau_R} - \frac{V_b}{H_b} \right) & \tau_R \leq \frac{H_b}{V_b} \\ 0 & \tau_R > \frac{H_b}{V_b} \end{cases} \quad 7.20$$

where  $\tau_R$  is the time a bubble spends at the liquid/vapor interface before rupturing and can be a function of  $R$ . Adding to this expression the rupture rate by mechanical shearing,  $E_{M.S.}$

$$E_{M.S.} = \frac{2 R V_b f}{A_t} \quad 7.21$$

gives an expression for the total rupture rate

$$E = \begin{cases} \frac{2 R H_b f}{A_t \tau_R} & \tau_R \leq \frac{H_b}{V_b} \\ \frac{2 R V_b f}{A_t} & \tau_R > \frac{H_b}{V_b} \end{cases} \quad 7.22$$

We are not aware of any studies of the rupture time,  $\tau_R$ , of a bubble driven to the interface of a free surface cavity flow. Since an expression for  $\tau_R$  is not available, for preliminary studies we will assume it to be a constant for all bubbles. As well, we will assume that  $\tau_R < H_b/V_b$ , where  $H_b/V_b$  is the maximum time a fluid element can spend at the surface before reaching the convergence point. This allows that bubbles can rupture by film draining before the bubbles reach the convergence point of the bulk and barrel films. Otherwise, if  $\tau_R > V_b/H_b$ , rupture will occur by mechanical shearing only.

Replacing this expression for the death rate with that in the population balance equation of the mechanical shearing rolling drum devolatilizer model (which will be referred to as the M.S. Model), equation 5.1b, gives a new expression for the population balance which includes rupture by film draining



$$\frac{\partial f}{\partial t} + \frac{\partial f}{\partial \tau} = -4\sqrt{\frac{3}{\pi}} \left( \frac{D^{1/2} H_b}{\rho_g A_t \tau_R} \right) \Delta C \tau^{1/2} f \quad 7.23$$

This new model will be termed the Film Draining Model (F.D. Model). Note that in equation 7.23, the bubble radius has been expressed in terms of its age using the bubble growth rate expression.

The model equations will be nondimensionalized by the same reference scales used for nondimensionalizing the M.S. Model in Chapter 5, with the exception that the characteristic time will be redefined as

$$\tau^* = \frac{A_c^{1/3} \tau_R^{2/3}}{D^{1/3}} \left( \frac{\rho_g}{C_{\max}} \right)^{2/3}$$

The nondimensional equations of the F.D. model are

$$\frac{dY}{d\Gamma} = -48\sqrt{\frac{3}{\pi}} \alpha_1 M_{1/2} Y^3 - \frac{2}{\pi^{1/4}} \alpha_2 \left[ \frac{A_t}{A_c} \right]^{1/4} Y \quad 7.24a$$

$$\frac{\partial \Psi}{\partial \Gamma} + \frac{\partial \Psi}{\partial \Gamma} = -4\sqrt{3} \left( \frac{A_c}{A_t} \right)^{1/2} \Gamma^{1/2} Y \Psi \quad 7.24b$$

$$\text{at } \Gamma = 0 \quad \begin{cases} Y = 1 \\ \Psi = 0 \end{cases}$$

$$\text{at } \Gamma = 0 \quad \Psi = \exp \left[ \alpha_3 \left( 1 - \frac{1}{Y^2} \right) \right]$$

where the definition of  $A_t/A_c$  is identical to that presented for the M.S. Model in Chapter 5.

$$\frac{A_t}{A_c} = 1 + 32\sqrt{\frac{3}{\pi}} \alpha_1 \alpha_4 Y^3 M_{3/2}$$

Only the expressions for  $\alpha_1$  and  $\alpha_2$  have changed

$$\alpha_1 = A_c^{5/6} \tau_R^{5/3} D^{2/3} \left( \frac{C_{\max}}{\rho_g} \right)^{1/3} F \exp(-\alpha_3)$$

$$\alpha_2 = \frac{D^{1/6} V_b^{1/2} \tau_R^{2/3}}{A_c^{5/12}} \left( \frac{\rho_g}{C_{\max}} \right)^{2/3}$$

Note that the mechanical shearing rupture rate decreases inversely with the extent of foam expansion,  $A_t/A_c$  (see equation 5.2b), whereas, the film draining rupture rate decreases inversely with the square root of  $A_t/A_c$  (equation 7.24b). Volume expansion reduces the rate of bubble rupture by film draining less than it does the rupture rate by mechanical shearing. This can be explained by the fact that the mechanical shearing occurs at a point on the surface (i.e. at the convergence point of the bulk and barrel films) rather than over the entire surface, as does rupture by film draining. Volume expansion increases the surface area of the interface which allows more bubbles to rupture by film draining. This moderates the reduction in the film draining rupture rate caused by volume expansion. Since rupture by mechanical shearing occurs at a point on the surface, the increasing surface area has no effect on its rate.

The reduced effect of foam expansion on the rate of bubble rupture by film draining can be seen clearly in the surface plot of the bubble age distribution calculated from the F.D. Model presented in Figure 7.9. The values of the model parameters input into the F.D. Model to produce this distribution are the same parameters that were used to correlate data 3 of Biesenberger and Lee (1986) using the M.S. Model:  $\alpha_1 = 0.02$ ,  $\alpha_2 = 0.00136$ ,  $\alpha_3 = 0.4$  and  $\alpha_4 = 336$ . Comparison with the distribution presented in Figure 7.3 calculated from the M.S. Model at identical values of the dimensionless model parameters reveals that the ridge running along the characteristic  $T = \bar{T}$  is absent and the model exhibits near quasi-steady behavior. As was done for the M.S. Model, the F.D. Model was solved for identical values of  $\alpha_2$ ,  $\alpha_3$  and  $\alpha_4$  but for  $\alpha_1$  reduced an order of magnitude to  $\alpha_1 = 0.002$ . The bubble distribution predicted at these conditions is plotted in Figure 7.10. The F.D. Model clearly predicts a quasi-steady state distribution which was not exhibited by the

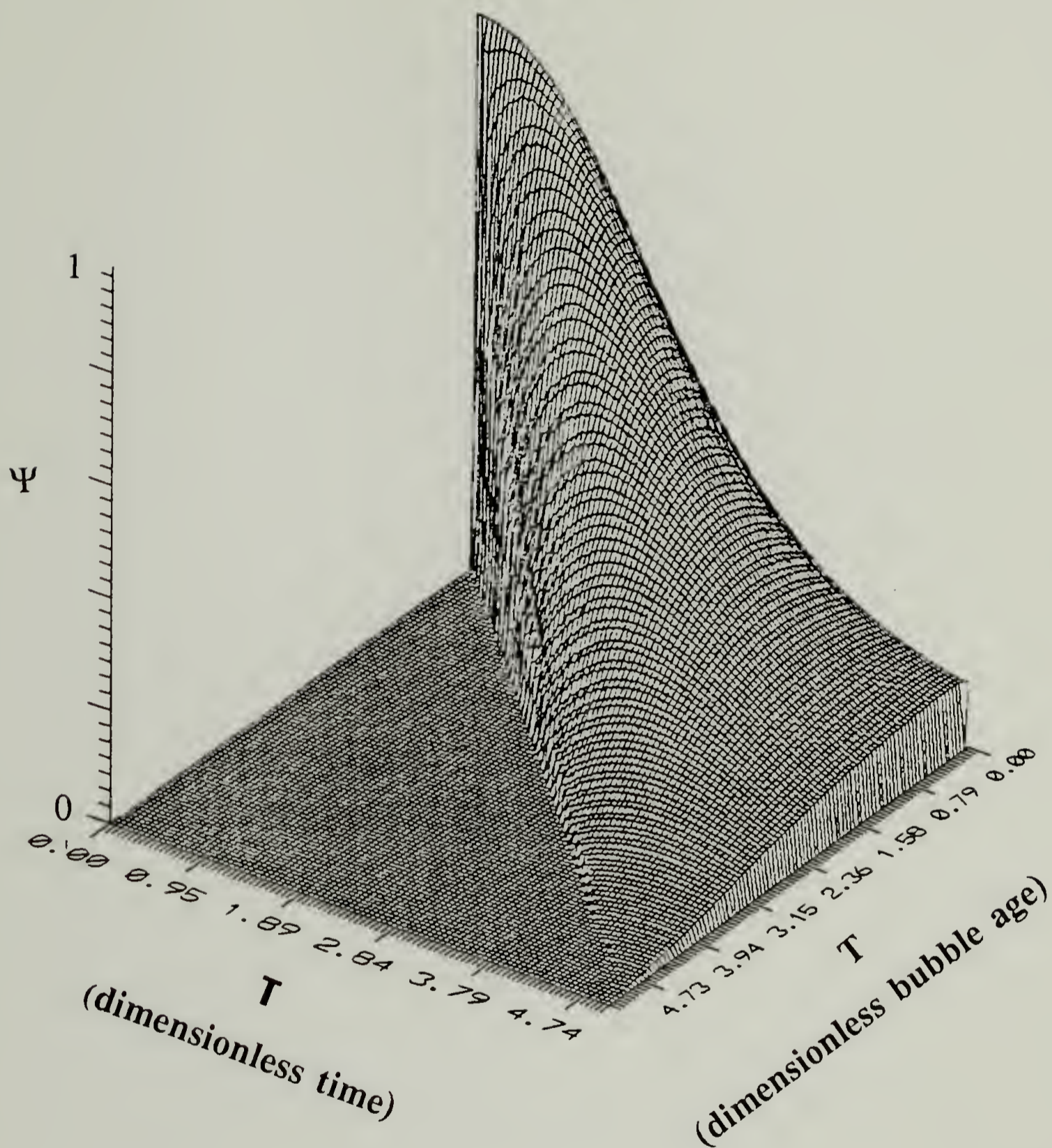


**Figure 7.9** Surface plot of the bubble age distribution predicted by the F.D. Complete Model of the rolling drum devolatilizer.  $\alpha_1 = 0.02$ ,  $\alpha_2 = 0.00136$ ,  $\alpha_3 = 0.4$  and  $\alpha_4 = 336$ .

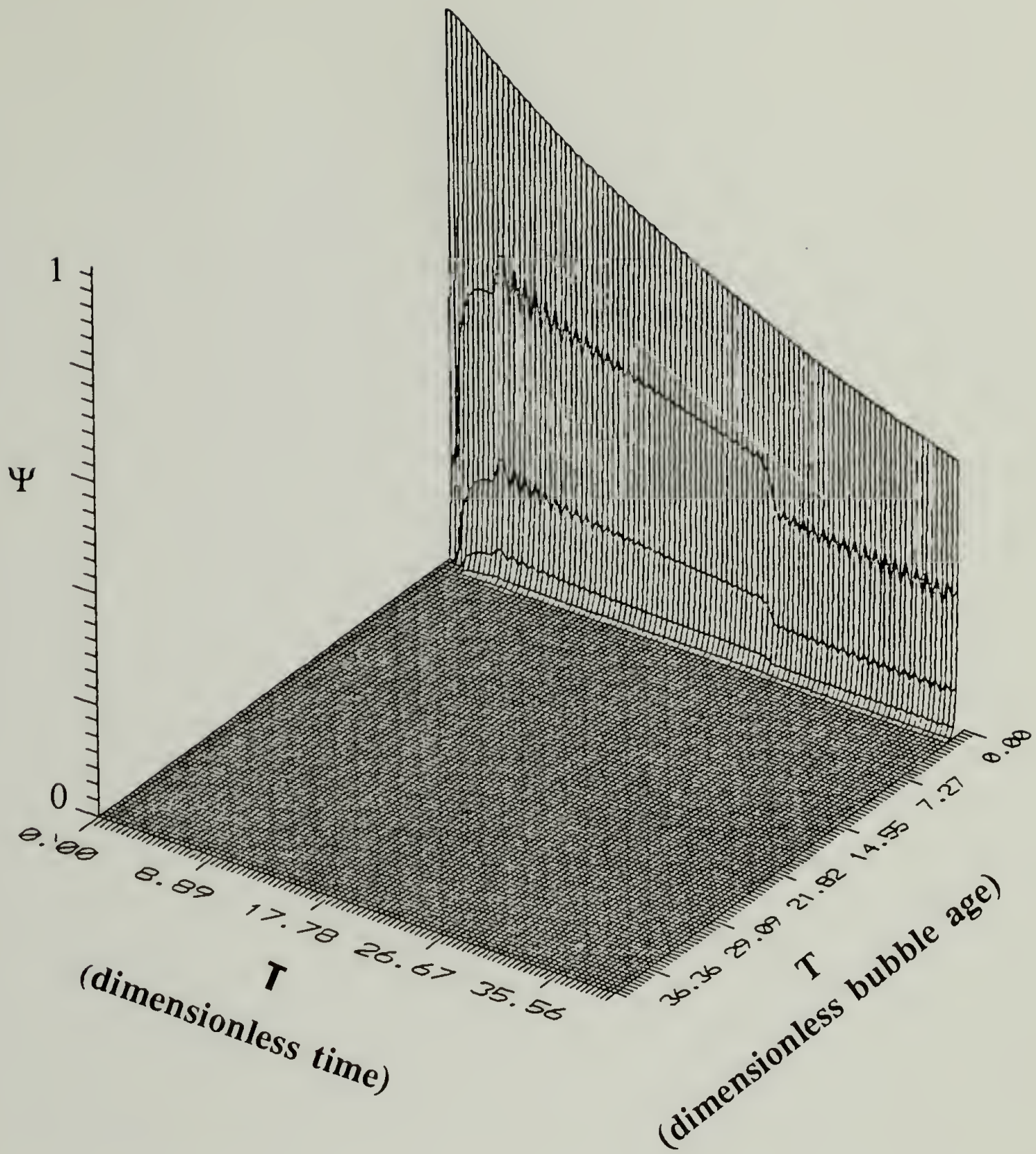


**Figure 7.10** Surface plot of the bubble age distribution predicted by the F.D. Complete Model of the rolling drum devolatilizer.  $\alpha_1 = 0.002$ ,  $\alpha_2 = 0.00136$ ,  $\alpha_3 = 0.4$  and  $\alpha_4 = 336$ .

M.S. Model in Figure 7.5 at identical conditions. It is evident from these results that volume expansion has less of an effect on the rupture rate in the F.D. Model than in the M.S. Model.

The ability of the F.D. Model to predict a realistic foam phase and simultaneously fit the measured DV rates will be investigated next. The F.D. Model was fit to Data 3 of Biesenberger and Lee's rolling drum experiments for increasing values of the nucleation and rupture rates. By choosing  $\tau_R = 0.005$  s, the rupture rate was increased approximately five times larger than the rupture rate specified by the Complete M.S. Model in correlating data 3 of Biesenberger and Lee (1986). The descriptors of the bubble distribution predicted by the F.D. Model for  $\tau_R = 0.005$  s are presented in Figure 7.11. The extent of volume expansion decreased as anticipated to a maximum of  $R_V/R_C = 5$  from  $R_V/R_C = 6$  for the M.S. Model (see Figure 7.8). Also, the average bubble radius decreased from a maximum of  $R_{av} = 0.7$  cm to  $R_{av} = 0.2$  cm. The values of  $F$  and  $E_a$  that best correlate the data are  $19500 \text{ cm}^{-3} \text{ s}^{-1}$  and  $15.2 \text{ atm}^2 \text{ K}$ .

There is a simple physical explanation why increasing the nucleation and rupture rates can reduce the volume fraction of foam, yet maintain the same DV rate. Increasing the nucleation and rupture rates results in a greater number of smaller bubbles, as predicted by the descriptor expressions. Since the DV rate is proportional to the total surface area of the bubbles, to maintain equivalent DV rates, the number of smaller bubbles must be that number which preserves roughly the total surface area of the bubbles. However, since the surface-to-volume ratio is larger for smaller bubbles, the total volume of the smaller bubbles must be smaller than that of the larger bubbles.

As the extent of volume expansion for this rupture rate is still unrealistically large, the rupture rate was increased an order of magnitude to  $\tau_R = 0.0005$  s. The descriptors predicted by the F.D. Model are shown in Figure 7.12. The maximum radial expansion ratio was reduced to approximately 1.5 which corresponds to a volume fraction of 0.6. The average bubble radius was also reduced to approximately 0.07 cm. The nucleation rate

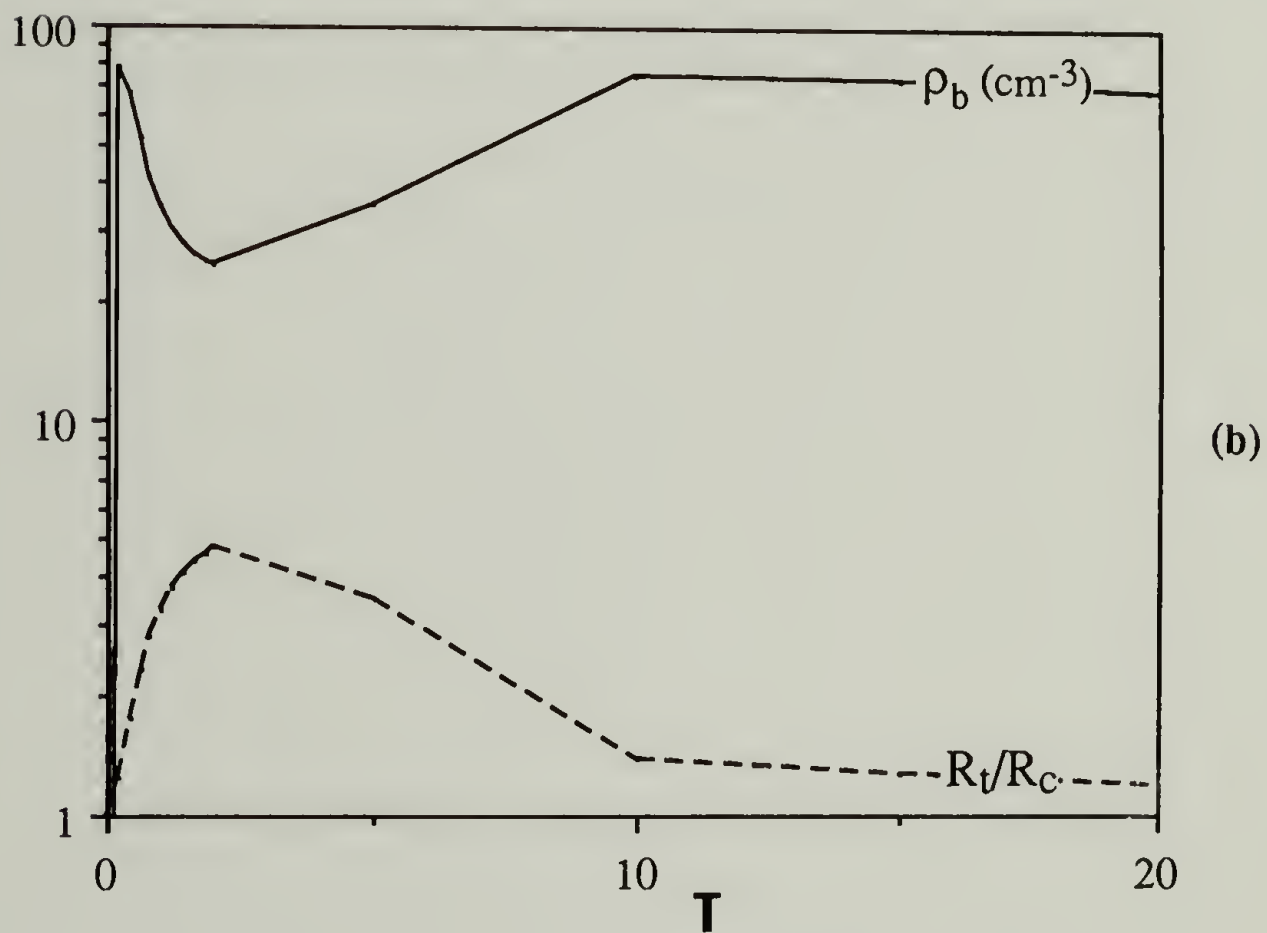
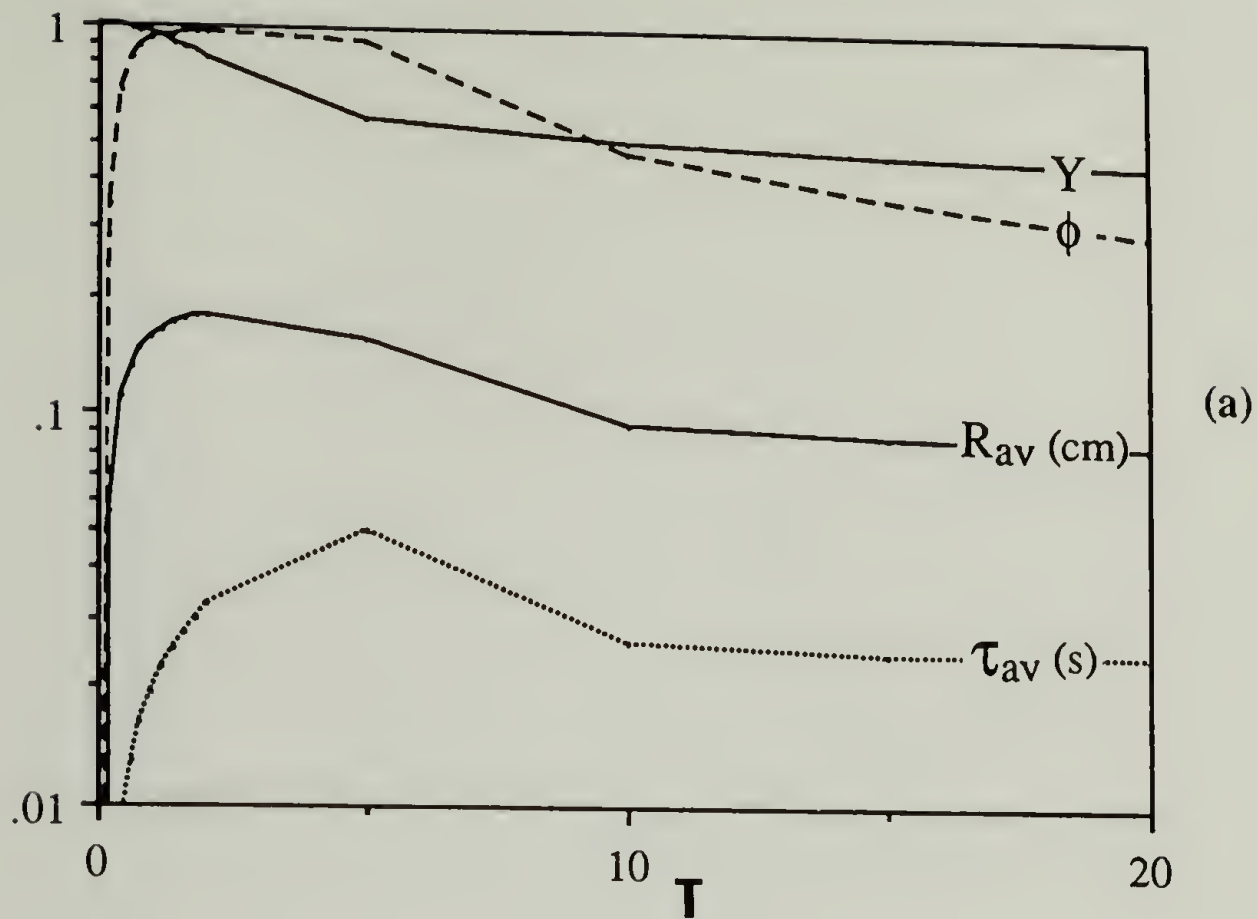


**Figure 7.11** Plots of the descriptors predicted by the F.D. Complete Model of the rolling drum devolatilizer for conditions of experiment 3 of Biesenberger and Lee (1986).  $F = 19500 \text{ cm}^{-3} \text{ s}^{-1}$ ,  $E_a = 15.2 \text{ atm}^2 \text{ K}$ ,  $\tau_R = 0.005 \text{ s}$ ,  $\alpha_1 = 0.008$ ,  $\alpha_2 = 0.000263$ ,  $\alpha_3 = 0.4$  and  $\alpha_4 = 336$ .

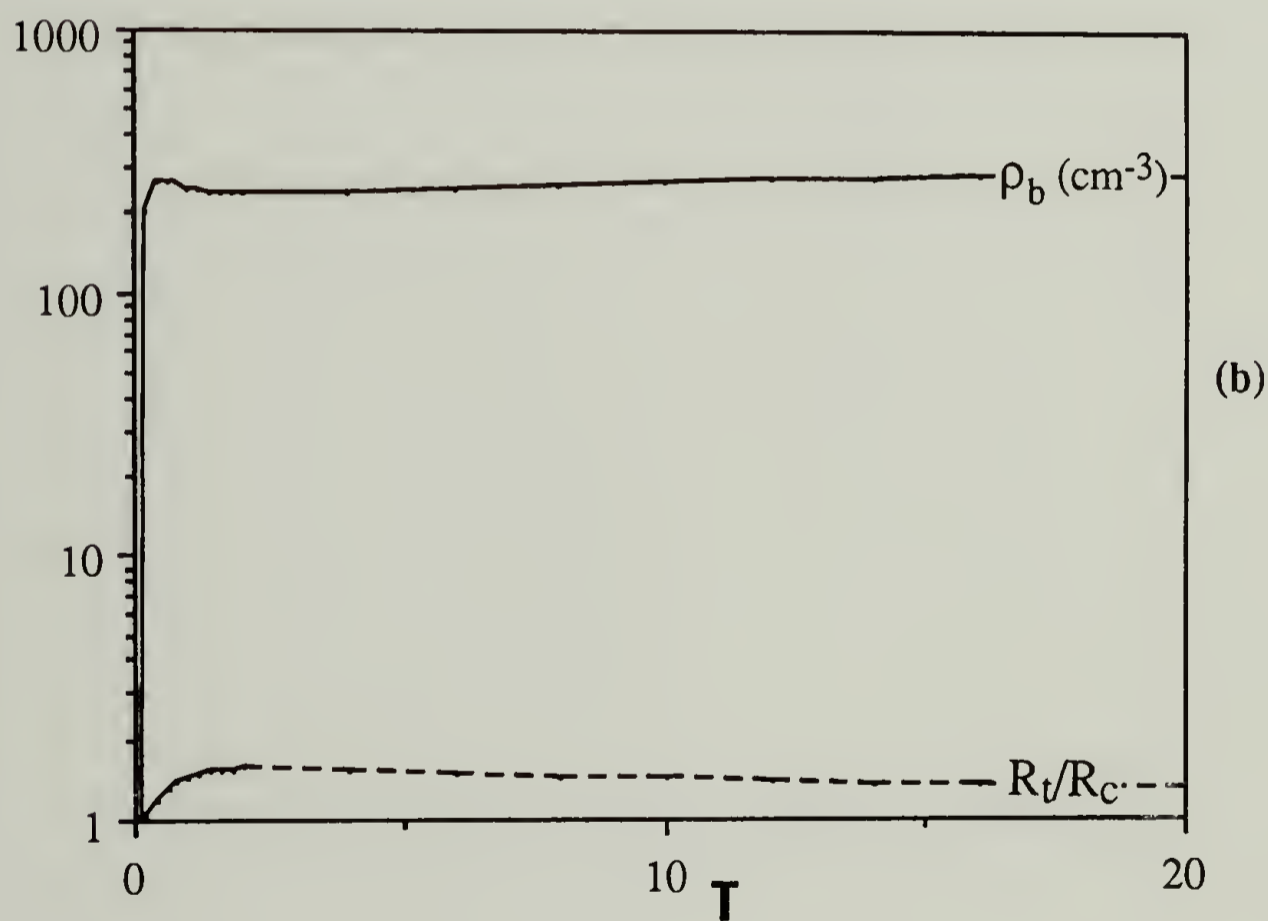
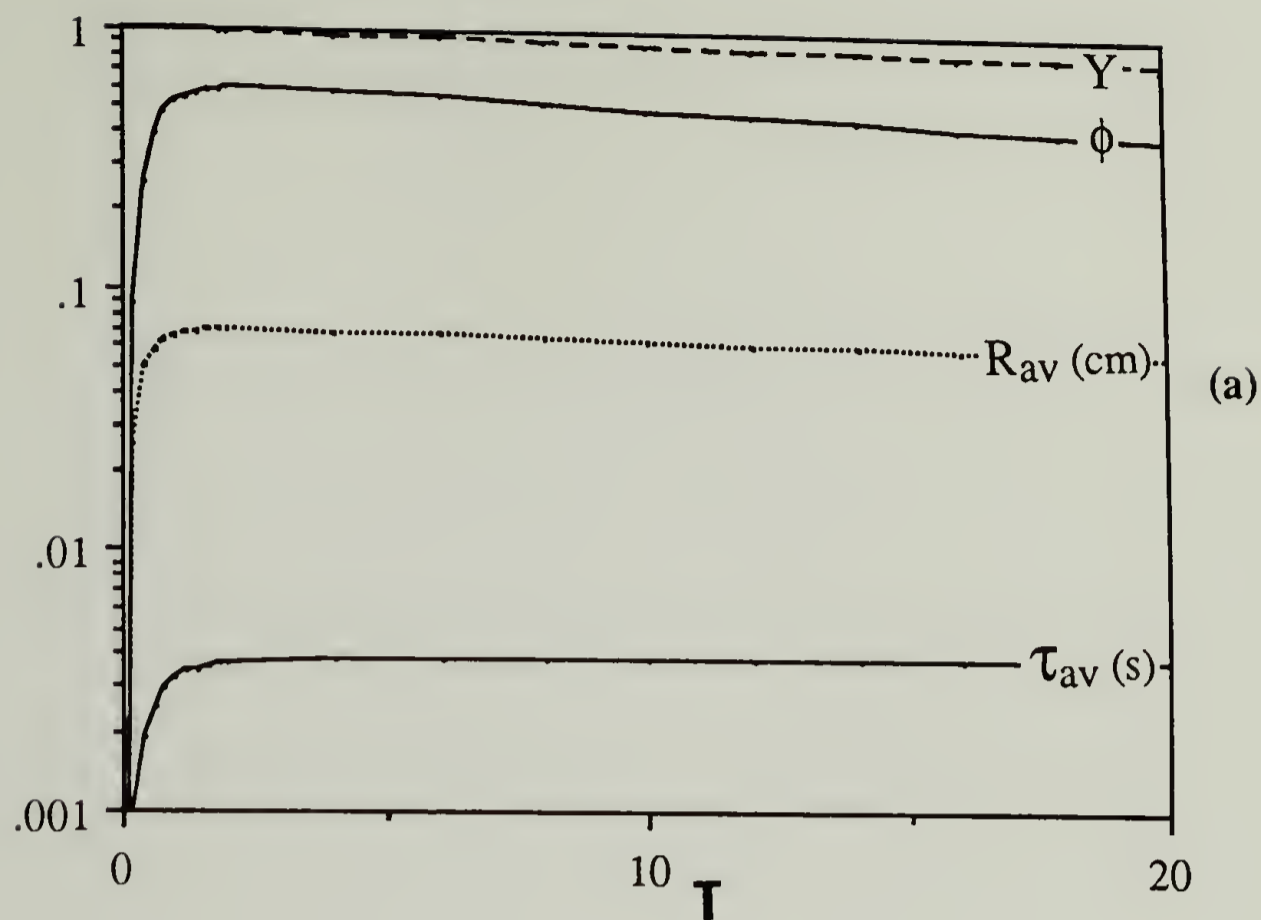


**Figure 7.12** Plots of the descriptors predicted by the F.D. Complete Model of the rolling drum devolatilizer fit to data 3 Biesenberger and Lee (1986).  $F = 1.7 \times 10^5 \text{ cm}^{-3} \text{ s}^{-1}$ ,  $E_a = 15.2 \text{ atm}^2 \text{ K}$ ,  $\tau_R = 0.0005 \text{ s}$ ,  $\alpha_1 = 0.0015$ ,  $\alpha_2 = 5.67 \times 10^{-5}$ ,  $\alpha_3 = 0.4$  and  $\alpha_4 = 336$ .

was increased an order of magnitude to  $F = 1.7 \times 10^5 \text{ cm}^{-3} \text{ s}^{-1}$  to maintain the same DV rate. The value of  $E_a$  was not changed. Note that proportional increases in the nucleation and ruptures rates maintained the DV rate at its previous value, as predicted by the descriptor expressions.

Increasing the nucleation rate and the film draining rupture rate reduced the extent of volume expansion and the average bubble radius to reasonable values. However, the average bubble age is predicted to be approximately 0.004 s, which is unrealistically small. This could have been foreseen if the expression for  $\tau_{av}$  were inspected. Increasing the death rate must decrease the bubble age. Although the F.D. Model can give a good correlation of the DV rate, its description of the bubble age distribution is not wholly realistic.

One explanation why the model predicts unrealistic foaming behavior may be that the hydrodynamic pressure in the fluid could be raised above that of the ambient pressure due to the applied flow. Evidence that pressure increases accompany increases in the screw rotation rate was found by Biesenberger and Lee (1986) during their observation of foaming in the rolling drum devolatilizer. They noted that increases in the barrel rotation rate caused the foaming pool to shrink in volume. Biesenberger et al. attributed this to an increase in the fluid pressure due to flow. This is plausible, however, a contributing factor to the reduction in foam expansion could be the increase in the bubble rupture rate by mechanical shearing, which is predicted by our model to accompany increases in the screw rotation rate. Yet, additional evidence for an increase in pressure was given by Biesenberger et al.. They observed bubbles to grow slower at higher drum rotation rates. Also, at high rotation rates, bubbles were observed to be compressed out of existence.

The pressure increase expected to occur in a typical single screw devolatilizer can be estimated using the analysis by Tadmor and Gogos (1979) of pressurization in the single screw extruder. For styrene/polystyrene solutions at operating conditions typical of the conditions studied by Coughlin and Canevari (1969), the cross channel pressure gradient,



$dP/dx$ , was estimated to be of order 10 psi/cm. This indicates that large pressure gradients may indeed occur in the cross section of the bulk film.

If the fluid pressure increases significantly in excess of the applied pressure, a more realistic bubble distribution is expected. The volume fraction of bubbles would be reduced and their residence time in the fluid would be increased. This is evident from the descriptor expressions for the rolling drum model, equations 7.2. Increasing the pressure would increase the gas density in the bubbles,  $\rho_g/C_{\max}$ , and decrease the foam volume fraction,  $\phi$ . From equations 7.2a and e, it is evident that increasing  $\rho_g$  will increase the average bubble age,  $\tau_{av}$ , and decrease the film expansion ratio,  $R_f/R_c$ . Since the values of the applied pressures used in the model simulations were very small (approximately 5 torr), small absolute increases in the fluid pressure could result in a many fold increase in  $\rho_g/C_{\max}$  and would have a large effect on the state of the foam.

There could be many more reasons why our models give unrealistic descriptions of foaming. The approximate descriptions of bubble nucleation, growth and rupture could introduce significant inaccuracies. Also, bubble coalescence, breakage and deformation could significantly affect the foaming behavior. Their exclusion from our models might explain their unrealistic predictions. To identify any serious flaws in our models, information on the nature of foam-enhanced DV is essential. Unfortunately, physical information on foam-enhanced DV is scarce. Without additional information, hypotheses as to the sources of our model's inadequacies would be high speculative.

## CHAPTER VIII

### CONCLUSIONS AND RECOMMENDATIONS

#### 8.1 Conclusions

The major conclusions of this thesis are:

- 1) The methodology proposed for modelling foam-enhanced DV, which includes a population balance to track the evolution of the foam phase (described as a distribution over bubble sizes) coupled with a mass balance to track the reduction in the solvent concentration, is novel to DV modelling and is the first to allow incorporation of realistic descriptions of bubble birth, growth and death into models of the process.
- 2) The single screw and rolling drum devolatilizer models constructed using this methodology give a good correlation of devolatilizer performance data.
- 3) The models constructed for the rolling drum and single screw devolatilizers offer significant improvements over Latinen's (1962) model, which is the model most commonly used for sizing single screw devolatilizers. These models correlate available DV performance data better than Latinen's Model, while using the actual value of the diffusivity. As well, they can correlate both the foaming and interfacial diffusion-controlled regimes of DV, whereas Latinen's model cannot. This indicates that any realistic model of foam-enhanced DV must include two time scales to adequately fit the two regimes of DV.
- 4) The approximate models of DV that we have developed, which agree closely with the complete model if the bubble distribution approaches a quasi-steady state, are simpler than the complete model and require computation times for their numerical solution that are two orders of magnitude smaller than those required to solve the complete model. The model predicts that a QSS distribution can occur at operating conditions typical of industrial operations.
- 5) A Design Model, derived from the approximate QSS Model, is suitable for devolatilizer design as it has an explicit, analytical solution and includes two time scales for DV.

- 6) Descriptors of the bubble distribution have been introduced and shown to be valuable for describing the state of the foam. These measures of the foam's character are often of greater practical value than the distribution itself, since they usually can be more easily measured than the distribution. Descriptor expressions derived for the rolling drum model indicate how the process and physical property variables affect the state of the foam and the DV performance. They reveal that the model contains physical inaccuracies, however, as it predicts unrealistically large foam volume fractions and bubble radii.
- 7) A general model constructed for foam-enhanced DV is valuable for providing insight into how the rates of bubble birth, growth and death affect the state of the foam phase and the DV performance. This model reveals how the modelling methodology used by preceding investigators can introduce significant errors into predictions of the DV performance. As well, it indicates that inaccuracies in the rolling drum model might be caused by an underestimation of the rates of nucleation and rupture of bubbles.
- 8) The F.D. rolling drum devolatilizer model, which includes an empirical description of rupture by film draining as a means for increasing the bubble rupture rate, predicts realistic values for the foam volume fraction and average bubble radius. However, it does not give a wholly realistic description of the DV process, as it grossly underestimates the average bubble age.

## 8.2 Recommendations for Future Work

The ultimate objective of future investigations on foam-enhanced DV would be to construct models of DV which have predictive capabilities. We expect that the methodology proposed in this study, which is based on population balances and allows the incorporation of conceptually realistic descriptions of bubble birth, growth and death into models of foam-enhanced DV, is the proper methodology to be used in the construction of future models. The problems lie in the development of realistic descriptions of the rates of bubble birth, growth and death occurring during foam-enhanced DV.

Due to the paucity of experimental data on foam-enhanced DV and due to the complex nature of and the intricate interactions among the bubble birth, growth and death processes, it is unlikely that, at present, theoretical investigations into foam-enhanced DV could provide sufficiently accurate models of the process. We believe it would be most efficacious to undertake a fundamental experimental study of foam-enhanced devolatilization first. This would provide a better physical understanding of foam-enhanced DV, essential in guiding the rational construction of accurate models of the process.

There are many fundamental research topics on the component processes of foaming occurring during DV that should be explored. Some of these important areas of research that could be addressed experimentally are discussed below.

**Nucleation:** The mechanism(s) of bubble nucleation occurring during foam-enhanced DV, that is, the birth of bubbles from solution unaided by the presence of other entrained bubbles (i.e. as distinct from birth by bubble coalescence and breakage), is unknown. Experimental studies of nucleation are recommended to reveal this mechanism(s), as the nucleation mechanism(s) must be known before descriptions of the nucleation frequency required in models of DV can be developed. A primary objective of this study should be to determine how fluid flow and the presence of nucleating agents (i.e. such as surfactants and heterogeneous impurities) affect the frequency of bubble nucleation.

**Growth:** The growth of bubbles in devolatilizers is a very complex process and is not well understood. The first question that should be answered is whether the growth of bubbles in devolatilizers is controlled by diffusion, by viscous forces, by elastic forces or by a combination of the three. Experimental studies of the effect of imposed flow, preferably both shearing and elongational, on the bubble growth rate are suggested. Also, studies of the effects on the bubble growth rate of interactions with neighboring bubbles are recommended.

**Rupture:** Experiments should be conducted to measure the frequency of bubble rupture in devolatilizers by the mechanisms of film draining and mechanical shearing. Understanding the effects of elongational flows on the rupture rate is of particular interest as bubbles at the free surface in screw devolatilizers are subjected to elongational flow.

**Breakage and Coalescence:** The focus of preliminary experimental studies of bubble coalescence and breakage in devolatilizers should be to measure the frequency of bubble coalescence and breakage occurring during devolatilization. This will be useful in determining if these processes are important and whether they should be included into models of DV. If important, additional studies should be directed at determining the dependence of the breakage and coalescence frequency on the bubble radius, volume fraction of bubbles and flow strength and type.

**Deformation:** As for the studies suggested on bubble coalescence and breakage, preliminary studies on bubble deformation during DV should be directed at measuring the extent of deformation to determine if it need be included into models of DV. If important, the dependence of the extent of bubble deformation on physical property and process variables such as bubble radius, viscosity and flow strength and type should be investigated.

**Rolling Drum Devolatilizer Performance Studies:** In addition to experimental studies on the physical processes which comprise foaming, *in situ* measurements of the DV rate and of the state of the foam phase occurring in industrial devolatilizers would be very valuable in evaluating the accuracy and limitations of DV models. Particularly, to elucidate the limitations in the screw devolatilizer models constructed in this study (i.e. for the single screw and rolling drum devolatilizers), careful measurements of the DV rates and the bubble radius and age distributions occurring in the rolling drum devolatilizer are suggested. The rolling drum devolatilizer is probably the most basic of all devolatilizers and is ideal for preliminary investigations. Photographic methods could be used to measure the bubble distribution directly, or, it could be inferred

from measurements of descriptors of the distribution, such as from measurement of the mean bubble radius or foam volume fraction. As short time measurements were shown in this study to be crucial to precise estimation of the empirical model parameters, techniques must be developed to accurately measure the DV rate and the evolution of the state of the foam at short times when foaming is rapid and DV rates are high.

## APPENDIX A

### BUBBLE GROWTH IN QUIESCENT POLYMER SOLUTIONS AND THE EFFECT OF SHEAR ON THE BUBBLE GROWTH RATE

The growth rate of bubbles in polymer/solvent solutions can be controlled by a number of physical processes; viscous forces, elastic forces, bubble-bubble interactions and finite rates of solvent diffusion can all impede the growth. The low diffusivity of solvents in polymer melts (usually from  $10^{-7}$  to  $10^{-10}$  cm<sup>2</sup>/sec) results in slow solvent diffusion. It is likely that diffusion of solvent to the bubble is the rate limiting step in bubble growth during DV. In this appendix, the assumption that bubble growth during devolatilization is controlled by diffusion will be addressed for a bubble growing in a quiescent polymer/solvent solution. Also, since bubbles in the single screw devolatilizer are translating in a free surface cavity flow, they can experience shear and elongational flows that will increase the mass transfer coefficient to the bubble. The effect of flow on the bubble growth rate will be also addressed in this appendix.

#### A.1 Bubble Growth in Quiescent Polymer Solutions

Barlow and Langlois (1962) developed a model of a bubble growing in a quiescent, infinite, Newtonian fluid containing a dissolved gas. The time dependence of the bubble radius was calculated numerically for a system with physical properties typical of polymer/solvent solutions:  $\mu = 10^6$  (dynes s/cm<sup>2</sup>),  $D = 10^{-9}$  (cm<sup>2</sup>/s) and  $\sigma = 20$  (dynes/cm). Hydrodynamics was shown to control the early period of growth. Diffusion-controlled growth was predicted to follow. Using criteria presented by Barlow and Langlois, the bubble diameter at which diffusion-controlled growth could be expected was calculated. Our calculations indicate that the bubble growth is diffusion-controlled for bubbles which grow beyond a radius of 7 microns. Since most bubbles are expected to

grow from 100 to 1000 times this value, the diffusion controlled growth assumption should apply.

Villamizar and Han (1978) measured the growth rate of bubbles growing in a polystyrene melt containing carbon dioxide released by the chemical degradation of sodium bicarbonate, a blowing agent. The observed time dependence of the bubbles are well fit by the expression  $R = \alpha t^n$ . The values of the exponent  $n$  that best fit the data range from 0.33 to 0.47. For diffusion-controlled growth, a value of  $n = .5$  is predicted. The data of Villamizar and Han show a slightly weaker time dependence of the bubble radius than is predicted for diffusion-controlled growth. This suggests the presence of some other process affecting the growth, possibly an elastic or bubble interaction effect. Nevertheless, the measured growth exponents are close enough to the diffusion controlled growth exponent such that the diffusion controlled growth model would be an adequate approximation for this system.

It should be noted that the devolatilization model is not limited to the case of diffusion-controlled bubble growth, for which  $n = .5$ . If the proper power law exponent is known, the devolatilization model can be easily altered to account for the new value of the exponent. Thus, the square root of time dependence of the bubble growth rate is not a model prerequisite. In addition, for bubble growth described by a mathematical expression not of the power law form, the general modelling methodology is still applicable, although the model's solution may be more difficult.

## A.2 Effect of Shear on the Bubble Growth Rate

The bubble growth rate model included in the single screw and rolling drum devolatilizer models assumes the bubbles to be growing in a quiescent fluid. Actually, bubbles in the bulk film of the single screw devolatilizer are entrained in a free surface cavity flow. The bubbles are exposed to mainly shear flow in the interior of the bulk film



and to elongational flows near the surface (Canedo, 1985). Flow can enhance the mass transfer of solvent to the bubbles and increase the bubble's growth rate.

Many investigators have analyzed the effect of an applied external flow field on the mass transfer to bubbles. A few of the more notable investigations include Levich, 1962; Acrivos and Taylor, 1962; Darby, 1964; Florschuetz, Henry and Khan, 1969 and Ruckenstein and Davis, 1970. All of these investigators considered bubbles growing and translating in a uniform flow field, such as for a bubble rising by buoyancy in a stagnant fluid. However, documentation of studies on bubbles growing in a shear flow, to which bubbles in the single screw devolatilizer are exposed most often, was not found in the literature.

Acrivos (1971) has analyzed mass transfer to rigid spheres freely suspended in a shear flow. Although the fluidity of the bubble and the growth induced radial convection are not exhibited in the rigid sphere problem, the two problems are analogous. Qualitative insight into the bubble growth problem can be gained and an estimate of the magnitude of the mass transfer enhancement due to flow can be inferred from Acrivos' study. In addition, Acrivos' study may yield a quantitative description of the mass transfer if the bubble rotates as a rigid sphere and if the radial velocity induced by bubble growth is negligible compared with the tangential velocity of the imposed flow.

Ruckenstein and Davis (1970) showed that growth induced radial convection can be neglected when modelling the growth of a low solubility (slowly growing) gas bubble rising in water. Due to the small diffusivities of solvents in polymers, it is possible that bubbles grow slowly enough in the shear fields generated during single screw extrusion so that they can be analyzed sufficiently accurately while neglecting the radial flow induced by the bubble growth. Also, it is possible that the bubble will rotate as a rigid sphere due to the immobilization of the interface caused by the surface active agents present as impurities in most industrial polymer production operations (Chen, Hahn, and Slattery; 1984). Further investigation would be required to determine if both of these conditions are met.

So Acrivos' analysis is expected to provide, at least, a qualitative description of the mass transfer enhancement, and possibly, a quantitative description.

Acrivos (1971) derived an asymptotic expression for the Sherwood number describing the mass transfer to a rigid sphere immersed in a simple shear flow. For the limiting case  $Re \rightarrow 0$  and  $Pe \rightarrow \infty$ , Acrivos' result is  $Sh \cong 4.5$  where

$$Sh = \frac{k_c R}{D}$$

$$Re = \frac{G R^2}{\nu}$$

$$Pe = \frac{R^2 G}{D}$$

and  $k_c$  is the liquid phase mass transfer coefficient,  $R$  is the bubble radius,  $G$  is the shear rate far from the bubble,  $D$  is the diffusivity and  $\nu$  is the kinematic viscosity

Acrivos predicts that the mass transfer coefficient approaches an upper bound and is independent of  $Pe$ , and hence, the strength of the flow, in the limit as  $Pe$  approaches infinity. This is in contrast to the dependence of  $Sh$  on  $Pe^{1/3}$  at the identical limit for mass transfer to a sphere translating in a stagnant fluid. This counter intuitive result is explained by the presence of closed streamlines encircling the bubble in the shear flow case. Only open streamlines occur for a bubble translating in a uniform flow. These closed streamlines form a constant width bounding layer, independent of flow strength, over which mass is transferred by diffusion only.

For the experiments of Coughlin and Canevari (1969), representative values of the Reynolds number for bubbles in the single screw channel are less than  $10^{-2}$  and the Peclet number is on the order of  $10^{11}$ . The constraints from Acrivos' analysis are met in this system and should be met for bubbles in any conventional single screw devolatilizer. From the relation between the growth rate,  $dR/dt$ , and the mass transfer coefficient given in equation 7.5, and estimating  $k_c \cong 4.5 D/R$ , the time-dependence of the radius of a bubble

with an immobilized interface and growing in a shear flow can be estimated by integrating the bubble's growth rate over its age. The resulting expression is

$$R = 3\sqrt{D \frac{\Delta C}{\rho_g}} \tau^{1/2} \quad \text{A.1}$$

where the bubble radius at birth,  $\tau = 0$ , was taken to be zero.

From Acrivos' expression for the mass transfer coefficient, we predict that the radius of a bubble undergoing simple shear will scale with the bubble's age to the 1/2 power. This value of the exponent was also predicted for the growth of bubbles in a quiescent solution by Scriven's (1959) model, which is the basis for the bubble growth rate expression used in our work. Acrivos' study indicates that the cell model used by previous investigators to account for the interaction of the diffusion fields of neighboring bubbles (Amon and Denson, 1984; Chella and Lindt, 1986) might not be necessary. If the average distance between bubbles is much larger than the thickness of the diffusion boundary layer, the diffusion fields will not interact and the bubbles may be treated as being wholly isolated from each other.

Comparison of the growth rate expressions derived with and without shear (c.f. equations A.1 and 4.2) reveals that the bubble growth rate without shear is predicted to be  $(4\Delta C/3\pi\rho_g)^{1/2}$  times greater than the growth rate with shear. Since this factor is significantly greater than one, the expression for the growth rate with shearing significantly underestimates the growth rate. This is probably due to the neglect of radial flow in the derivation of equation A.1. Radial flow stretches the fluid surrounding the bubble increasing the radial concentration gradient which enhances mass transfer. This indicates that radial flow can contribute significantly to the growth rates of bubbles in the shear fields of the single screw devolatilizer and should be considered in any model of the process.

## APPENDIX B

### BUBBLE RUPTURE RATES BY FILM DRAINING AND MECHANICAL SHEARING IN A SINGLE SCREW DEVOLATILIZER

Bubbles at the surface of the bulk film in the rolling drum devolatilizer have been observed by Biesenberger and Lee (1986) to rupture by the mechanisms of mechanical shearing and film draining. Descriptions of both processes will be presented in this appendix and expressions will be derived for the rates of bubble rupture by both mechanisms in the single screw devolatilizer.

#### B.1 Rupture by Mechanical Shearing

Bubbles at the surface of the bulk film can rupture by mechanical shearing as they travel through the convergence point of the bulk and barrel films (see Figure 4-2). In this model we will assume that all bubbles that reach the convergence point rupture. To derive the rate of death of bubbles of age  $\tau$  over a differential element  $dz$ , we only need to estimate the surface density of bubbles,  $\rho_{\text{surf}}$ , where  $(\rho_{\text{surf}} d\tau dz)$  is defined as the number of bubbles jutting through the surface between ages  $\tau \rightarrow \tau + d\tau$  and between positions  $z \rightarrow z + dz$  per surface area of interface. The death rate by mechanical shearing,  $E_{\text{M.S.}}$ , is equal to the product of the surface density of bubbles and the flux of the surface through the convergence point,  $V_b dz$ .

$$E_{\text{M.S.}} d\tau dz = (\rho_{\text{surf}} d\tau dz) V_b dz$$

To derive an expression for  $\rho_{\text{surf}}$ , we will assume that the bubbles are homogeneously distributed over the channel cross section. A bubble of radius  $R$  will occupy the surface if its center is located a distance  $R$  or less above or below the surface. This is illustrated in Figure B-1. The fraction of bubbles in the cross section which breach the surface is simply that fraction of bubbles located in this region, which for homogeneously distributed

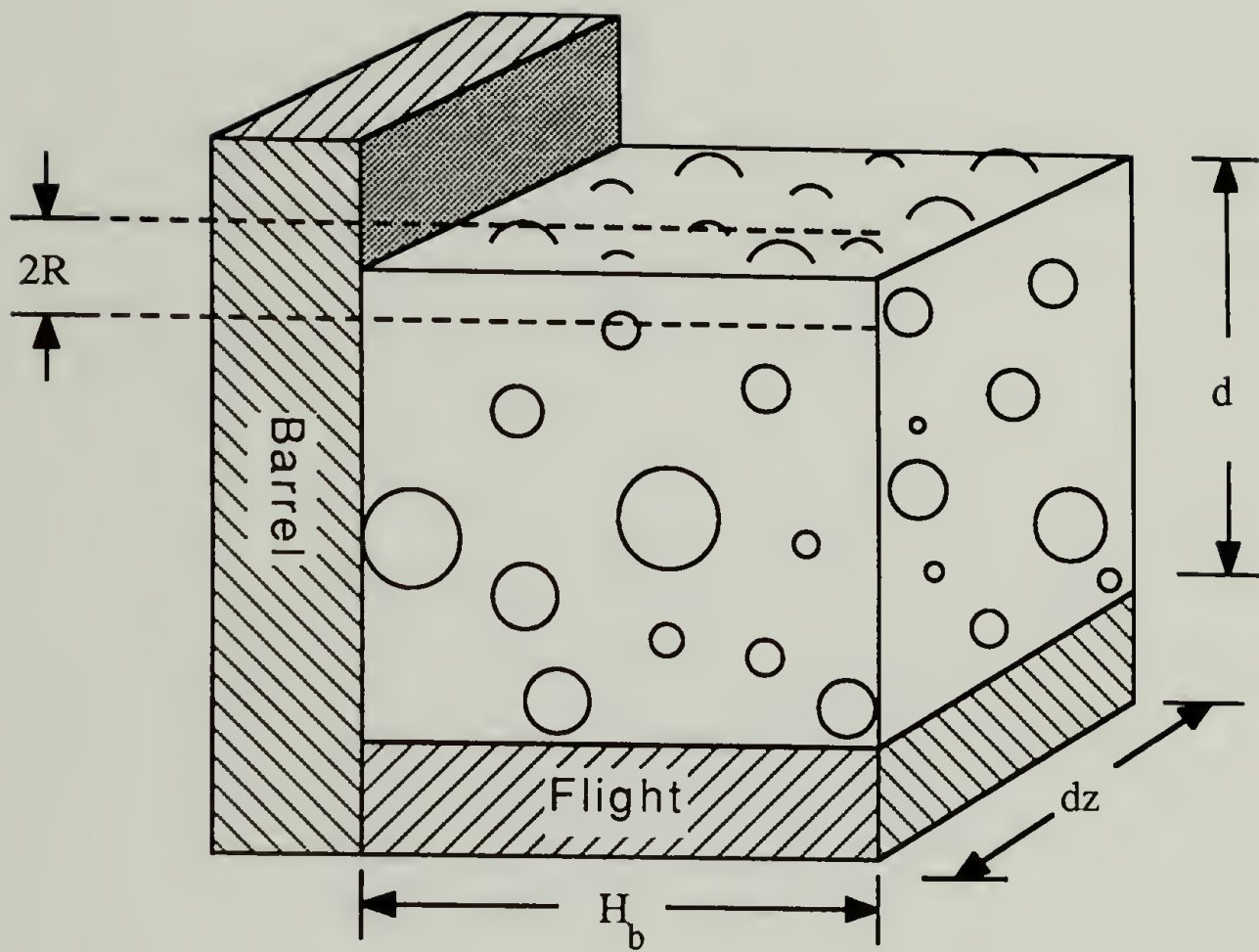


**Figure B-1** Schematic of a cross sectional element of the single screw devolatilizer.

bubbles is  $2R/d$ . The number of surface bubbles in the cross section per area,  $\rho_{\text{surf}} d\tau dz$ , is then given by the product of the fraction of bubbles of radius  $R(\tau)$  at the surface and the total number of bubbles in the element, which is  $f d\tau dz$ , divided by the surface area of the element,  $H_b dz$ .

$$\rho_{\text{surf}} d\tau dz = \frac{\left(\frac{2R}{d}\right)(f d\tau dz)}{H_b dz}$$

so that the surface density of bubbles is given by

$$\rho_{\text{surf}} = \frac{2 R f}{d H_b dz}$$

Substituting into the death rate expression for  $\rho_{\text{surf}}$  gives

$$E_{\text{M.S.}} = \left(\frac{2 V_b}{d H_b}\right) \left[ R_0 + \sqrt{\frac{12 D}{\pi}} \left(\frac{\Delta C}{\rho_g}\right) \tau^{1/2} \right] f$$

where the bubble radius, shown in brackets, has been expressed in terms of the bubble's age  $\tau$  using the bubble growth rate expression given in equation 4.2.

## B.2 Rupture by Film Draining

As a bubble is driven towards the liquid/vapor interface, fluid between the bubble and the interface is displaced. When the bubble breaches the surface, a thin fluid film remains surrounding the bubble, since the fluid cannot drain fast enough to allow immediate rupture. Draining of this film into the surrounding fluid is induced by pressure gradients caused by the spatially varying curvature of the film surrounding the bubble. As the fluid in the film drains, a critical film thickness (on the order of 500 angstroms) is reached where London-van der Waal's forces lead to instability and rupture (Chen, Hahn and Slattery; 1984)

Surface-active agents, if present, will accumulate at the fluid-fluid interfaces and set up interfacial surface tension gradients which will immobilize the gas-fluid interfaces between the bubble and the fluid and between the fluid and the vapor space.

Immobilization of these interfaces causes the fluid to drain from the interior of the film only. This significantly decreases the draining rate. Very small concentrations of surface-active agents are required for interface immobilization (Lin and Slattery; 1982) and it is likely that industrially produced polymers contain sufficient concentrations to cause immobilization.

Chen et. al. (1984) developed a model for the film draining and rupture of a bubble driven to a fluid-fluid interphase by buoyancy. They derived an expression for the rupture time which we reduced to the following form.

$$\tau_R = 1.06 \mu \frac{R^{17/5} (\Delta\rho g)^{3/5}}{B^{2/5} \sigma^{6/5}}$$

where B is the interaction potential per unit volume, which is a measure of the pressure acting to attract two parallel fluid-fluid interfaces,  $\Delta\rho$  is the density difference between the two phases,  $\mu$  is the fluid viscosity,  $\sigma$  is the surface tension and g is the gravitational constant. This expression predicts that a bubble's rupture time is a function of the bubble radius. This behavior has been observed by most investigators: Gillespie and Rideal (1956), Charles and Mason (1960) and Woods and Burrill (1972, 1973).

Bubble rupture in single screw devolatilizers differs from that modelled by Chen et. al.. In single screw devolatilizers bubbles are not driven to the surface by buoyancy forces, since, for polymer melts, the high viscosity arrests the buoyancy induced bubble motion. Rather, bubbles are driven to the surface by the elongational flow of the fluid at the surface of the bulk film. There have been no investigations conducted on the rate of bubble rupture by film draining at the surface of an elongating fluid. However, a related problem of protrusion of rigid spheres through surfaces undergoing elongational flows during mold filling has been analyzed by Hoffman (1985). Hoffman presents a simple model revealing that, for a particle near a fluid surface undergoing an elongational flow, unbalanced drag forces will act on the particle and drive it towards the surface.

Although Chen's analysis is not strictly applicable to the rupture of bubbles in the single screw devolatilizer, we expect that the two rupture processes are similar, as film draining and instability onset are common to both. We anticipate that, for bubbles in the single screw devolatilizer, the rupture times will also be a function of the bubble's radius. A general rupture time function,  $\tau_R$ , will be introduced and defined as the time required by a surface bubble with a radius  $R$  to rupture by film draining.

Given an expression for  $\tau_R$ , we may develop a model for the film draining rupture rates based on the following description of the rupture process. Surface bubbles are assumed to translate to the convergence point of the bulk and barrel films at the velocity of the fluid surface,  $V_b$ . For reference, a schematic of the bulk film surface is shown in Figure B-2. If the surface residence time of any of these bubbles is larger than the film draining rupture time,  $\tau_R$ , corresponding to its radius, it will rupture. If not, bubbles will reach the convergence point and either rupture by mechanical shearing or pass back into the interior of the bulk film. If both mechanical shearing and film draining occur, the total death rate is simply obtained from the sum of the death rates by both mechanisms.

The model for bubble rupture by film draining is derived from this physical picture as follows. Bubbles are assumed to continuously breach the surface at random positions on the film surface. The surface density of bubbles,  $\rho_{\text{surf}}$ , is therefore homogeneous over the surface and will be assumed to be identical to that derived earlier for rupture by mechanical shearing. For illustrative purposes, we'll assume that all surface bubbles have breached the surface simultaneously at time  $t = 0$ . This idealization will not affect the resulting rupture rate expression. All bubbles of age  $\tau$  (or equivalently of radius  $R(\tau)$ ) will be assumed to have a corresponding rupture time,  $\tau_R$ , associated with it. Bubbles of radius  $R$  at the film surface over a differential cross section,  $dZ$ , (see Figure B-2) will be assumed to rupture if they reside on the surface for times greater than  $\tau_R$ . Focussing on a differential surface element,  $dy$ , a distance  $q$  from the convergence point, surface bubbles at  $q$  will travel with a velocity  $V_b$  towards the convergence point. If the time spent in travelling from  $q$  to the



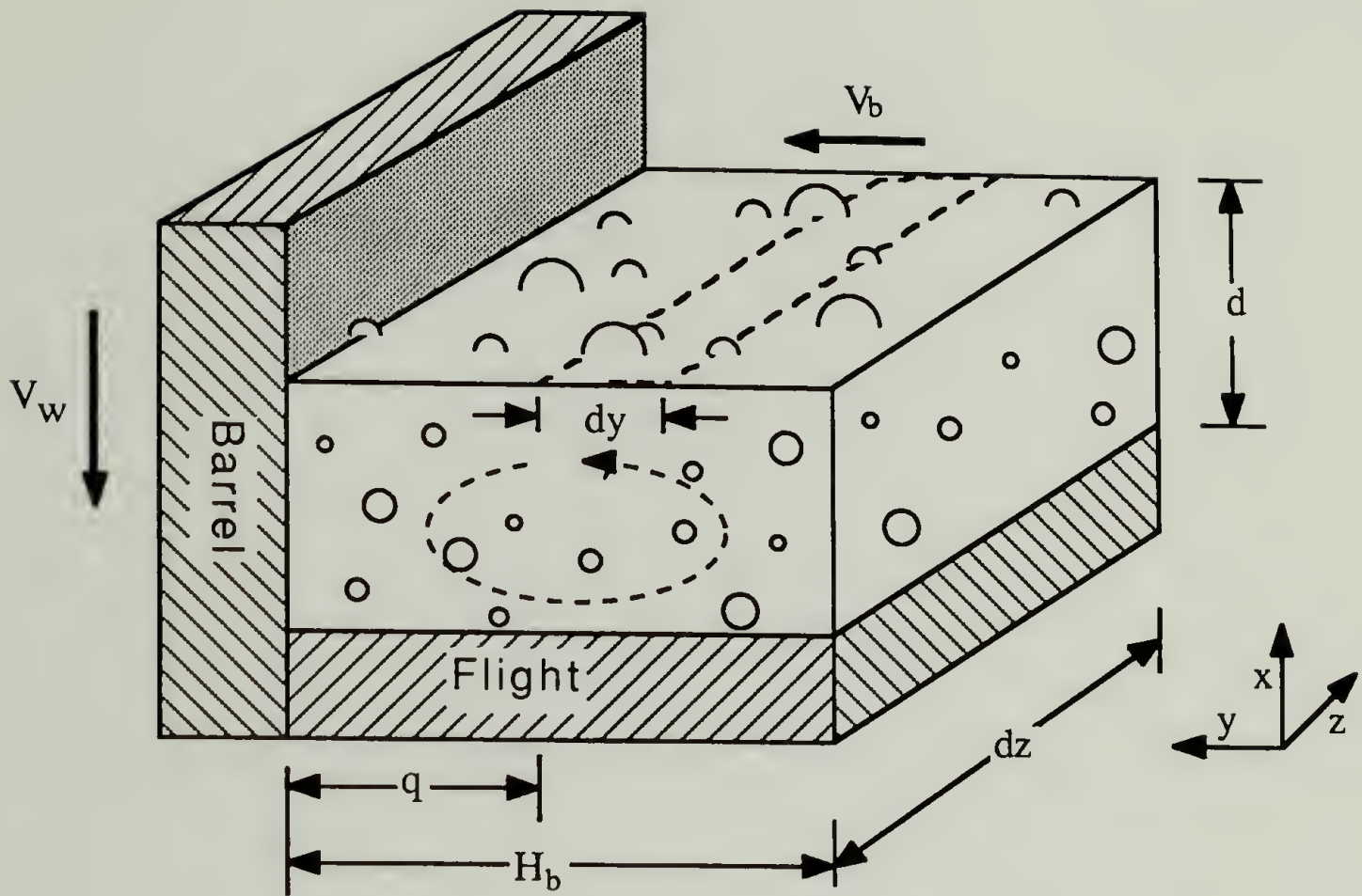


**Figure B-2** Schematic of a cross sectional element of the single screw devolatilizer.

convergence point,  $q/V_b$ , is greater than  $\tau_R$ , the bubbles will rupture by film draining before reaching the convergence point. Otherwise, bubbles will travel to the convergence point and incur the consequences dictated by the rupture model for bubbles passing through the convergence point.

Any bubble of age  $\tau$  a distance  $\tau_R/V_b$  from the convergence point and beyond will rupture by film draining over the time  $\tau_R$ . From this relation, the fraction of surface bubbles of age  $\tau$  that rupture can be determined and an expression for the bubble death rate by film draining,  $E_{F.D.}$ , can be derived from the following identities.

$$E_{F.D.} d\tau dz = \frac{\left\{ \begin{array}{l} \# \text{ of surface bubbles} \\ \text{of age } \tau \rightarrow \tau + d\tau \\ \text{between } z \rightarrow z + dz \end{array} \right\} \left\{ \begin{array}{l} \text{fraction of surface} \\ \text{bubbles of age } \tau \\ \text{that rupture} \end{array} \right\}}{\left( \text{rupture time of bubbles of age } \tau \right)}$$

$$\left\{ \begin{array}{l} \# \text{ of surface bubbles} \\ \text{of age } \tau \rightarrow \tau + d\tau \\ \text{between } z \rightarrow z + dz \end{array} \right\} = \left[ \rho_{\text{surf}} d\tau dz \right] H_b dz = \frac{2R}{d} f d\tau dz$$

$$\left\{ \begin{array}{l} \text{fraction of bubbles} \\ \text{age } \tau \text{ that rupture} \end{array} \right\} = \frac{\left\{ \begin{array}{l} \# \text{ of surface bubbles of age } \tau \\ \text{in the region } \tau_R V_b < x < H_b \end{array} \right\}}{\left\{ \begin{array}{l} \text{total } \# \text{ of surface bubbles} \\ \text{of age } \tau \text{ in element} \end{array} \right\}}$$

$$= \frac{\rho_{\text{surf}} (H_b - \tau_R V_b) dz}{\rho_{\text{surf}} H_b dz}$$

Simplifying the above expression and forcing it to zero for bubbles with rupture times greater than the surface residence time of a fluid element,  $H_b/V_b$ , gives

$$\left\{ \begin{array}{l} \text{fraction of bubbles of age } \tau \text{ that rupture} \end{array} \right\} = \begin{cases} \left( 1 - \frac{\tau_R V_b}{H_b} \right) & \tau_R < \frac{H_b}{V_b} \\ 0 & \tau_R \geq \frac{H_b}{V_b} \end{cases}$$

Substituting the expressions for the bracketed terms into the expression for  $E$  gives the

expression for the bubble rupture rate by film draining

$$E_{F.D.} = \begin{cases} \frac{2 R f}{d} \left( \frac{1}{\tau_R} - \frac{V_b}{H_b} \right) & \tau_R < \frac{H_b}{V_b} \\ 0 & \tau_R \geq \frac{H_b}{V_b} \end{cases}$$

All that remains to apply the film draining death rate expression into a model of DV is to express  $\tau_R$  and  $R$  as a function of bubble age,  $\tau$ .

## APPENDIX C

### ESTIMATION OF $E_a$ FROM NUCLEATION ONSET STUDIES AND THE SHEAR RATE DEPENDENCE OF THE BUBBLE BIRTH RATE

As discussed in Chapter 4,  $E_a$  determines the superpressure, or similarly, the supersaturation, at which the onset of nucleation occurs. It could be determined from experimental studies of the onset of nucleation. In this appendix, a method of estimating  $E_a$  from nucleation onset studies will be presented and values of  $E_a$  will be estimated from results of nucleation onset studies presented in the literature. Also, the shear rate dependence of the nucleation rate and a mechanism of nucleation proposed by Biesenberger and Lee (1986) to explain it will be discussed.

#### C.1 Estimation of $E_a$ from Nucleation Onset Studies

Inspection of Figure 4.5 shows that classical nucleation theory predicts that a critical superpressure must be exceeded before significant nucleation can occur. This behavior was observed experimentally by Villamizer and Han (1978), by Biesenberger and Lee (1986) and by Hoque (1986). As is also evident in Figure 4.5, the value of  $E_a$  determines the value of this critical superpressure. From measurements of the superpressure required for the onset of nucleation, an estimate of  $E_a$  may be made. For example, if the superpressure required for nucleation was measured to be 10 psi, from Figure 4.5 we could estimate  $E_a$  to be between  $2.5 \times 10^5$  and  $10^6$  psi<sup>2</sup> K.

Villamizar and Han (1978) conducted experiments on the onset of nucleation in polyethylene/carbon dioxide solutions during foam molding. The solution was forced under pressure through a rectangular, transparent die and the position and pressure at which nucleation was first observable was recorded. At 220 degrees centigrade and a 2% concentration of Celogen (a blowing agent which produces carbon dioxide), the superpressure at which nucleation was first observed by Villamizar et al. is calculated to be

17.4 psi. From Figure 4.5, the activation energy at which nucleation just becomes observable at  $\Delta P=17.4$  psi can be estimated to be within the range of 250,000 to 500,000  $\text{psi}^2 \text{K}$ . Over this range of  $E_a$ ,  $J/F$  varies from 0.03 to 0.15.

We also estimated values of  $E_a$  from the experimental studies of nucleation onset by Biesenberger and Lee (1986) and by Hoque (1986). Biesenberger et al. measured the superpressure at which nucleation first became observable in a solution of polydimethylsiloxane/methyl chloride undergoing a free surface cavity flow (chosen to simulate the flow in the single screw extruder channel). A value of  $E_a$  for this system was estimated to be  $8 \times 10^3$  ( $\text{psi}^2 \text{K}$ ). Hoque measured the system pressure at which nucleation became observable in a solution of polybutene/n-pentane flowing in a two roller apparatus (chosen to simulate flow in a twin screw extruder). We estimated the superpressure required for the onset of nucleation to be the difference between the local fluid pressure (estimated from lubrication theory) and the vapor pressure. A value of  $E_a$  for this system was estimated to be  $4 \times 10^5$  ( $\text{psi}^2 \text{K}$ ). Values of  $E_a$  for these three different polymer/solvent solutions range from  $8 \times 10^3$  to  $5 \times 10^5$  ( $\text{psi}^2 \text{K}$ ), suggesting that values of  $E_a$  for other polymer/solvent solutions might be close to or within this range.

A value of  $E_a$  equal to 3,200  $\text{psi}^2 \text{K}$  (i.e. 15  $\text{atm}^2 \text{K}$ ) was found to give a good correlation of the devolatilization data of Biesenberger and Lee (1986) using our devolatilization model. We estimated  $E_a$  to be 8,000  $\text{psi}^2 \text{K}$  (37  $\text{atm}^2 \text{K}$ ) for this polymer solution from the nucleation onset studies of Biesenberger and Lee (1986). This indicates that the procedure for estimating  $E_a$  from nucleation onset studies may be suitable for providing an order of magnitude estimate of  $E_a$ .

## C.2 The Shear Rate Dependence of the Bubble Birth Rate

From their observations of foaming occurring during DV, Biesenberger and Lee (1986) proposed that the bubble birth rate increases with the applied shear rate. Biesenberger et al. attribute this phenomenon to invisible pockets of gas which act as

nucleation sites. These are metastable at rest but become unstable with increasing shear rate, leading to bubble birth.

This indicates that the primary mechanism of bubble birth during devolatilization may not occur by random molecular fluctuations leading to a stable bubble nucleus, as postulated by classical nucleation theory. Rather, bubbles may originate from stable gas pockets trapped in the crevices of heterogeneous impurities or container walls. Imposition of a reduced pressure will cause these pockets of gas to grow. At some critical inflation, the gas pockets may pinch off, sending a new bubble into solution. However, part of the vapor could remain in the crevice and act as the nucleus for the growth and pinch-off of another bubble. This mechanism would allow for the birth of a continuous stream of bubbles from a single crevice. Indeed, this is the mechanism of birth of bubbles in a glass of beer which the socially-disposed among us may be quite familiar. A continuous stream of bubbles can be observed to issue from a single spot on the surface of the glass at which is located a gas-filled crevice. However, this mechanism of bubble pinch-off is different from that proposed in devolatilizers, as bubbles in devolatilizers are thought to be torn from the crevice by viscous rather than by buoyancy forces.

Bubble birth by this pinch-off mechanism was studied by Darby (1964) for vapor bubbles of superheated Freon and water issuing from an isolated nucleation site (i.e. a pocket of vapor occupying a crack) on a solid surface. We expect that, in the presence of a shear field, this pinch-off rate will accelerate resulting in a higher pinch frequency. Higher shear rates would result in more frequent pinching, and hence, higher birth rates as proposed by Biesenberger et al.

The metastable bubble theory is speculative, however. Further study is necessary to evaluate its validity. If growth and pinch-off of stable gas pockets is the predominant nucleation mechanism during DV, nucleation models based on classical nucleation theory would be rendered purely empirical. Attempts at inferring physical insight from these models may be misguided. Until the bubble birth mechanism in devolatilizers is elucidated,

modelling the process using classical nucleation theory should be done with the reservation that it may represent only empiricism.

## REFERENCES

- Acrivos, A. and T. D. Taylor; "Mass Transfer from Single Spheres in Stokes Flow", *Phys. Fluids*, 5, 387-393 (1962).
- Acrivos, A.; "Heat Transfer at High Peclet Number from a Small Sphere Freely Rotating in a Simple Shear Field", *J. Fluid Mech.*, 46, 233-240 (1971).
- Aiken, R. C. and L. Lapidus; "An Effective Numerical Integration Method for Typical Stiff Systems", *AIChE J.*, 20, 368-375 (1974).
- Alabak, R. J., Z. Tadmor and Y. Talmon; "Scanning Electron Microscopy Studies of Polymer Melt Devolatilization", *AIChE J.*, 5, 808-818 (1987).
- Amon, M. and C. D. Denson; "A Study of the Dynamics of Foam Growth: Analysis of the Growth of Closely Spaced Bubbles", *Pol. Eng. Sci.*, 24, 1026-1034 (1984).
- Barlow, E. J. and W. E. Langlois; "Diffusion of Gas from a Liquid into an Expanding Bubble", *IBM J.*, July, 329-337 (1962).
- Bayens, C. A. and R. L. Laurence; "A Model for Mass Transfer in a Coalescing Dispersion", *Ind. Eng. Chem. Fund.*, 8, 71-76, (1969).
- Biesenberger, J. A.; "Polymer Devolatilization: Theory of Equipment", *Pol. Eng. Sci.*, 20, 1015-1022 (1980).
- Biesenberger, J. A. and G. Kessidis; "Devolatilization of Polymer Melts in Single-Screw Extruders", *Pol. Eng. Sci.*, 22, 832-835 (1982).
- Biesenberger, J. A. and S. T. Lee; "A Fundamental Study of Polymer Melt Devolatilization", *Soc. Plast. Eng. ANTEC Nat'l Meet.*, 2-7 (1985).
- Biesenberger, J. A. and S. T. Lee; "A Fundamental Study of Polymer Melt Devolatilization II. A Theory for Foam-Enhanced DV", *Soc. Plast. Eng. ANTEC Nat'l Meet.*, 846-850 (1986).
- Biesenberger, J. A. and S. T. Lee; "A Fundamental Study of Polymer Melt Devolatilization III. More Experiments on Foam-Enhanced DV", *Pol. Eng. Sci.*, 27, 510-517 (1987).
- Bigg, D. and S. Middlemann; "Mixing in a Screw Extruder. A Model for Residence Time Distribution and Strain", *Ind. Eng. Chem. Fundam.*, 13, 66-71 (1974).
- Blanks, R. F., J. A. Meyer and E. A. Grulke; "Mass Transfer and Depolymerization of Styrene in Polystyrene", *Pol. Eng. Sci.*, 21, 1055-1062 (1981).
- Blander, M. and J. L. Katz; "Bubble Nucleation in Liquids", *AIChE J.*, 21, 833-848 (1975).
- Burrill, K. A. and D. R. Woods, "Film Shapes for Deformable Drops at Liquid-Liquid Interfaces II. The Mechanisms of Film Drainage", *J. Coll. Int. Sci.*, 42, 15-25 (1973).



- Canedo, E. L.; "Flow and Mass Transfer in Driven Cavities with a Free Surface", Doctoral Dissertation, Chemical Engineering Department, University of Delaware (1985).
- Chan, R. K. S., C. B. Patel, R. Gupta, C. H. Worman and R. E. Grandin; "Batch Stripping of Vinyl Chloride", *J. Macromol. Sci.-Chem.*, A17, 1045-1064 (1984).
- Charles, G. E. and S. G. Mason; "The Coalescence of Liquid Drops with Flat Liquid/Liquid Interfaces", *J. Coll. Sci.*, 15, 236-267 (1960).
- Chella, R. and J. T. Lindt; "Polymer Devolatilization II. Model for Foaming Devolatilization", *Soc. Plast. Eng. ANTEC Nat'l Meeting*, 851-854 (1986).
- Chen, J. D., P. S. Hahn and J. C. Slattery; "Coalescence Time for a Small Drop or Bubble at a Fluid-Fluid Interface", *AIChE J.*, 30, 622-630 (1984).
- Collins, G. P., C. D. Denson and G. Astarita; "The Length of a Transfer Unit (LTU) for Polymer Devolatilization Processes in Screw Extruders", *Pol. Eng. Sci.*, 23, 323-327 (1983).
- Collins, G. P., C. D. Denson and G. Astarita; "Determination of Mass Transfer Coefficients for Bubble-Free Devolatilization of Polymeric Solutions in Twin-Screw Extruders", *AIChE J.*, 31, 1288-1296 (1985).
- Colton, J. S.; "The Nucleation of Microcellular Thermoplastic Foam", Doctoral Dissertation, Chemical Engineering Department, M.I.T. (1985).
- Coughlin, R. W. and G. P. Canevari; "Drying Polymers During Screw Extrusion", *AIChE J.*, 15, 561-565 (1969).
- Darby, R.; "The Dynamics of Vapour Bubbles in Nucleate Boiling", *Chem. Eng. Sci.*, 19, 39-49 (1964).
- Denson, C. D.; "Stripping Operations in Polymer Processing", *Adv. Chem. Eng.*, 12, 61-106 (1983).
- Florschuetz, L. W., C. L. Henry and A. R. Khan; "Growth Rates of Free Vapor Bubbles in Liquids at Uniform Superheats Under Normal and Zero Gravity", *Int. J. Heat Mass Transfer*, 12, 1465-1474 (1969).
- Gaines, G. L., "Surface and Interfacial Tension of Polymer Liquids - A Review", *Pol. Eng. Sci.*, 12, 1-11 (1972).
- Gear, C. W.; "Numerical Initial Value Problems in Ordinary Differential Equations", Prentice-Hall, Englewood Cliffs, N.J. (1971).
- Gillespie, T. and E. K. Rideal; "The Coalescence of Drops at an Oil-Water Interface", *Trans. Far. Soc.*, 52, 173-183 (1956).
- Gras, D. and K. Eise; "The Use of Multi-Screw Extruders for Devolatilizing Low Solids Polymer Solutions", *Soc. Plast. Eng. ANTEC Nat'l Meeting*, 386-389 (1975).
- Han, H. P. and C. D. Han; "The Mechanism of Foam Devolatilization in Partially Filled Screw Devolatilizers", *Soc. Plast. Eng. ANTEC Nat'l Meeting*, 8-11 (1985).

- Han, C. D. and H. P. Han; "A Study of Bubble Nucleation in Concentrated Polymer Solutions", Presentation at the AIChE Nat'l Meeting, New York (1987).
- Hinch, E. J. and A. Acrivos; "Long Slender Drops in a Simple Shear Flow", *J. Fluid Mech.*, 98, 305-328 (1980).
- Hoffman, R. L.; "Response of a Rigid Sphere to an Extensional Flow Field Near a Liquid-Gas Interface", *J. Rheol.*, 29, 579-604 (1985).
- Hoque, R. N.; "The Onset of Boiling and its Importance in Polymer Devolatilization", Masters Thesis, Chemical Engineering Department, University of Massachusetts (1986).
- Hulburt, H. M. and S. Katz; "Some Problems in Particle Technology: A Statistical Mechanical Formulation", *Chem. Eng. Sci.*, 19, 555-574 (1964).
- Ince, E. L.; Ordinary Differential Equations, Dover, New York, N.Y. (1956)
- Kearney, M. and P. Hold; "A Rotating Drum Devolatilizer", Soc. Plast. Eng. ANTEC Nat'l Meeting, 17-22 (1985).
- Latinen, G.; "Devolatilization of Viscous Polymer Systems", *A.C.S. Adv. Chem. Series*, 34, 235-246 (1962).
- Lee, S. T.; "Study of Foam Enhanced Devolatilization: Experiments and its Theories"; Doctoral Dissertation, Stevens Institute of Technology (1986).
- Lee, S. T. and J. A. Biesenberger; "A Fundamental Study of Polymer Melt Devolatilization: IV. Some Theories and Models for Foam-Enhanced DV", Soc. Plast. Eng. ANTEC Nat'l Meet., 81-86 (1987).
- Levich, V. B., Physicochemical Hydrodynamics, Prentice-Hall, Englewood Cliffs, N.J. (1962)
- Mack, M. H.; "Choosing an Extruder for Melt Devolatilization", *Plastics Eng.*, July, 47-51 (1986).
- Meder, S.; "Progress in Devolatilization of Polymer Melts in Injection Molding and Extrusion", Soc. Plast. Eng. ANTEC Nat'l Meeting, 77-80 (1987).
- Mehta, P. S., L. N. Valsamis and Z. Tadmor; "Foam Devolatilization in a Multi-Channel Corotating Disk Processor", *Pol. Proc. Eng.*, 2, 103-128 (1984).
- Moffat, H. K. J.; "Viscous and Resistive Eddies Near a Sharp Corner", *J. Fluid Mech.*, 18, 1-9 (1964).
- Millen, W. and S. Hawkes; "Diffusion and Partition of n-Alkanes in Dimethylsilicone Stationary Phases", *J. Chrom. Sci.*, 15, 148-150 (1977).
- Newman, R. E. and R. H. M. Simon; "A Mathematical Model of Devolatilization Promoted by Bubble Formation", 73'rd Annual AIChE Meet., Chicago, Ill. (1980).

- Nichols, R. J. and P. E. Lubiejewski; "Extrusion Isolation of Polymers from Solution", Soc. Plast. Eng. ANTEC Nat'l Meeting (1985).
- Pasiuk-Bronikowska, W. and K. J. Rudzinski, "A Mathematical Model of Bubble Gas Desorption from Liquids", Chem. Eng. Sci., 35, 512-518 (1980).
- Pasiuk-Bronikowska, W. and K. J. Rudzinski, "Gas Desorption from Liquids", Chem. Eng. Sci., 36, 1153-1159, (1981).
- Powell, K. G. and C. D. Denson "A Model for the Devolatilization of Polymeric Solutions Containing Entrained Bubbles", 75'th Annual AIChE Meet., Washington, D.C., (1983).
- Prud'homme, R. K., W. J. Gregory and R. P. Andres, "Homogeneous Nucleation Temperature for Concentrated Polystyrene/Benzene Solutions", J. Pol. Sci., 72, 263-275 (1985).
- Rallison, J. M.; "The Deformation of Small Viscous Drops and Bubbles in Shear Flows", Ann. Rev. Fluid Mech., 16, 45-66 (1984).
- Randolph, A. D., and M. A. Larson; Theory of Particulate Processes, Academic Press, New York, N.Y., (1971).
- Roberts, G. W.; "A Surface Renewal Model for the Drying of Polymers During Screw Extrusion", AIChE J., 16, 878-881 (1970).
- Ruckenstein, E. and E. J. Davis; "Diffusion-Controlled Growth or Collapse of Moving and Stationary Fluid Spheres", J. Coll. Int. Sci., 34, 142-158 (1970).
- Sakai, T. and N. Hashimoto; "Application of Novel Counter-Rotating Intermeshed Twin Extruder for Degassing Operation", Soc. Plast. Eng. ANTEC Nat'l Meet., 860-863 (1986).
- Scriven, L. E.; "On the Dynamics of Phase Growth", Chem. Eng. Sci., 10, 1-14 (1959).
- Secor, R. M.; "A Mass Transfer Model for a Twin-Screw Extruder", Pol. Eng. Sci., 26, 647-652 (1986).
- Shah, S., S. F. Wang, N. Schott and S. Grossman; "Counter-Rotating Twin Screw Extruder as a Devolatilizer and as a Continuous Polymer Reactor", Soc. Plast. Eng. ANTEC Nat'l Meet., 122-127 (1987).
- Szekely, J. and G. P. Martins; "Nonequilibrium Effects in the Growth of Spherical Gas Bubbles due to Solute Diffusion", Chem. Eng. Sci., 26, 149-147 (1971).
- Tadmor, Z. and C. G. Gogos; Principles of Polymer Processing, John Wiley and Sons, New York, N.Y. (1979).
- Tirrell, M., R. Galvan and R. L. Laurence; "Polymerization Reactors", Chapter 11, 735-778, in Chemical Reaction and Reactor Engineering, Ed's J. J. Carberry and A. Varma, Marcel Dekker Inc., New York (1987)
- Todd, D. B.; "Polymer Devolatilization", Soc. Plast. Eng. ANTEC Nat'l Meet., 472-475 (1974).

- Villamizer, C. A. and C. D. Han, "Studies on Structural Foam Processing. II. Bubble Dynamics in Foam Injection Molding", *Pol. Eng. Sci.*, 18, 699-710 (1978).
- Vrentas, J. S., J. L. Duda and M. K. Lau; "Solvent Diffusion in Molten Polyethylene", *J. Appl. Pol. Sci.*, 27, 3987-3997 (1982).
- Vrentas, J. S., J. L. Duda and H. C. Ling; "Enhancement of Impurity Removal from Polymer Films", *J. Appl. Pol. Sci.*, 30, 449-4516 (1985).
- Werner, H.; Devolatilization of Plastics, Verein Deutscher Ingenieure, Dusseldorf, 99 (1980).
- Wolf, D. and D. H. White; "Experimental Study of the Residence Time Distribution in Plasticating Screw Extruders", *AIChE J.*, 22, 122-132 (1976).
- Woods, D. R. and K. A. Burrill; "The Stability of Emulsions", *Electroanal. Chem. Int. Electrochem.*, 37, 191-213 (1972).
- Yoo, H. J. and C. D. Han; "Development of a Mathematical Model of Foam Devolatilization", *Pol. Proc. Eng.*, 2, 129-151 (1984).

